DESIGN, SYNTHESIS, KINETIC ANALYSIS, MOLECULAR MODELING, AND PHARMACOLOGICAL EVALUATION OF NOVEL INHIBITORS OF PEPTIDE AMIDATION

A Thesis
Presented to
the Academic Faculty

by

Michael Scott Foster

In Partial Fulfillment
Of the Requirements for the Degree
Doctor of Philosophy in Chemistry

Georgia Institute of Technology

December 2008

DESIGN, SYNTHESIS, KINETIC ANALYSIS, MOLECULAR MODELING, AND PHARMACOLOGICAL EVALUATION OF NOVEL INHIBITORS OF PEPTIDE AMIDATION

Approved by:

Dr. Sheldon W. May
School of Chemistry and Biochemistry
Georgia Institute of Technology

Dr. Stanley H. Pollock
Pharmaceutical Sciences
Mercer University

Dr. James C. Powers
School of Chemistry and Biochemistry
Georgia Institute of Technology

Dr. Niren Murthy
School of Biomedical Engineering
Georgia Institute of Technology

Dr. Nicholas V. Hud
School of Chemistry and Biochemistry
Georgia Institute of Technology

Date Approved: August 12, 2008

For Dr. Sheldon W. May, without whose indefatigable kindness, patience, good humor, and positive attitude, I surely would never have completed this work.

For Amanda, whose loyalty, love, and trust throughout these many years have ever been a blessing to me.

For Dave, the best brother a person could ask for.

And for my mother, who gave me everything. I am sorry you could not be here to share in my success.

ACKNOWLEDGEMENTS

I give, again, my deepest thanks to Dr. Sheldon May for the opportunity to work alongside him and with his group for these wonderful years. Also, many thanks to Dr. Charlie Oldham for listening to me gripe about ill-conceived software default settings and shoddy instrument engineering without every becoming more than mildly irritated with me. His encyclopedic knowledge of many different scientific and technical fields has been a wonderful benefit to my graduate career.

I also wish to thank Dr. Stanley Pollock of Mercer University for allowing me to expand my research horizons into pharmacological studies. Thanks also to the following for various contributions to my knowledge, technique, and my general welfare: Dr. Kristi Burns, Dr. Veronica de Silva, Dr. Jennifer Overcast Lane, Dr. Jeffrey Sunman, Dr. John Bauer, Dr. Michael Kulis, Mr. Jeremy Thompson, Mr. Jacob Lucrezi, Ms. Elizabeth Cowan, and Ms. Maggie Schwab.

I also wish to thank the other members of my Thesis Committee, Dr. James Powers, Dr. Nicholas Hud, and Dr. Niren Murthy. I appreciate the personal time that everyone has spent on my behalf.

Finally, I would like to thank the National Institutes of Health (NIH) and the National Arthritis Foundation for their generous supports of the work presented herein.

TABLE OF CONTENTS

LIST OF TABLES

LIST OF FIGURES

LIST OF SYMBOLS AND ABBREVIATIONS

APAA	5-(Acetylamino)-4-Oxo-6-Phenyl-Hexenoic Acid
APAA-OMe	Methyl-5-(Acetylamino)-4-Oxo-6-Phenyl-Hexenoate
BEV	Baculovirus Expression Vector
BSA	Bovine Serum Albumin
CGRP	Calcitonin Gene-Related Peptide
COX	Cyclooxygenase
DBM	Dopamine β-Monooxygenase (EC 1.14.17.1)
DMSO	Dimethylsulfoxide
EtOAc	Ethyl Acetate
FBS	Fetal Bovine Serum
FPLC	Fast Protein Liquid Chromatography
HEPES	N-2-Hydroxyethylpiperazine-N'-2-ethanesulfonic Acid
HPLC	High Performance Liquid Chromatography
IYG	N-Acetyl-3,5-Diiodo-(L)-Tyrosine-Gly
K_M	Michaelis Constant
MES	2-(N-Morpholino)ethanesulfonic Acid
NSAIDs	Non-Steroidal Anti-Inflammatory Drugs
PAM	Peptidylglycine α-Amidating Monooxygenase (EC 1.14.17.3)
PBA	4-Phenyl-3-Butenoic Acid
PBA-OMe	Methyl-4-Phenyl-3-Butenoate
PGL	Peptidoamidoglycolate Lyase (EC 4.3.2.5)

SP	Substance P
TNP	2,4,6-Trinitrophenyl Group

SUMMARY

Novel, rationally-designed acrylate analogs of various known dipeptide substrates were found to be mechanism-based inactivators of the enzyme peptidylglycine α-amidating monoxygenase (PAM, EC 1.14.17.3). This enzyme is responsible for the rate-limiting and final bioactivation step, a C-terminal amidation of glycine-extended peptides, of a variety of peptide hormones including the potent pro-inflammatory compound Substance P. Protein-ligand docking studies, in tandem with *in vitro* kinetic analysis of these inactivators, indicated that the rational design of this class of compounds was successful in creating potent competitive inactivators of this enzyme. Pharmacological evaluation, via both acute and chronic models of inflammation in Sprague-Dawley rats, of these compounds indicates that they are highly potent anti-inflammatory agents which ameliorate both acute carrageenan-induced edema and the deleterious effects of chronic adjuvant-induced polyarthritis. Furthermore, these compounds were also able to induce a return toward a more normal phenotype in cancerous WB-Ras epithelial cells, via the interruption of the growth factor-stimulated pathway precipitated by Substance P. Finally, our modeling studies provide a structural basis for both the reaction and subsite stereospecificity of PAM toward its substrates, competitive inhibitors, and mechanism-based inactivators.

Part 1

Design, Synthesis, Kinetic Analysis and Molecular Modeling of Novel Inhibitors of Peptide Amidation

Chapter 1: Introduction

General Introduction

Neuropeptides, also known as peptide hormones, were first discovered by von Euler and Gaddum in 1931 (von Euler, 1931) with the identification of Substance P (SP). Unlike a wide variety of non-peptide hormones or messengers which are either inherently unstable (such as prostaglandins) or quickly degraded by various enzymes (such as acetylcholine) and as such act only in an autocrine or paracrine fashion, the amino acid chain of a neuropeptide is remarkably robust and may persist long enough in the circulation to act at targets far removed from the site of production in a truly endocrine manner. In 1953, Tuppy and Michl found, surprisingly, that the active form of the peptide hormone oxytocin contains a C-terminal amide functionality, rather than a free carboxylic acid group. (Tuppy, 1953) Although Substance P had been known since its discovery in 1931, many years passed before Susan Leeman and colleagues demonstrated that SP possesses an amide moiety at its C-terminus (Leeman, 1980). Since then, many neuropeptides have been isolated and characterized. Nearly 50% of these peptides require C-terminal amidation for full biological activity.

Although the existence of amidated neuropeptides was well-known by the time that Leeman et al. proved that Substance P (Arg-Pro-Lys-Pro-Gln-Gln-Phe-Phe-Gly-Leu-Met-NH_2) fell into this category, the amidation mechanism remained unknown. The list of known amidated peptides included sequences which terminated in every natural amino acid amide. Moreover, there seemed to exist no regularity with regard to residues at the

penultimate position or those located further toward the N-terminus of the C-terminal amide. This seemed to rule out the possibility that the amidation reaction proceeded via any type of process in which either the C-terminal residue or sequence of residues of a given amidated peptide participated in or directed the mechanism of peptide amidation. Indeed, SP terminates in Gly-Leu-Met-NH_2 while oxytocin terminates in Pro-Leu-Gly-NH_2 and vasoactive intestinal peptide (VIP) in Ile-Leu-Asn-NH_2, illustrating the lack of consensus of the residues which precede the C-terminal amidated residue. Since approximately half of known neuropeptides are not amidated at the C-terminus, any type of transamidase activity (which would proceed regardless of the sequence of the peptide substrate, since there seemed to be few, if any, restrictions engendered by the nature of the residues to the N-terminal side of the amide) would have to be extensively colocalized only with those particular peptides for which amidation is absolutely required, and to the exclusion of all non-amidated neuropeptides. *A priori*, this would completely obviate the possibility that amidation could occur extracellularly, and would indicate a complex process of sequestration of both enzyme and peptide substrates within subcellular compartments. Alternatively, if the product peptide amide were generated from a larger precursor, any extra residues to the C-terminal side of the ultimately amidated amino acid would be able to lend specificity to the amidation reaction and restrict any peptide without such a sequence (or residue) from being subject to amidation.

In 1977, Suchanek and Kreil (Suchanek, 1977) expressed melittin (terminating in Arg-Gln-Gln-NH_2) mRNA from queen bee venom glands in a cell-free wheat germ system and found that while, unsurprisingly, no peptide amide product was detected, a prepromelittin peptide was expressed which terminated in the sequence Gln-Gln-Gly-

COOH. The authors suggested that, if the residue Gly could be shown to be present immediately to the C-terminal side of the ultimately amidated residue of other potential amidation substrates, then perhaps the extra glycine residue is both necessary and sufficient to target a peptide sequence for amidation. Moreover, this glycine would also suggest a possibility for the mechanism of amidation, which they reasoned could plausibly proceed via the involvement of some currently unknown (but C-terminal glycine-specific) aminotransferase activity. Their hypothesis was strengthened by the fact that the sequence of corticotropin (Scott, 1973), an α-melanotropin precursor (α-melanotropin itself terminates in Val-NH_2 (Harris, 1957)), contains two potential protease cleavage sites (for trypsin- and carboxypeptidase-B-like activities) which, following proteolysis, would yield a C-terminus of Val-Gly-COOH and be subject to that putative activity which amidates peptides terminating in X-Gly-COOH (where X = any amino acid residue).

Several years later, Bradbury et al. succeeded in isolating a peptide amidating activity from gel-filtration fractions (corresponding to MW of approximately 60,000 daltons) of porcine pituitary homogenate. (Bradbury, 1982) The synthetic peptide D-YVG was chosen as the substrate in the amidation assays based on the perception that the C-terminal sequence Val-Gly likely contained "the minimal structural elements of corticotropin necessary for the formation of the valine amide group present at the C-terminus of α-melanotropin." The N-terminal D-tyrosine was chosen for two reasons: first, a D-amino acid residue at the N-terminus of peptides was known to inhibit degradation from aminopeptidases likely to be present in the pituitary homogenate fractions; secondly, tyrosine is readily radioiodinated by ^{125}I at both carbons ortho to the

phenolic hydroxyl group, which obviously vastly increases the sensitivity of any subsequent chromatographic analysis of both the substrate and product (D-YV-NH_2). Additionally, when D-YVG synthesized with ^{15}N-glycine was incubated with the fractionated pituitary homogenate, the product amide D-YV-NH_2 invariably terminated with ^{15}N-labeled amide. This proved that the C-terminal glycine is the source of the nitrogen atom found in the amidated product. Inclusion of the ammonium ion or the aminotransferase donors glutamine or asparagine failed to increase the efficiency of the amidation reaction, effectively ruling out any type of aminotransferase activity as the amidating enzyme. Further investigations served to demonstrate that the amidating activity was eliminated when the C-terminal glycine was replaced by (L)-Sar, (L)-Ala, (L)-Leu, (L)-Lys or (L)-Glu. The reaction proceeded when (L)-Val (the penultimate residue) was replaced with (L)-Phe or Gly, but not when replaced by (D)-Ala, (L)-Lys, or (L)-Asp. This was consistent with the knowledge (at the time) that no peptides were known to terminate in (D)-Ala, (L)-Lys, or (L)-Asp amides. Finally, based on the fact that glyoxylate was identified as the second product of the amidation of glycine-extended tripeptides, the mechanistic conjecture was refined to include the oxidative formation of an imine intermediate followed by aqueous hydrolysis.

At this point, the door was opened to a full investigation of the properties of this amidating activity. If this enzyme were responsible for the bioactivation of all amidated neuropeptides, it was evident that the development of amidation inhibitors would provide a new tool for the amelioration of a potentially immense variety of pathophysiological conditions arising from excessive production of these hormones. Indeed, Substance P, the first neuropeptide to be identified back in 1931, is now known to be involved in the

transmission of chronic pain signals and is also a potent pro-inflammatory mediator that serves to "prime" a great many cells of the immune system. Reduction of SP levels in patients with chronic pain, inflammation, or autoimmune disorders could prove an invaluable tool in the amelioration of these conditions. Most of the thrust of this thesis is based on the design, development, and analysis of inhibitors of the α-amidating enzyme (now called peptidylglycine α-amidating monooxygenase, or PAM; EC 1.14.17.3), more specifically toward the goal of reducing *in vivo* levels of Substance P and mitigating its deleterious effects as a pro-inflammatory agent run amok in, for example, the devastating condition of rheumatoid arthritis.

The rest of this portion of the Introduction will investigate many aspects and properties of this fascinating enzyme. Initially, we will explore the expression and localization of PAM in various tissues and at various levels of subcellular organization and sequestration, and any different isozymes which may be present from one tissue to another. We will discuss substrate specificity and cofactor requirements of the various isozymes of this enzyme known to be expressed in various tissues. The processing, routing, trafficking, storage, and secretion of PAM will be explored. We will discuss a wide variety of competitive inhibitors (and briefly touch upon several uncompetitive inhibitors) in relation to the structure of the PAM active site. Finally, the mechanism of PAM will be extensively explored, especially in the context of the mechanism-based inactivators developed in this laboratory. The second portion of the introduction will concentrate more upon Substance P and its physiological effects, especially as they relate to the problem of chronic inflammation and its resolution. We will also discuss several

autocrine growth loops evident in many neoplastic pathologies which are thought to be governed and reinforced by a variety of amidated neuropeptides.

PAM Localization and Expression

In 1986, Mizuno, et al., developed a sensitive radioassay for monitoring PAM activity *in vitro* using (^{125}I)-Ac-D-YFG and were the first group to purify the enzyme to homogeneity, using frog skin (*X. Laevis*) as the enzyme source. (Mizuno, 1986) After several purification steps, a hydroxylapatite column resolved the amidating activity into two different fractions, AE-I (amidating enzyme-I) and AE-II (amidating enzyme-II), with AE-1 being the major, and later-eluting, fraction. After further purification (c. 8300-fold), AE-1 was found to be homogeneous with a molecular weight of approximately 39,000 Daltons. Further purification of AE-II failed to yield a homogeneous product and instead was composed of two active fractions, with molecular weights of 39,000 (AE-IIa) and 34,000 (AE-IIb). Sequence analysis by Edman degradation revealed that all three proteins were possessed of the same N-terminal sequence (Ser-Leu-Ser), which indicated that the three isozymes were related and most likely expressed from the same gene. Indeed, in the same year, experiments by Murthy, et al. (Murthy, 1986) to purify PAM from bovine pituitary also revealed the presence of multiple forms of PAM. AE-I was then incubated with a variety of glycine-extended peptides (YFG, N-Ac-YFG, (D)-YVG, and (D)-YGG), yielding the following activity profile: YFG > N-Ac-YFG > (D)-YVG > (D)-YGG. Two peptides which do not contain a C-terminal glycine (des-amidoadrenorphin and BAM-12P) were unaffected following

incubation with purified AE-I. The optimal pH range was between 6.0 and 7.0. Activity was abolished upon addition of 0.1 mM EDTA, and subsequently rescued by the addition of excess copper sulfate (0.12 mM). Addition of 1 mM dithiothreitol, likely via copper ligation, also greatly inhibited the amidation activity, which could again be rescued by the addition of excess copper sulfate, or by 5 mM N-ethylmaleimide, a sulfhydryl alkylating reagent. Activity was found to be much lower in the absence of exogenously-applied ascorbic acid, or when the enzyme ascorbate oxidase was included in the assay solution.

The same year, Sakata et al. performed ammonium sulfate precipitations on a wide variety of tissues from adult male Wister rats (Sakata, 1986) and assayed the precipitates for amidating activity. Surprisingly, the activity was found in nearly every tissue assayed, with the notable exceptions of the thymus and liver. The highest activities were found in the pituitary, heart atrium, submaxillary gland, parotid gland, and thyroid gland, respectively (c. 45/18/11/8/6). The lowest detected levels were found in the kidney, spleen, cerebellum, and esophagus, respectively (c. 0.034/0.054/0.132/0.220). These findings indicated that the amidation activity responsible for the bioactivation of *neuro*peptides was to be found throughout the entire body of the rat, and suggested that the systemic importance of neuropeptides in controlling or influencing various metabolic functions was much greater than had been previously anticipated.

Interestingly, the same year Mollay et al. also attempted to isolate homogeneous amidating enzyme from the skin of *X. Laevis*. Although they failed to achieve the degree of purity of Mizuno et al. (150-fold vs. 8,300-fold), they nevertheless discovered several important results. First, their amidating enzyme was characterized by *two* pH maxima at

5.5 and 8.4, rather than the 6.0-7.0 optimum range found with Mizuno's enzyme. This was actually the hint of a two-step mechanism in the formation of C-terminal amides from glycine-extended precursors, one with an acidic optimum and one with an alkaline optimum. Conceivably, then, it was possible that *two* distinct enzymes (or a single bifunctional enzyme) were responsible for the production of amidated peptides. In the absence of added cofactors, the rates of amide formation at the two pHs were nearly identical (540/460 @ pH 5.5/8.4). Addition of exogenous copper and ascorbate (2 μM and 2 mM, respectively) selectively increased the rate of amide formation at pH 8.4 vs. pH 5.5 (4.2 fold to 1.5 fold, respectively). Also, at pH 5.5 this enzyme, in contrast to findings from the mammalian amidating enzyme which was stimulated only by the addition of Cu^{+2}, was greatly increased by addition of Cu^{+2} or Fe^{+3}, Mn^{+2}, Zn^{+2}, or Fe^{+2}.

Subsequently, work by von Zastrow et al. (von Zastrow,1986) demonstrated that the amidating enzymes were also to be found in the pancreas, and the submaxillary, lachrymal, and parotid glands. This was the first time that PAM was found to be actively expressed in exocrine tissues, which secrete their products into ducts (endocrine glands secrete products directly into the bloodstream). Indeed, as with prior work with pituitary PAM, it was found that the majority of the activity was found to coelute with α-amylase in the secretory granule fraction. About 15% of the total amidating activity was associated with the endoplasmic reticulum and Golgi fractions. *In* vivo, administration of the β-adrenergic agonist isoproterenol allowed the collection of exocytosed secretory granules via cannula. The contents of the secretion were found to be nearly identical in content to the purified secretory granules. With regard to kinetic parameters, while this enzyme was not subject to further purification (and hence was of unknown molecular

weight), the pH optimum with respect to the substrate D-YVG was found to be between 6.5 and 7.0. The amidating activity was, again, stimulated by exogenous copper and ascorbate. Addition of 2 mM ascorbate increased both the V_{max} and, to a lesser degree, the K_M values.

Concurrently, Murthy et al. (Murthy, 1986) analyzed the anterior, neural, and intermediate lobes of the bovine pituitary for amidating enzyme activity. In all cases, the PAM activity was highly localized to the secretory granule fractions. The ratio of activity for the anterior, neural, and intermediate lobes was found to be approximately 10:10:1, respectively. Further purification of the PAM activity yielded two forms of PAM, PAM-A and PAM-B (M.W. = 54K and 38K, respectively); tryptic digests indicated that the two forms of the enzyme were related, with PAM-B likely a further modified form of PAM-A. Crude PAM, PAM-A, and PAM-B all behaved identically with regard to pH optima (alkaline) and exogenously added Cu^{+2} and ascorbate (all stimulated above baseline). Interestingly, initial attempts to purify PAM directly from secretory granules resulted in very low yields of enzyme. The authors estimate that there are, at most, several molecules of PAM per secretory granule.

In 1987, Mizuno et al. (Mizuno, 1987) were able to clone the amidating enzyme from frog skin (*X. Laevis*). All introns were removed from the mRNA and a cDNA construct was synthesized and expressed in stably transfected *E. Coli*. The molecular weight of this purified, cloned enzyme was approximately 38,500 Daltons. Naturally, this was to be a very important step in the later mechanistic analysis of the amidating enzyme, allowing for mutagenesis studies and for easy isolation of much greater amounts of purified enzyme.

Since the evidence that the amidating enzyme was actually a bifunctional enzyme with both monooxygenase and lyase activities (or two soluble monofunctional enzymes acting sequentially) was not known until 1990 when PGL was discovered in this laboratory, assays performed on various substrates, and their reported pH optima, K_M and V_{max} values acquired prior to this date must be very carefully parsed in order to gain meaningful insight into the nature of the enzymatic reaction. Four tripeptides of the sequence D-Tyr-Xxx-Gly, where the middle residue was either Val, Trp, Glu, or Pro, were tested as substrates in the presence of purified PAM-B (M.W. = 38,000 Daltons) from bovine neurointermediate pituitary (Murthy, 1987). As an important aside, later studies (Katopodis, 1990) demonstrated that purified monofunctional PAM has a molecular weight of approximately 39,000 Daltons, and that PGL activity elutes from an analytical gel filtration column with an apparent molecular weight of 45,000 Daltons. Therefore, in hindsight, the 38,000 Dalton bovine neurointermediate pituitary PAM can only be the monofunctional monooxygenase enzyme. Furthermore, it is now known that the monooxygenase reaction yields an α-hydroxyglycine intermediate which is stable at acidic pH and requires the action of the lyase (PGL) to yield the amidated peptide product under acidic conditions (as in the secretory granule). However, at alkaline pH the hydroxylated peptide intermediate is spontaneously dealkylated via a base-catalyzed reaction. So, the authors in this case are measuring the rate of formation of the amidated product and thus are really measuring the product of two rates: first, that of PAM; second, that of the spontaneous dealkylation. Whether the former or the latter mechanistic step is rate-limiting is impossible to determine (in the absence of direct analysis of the α-hydroxyglycine intermediate) under these conditions, so only general

assumptions can be made about the relative efficacy of the enzyme with regard to one tetrapeptide substrate *vis-a-vis* the next.

Nevertheless, the results of the amino acid substitutions at the P2 position proved interesting. Valine and tryptophan are hydrophobic residues, although the latter is of much greater size. With proline at the P2 position, owing to the rotational restriction imposed by the nature of its side chain, the peptide substrate cannot adopt as wide a range of conformers as those tripeptides with Trp, Val, or Glu at the P2 position. This restriction, if it locks the molecule in a conformation amenable to the residues of the enzyme's active site, can allow for an extremely favorable substrate. On the other hand, this same conformational restriction may result in a very poor substrate, relative to one containing any of the other 19 naturally-occurring amino acids. Glutamic acid, with a side chain pK_a of approximately 4.0, is expected to exist almost entirely as the anionic form (90% at pH = 5.0; 99% at pH =6.0, etc.) over the range of pH values used in the assays (5.0-9.0). Again, this ionization may be either highly favorable as regards substrate binding to the active site or highly unfavorable depending on the nature of the microenvironment in which the side chain must bind. Obviously, the rate of reaction may be affected by the nature of the P2 residue as well.

Basically, it was found that the Val and Trp-containing peptides were about equipotent substrates with regard to k_{cat}/K_M at 0.25 mM ascorbate, with the larger Trp possessed of a slightly lower substrate binding constant (1.1 μM vs. 1.9 μM for Val) and also a slightly higher value for k_{cat} (8.4 nmol/μg*h vs. 7.5 nmol/μg*h for Val). When the concentration of ascorbate in the assay mixture was raised to 1.25 mM, K_M values tripled for both peptides, while k_{cat} values increased 4-fold. At the lower ascorbate concentration, the

Pro-containing peptide was found to have a significantly higher K_M value (30.6 μM) but a k_{cat} value approximately equal to the Trp- and Val-containing peptides (9.7 nmol/μg*h). At the higher ascorbate concentration, the trend was the same as for Trp and Val; K_M and k_{cat} each increasing 3- or 4-fold. However, the Glu-containing tripeptide, at the lower ascorbate concentration, has K_M and k_{cat} values of 129 μM and 45.9 nmol/μg*h, respectively. Interestingly, at the higher concentration of ascorbate, the K_M value jumped (in line with the other tripeptides) approximately 3-fold while the k_{cat} value increased to 1970 nmol/μg*h, approximately a 50-fold increase. The pH optima for Val, Trp, and Pro were approximately 8.5, while that for the Glu-containing tripeptide was about 5.5. The only explanation for these phenomena appears to be the following: it is now known that monofunctional PAM generally has a pH optimum of approximately 5.5 and is the rate-limiting step in the overall amidation reaction. PGL is also functional at this pH and serves to catalyze the dealkylation of the α-hydroxy intermediate to the des-Gly amide product, which can also occur non-enzymatically by general base catalysis at alkaline pH. For Trp, Val, and Pro, the alkaline pH optima likely reflects a much kinetically-subdued PAM reaction, but allows for an accelerated rate of non-enzymatic dealkylation to yield the product amide (recall that only the final amide product is being assayed here, and not the PAM-catalyzed hydroxyglycine intermediate). At the pH optimum for the Glu-containing tripeptide, the acidic conditions allow for amide formation from the hydroxyglycine intermediate at a very slow rate (possibly the rate-limiting step) for Trp, Val, and Pro. However, because Glu contains a second ionizable carboxylate functionality in close proximity to the PAM-added hydroxyl group the Glu-containing hydroxyglycine intermediate may be autocatalytically dealkylated via general base

catalysis at a rate commensurate with the incredibly elevated k_{cat} values of this molecule. So the acidic pH optimum for the Glu-containing peptide allows for a much higher rate of formation of the α-hydroxyglycine (since the PAM pH optimum is about 5.5), while the side chain carboxylate group is able to catalyze the dealkylation of the intermediate to the detectable amide product. These types of data and their subsequent analysis illustrate the difficulty in describing an enzymatic system in the absence of all relevant facts, especially as relates to a bifunctional enzymatic system such as PAM/PGL proved to be in later experiments.

PAM was also later discovered to be expressed at an appreciable rate and quantity by rat and bovine atrial cardiocytes. (Eipper, 1988) It had recently come to be known that the heart also functioned as an endocrine organ, insofar as it secretes the peptide hormones atrial natriuretic peptide (ANP) and brain natriuretic peptide (BNP). Neither peptide is amidated at the C-terminus in its active, fully-processed form (deBold, 1985). Eipper et al. found that PAM is localized in the secretory granule fractions of atrial myocytes, initially both in a membrane-associated form (70% in the rat) and a soluble form (30% in the rat). Moreover, the specific activity of the PAM collected from the rat atrial myocytes was between 5- and 20-fold higher than in the anterior pituitary. The distribution of PAM was found to be colocalized with ANP in the crude granule and microsomal fractions. As later work by this laboratory indicates (presented in Results section and Discussion section), there is an appreciable amount of soluble PAM found in the bloodstream (serum PAM) which is inactivated *in vivo* by our acrylate inhibitors (and PBA), and the amount of inactivation is proportional to a large degree to the anti-inflammatory effects of these compounds. It is possible that atrial myocytes are the main

source of PAM found in rat serum. With the amidating enzyme present in the bloodstream, it is possible that glycine-extended peptides, requiring amidation for full biological activity, may be secreted in an inactive form (by various cells of the innate or humoral immune system, for instance) and activated by serum PAM (bloodstream pH is alkaline, pH 7.4, and the intermediate is readily dealkylated non-enzymatically and does not necessarily require PGL activity). In this way, various cell types could express initially inactive peptide hormones which could be activated in the bloodstream or extracellular space without also expressing active PAM themselves.

In 1988, Fenger et al. (Fenger, 1988) demonstrated that dietary ascorbate was a major influence on the levels of peptide amidation in guinea pig pituitary. Animals from the experimental group were fed an ascorbate-depleted diet (resulting in 6-fold less ascorbate than control animals; 1.2 μmol/g tissue) while control animals consumed a normal diet with respect to ascorbate. Following ascorbate depletion, the pituitary glands were assayed for variously processed derivatives of adrenocorticotrophic hormone (ACTH): ACTH (1-39), the amidated peptide α-MSH (ACTH (1-13-NH_2), and ACTH (1-14), which has a C-terminal glycine. In the depleted animals, α-MSH levels dropped to approximately 50% of controls, while ACTH (1-14) accumulated to approximately 300% of controls. Interestingly, although the ascorbate-depleted animals' average body weight was only about 60% of control animals, the difference in mass of the pituitary glands of both groups was statistically insignificant. The authors did not investigate whether levels of ascorbate in the bloodstream or in other bodily tissues of the experimental animals were depleted to a greater or lesser extent than the pituitary gland (which could possibly

be able to maintain higher levels of ascorbate in general during a systemic depletion in order to maintain its function, relative to other tissues).

Various regions of sheep brain were assayed for amidating enzyme by Gale, et al. (Gale 1988). As expected from previous results, high levels of PAM activity were found in the anterior pituitary and the hypothalamus (specifically the medial basal hypothalamus). The highest levels were found in the median eminence of the hypothalamus, the region which, via the hypophyseal portal system, connects the anterior pituitary and hypothalamus. Both the synaptosomal fractions (synaptosomes are artifacts of the homogenization process, formed from cell-membrane phospholipids and including many proteins, peptides, and receptors originally localized at the synapse) and the neurosecretory granule fractions were especially enriched with PAM activity. Also in line with previous work, the enzyme was stimulated by the addition of exogenous ascorbate and copper and was found to have an alkaline pH optimum with D-Tyr-Pro-Gly-Gly, the C-terminal sequence of gonadotropin-releasing hormone, as the substrate. This is an interesting substrate for several reasons. First, Gly and Pro are found at the P2 and P3 positions of the peptide substrate, respectively, and both are known to adopt peculiar φ and ψ values as a function of the rigid conformational restriction of dihedral angle values available to Pro and the relatively rich availability of conformational freedom with regard to Gly. Moreover, after D-Tyr-Pro-Gly-Gly undergoes amidation by PAM, the peptide terminates in a glycyl amide. Since no D-Tyr-Pro-NH_2 was evident in the PAM assay, it seemed safe to assume that C-terminal glycine amides are not PAM substrates, indicating that the free carboxylate is obligatory for PAM catalysis. The K_M value for this peptide was reported as between 30-70 μM, about 20-fold higher than that

reported for D-YVG. Addition of ascorbate, catalase (to degrade any hydrogen peroxide formed by non-enzymatic reduction of water/oxygen by ascorbate), and copper (as copper (II) sulfate) stimulated activity, increasing both the K_M and V_{max} in parallel, as was previously described for a variety of other peptide substrates. Production of D-Tyr-Pro-Gly-NH_2 was inhibited by concurrent incubation with D-Tyr-Val-Gly, and production of D-Tyr-Val-NH_2 was inhibited by the addition of D-Tyr-Pro-Gly-Gly. This implies a competitive inhibition of one peptide by the other. Lastly, very little activity with respect to D-Tyr-Pro-Gly-Gly was found in either the cerebral cortex or the pineal gland, areas of the brain known to synthesize amidated peptides other than gonadotropin-releasing hormone, which could, perhaps, imply some varying substrate specificity in PAM from different tissues.

Further investigations by May et al. (May, 1988) into PAM distribution in rat anterior and neurointermediate pituitary reinforced the idea that both membrane-associated and soluble PAM have basically identical properties with regard to copper and ascorbate requirements, pH optima, and K_M values with respect to various glycine-extended peptide substrates. Interestingly, at least half of the amidating activity in the anterior pituitary was membrane-associated, while only about 10% of the activity in the neurointermediate pituitary was membrane-associated. Typically, approximately 5-fold more PAM was found in secretory granules relative to rough endoplasmic reticulum/Golgi fractions. Moreover, as the PAM is packaged in early granules and transported from the Golgi apparatus, the enzyme is increasingly processed to a soluble form which is released upon secretion. The authors could not determine to what extent the rate of peptide amidation

was affected by the location in the transport chain from rough ER to mature secretory granules.

PAM was next found to be expressed to a remarkably high degree in rat medullary thyroid carcinoma cells. Since many cellular growth factors are amidated peptides, it was not surprising that a cancerous cell-line was thusly enriched with amidating enzyme. Mehta, et al., (Mehta 1988), described four gel-filtration chromatography peaks with amidating activity, or which Peak III (M.W. = 75,000) was purified to homogeneity. In contrast to PAM from other sources (porcine and bovine pituitary and frog skin), this enzyme had an acidic pH optimum (5.0-5.5). In hindsight, the larger size of this enzyme indicates that PGL is also present in a bifunctional enzyme (PAM and PGL). Since the authors are still assaying for the amide product (rather than the then unknown hydroxyglycine intermediate), results for this enzyme are likely more reflective of the overall kinetic parameters of the amidation reaction than those investigations where only monofunctional PAM was used and the pH optima were found to be more alkaline than in this particular case. During these years, prior to the discovery of PGL, it is very difficult to compare the kinetic parameters of PAM from tissue to tissue or species to species because of the multiple substrates used by various research groups and, more importantly, the varying concentrations of exogenously added copper and ascorbate used in the various assays. Finally, the specific activity of the PAM from the carcinoma cells was found to be higher than that described for bovine/porcine pituitary and frog skin. The amount of PAM relative to total protein was two orders of magnitude greater in the thyroid carcinoma cells than these other cell types. Clearly, these carcinoma cells are wont to dedicate a great deal of metabolic energy to the production of PAM, the first

indication that PAM might in fact be a desirable target for inhibition in the treatment of various neoplastic pathologies.

Subsequently, significant amidating enzyme activity was found in both mouse atrial myocytes (previously investigated in rats) and in AtT-20 cells, a mouse corticotropic tumor cell line (corticotropes are cells in the anterior pituitary which express and secrete adrenocorticotropic hormone, as well as α-MSH, and which are sensitive to the polypeptide corticotropin-releasing factor (CRF, also known as corticotropin-releasing hormone, or CRH). Thiele, et al., (Thiele, 1989) investigated the degree to which the expression of PAM in both of these cell types varied in the presence of either the synthetic glucocorticoid dexamethasone or the cyclic-AMP analog $(Bu)_2$cAMP. Dexamethasone is a potent immunosuppressant and anti-inflammatory agent which exerts its effects through the HPA axis (hypothalamus/pituitary/adrenal axis). $(Bu)_2$cAMP activates protein kinase A (PKA), which in turn activates a variety of intracellular enzymes via phosphorylation, and can ultimately result in the activation of specific promoter regions in the DNA of the cell nucleus which causes the activation and expression of genes stimulating the production of growth hormones and a variety of pro-inflammatory mediators.

Treatment of the AtT-20 (pituitary-derived) cell with dexamethasone, unsurprisingly, resulted in an appreciable decrease in PAM mRNA (to 55% controls) while treatment with $(Bu)_2$cAMP resulted in an increase in the transcription of PAM mRNA (to 132% controls). The specific activity of the extracted, cell-associated PAM enzyme (M.W. = 100,000 and likely bifunctional PAM/PGL) decreased in both cases to approximately 60% of controls. In the case of the cAMP analog, the reduction was attributed to the

stimulation of secretion of PAM into the cultural medium. Interestingly, the heart atrial cultures responded in a similar manner to both compounds, with PAM mRNA increasing in both cases to approximately 220% of the controls. Secretion also increased by the same proportion. The effects of the coadministration of both compounds resulted in an additive effect, where secretion increased to nearly 350% of controls. AtT-20 cells were unable to maintain baseline levels of PAM in the face of higher secretion levels, whereas the cellular PAM levels of atrial cardiocytes were unaffected, even as secretion increased dramatically. This provides further evidence that atrial myocytes might be the major source of amidating enzyme in the bloodstream. Naturally, only soluble amidating enzyme is secreted. The authors do not describe the molecular weight of the soluble, secreted enzyme, but it is extremely likely that it is the monofunctional PAM monooxygenase.

Later that year, PAM was also discovered in chromaffin granules of bovine adrenal medulla (as well as other ganglia of the sympathetic nervous system) (Bastiaensen, 1989). This is interesting for an additional reason, namely that these neuroendocrine cells are known for the secretion of the catecholamines epinephrine and norepinephrine, the latter of which is a β-hydroxylated product that is formed from dopamine by the action of the enzyme dopamine β-monooxygenase (DBM), an enzyme with considerable sequence homology to PAM and also requiring the cofactors copper and ascorbate. The amidated peptides Neuropeptide Y (NPY), metorphamide, and amidorphin were also known to be present in chromaffin granules. These cells are innervated by the splanchic nerve and are readily stained by chromium salts (hence the name “chromaffin”). While low levels of PAM activity were found in the cell homogenate, activity was much higher

in the soluble fraction of the secretory granules. The molecular weight of the enzyme was found to be 40,000 Daltons and had a pH optimum of approximately 8.0. This alkaline pH optimum and lower molecular weight indicates, again, that the soluble form of the enzyme investigated here is monofunctional PAM.

In 1990, Rhodes et al. (Rhodes, 1990) further investigated the distribution of PAM throughout the nervous system of the rat, finding PAM in a wide variety of both neuronal and non-neuronal cell types. Immunostaining of PAM was effected via an antiserum raised against seventeen amino acid residues of the N-terminus of the enzyme. Unsurprisingly, a great deal of immunoreactivity was detected in the perikarya (neuronal cell bodies) of various neuronal cells, including pituitary, the hypothalamic periventricular and supraoptic nuclei, the neocortex, and sensory ganglia. Immunoreactivity was highest in regions known to receive amidated peptidergic afferents, as well as some neurons not known to produce amidated peptides (such as the pyrimidal cells of the hippocampus, a structure known to be involved in long-term memory and spatial navigation). Moreover, some of the most intensely-stained areas of the brain involved a variety of non-neuronal cell types, especially in the ependyma (neuroglia in the epithelial lining of the ventricular system of the brain) and choroid plexus (modified ependymal cells in the ventricular system which are involved in the production of cerebrospinal fluid). The following glial cells (glial cells are a wide variety of cells which support neurons in a number of different fashions) also exhibited a considerable amount of PAM immunoreactivity: oligodendroglia, cells involved in the insulation of axons of neurons in the central nervous system, each capable of supporting up to fifty neurons; astrocytes (astroglia), cells involved in the repair of neuronal injury

as well as basic biochemical support of the endothelial cells which form the blood-brain barrier; and Schwann cells, glia which insulate the axons of the peripheral nervous system, and which are associated with, in contrast to oligodendroglia, only one neuronal axon. Finally, a comparatively huge degree of PAM immunoreactivity was found in the sciatic nerve, the largest nerve in the body, which runs from the lower back through the lower limb. Braas et al. (Braas, 1992) also found PAM immunoreactivity in the heart, salivary glands, thyroid, adrenal glands, the α-islet cells of the pancreas, the kidneys, and the testis.

By 1992, the bifunctional nature of the amidating enzyme had been demonstrated by this laboratory (Katopodis, 1990) with the discovery of PGL (Peptidoamidoglycolate Lyase, E.C. 3.2.1.15), the enzyme which catalyzes the dealkylation of the α-hydroxyglycine product of the PAM (monooxygenase) reaction. Our laboratory (Oldham, 1992) investigated whether PAM and/or PGL was expressed in endothelial cells, and found both the monooxygenase and lyase activities to be present therein. Endothelial cells release a variety of vasoconstrictors (endothelin and angiontensin II) and vasorelaxants (endothelium-derived relaxing factor and the eicosanoid prostaglandin prostacyclin) and also express a variety of cell-surface attachment proteins (intracellular adhesion molecule, or ICAM, and vascular cell-adhesion molecule, or VCAM, e.g.) involved in the recruitment, diapedesis, rolling, and extravasation of leukocytes into areas of inflammation, infection, or cellular damage in the extravascular space. The monooxygenase and lyase reactions were measured simultaneously by monitoring the conversion of trinitrophenyl-D-YVG (TNP-YVG) to both TNP-YV(OH)G and TNP-YV-NH_2. The isolated PGL reaction was monitored by the conversion of α-

hydroxybenzoylglycine to benzamide. The full amidation reaction (requiring both PAM and PGL) was ascorbate dependent, whereas the isolated PGL reaction showed no such dependency. Preincubation of the cell extracts with 4-phenyl-3-butenoic acid (PBA), a known inactivator of PAM, abolished all activity in the PAM assay, while the PGL reaction was unaffected by this preincubation.

Eipper et al. (Eipper 1992) demonstrated that, although PAM/PGL is encoded by a single gene in the rat, alternative splicing in various tissues results in as many as seven different forms of amidating-enzyme mRNA. Five encode the full bifunctional enzyme. Of these five, three are translated into the membrane-bound form while two encode soluble proteins. One mRNA encodes a soluble, monofunctional PAM. The final mRNA, strangely, encodes only part of the PAM domain (it does not include the region of sequence homology to DBM), which is completely inactive toward common PAM substrates. Of the five bifunctional enzymes, only one, rPAM-1, contains the dibasic cleavage site (Lys-Lys, in Exon A) which allows for the proteolytic cleavage of a soluble PAM from PGL, leaving the PGL membrane-bound. The different enzyme forms may lead to targeting of the newly formed enzymes along different trafficking pathways to various subcellular locations, or allow for different N-glycosylation sites, or may allow for endocytosis and recycling of certain forms of PAM to the exclusion of others. There do not appear to exist any monofunctional PAM derivatives which could conceivably remain associated with the cellular membrane. Interestingly, concurrent work by Kato et al. (Kato, 1992) detected significant PAM/PGL in the saliva and submaxillary gland (exocrine) of the rat. The salivary PAM had a molecular weight of 75,000 Daltons, whereas the PAM localized to the submaxillary gland was found to be about 25,000

Daltons. A trypsin digest (a protease which cleaves peptides to the carboxy side of Lys and Arg residues) of the salivary PAM resulted in PAM with a molecular weight of 25,000, identical to that found originally in the submaxillary gland.

Saldise et al. (Saldise, 1996) found an abundance of amidating enzyme in both normal human lung and a variety of lung cancer resections, including adenocarcinomas, small-cell lung carcinomas, large-cell carcinomas, and well-differentiated neuroendocrine carcinomas. Interestingly, PAM activity was found to some degree in all tumor types, but PGL was absent in many resections, or present only to a much smaller degree than PAM. Not surprisingly, the neuroendocrine tumors were richest in PAM and PGL activity. In normal human lung, PAM immunoreactivity was found in airway epithelium, endothelium, some chondrocytes, alveolar macrophages, smooth muscle cells, and both myelinated nerves and neurons of the intrinsic ganglia.

Guembe, et al. (Guembe, 1999) followed the expression of PAM and PGL in adult mouse lung, finding significant immunoreactivity in epithelial cells, smooth muscle cells, and pulmonary parenchymal cells (the authors assume these to be macrophages). More interestingly, the authors found that some cells were immunoreactive to either PAM or PGL, but not both. Since both enzymes are encoded by the same gene, the fact that some cells express one but not the other implies that a preferential secretion or degradation of one enzyme or the other may occur in a given cell type. This may imply a heretofore unknown function for either glycine-extended PAM substrates in their own right (by virtue of cells lacking PAM immunoreactivity) or for α-hydroxyglycine intermediates of various peptides (no PGL activity). Indeed, CGRP-positive (a known amidated peptide) cells have been found to be negative for PAM activity or immunoreactivity (Martinez,

1993; Steel, 1994). Such a functional role for either of these types of species would greatly increase the known complexity and flexibility of the neuroendocrine system. Indeed, it was later shown that SP-Gly is equipotent with SP in the stimulation of NO release from cultured bovine cardiac endothelial cells (Abou-Mohammed, 2000). However, it is possible that this effect is derived from the N-terminus of SP/SP-Gly, rather than from the C-terminus, associating with the appropriate receptor. Differential, rather than similar, effects of a given glycine-extended peptide relative to its des-Gly amide would serve to increase the complexity of a given system.

Substrates and Inhibitors

For reference, the overall amidation reaction is shown in Figure 1. Among the earliest investigations into the substrates of Peptidylglycine α-Amidating Monooxygenase were those begun in the early 1980's by Bradbury and coworkers. The first known synthetic PAM substrate was the tripeptide D-YVG, utilized in these early experiments (Bradbury, 1983). This same tripeptide, albeit modified with a trinitrophenyl adduct to increase UV activity, has been utilized exhaustively as a PAM substrate in inhibition experiments by this laboratory for many years (Katopodis 1988). Other laboratories have utilized dansylated or N-acetylated derivatives of this tripeptide as their standard PAM substrate. As mentioned previously, the sequence is based on the R-Val-NH_2 carboxy terminus of α-MSH (melanocyte-stimulating hormone) and the fact that corticotropin (the α-MSH precursor) contains the MSH sequence followed by a glycine residue. D-Tyrosine, easily radioiodinated for increased assay sensitivity of both substrate and potential product, was

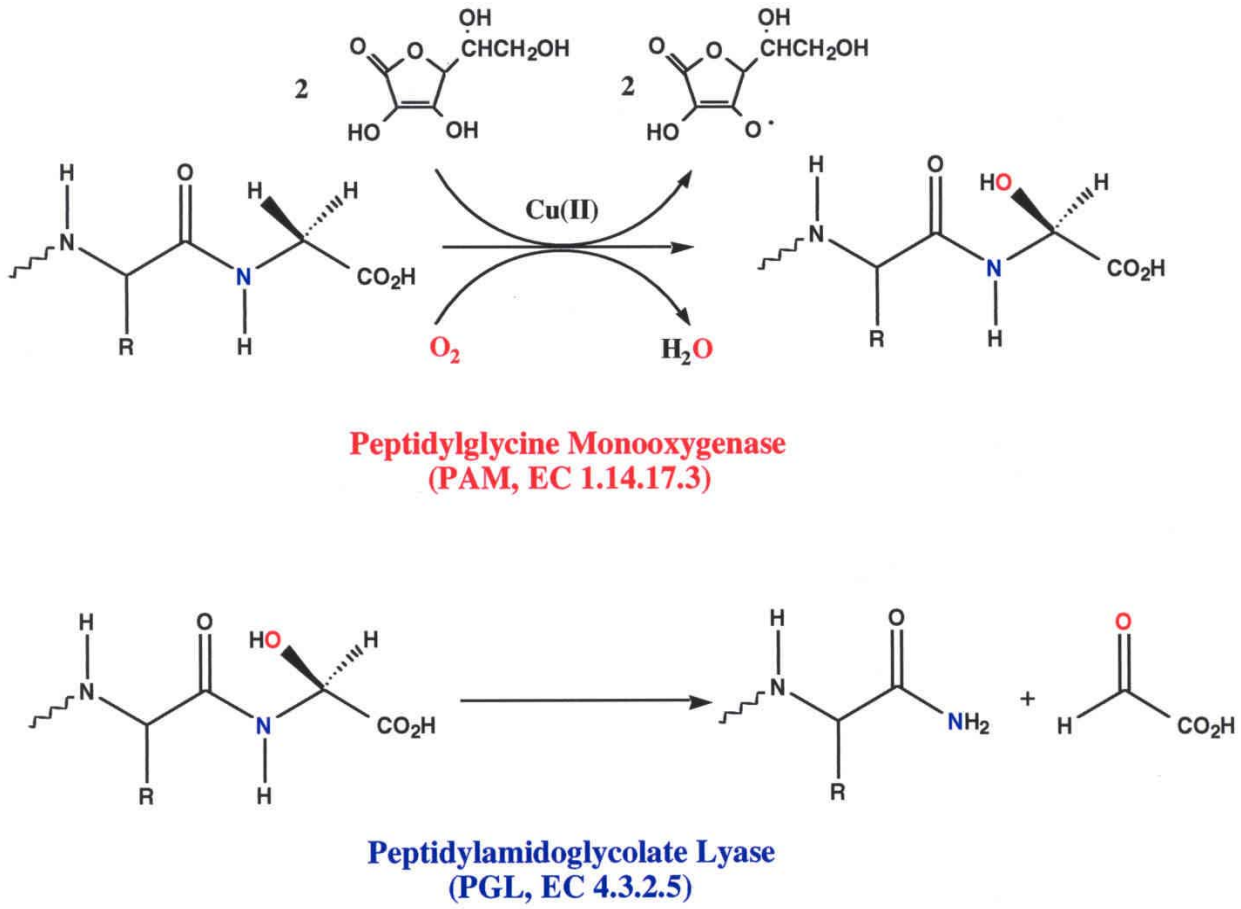

Figure 1. Reaction scheme for PAM and PGL, including appropriate stereochemistry and cofactors. The monooxygenase incorporates one atom of molecular oxygen into the peptide substrate, the other is reduced to water. Ascorbate reduces both active-site copper ions to Cu(I), and is oxidized to semidehydroascorbate. PGL catalyzes the oxidative dealkylation of the PAM product to the des-Gly amide and glyoxylate.

included as the residue at the P3 position of the substrate. The incorporation of a (D)-residue may also serve to decrease the rate of substrate hydrolysis by any proteases present in biologically-derived samples. D-YVG was converted to D-YV-NH_2 by purified amidating enzyme. Replacement of Gly by either negatively charged Glu, positively charged Lys, or the small hydrophobic Ala, resulted in no amide formation. This was the first demonstration that only glycine-extended peptides are accepted as PAM substrates. Further studies revealed that all (L)-amino acids are tolerated at the P2 position, but that neutral hydrophobic residues are preferred. The tripeptide D-Tyr-D-Ala-Gly was found not to be a PAM substrate, demonstrating stereospecificity at the P2 position as well. Obviously, (D)-amino acids are tolerated at the P3 position. It was hypothesized that peptide amidation was the final step of a three-step process whereby ACTH is initially cleaved to the carboxy-side of a pair of dibasic residues by a prohormone convertase, followed by cleavage to the N-terminal side of the dibasic pair of residues by a Carboxypeptidase B-like activity, followed by amidation of the glycine-extended peptide by PAM.

With the knowledge that glyoxylic acid was a product of the amidation reaction (Bradbury 1987) and that amidation does not occur under anaerobic conditions, Bradbury et al. hypothesized that the amidation reaction involved the incorporation of a hydroxyl group into the glycine-extended precursor followed by a dealkylation to yield, in addition to free glyoxylate, the amidated peptide product. To that end, a series of glyoxylate phenylhydrazones, thiosemicarbazones, and semicarbazones were synthesized as potential substrates for the amidating enzyme. The interesting feature common to these molecules is the presence of an sp2 carbon atom bound to the carboxylate, rather than the

sp3 methylene carbon present in peptide substrates possessed of a C-terminal glycine residue. Assuming an enzyme mechanism involving substrate hydroxylation, the product of the reaction of glyoxylate phenylhydrazone and purified PAM was expected to be oxalate phenylhydrazide, and indeed this was the sole product of the reaction. This involved oxidation of the putative alcohol intermediate concomitant with reduction of the imine. Glyoxylate phenylhydrazone was found to inhibit the formation of D-YV-NH_2 with a K_I value of 15 μM (approximately equal in value to the K_M of the substrate used). At 0.1 mM, this compound was found to exhibit about 96% inhibition. Interestingly, the pyruvate phenylhydrazone derivative not only was not a substrate for PAM, but was also unable to inhibit the enzyme to any degree in the presence of known substrates. They also showed that [^{14}C]-glyoxylic acid was formed from D-Tyr-Val-[^{14}C]-Gly.

At about the same time, Tamburini et al. were conducting experiments regarding structural requirements for amidation substrates along the same lines as Bradbury (Tamburini 1990). They also found the C-terminal glycine residue was obligatory for activity, with all substitutions/additions for glycine at the C-terminus resulting in no product formation, amide or otherwise. Neither peptide amides corresponding to formerly glycine-extended peptides, nor C-terminal glycine methyl esters were PAM substrates, although they were weakly competitive inhibitors (15-30 fold decrease in binding affinity relative to C-terminal glycine substrates). Any additional C-terminal residues beyond Gly also abolished binding. Furthermore, P2 and P3 amino acid residues also heavily influenced the binding affinity of various glycine-terminal peptides. At the P2 position, the effect on binding affinity was found to correspond to: sulfur-containing > aromatic > histidine > nonpolar > polar > charged. Pentapeptides with the same C-

terminal sequence as a variety of prohormones exhibited very nearly the same binding affinity as the prohormones themselves. This indicated that the secondary and/or tertiary structure of larger prohormones does not influence substrate binding, for better or for worse. Replacement of the amide nitrogen with a methylene group (i.e. C-terminal β-alanine) abolished binding affinity, as does C-terminal sarcosine (i.e. C-terminal glycine with a pendant methyl group on the amide nitrogen). One final interesting finding in this study was the fact that although the PAM used was derived from AtT-20 thyroid carcinoma cells, the prohormones with the greatest binding affinity were Substance P-Gly and Neuropeptide Y-Gly, both peptides associated with the central nervous system rather than the thyroid gland. This indicated that PAM from different tissues have very similar affinities for a given substrate.

In 1988, this laboratory (Katopodis, 1988) developed a highly UV-active tripeptide PAM substrate (TNP-(D)-YVG) which greatly improved the ease of detection of the hydroxyglycine intermediate and amidated product by HPLC. Previously, radioiodinated tyrosyl substrates and fluorescent (dansyl) peptides were used to quantify PAM products, as the working substrate concentrations (c. 2-20 μM) without these modifications provided a UV response too low to detect by UV-Vis HPLC. Unlike D-YVG, the trinitrophenylated TNP-YVG substrate has no charge at the N-terminus. This lack of charge, and the inclusion of another large aromatic residue, resulted in a substrate with increased binding affinity (3 μM).

The most involved and detailed study of PAM (the bifunctional enzyme) substrates and inhibitors to date was undertaken by this laboratory in 1990 (Katopodis and May, 1990), when a variety of hippuric acid (i.e. N-benzoylglycine) analogs were developed,

including O-glycolate esters, S-glycolate ethers, N-glycolate amines, O-glycolate ethers, and benyoylacrylate (Figure 2). This was the first elucidation of a series of non-peptide substrates for the amidating enzyme and represented a conceptual breakthrough in the evaluation of its substrates and inhibitors. First, the kinetic parameters of hippuric acid, 4-nitrohippuric acid, and 4-methoxyhippuric acid were found to depend on the substitution (or lack thereof) at the para position. The best substrate was 4-nitrohippuric acid, with a K_M value of 1.0 mM and a V_{max} of 1370 nmol/mg/h. The nitrophenyl group is strongly electron-withdrawing. Hippuric acid itself had a slightly higher K_M (1.6 mM) and a greatly reduced V_{max} (493 nmol/mg/h). Inclusion of the electron-donating methoxy group resulted in a further decline in V_{max} (109 nmol/mg/h) while the K_M slightly increased to 1.7 mM. All were converted to the corresponding amide product. The 4-nitro ether (uncharged) analog was an especially good substrate, converted to the corresponding alcohol with K_M and V_{max} values of 0.16 mM and 1360 nmol/mg/h, respectively. The positively-charged 4-nitro secondary amine analog displayed a much poorer binding affinity (K_M = 1.7 mM) but a higher V_{max} value (2930 nmol/mg/h) and was converted to the dealkylated primary amine. Since we are dealing with the bifunctional enzyme, it is likely that the positive charge of the amino moiety impairs binding to PAM, but allows for more efficient dealkylation by PGL relative to the uncharged ether analog. When the corresponding 4-methoxy O-glycolate ester was incubated with the bifunctional enzyme, no dealkylation product (i.e. 4-methoxybenzoic acid) was detected. However, this compound was a weak competitive inhibitor (K_I = 0.48 mM). The 4-nitro S-glycylthioether was also a very good substrate (K_M = 0.34 mM, V_{max} = 2310 nmol/mg/h), but yielded the corresponding sulfoxide rather than the

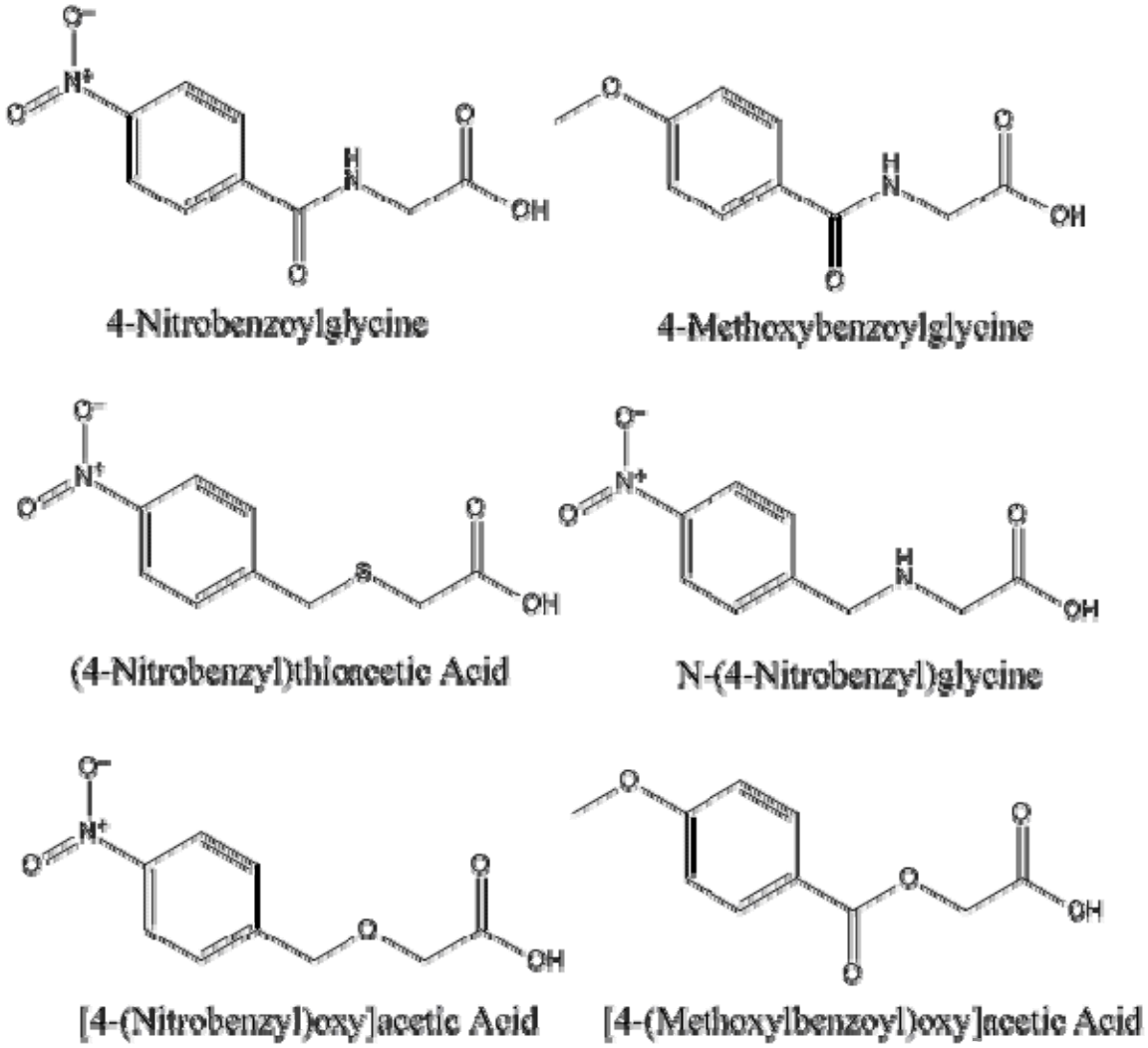

Figure 2. Structures of hippuric acid analogs. All are PAM substrates, except for the ester which is a competitive inhibitor. The thioether yields the corresponding sulfoxide product.

expected sulfhydryl dealkylation product. This is likely exclusively a rearrangement product of the PAM reaction (presumably forming the α-hydroxy product initially), without any subsequent PGL catalysis.

Trans-benzoylacrylic acid was found, like 4-phenyl-3-butenoic acid (PBA), to be a mechanism-based inactivator of the amidation reaction (K_I = 0.16 mM, k_{inact} = 3.6 min^{-1}). It is certainly interesting that both 2- and 3-alkenyl carboxylic acids are able to serve as mechanism-based inactivators of the amidation reaction, since the former lacks the requisite sp3-hybridized methylene group adjacent to the carboxylic acid requisite for substrate hydroxylation. Noteworthy was the lack or any epoxide or diol product following the incubation of trans-benzoylacrylate with PAM. Moreover, incubation with the corresponding epoxide failed to inactivate the enzyme, suggesting another pathway of inactivation. Monoethyl fumarate was also found to weakly inactivate the enzyme, indicating that the phenyl ring of trans-benzoylacrylate is not obligatory for inactivation. Also notable for failure to inactivate PAM was CBZ-dehydroalanine, which contains a terminal alkene functionality at the α-carbon, rather than an internal alkene. The consequences of these findings will be developed more exhaustively in the Discussion section of this thesis when comparisons to the second-generation peptidyl-acrylates (e.g. N-Ac-(L)-Phe-acrylate, N-Ac-(D)-Phe-acrylate, and N-Ac-(L)-Met-acrylate) are investigated.

In 1992 and 1993, this laboratory fully elucidated the stereochemistry (reaction and subsite) of the PAM and PGL reactions (Ping, 1992; Ping, 1995). Incubation of TNP-(D)-Tyr-(L)-Val-NH_2 with glyoxylic acid monohydrate under reflux resulted in the formation of two TNP-YV(OH)G diastereomers (RP-HPLC). Incubation of TNP-YVG

with PAM resulted in the formation of a single hydroxyglycine intermediate which coeluted with the later-eluting synthetic hydroxyglycine, indicating that the PAM reaction is stereospecific. Incubation of both synthetic hydroxyglycine diastereomers with PGL resulted in the decrease of only the later-eluting peak. This proved that PAM catalyzes the production of only one of the two possible hydroxyglycine diastereomers of TNP-YV(OH)G, and that PGL stereospecifically catalyzes the N-dealkylation of the PAM product only. Further experiments with PGL and Acylase I (i.e. N-acyl-(L)-amino acid amidohydrolase, E.C.3.5.1.14) using racemic N-cinnamoyl-α-hydroxy-Gly showed that both enzymes reacted with the same enantiomer (reaction with PGL yields cinnamide, reaction with Acylase I yields cinnamic acid). Since it is known that (S)-cinnamoyl-α-hydroxy-Gly is stereotopically equivalent to an N-acyl-(L)-amino acid, it was concluded that PGL reacts only with (S)-α-hydroxyglycines. Therefore the PAM reaction itself yields (S)-α-hydroxyglycines exclusively.

Although peptides and peptide analogs with (D)-amino acids in the P2 position had previously been shown to be poor PAM substrates in the past (Bradbury 1982, Bradbury 1983), these studies were carried out without the knowledge that the process of peptide amidation actually was the product of two separate and distinct catalytic functionalities. As mentioned previously, this discovery obviously cast a new light upon many of the kinetic parameters and binding constants for various substrates and inhibitors which had been evaluated (unknowingly) in the presence of both enzymes. When assaying a potential inhibitor, for instance, for its efficacy in impeding the amidation process when both PAM and PGL are present, it is impossible to determine to what degree a given compound inhibits one enzyme or the other, especially when only the final amide product

is assayed, and not both the amide and hydroxyglycine intermediate. Thus, although it was known that certain molecular functionalities and spatial orientations did indeed inhibit overall amidation, it remained to be seen exactly which of these properties was effective in inhibiting PAM vs. PGL. Thus, this laboratory set out to determine to what extent the stereochemical properties of various substrates and inhibitors affected PAM and PGL catalysis on an individual basis.

To this end, a variety of derivatives with varying stereochemistry at the P2 position were evaluated. Incubation of purified PAM with N-Ac-(L)-Phe-Gly and N-Ac-(D)-Phe-Gly resulted in stark differences in product formation. The former was about as effective a substrate, with respect to kinetic parameters, as TNP-YVG, and underwent 100% conversion to the hydroxyglycine intermediate. The (D)-enantiomer, on the other hand, evinced only about an initial 0.5% conversion which did not increase after extended incubation times. This product coeluted with the (L)-Phe-(S)-hydroxy-Gly seen from the (L)-Phe-Gly incubation (recall that diastereomeric hydroxyglycines were resolved previously by RP-HPLC) and was therefore either, firstly, (L)-Phe-(S)-hydroxy-Gly resulting from a slight enantiomeric impurity in the (D)-Phe-Gly preparation, or secondly, (D)-Phe-(R)-hydroxy-Gly (which, as an enantiomer of (L)-Phe-(S)-hydroxy-Gly would indeed coelute with that compound). The failure of extended incubations to increase the size of the product peak after the initial 0.5% conversion argues for the presence of a very slight enantiomeric impurity in the (D)-Phe-Gly preparation. Interestingly, not only was the (D)-Phe-Gly not a PAM substrate but was also an exceedingly poor competitive inhibitor (K_I = 1.3 mM) of PAM, indicating that its spatial configuration precludes not only catalysis, but effective binding in the active site. By

comparison, the apparent K_I of N-Ac-(L)-Phe-Gly in the presence of TNP-YVG substrate was found to be 2.0 μM, nearly 3 orders of magnitude less than the (D)-enantiomer. Similar trends were seen with the enantiomeric pair (S)-O-Ac-mandelyl-Gly and (R)-O-Ac-mandelyl-Gly (O-acetylated-α-hydroxybenzeneacetic acids) and the diastereomeric pair N-Ac-(L)-Phe-(L)-Phe-Gly and N-Ac-(L)-Phe-(D)-Phe-Gly. These results plainly indicated the stringent subsite stereospecificity of PAM with respect to its substrates. The same subsite specificity was evident with N-Ac-Phe-O-glycolate enantiomers, and although neither underwent PAM catalysis the (L)-enantiomer was found to be a potent competitive inhibitor (K_I = 45.2 μM) whereas the (D)-enantiomer was very ineffective (K_I = 2.25 mM). PGL was found to exhibit very low subsite specificity, converting (S)-hydroxyglycines to the amide in a nondiscriminant manner regardless of the stereochemistry at the P2 position.

Another important advance in the study of peptide amidation were the crystal structures of oxidized PAM, ascorbate-soaked reduced PAM, and oxidized PAM with bound substrate in the active site (Prigge, 1997). Obviously, the solving of the crystal structures is an extremely important step in the ability to design, tailor, and refine effective enzyme inhibitors. PAM (Figure 3) was found to be a prolate ellipsoid, with dimensions of approximately 55 X 45 X 25 Å. Two domains are associated through an extensive hydrophobic interface in an overall horseshoe-shaped structure, with the rest of the interface separated by a broad solvent accessible cleft approximately 8 Å in width. Two copper ions (Cu_A and Cu_B, also Cu_H and Cu_M, respectively), separated across the solvent-accessible cleft by approximately 11 Å, are each ligated by three amino acid residues (Cu_A by three Histidines and Cu_B by two Histidines and one Methionine). The

Figure 3. Cartoon of the X-ray crystal structure of oxidized PAM (PDB ID: 1OPM). Bound copper ions represented as green spheres, one on each side of the solvent-accessible cleft. Substrate binds above Cu_B. The copper ions are 11 Å distant from each other. Reproduced from Prigge et al., 1997.

substrate (diiodo-Tyr-Gly) binds at the top of the cleft, offset to one side so as to place the reactive pro-(S) glycyl hydrogen in close proximity to Cu_B. The carboxylate of the substrate is anchored by a bidentate salt-bridge to the guanidinium group of R240, also forming a hydrogen bond with the phenolic hydrogen of Y318. The main chain amide of the peptide bond forms another hydrogen bond with the amide side chain of N316. The aromatic ring projects upwards into a large hydrophobic pocket bordered by a variety of Ile, Phe, Tyr, and Met residues. Other van der Waals' contacts are formed with M314, which is ligated to Cu_B. Neither the oxidation state of the copper ions or the binding of substrate appears to significantly influence the structure of the active site of the enzyme (R.M.S. of 0.3 Å for the protein α-carbons). The only noticeable change upon substrate binding is the loss of a hydrogen bond between Y318 and N316, with the latter instead forming a hydrogen bond with the substrate as mentioned previously. The formation of the salt-bridge between the substrate carboxylate and the guanidinium of R240 helps to explain the poor binding of C-terminal amide and ester-derivatives of known substrates. The formation of the α-hydroxyglycine intermediate requires an overall two-electron reduction of molecular oxygen, one electron each donated from Cu_A and Cu_B, so the most obvious question which arises from the crystal structure is the mechanism by which an electron is transferred from Cu_A (11 Å distant) to the ROS at Cu_B. The mechanism of the PAM reaction will be discussed in far more detail below.

Subsequently, Prigge et al. (Prigge, 2004) were able to crystallize reduced PAM with both substrate and molecular oxygen bound to the active site of the enzyme. In this case, since the enzyme is catalytically competent in the presence of reduced copper and molecular oxygen, it was necessary to find a substrate with an appropriate pro-(S)

hydrogen (to illustrate the proximity of said hydrogen to molecular oxygen) which either failed to undergo catalytic turnover or was an exceedingly slow substrate on the time-scale of the crystallization experiments. To this end, the "substrate" diiodo-Tyr-(D)-Thr was cocrystallized with reduced PAM under aerobic conditions, and again with oxidized PAM. In both cases the substrate docked in essentially the same position relative to the active site residues, but molecular oxygen bound only in an "end-on" manner to Cu_B in the case of reduced, catalytically competent PAM. All other interactions of the substrate and enzyme were the same as described for the case of diiodo-Tyr-Gly above, with the sole exception that an additional hydrogen bond was formed between the hydroxyl group of the threonine side chain and Y318. The Cu_B-O-O bond angle was found to be approximately 110°, and the O-O bond length 1.23 Å. This bond length is indicative of dioxygen either in the dioxygen or superoxo (reduced by one electron) form, but not in the peroxo (reduced by two electrons) form. The latter would also present a Cu_B-O-O bond angle closer to 90°. It is likely, however, based on mechanistic evidence to be presented later, that the O_2 is found in the unreduced dioxygen form in the case of this poor substrate. The two oxygens are within 4.13 and 4.73 Å of the glycyl C_α, and predicted to be within 3.16 Å of the pro-(S) glycyl hydrogen (which cannot be explicitly seen in the crystal structure), an appropriate distance for abstraction of this hydrogen atom from the substrate. The authors propose that, ultimately, an electron is transferred from Cu_A to Cu_B-O_2 via H108 (a Cu_A ligand), a solvent water, and the substrate carboxylate moiety. This is the "substrate-mediated electron-transfer pathway" mechanistic hypothesis. Again, oxygen only binds under aerobic conditions in the presence of substrate and an appropriate copper-reducing agent (e.g., ascorbate).

In recent years, a spate of research has shown that PAM is capable of hydroxylating (and PGL dealkylating) many physiological non-peptide substrates which are either possessed of a CH_2-COOH moiety, or glycine-extended in their own right. These include various N-acylglycines such as N-myristoylglycine (Merkler, 1996) and N-lauroylglycine (Wilcox, 1999). Indeed, physiologically, a variety of carboxylic acids are conjugated to glycine via the enzyme Acyl-CoA: Glycine N-Acyltransferase (E.C.2.3.1.13), including nicotinic acid. The glycine-extended conjugate is a PAM substrate which is converted to nicotinamide (vitamin B3) by the tandem activities of PAM and PGL (Merkler, 1999). Aspirin (acetylsalicylic acid) is perhaps the most widely used pharmaceutical product in existence. *In vivo,* aspirin is initially hydrolyzed to salicylic acid and then further metabolized by glycine conjugation in the liver to salicyluric acid (which is then maintained at nearly constant concentrations in the bloodstream for extended periods of time. DeBlassio et al. found that salicyluric acid and gentisuric acid (ring-hydroxylated salicyluric acid) are converted to the corresponding amides by PAM and PGL activities (DeBlassio, 2000). Whether or not these amides have any significant biological activity remains to be determined, but it is possible that concentrations of these compounds in the bloodstream is high enough to inhibit serum PAM (with respect to other substrates) following common aspirin dosages. Also, glycine-conjugated bile acids, which are released into the bloodstream under pathological conditions in the liver, have been found to be PAM substrates. (Merkler, 1988)

Further work by Merkler et al. (Merkler, 2003) found that glutathione, S-substituted glutathiones, and leukotriene C_4 (a pro-inflammatory mediator conjugated to glutathione) were all PAM substrates on a par with various tripeptide substrates as regards V/K_{app}

values. All were found to proceed via the corresponding α-hydroxyglycine intermediate, with glyoxylate production lagging until the amide is formed (ultimately 1:1 ratio amide/glyoxylate). Interestingly, amidated glutathione is an exceedingly poor substrate for the enzyme glutathione-S-transferase (E.C.2.5.1.18), an enzyme involved in the detoxification of peroxidized lipids and various xenobiotics via conjugation with reduced glutathione. Amidated glutathione, being a poor substrate for glutathione-S-transferase, is effectively rendered physiologically useless in this regard, although it may have various potentially unknown physiological functions. Glutathione and PAM are known to be colocalized in a variety of tissues, such as the anterior pituitary, hypothalamus, choroid plexus, heart atrium, secretory vesicles of small-cell lung carcinoma cells, cerebrospinal fluid, and the bloodstream. The C-class leukotrienes, conjugated to glutathione, are the so-called "slow-reacting substance of anaphylaxis". It is unknown whether amidation of the attached glutathione either inhibits or exacerbates these adverse effects. Finally, the protein ubiquitin, when conjugated to peptides/proteins, targets them for destruction by the proteasome. Ubiquitin terminates in the sequence Gly-Gly and is therefore a candidate for amidation by PAM. Chew et al. (Chew 2005) found that ubiquitin is indeed a PAM substrate (K_M = 600 μM vs. 220 μM for D-YVG in their hands) and that amidation of ubiquitin (i.e. to ubiquitin 1-75-NH_2) eliminates its ability to label peptides and proteins for subsequent proteasome degradation.

As the recent work with various substrates has shown, although PAM has a strict requirement for a carboxylate functionality and an α-methylene (or methine, if the hydrogen is pro-(S) and the other hydrogen has been replaced with a small group such as methyl or hydroxymethyl) group in order for catalysis to proceed, the enzyme is fairly

indiscriminant beyond these minimal requirements. Of course, molecules with inappropriate stereochemistry in a position analogous to the P2 residue in peptidyl substrates are exceedingly poor substrates, but a wide variety of fatty acids and N-acylglycines have been shown to be substrates for amidation. A variety of competitive inhibitors have been identified, including O-glycolate esters (Ping 1995), C-terminal homocysteines, and the glycine-terminal dipeptide analogs thiorphan and tiopronin. The sulfur-containing compounds appear to interact strongly with $Cu_{B,}$ with the homocysteines possessed of a sulfhydrylethyl group which is stereotopically equivalent to the reactive pro-(S) hydrogen of glycine-extended peptides. Other copper-chelating compounds, such as disulfiram and diethylthiocarbonate, have been shown to inhibit the amidation reaction in cultured cells, but these presumably do not affect the enzyme directly as exogenous copper is able to overcome these inhibitory effects. Also, dietary copper deficiency, like dietary ascorbate deficiency, results in a net decrease in amidation, with the PAM in the brain less affected than PAM in the periphery, possibly due to some sort of "copper-hoarding" mechanism by the applicable brain cells. (Mains, 1986; Mueller, 1993; Mueller, 1995) N-Ac-(L)-Phe-Pyruvate and other pyruvate-extended amino acids, developed by this laboratory, are the only known noncompetitive inhibitors of PAM, competing instead with ascorbate at the site of copper reduction. The most interesting compounds, from both a chemical and pharmacological viewpoint, are the competitive mechanism based inactivators. These include two classes of compounds: first, the commercially available 4-phenyl-3-butenoic acid (PBA) and any related 3-enoic acids; and secondly, the 2-enoic peptide acrylate class of compounds developed by this laboratory (e.g., N-Ac-Phe-Acrylate, N-Ac-Met-Acrylate, and N-Ac-2'-Thienyl-

Acrylate). Finally, unsaturated thioacetic acid derivatives, such as *trans*-styrylthioacetic acid (K_I = 0.1 mM, k_{inact} = 0.2 min^{-1}), were found to be reasonably effective with regards to PAM inactivation (Casara, 1996). These compounds, although they contain a main-chain sulfur atom, are structurally and electronically equivalent to 4-alkenyl carboxylic acids. Only the *trans* isomer was found to be capable of enzyme inactivation.

The 3-enoic acid PBA (4-phenyl-3-butenoic acid), along with its potent PAM inactivation properties, satisfies the basic structural requirements (R-CH_2-COOH) for a PAM substrate and has a pro-(S) methylene hydrogen available for extraction by the ROS generated at Cu_B. Although PBA has been studied and utilized as a PAM inactivator *in vivo*, *in vitro,* and *ex vivo* for many years as described previously, its powerful inactivation properties, coupled with a rather meager UV-Vis activity, made it difficult to generate enough products from PBA (in the absence of huge quantities of purified PAM) to be readily analyzed by HPLC. To this end, Driscoll et al. utilized PBA radiolabeled by tritium exchange as a PAM substrate/inactivator and found that two hydroxylated products were formed: 2-hydroxy-4-phenyl-3-butenoic acid and 4-hydroxy-4-phenyl-2-butenoic acid (Driscoll, 2000). Pulse-chase experiments indicated that both were direct products of PAM catalysis, and not formed one from the other in solution. Additionally, product formation was stereoselective rather than stereospecific (strictly stereospecific with regard to peptide substrates) with the (R)-stereoisomer formed preferentially at a ratio of 70:30 for the 2-hydroxy product and spatially the same as (S)-hydroxyglycines derived exclusively from peptide substrates. For the 4-hydroxy product, no absolute configuration was derived, but one stereoisomer was formed over the other at a ratio of 80:20. Interestingly, neither of the two products was able to inactivate the enzyme,

which was unexpected owing to the structural similarity of both to known inactivators, the 4-hydroxy product to 2-enoic inactivating compounds, and the 2-hydroxy product to PBA itself. Clearly, since both (R) and (S)-stereoisomers of the 2-hydroxy are formed, and because peptides terminating in (D)-alanine are, albeit very poor, PAM substrates, one of the isomeric products would necessarily possess a pro-(S) hydrogen and therefore inactivate the enzyme. The fact that they do not suggests, therefore, a mechanistic or electronic, rather than structural, impediment to inactivation by this species (especially the 4-hydroxy product). The partition ratio was found to be approximately ninety (90 pmol product produced/pmol PAM inactivated). The high partition ratio, coupled with the knowledge that both 2-hydroxy and 4-hydroxy products are formed rather than exclusively, as would be expected, the 2-hydroxy product, indicates that PBA, following hydrogen atom abstraction, binds less tightly to the active site than does PBA itself. Therefore, it is possible that a PBA radical may, one time out of ninety, escape the active site and leave an activated ROS bound to Cu_B which may lead to a reaction with an active site residue (possibly Y318) which permanently inactivates the enzyme. The fact that PBA lacks a hydrogen-bond donor (no amide functionality) obviates the possibility of a hydrogen bond forming with N316 (as it does with peptide substrates) and may contribute to a "loose" binding in the active site, explaining the existence of both 2-hydroxy and 4-hydroxy products, as well as enzyme inactivation. Finally, no ^{3}H radioactivity was seen to coelute with inactive PAM. Therefore, no covalent adduct is formed during the inactivation of PAM by PBA. This finding contradicts the results of Bradbury's work with ^{14}C-labeled PBA which showed by HPLC that radioactivity coeluted with the inactivated enzyme.

The peptidylacrylate class of compounds developed by this laboratory in the 1990s (Feng, 2000) remain the most potent mechanism-based PAM inactivators known today. Based on the idea that a transient cationic radical intermediate may form during the course of PAM catalysis, it was posited that a 2-alkenyl group would stabilize and trap the nascent radical such that further chemistry may occur with active site residues resulting in the irreversible inactivation of the enzyme. Moreover, structural similarity to peptide substrates with relatively higher binding affinities was expected to yield more potent inactivation properties. NMR analysis of the acrylates indicates that they exist entirely in the *trans* configuration when synthesized by our protocol. The molecule N-Ac-Phe-acrylate is essentially a rational modification of N-Ac-(L)-Phe-Gly, one of the most efficient dipeptide PAM substrates, where the main-chain -N-C_α- group of the glycine residue is replaced by a –C=C- functionality. Essentially, this change creates an α-β-unsaturated ketoacid. Feng et al. found that N-Ac-(L)-Phe-acrylate was a cofactor-dependent, time-based irreversible competitive inhibitor of PAM ($K_I = 95 \pm 12$ μM, $k_{inact} = 1.1 \pm 0.2$ min^{-1}, $k_{inact}/K_I = 12, 000$ M^{-1} min^{-1}).

Also, with a view to optimizing active-site binding via ligation with the active-site Cu_B ion, N-Ac-Phe-acrylate was further modified by the replacement of the phenyl group with a 2'-thienyl group to yield N-Ac-2'-thienyl-acrylate (4-oxo-5-acetamido-6-(2-thineyl)-hex-2-enoic acid). The thienyl ring is a five-membered sulfur-containing aromatic ring, similar in size to a phenyl group, and is electron-rich relative to benzene by virtue of possessing a complement of 6 e^- distributed over a 5-membered, rather than 6-membered, ring. Thiophene is a well-known and potent ligator of copper ions. Indeed, N-Ac-(L)Thienyl-acrylate was found to be an even more potent inactivator than the

corresponding phenylalanine derivative (K_I = 31.9 ± 0.2 μM, k_{inact} = 0.56 ± 0.1 min^{-1}, k_{inact}/K_I = 17,600 M^{-1} min^{-1}). Interestingly, however, although the binding of the thienyl derivative was approximately 3-fold more potent than the phenylalanyl derivative, its rate constant of inactivation dropped by about one-half. An appeal to Prigge's crystal structure provides some explanation for this divergence of potency relative to the individual kinetic parameters of the thienyl derivative. The tyrosine of IYG bound to oxidized PAM in the crystal structure is oriented upwards into the large hydrophobic pocket of the PAM active site, whereas Cu_B (to which the thiophene ring could presumably ligate) lies in the opposite direction. It is not possible for the thiophene ring to interact with both Cu_B *and* the hydrophobic residues of the active site. Presumably, the difference in binding energy *vis-a-vis* the hydrophobic pocket between thiophenyl and phenyl rings should be negligible, when size and hydrophobicity of the rings are taken into account. This leads to the assumption that the thiophene ring does indeed interact directly with Cu_B, and if this is the case it explains both the increase in binding affinity and the decrease in the rate of inactivation. The latter is decreased because the ligation of the inhibitor to the active-site copper would be expected to interfere with the actual electron-transfer catalysis by either displacing one of the copper ligands (M318, H108, or H109) or by occupying the fourth position which is normally taken by molecular oxygen. It would not be surprising that this would result in a less efficient mechanistic inactivation than that seen with the phenylalanyl derivative where the active-site copper is expected to be unmolested.

As this laboratory had illustrated the stereochemical requirements of peptidyl PAM substrates and competitive inhibitors in the past, it was important to establish whether the

same requirements extended to our acrylate inactivators. Racemic N-Ac-Thienyl-acrylate was also synthesized, with both kinetic parameters moving in an unfavorable direction with regard to the pure (L)-enantiomer (racemate: $K_I = 60.5 \pm 0.3$ μM, $k_{inact} = 0.40 \pm 0.01$ min^{-1}). Extrapolation of this result, as regards binding of the (D)-enantiomer, indicates that, theoretically, this compound would have a binding constant at least one order of magnitude greater than that of the pure (L)-enantiomer. Since the acrylate inactivators do not possess a glycyl sp3 hydrogen (as do C-terminal glycine substrates or the inactivator PBA) near the carboxy terminus, but instead an alkenyl sp2-hybridized hydrogen atom, it is worth mentioning that the mechanism of inactivation of PAM by these compounds likely proceeds through a mechanistic pathway entirely different than the hydroxylation of PBA or peptide substrates. All relevant structures are provided in Figure 4.

PAM Mechanism

Although the mechanism of the PAM reaction is academically interesting for a variety of a reasons, not least of which is the question of the mechanism of long-distance electron-transfer from the two copper ions to molecular oxygen and substrate, it remains rather tangential to our investigations here and therefore will not be discussed as exhaustively as the substrates, inhibitors, and inactivators mentioned above. Nevertheless, a brief recapitulation of which mechanistic aspects of the PAM monooxygenase reaction are known, and unknown, will be instructive to our discussion. Following years of mutagenesis studies, kinetic-isotope investigations, EPR spectroscopy, extended x-ray-absorption fine structure, X-ray crystallography, and the

evaluation of a vast array of different substrates, inhibitors, and inactivators, there is still no absolute consensus on the entirety of the PAM reaction mechanism. A feasible and complete mechanistic evaluation of the PAM reaction is complicated by the multistep nature of the catalysis, which includes copper binding, ascorbate binding and reduction of the active site coppers, peptide substrate binding, binding of molecular oxygen, two distinct electron transfers, reduction of molecular oxygen, hydrogen atom abstraction from substrate, hydroxylation of substrate, and product release. Much is known regarding the steps prior to electron-transfer, and there is a fairly established consensus as to the order of binding of substrates and cofactors. The difficulty lies largely in the electron-transfer steps, the nature of the activated reduced molecular oxygen species present at $Cu_{B,}$ and the nature of the species responsible both for hydrogen atom abstraction from the substrate and the subsequent hydroxylation. Molecular oxygen is reduced to superoxide, a radical anion, following a one-electron reduction. Superoxide, a relatively weak nucleophile, may either be protonated (acting as a base), or may undergo a subsequent one-electron reduction to the peroxy dianion which may exist in the singly protonated form (hydroperoxy anion) when ligated to Cu^{+1}. It is unknown which of these species is responsible for hydrogen atom abstraction and the subsequent hydroxylation.

Prior to 1992, owing to its extensive sequence homology to the copper- and ascorbate- and molecular oxygen-dependent monooxygenase dopamine-β-hydroxylase (DβM E.C.1.14.17.1), the PAM mechanism was largely taken for granted to be very similar to that of DβM. Although there are structural differences in the natural substrates (PAM hydroxylates the α-carbon of carboxylic acids whereas DβM hydroxylates the β-carbon of a primary amine), the identical cofactor requirements and sequence homology

(identical for the residues which ligate the two copper ions in each enzyme) argued strongly for both enzymes having very similar, if not necessarily identical, mechanisms. The first proof that PAM was itself a monooxygenase (i.e. one oxygen atom is incorporated into the substrate and the other is reduced to water) came in 1992 when Merkler et al. (Merkler, 1992) investigated the ^{18}O isotopic ^{13}C NMR shift of the product of the PAM reaction in the presence of isotopically labeled molecular oxygen or water. This isotopic shift in the product was only seen in the presence of $^{18}O_2$, and not in the presence of $H_2{}^{18}O$. The authors also showed that a 1:1 stoichiometry exists between all of the following pairs: glyoxylate formed/dansyl-YVG consumed, pyruvate formed/dansyl-Tyr-Val-(D)-Ala consumed, dansyl-YV-NH_2 formed/ascorbate oxidized, and dansyl-YV-NH_2 formed/O_2 consumed. The authors showed, via the use of the enzyme semidehydroascorbate reductase (SDR, E.C.1.14.17.11), that each ascorbate which participates in the PAM reaction is oxidized to semidehydroascorbate (which is reduced back to ascorbate by SDR). Any dehydroascorbate present in the final reaction mixture results from disproportionation of semidehydroascorbate. Therefore, each molecule of ascorbate reduces only one equivalent of enzyme-bound Cu(II).

Once the two copper centers of PAM have been individually reduced by two molecules of ascorbate, the enzyme becomes catalytically competent. At this point, the two substrates (O_2 and peptidyl substrate) must associate prior to substrate hydroxylation. With hippuric acid (K_M = 1.6 mM) as the substrate, an equilibrium-ordered mechanism predominates, indicating that the dissociation rate of the E-S complex is much faster than binding of molecular oxygen to the E-S complex. For substrates with higher binding affinities (lower K_M values), the addition of the two substrates becomes steady-state

ordered, where the E-S complex forms rapidly upon addition of substrate and molecular oxygen then binds to the E-S complex. In this case, the dissociation rate of the E-S complex is much slower than the association rate of molecular oxygen with the E-S complex (Francisco, 1998). In any event, O_2 does not bind to free enzyme to from an E-O_2 complex. Therefore, no reactive (reduced) oxygen species can be formed in the absence of substrate.

Further, it was shown that dideuteration of hippuric acid at the α-carbon resulted in significant primary and α-secondary deuterium isotope effects. The primary deuterium isotope effect (k_H/k_D) was found to be 10.9 ± 1.9, an extremely large value that fairly proved that C-H bond cleavage is the first irreversible step in the PAM reaction. The α-secondary deuterium isotope effect was found to be 1.17 ± 0.03. This bond (nor this deuterium) is directly involved in the PAM reaction. A value of 1.2 for the α-secondary deuterium isotope effect is indicative of an impediment (caused by the heavier D atom) in the rearrangement of an sp^3 to an sp^2 center. While a nascent sp^2 center in this case could indicate either the development of a neutral radical or cationic carbon species, it necessarily rules out the possibility of a carbanion intermediate (which would retain an sp^3 configuration). However, the development of a carbon-centered radical cation would involve a hydride migration from the peptidyl substrate to molecular oxygen, which would be without precedent as pertains to copper/oxygen chemistry. Also, if tunneling indeed contributes to the C-H bond cleavage step a hydride transfer is all the more unlikely as it requires the tunneling of two electrons and one proton, rather than simply the one electron and one proton of a hydrogen atom. All available evidence points the C-H bond cleavage step as involving the transfer of a hydrogen atom, with the resultant

formation of an uncharged carbon-centered glycyl substrate radical. The bond-dissociation energy for a glycyl C-H bond is approximately 87 kcal/mol. This mechanism is supported by a wealth of literature which establishes the relative ease of formation and stability of carbon-centered glycine radicals. (Barratt 2004) These results do not, of course, establish the nature of the reactive oxygen species which drives H-atom abstraction.

The question of the mechanism of electron-transfer from Cu_H to Cu_M and the nature of the ROS which activates the peptide substrate are perhaps the most difficult to answer with any degree of confidence. At which point the electron-transfer occurs will likely be instructive as to the nature of the ROS, independent of the mechanism of transfer. If the second electron transfer (Cu_H to Cu_M) occurs subsequent to substrate hydroxylation, for instance, then the reactive oxygen species at Cu_M responsible for hydrogen-atom abstraction can be only Cu(I)-superoxide. If, instead, both reducing equivalents are present at Cu_M prior to hydrogen-atom abstraction, then the reactive oxygen species may be Cu(I)-superoxide, Cu(II)-hydroperoxide, or Cu(II)-peroxide (depending on protonation of the ROS, in the latter two cases).

Based upon models of CO reactivity with PAM copper centers (Jaron, 1999), it was proposed that the reducing equivalent from Cu_H is transferred via an "assisted superoxide-channeling mechanism." Under anaerobic conditions, the stoichiometry of CO-binding per copper was found to be 1:2 in wild-type PAM, with CO binding exclusively to Cu_M (based on IR spectroscopy). Substrate-binding then provided a second site for CO binding, presumably at Cu_H. Naturally, the PAM mechanism does not necessarily require the presence of a second molecule of dioxygen (assuming that

dioxygen binds if CO binds) at Cu_H. The appearance of this second CO binding site upon substrate-binding led the authors to propose that a superoxide is formed at both Cu_M and Cu_H, with the latter then migrating, with the assistance of the active site residue Y79, toward the superoxide at Cu_M, at which point the two superoxides undergo dismutation, yielding either a Cu_M(II)-peroxo or Cu_M(I)-superoxo species and regenerating one dioxygen molecule (fitting with the earlier finding that molecular oxygen and substrate are consumed at a 1:1 ratio).

Subsequent studies (Francisco, 2003), however, using both $^{18}O_2$ and substrate deuterated at the glycyl pro-(S) hydrogen, showed a dependence of the oxygen isotope effects upon the deuteration (or lack thereof) of the substrate, indicating that ALL oxygen activation steps are reversible prior to the first irreversible catalytic step of hydrogen-atom abstraction. Certainly, the reversibility of a superoxide-channeling mechanism is not feasible. Once the reducing equivalent (superoxide) has been decoupled from Cu_H and transferred across the solvent-accessible cleft of the active site, it is quite unlikely that it could then return to Cu_H, reoxidize Cu(I) to Cu(II) and be released as molecular oxygen again. Even if this reversibility were indeed possible in principle, it does not seem possible that the long distance transfer of this ROS (and subsequent return to Cu_H) could possible proceed with 100% efficiency. In other words, the superoxide assisted-channeling mechanism would require at least some decoupling of product formation and oxygen consumption. By analogy with DβM, the only other known enzyme to exhibit an $^{18}O_2$ KIE dependent on substrate deuteration, there can be no decoupling of oxygen consumption from product formation/substrate depletion. (Evans, 2003) Using a non-DβM-substrate (β,β-difluorophenethylamine) structurally equivalent to the substrate

phenethylamine, but with a non-labile fluorine in place of the hydrogen atom of the substrate, and operating at concentrations three times the K_I value for the substrate analog, there was no evidence that the ratio of dioxygen consumption/product formation departed from unity. Comparison of three other "fast" substrates (dopamine, tyramine, and phenethylamine) to the very slow *p*-trifluorophenethylamine (k_{cat}/K_M three orders of magnitude smaller than any of the "fast" substrates) also failed to indicate any departure of this ratio from unity. Logically, the poorer a substrate, the more likely that activated oxygen species can escape from the active site after they are generated (whether reversibly or irreversibly), owing to the correspondingly much decreased rate of the irreversible step of hydrogen-atom abstraction. The fact that this is not the case is probably the best argument against the superoxide assisted-channeling mechanism, which is ripe with opportunity for the escape of ROS generated at Cu_H. Moreover, if any of the oxygen activations steps were irreversible, the $^{18}O_2$ isotope effect would not be dependent on substrate deuteration.

In light of the above, a long-range electron-transfer step occurring subsequent to the hydroxylation of substrate remains possible. Under this assumption, oxygen activation would remain reversible (consistent with the $^{18}O_2/^2H$ data) and hydrogen atom abstraction from substrate would remain the first irreversible step. Simply, dioxygen at Cu_M would be initially reduced to superoxide. Superoxide would abstract a hydrogen atom from the substrate, yielding a hydroperoxide anion. Substrate would then be hydroxylated by the hydroperoxide species, leaving a Cu(II)-O^{1-} radical, or its protonated form. Then, with product formation already completed, a second electron would be transferred (although not by the now unlikely superoxide assisted-channeling mechanism) from Cu_H to the

oxygen species at Cu_M, reducing it further to $Cu_M(II)$-O^{2-}. Following protonation, the product and one molecule of water would then be released, or, alternatively, hydroxide ion could remain ligated to $Cu_M(II)$, as seen in the crystal structure of oxidized PAM (Prigge, 1998). This mechanism is supported by *in silico* modeling studies by Chen and Solomon (Chen, 2004) which suggests that long-range electron-transfer would be driven more effectively by the reduction potential of the deprotonated hydroxyl radical at Cu_M (c. 2.18 V) than by either superoxide (0.94 V) or hydroperoxide (0.46 V). Although this is instructive with regard to reduction potentials, their mechanism assumed an initial "side-on" binding of dioxygen to Cu_M, with a subsequent ligation of a solvent water displacing one oxygen of the side-on-bound ROS to yield an "end-on" bound protonated superoxide. However, a crystal structure of reduced PAM with bound substrate and molecular oxygen revealed that dioxygen initially binds to the E-S complex in an "end-on" orientation (Prigge, 2004). Nevertheless, this late electron-transfer step remains feasible.

Regardless of the timing of the second electron-transfer event, and to the nature of the ROS to which it is transferred, a reversible superoxide migration seems exceedingly unlikely. It is possible, although improbable, that a solvated electron could migrate across a 7 to 8 Angstrom-wide solvent-filled cleft. Moreover, if the electron-transfer from Cu_H to Cu_M occurs prior to or concomitant with oxygen activation (which is reversible), this would imply that the solvated electron-transfer is also reversible. This too is very unlikely. The most reasonable explanation seems to be a substrate-assisted electron-transfer step, either through the substrate itself via the salt-bridge with Arg240, or possibly through a bridging water molecule hydrogen-bonded to the substrate carboxy

group and to Gln170 and H108 (a Cu_H ligand). This last case is supported by *in silico* electron-transfer dynamics simulations (de la Lande, 2007) of the active site with this bridging water molecule, also present in the PAM crystal structure. Moreover, to prevent the leakage of reducing equivalents from the system, in conjunction with the fact that oxygen is not activated in the absence of substrate, it seems likely that the pathway for electron-transfer from Cu_H to Cu_M must include at least a portion of the substrate, either directly (i.e. through the substrate carboxylate and the glycyl methylene group to molecular oxygen) or through a water molecule hydrogen-bonded to the substrate carboxylate, in close proximity to molecular oxygen. It also seems likely that the reducing equivalent from Cu_H is present before the first irreversible step of hydrogen atom abstraction. This is perhaps a borderline teleological argument, but it seems unlikely that the evolutionary "history" of the enzyme would yield such tight control of molecular oxygen activation (requiring presence of substrate, and with no leakage of ROS evident during the catalytic cycle based on the strict one-to-one correspondence of oxygen consumption to product formation), only to allow for the electron from Cu_H to float about freely AFTER the hydroxylation reaction, potentially allowing a release of both an ROS from Cu_M and a solvated electron from Cu_H into the active site of the enzyme, and leading to potentially irreversible damage therein. The various crystal structures, especially the most recent by Prigge et al., certainly allow for the possibility of the substrate/water-bridge pathway, outlined above.

The acrylate series of PAM inactivators, designed originally on the presumption of a cationic radical being formed during the course of the mechanism of natural substrate hydroxylation, are presumed to potentiate inactivation of the enzyme via some kind of

"radical trap" mechanism. The pharmacaphore of the acrylates has several important structural differences from a glycyl residue. First, the glycyl nitrogen present in peptide substrates is replaced with an sp^2 carbon atom in molecules of the acrylate series. This eliminates the possibility of the formation of a hydrogen bond with N316 of the PAM active site. Certainly, this association greatly restricts the freedom of rotation of the carboxy-terminus of peptide substrates bound to the PAM active site, and likely plays the most important role in the orientation of the labile pro-S hydrogen of glycine toward the ROS generated at Cu_M. Additionally, rotational freedom of peptide substrates is restricted by the partial double-bond character of the peptide bond. This restriction is not readily apparent from the molecular structure of the acrylate series, although the conjugated nature of its α,β-unsaturated ketone functionality may lend some double-bond character to this moiety and serve to restrict its rotational freedom as well. This would certainly be the case for a "common" unsaturated ketone, but the presence of the anionic carboxylate may lend further stability to this acrylate resonance form, stabilizing the developing positive charge. To what extent the neutralization of this effect would occur once the carboxylate of the acrylate associates with the positively-charged guanidinium of R240 is currently unknown, as no other instances of this type of molecular substructure can be found in the literature (save for *trans*-benzoylacrylate esters, which are poor models of the circumstance where the charge of a free carboxylate is neutralized by salt-bridge formation with the guanidinium moiety of R240). Nevertheless, it seems reasonable to expect that this resonance structure would be an important contributor to the overall structure of the acrylate molecule. The molecular docking simulations

presented in this thesis show that the carboxy-terminus of the acrylates, including the α,β-unsaturated ketone group, is largely coplanar.

Second, and perhaps more importantly, the sp^3-hybridized carbon atom from which the pro-S hydrogen is abstracted from glycine-extended peptides is replaced by an sp^2 center in the acrylates. Certainly, the acrylate sp^2 C-H is a stronger bond than the peptide sp^3 C-H bond, and, as such, homolytic cleavage would be more difficult in the case of the acrylates. Coupled with the deuterium isotope data indicating an extremely large primary isotope effect for natural substrates, the possibility of the abstraction of the corresponding hydrogen atom from the acrylates is certainly in question. Additionally, the superoxide anion radical has been shown to be insufficiently nucleophilic to productively undergo either 1,4 or 1,2-addition to α,β-unsaturated ketones. Instead, the nascent tetrahedral addition product readily dissociates back to the original molecule and superoxide in the case of benzaldehyde or benzophenone (Sawyer, 1979). Simple olefins are also unreactive, although chalcones have been shown to be susceptible (Frimer, 1976). The olefin radical anion was directly observed by ESR in some of these systems. However, this is the case only in aprotic solvents. In aqueous media (and the nascent ROS is adjacent to a water molecule in the PAM crystal structure), the relative basicity of the superoxide anion would dominate over any possible addition reaction, yielding instead the protonated superoxide (Sawyer, 1979). However, Gibian et al. (Gibian 1984) showed that aliphatic α,β-unsaturated ketones can be facilely reduced by superoxide, generating a carbon-centered radical/anionic oxygen species at the carbonyl functionality. This radical species, when the acrylate is bound at the PAM active site, would be in close proximity to the phenolic group of Y318, allowing, possibly, for an irreversible addition

reaction between the acrylate inactivator and this active site residue. In addition, dependent upon the order of electron transfer (i.e. either first from Cu_M or Cu_H), and the favorable reduction potential of the acrylates, it is also a possibility that the reducing equivalent from Cu_H, navigating a substrate-mediated electron-transfer pathway, could be subsumed by the acrylate PRIOR to any activation of molecular oxygen, generating the actual inactivating acrylate species (an anion radical). In any event, the nature of the inactivating species remains open for debate in the absence of any further data.

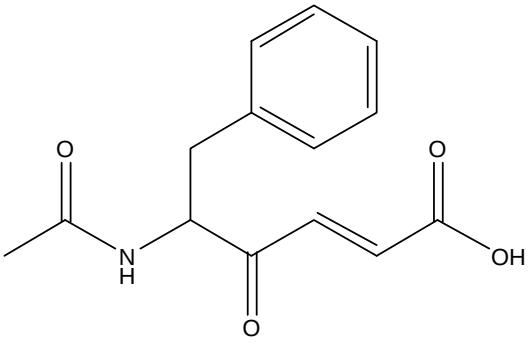

N-Ac-Phe-Acrylic Acid

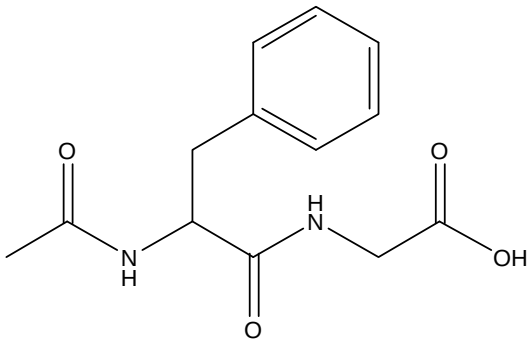

N-Ac-Phe-Gly-OH

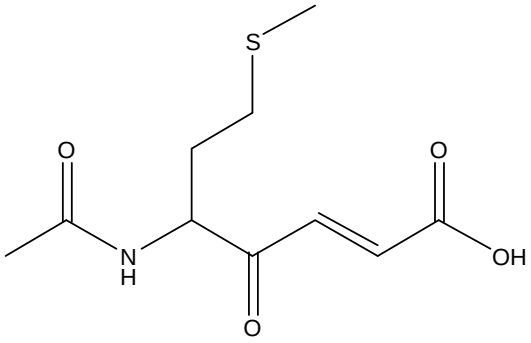

N-Ac-Met-Acrylic Acid

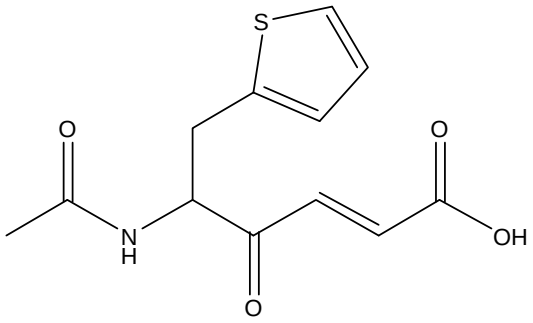

N-Ac-2'-Thienyl-Acrylic Acid

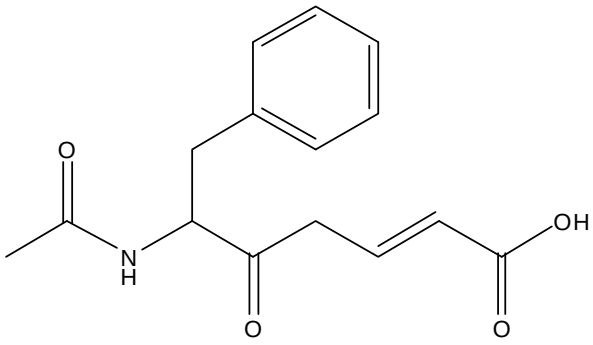

N-Ac-Phe-Crotonic Acid

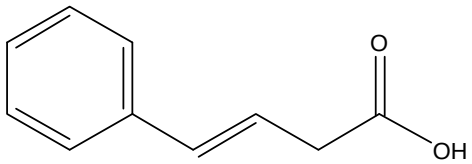

PBA

Figure 4. Molecular structures of compounds tested as PAM substrates and/or inhibitors, and evaluated as PAM ligands using docking simulations with Molecular Operating Environment

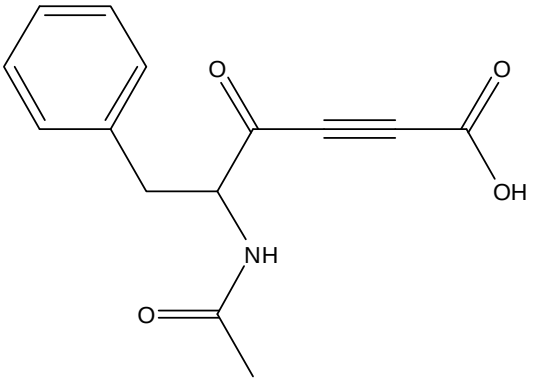

N-Ac-Phe-Propiolic Acid

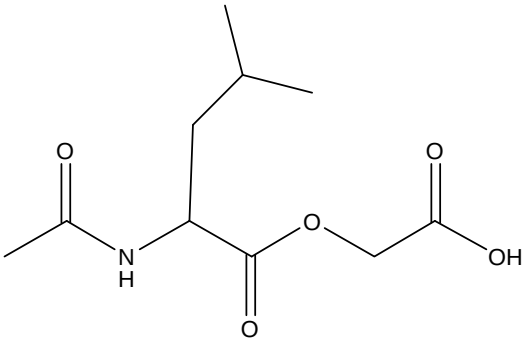

N-Ac-Leu-O-CH_2-COOH

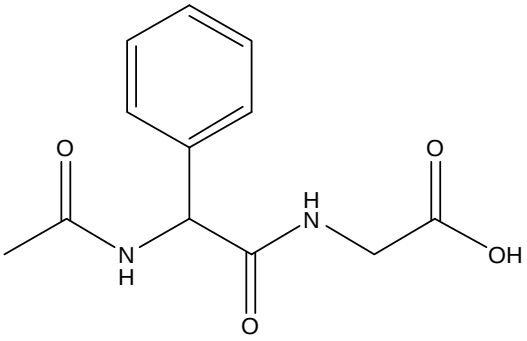

N-Ac-Mandelyl-Gly

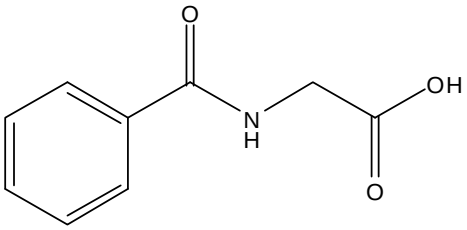

Hippuric Acid

Figure 4 (continued).

Chapter 2: Materials and Methods

TNP-D-Tyr-L-Val-Gly (TNP-YVG)

TNP-YVG was synthesized according to previously described procedures. (Katopodis 1988, Katopodis 1990) Briefly, 12 mg 2-4-6-Trinitrobenzenesulfonic acid hydrate and 11 mg D-Tyr-Val-Gly were dissolved in 20 mL of MeOH/water (1:4) in a foil-wrapped round-bottom flask. The reaction was initiated via the addition of 3 drops of Et_3N, upon which the reaction mixture turned a deep orange. After 30 minutes, 100 mL water was added and the reaction mixture was acidified to pH = 2.0 by the addition of 0.1 M HCl, turning yellow. The reaction mixture was extracted three times with 25 mL EtOAc, and the extracts were pooled, dried over $MgSO_4$, and evaporated to dryness under reduced pressure. The residue was dissolved in a minimum volume of 1:1 Et_2O:EtOAc, and hexanes were added until the solution turned cloudy. After storage overnight at -20º C, the yellow precipitate was collected by vacuum filtration, dissolved in approximately 5 mL of MeOH, and stored at -70ºC. Concentration was determined by UV-Vis spectroscopy. The extinction coefficient of TNP-YVG is 12.2 X 10^3 at 350 nm. A yield of 50% is typical for this synthesis. RP-HPLC analysis revealed no impurities.

TNP-D-Tyr-L-Val-(S)-α-Hydroxy-Gly (TNP-VY(OH)G)

This compound is enzymatically synthesized by reaction of the PAM substrate, TNP-YVG, with isolated, purified PAM and the appropriate cofactors. TNP-YV(OH)G is

used to create HPLC standard curves to quantify PAM product formation in kinetic and activity assays. Briefly, 2.5 mL Catalase (65,000 U/mg, 20 mg/mL) was dissolved in 5.0 mL TRIS buffer (pH 8.5). The above was added to 50 mL 50 mM MES buffer (pH 6.2) containing 4 mM ascorbic acid and 4 μM $CuSO_4$. TNP-YVG in MeOH from the above synthesis was added, and the enzymatic hydroxylation was initiated via the addition of purified PAM. The reaction was monitored at 344 nm on a C8 RP-HPLC column (eluting solvent 44.0% CH_3CN, 55.9% water, 0.1% TFA) at a flow rate of 1.5 mL/min. Additional purified PAM and/or ascorbate was added as necessary until the reaction went to 100% completion. The reaction mixture was then ultrafiltered through an Amicon YM-10 (10,000 M.W. cutoff) membrane. Catalase and purified PAM are retained above the membrane. The filtrate was rinsed once with 20 mL EtOAc (to remove any amide formed), acidified with 0.1M HCl (pH 2.0) and extracted three times with 20 mL EtOAc. The EtOAc solution was dried over $MgSO_4$ and evaporated to dryness under reduced pressure. The yellow film was dissolved in a minimum volume of MeOH and stored at -70º C. A yield of 90% or more is typical of this synthesis. RP-HPLC analysis revealed no impurities.

N-Ac-(D)-Phe-Acrylate

Methyl-N-Ac-(D)-Phe-Acrylate was synthesized according to a previously established procedure (Feng 2000). Both Methyl-N-Ac-(L)-Phe-Acrylate and Methyl-N-Ac-(L)-Met-Acrylate were synthesized by the same procedure, starting from (L)-Phe-OMe and

(L)-Met-OMe, respectively. The methionyl derivative was synthesized and analyzed under my supervision by Undergraduate Research Scholar (URS) Ms. Maggie Schwab.

N-Ac-(D)-Phe-OMe

First, 9.4 mL pyridine and 11.0 mL acetic anhydride were combined in a 100 mL round-bottomed flask at 0º C. Next, 5.0 g (D)-Phe-OMe was dissolved in the above solution and the ice bath was removed. The reaction was allowed to proceed overnight at room temperature, and turned a rich purple color. The reaction was quenched by the addition of 100 mL water/ice slurry. The resulting solution was again allowed to return to room temperature and then extracted four times with CH_2Cl_2. The extracts were pooled and then rinsed three times each with saturated $NaHCO_3$ solution, 0.1 M HCl solution, and water. The methylene chloride solution was dried over $MgSO_4$ and evaporated to dryness under reduced pressure, yielding 4.5 g of N-Ac-(L)-Phe-OEt as a white solid (yield 73%). ^{1}H NMR ([^{2}H]chloroform, tetramethylsilane (TMS) = 0.0 p.p.m.): δ 1.98 (s, 3H), δ 3.12 (q, 2H), δ 3.73 (s, 3H), δ 4.89 (m, 1H), δ 5.90 (broad, 1H), δ 7.09 (m, 2H), δ 7.27 (m, 3H).

N-Ac-(D)-Phe-α-Ketophosphonate

In a 3-necked 250 mL round-bottom flask at -78º C under argon, 4.4 mL dimethylmethylphosphonate was added to 45 mL dry THF (dried over sodium metal). 16.5 mL of n-BuLi (2.5 M in hexanes) was added dropwise over 30 minutes. A small

quantity of white precipitate was formed, which disappeared over 15 minutes. Then, 4.5 g N-Ac-(D)-Phe-OMe in 50 mL dry THF was added all at once. The reaction was allowed to proceed overnight and come to room temperature, turning yellow-orange. The reaction mixture was quenched by the addition of 100 mL water and washed twice with 50 mL diethyl ether. The aqueous layer was acidified by 0.1 M HCl (pH 1.0), and then extracted four times with 50 mL CH_2Cl_2. The methylene chloride extracts were pooled, dried over $MgSO_4$, and evaporated to dryness under reduced pressure, yielding a yellow oil. The crude N-Ac-(D)-Phe-α-Ketophosphonate was purified by silica gel chromatography from chloroform/methanol (20:1 v/v) yielding a yellow oil (6.1 g, 96%). ^{1}H NMR ([^{2}H]chloroform, TMS = 0.0 p.p.m.): δ 1.98 (s, 3H), δ 2.98-3.30 (m, 4H), δ 3.72-3.78 (m, 6H), δ 4.82-4.94 (q, 1H), δ 6.52 (d, 1H), δ 7.10-7.32 (m, 5H).

Methyl Glyoxylate

First, 3.6 g of glyoxylic acid monohydrate and 100 mg p-toluenesulfonic acid were dissolved in 4.6 mL methyl dimethoxyacetone in a 100 mL round-bottomed flask. The reaction mixture was heated under reflux overnight. The next morning, the reaction mixture was cooled to room temperature and 4 g phosphorous pentoxide were slowly added. The reaction mixture was again heated to reflux (80º C) for 4 hours, allowed to cool to room temperature and then distilled under reduced pressure. The product which distilled at 70º C was collected (3.0 mL) as a yellow oil. ^{1}H NMR ([^{2}H]chloroform, TMS = 0.0 p.p.m.) δ 3.76 (singlet).

Methyl-N-Ac-(D)-Phe-Acrylate

First, 6.1 g N-Ac-(D)-Phe-α-Ketophophonate was placed in a 100 mL round-bottomed flask over ice. Then, 10 mL water and 2.5 mL methyl glyoxylate were added, and after 5 minutes 20 mL of potassium carbonate solution (0.25 g/mL) were added. A white precipitate formed immediately upon addition of the carbonate solution. The reaction was allowed to proceed for 30 minutes. The white solid was collected by vacuum filtration, rinsed with cold water, and recrystallized from ethanol/water. The white solid was again collected by vacuum filtration and dried under vacuum over phosphorous pentoxide (1.1 g, 19%). ^{1}H NMR ([^{2}H]chloroform, TMS = 0.0 p.p.m.) δ 1.98 (s, 3H), δ 3.00-3.22 (o, 2H), δ 3.80 (s, 3H), δ 5.05-5.12 (q, 1H), δ 6.02-6.07 (d, 1H), δ 6.76-6.80 (d, 1H, J = 15.9 Hz), δ 7.05 (m, 2H), δ 7.08-7.16 (d, 1H, J = 15.9 Hz), δ 7.25 (m, 5H).

N-Ac-(D)-Phe-Acrylic Acid

Typically, 100 mg Methyl-N-Ac-(D)-Phe-Acrylate was dissolved in 8 mL EtOH, and slowly added to 40 mL 100 mM TRIS buffer (pH = 7.1) to prevent precipitation. In a separate tue, 6 mg of reconstituted Pig Live Esterase (E.C. 3.1.1.1, 15 U/mg) in one mL of water was added to initiate the reaction. The reaction was monitored on a C8 column at 260 nm (25.0% CH_3CN/74.9% water/0.1% TFA) at a flow rate of 1.5 mL/min. Typically, the reaction went to 99% completion after 24 hours. The reaction mixture was ultrafiltered through an Amicon YM-10 membrane, the filtrate was acidified (pH 2.0) by addition of 0.1M HCl, and extracted four times with 10 mL EtOAc, dried over $MgSO_4$,

and evaporated under reduced pressure to yield a white solid. The product was found to be pure by HPLC. Typical yields for this reaction were greater than 75%. ^{1}H NMR (DMSO-d_6, DMSO = 2.49 p.p.m.): δ 1.78 (s, 3H), δ 2.72-3.07 (m, 2H), δ 4.70 (m, 1H), δ 6.56 (d, 1H, J = 15.9 Hz), δ 7.09 (d, 1H, J = 15.9 Hz), δ 7.22 (m, 5H), δ 8.42 (d, 1H). Polarimetry: $[\alpha]_D^{25} = 12.5 \pm 1.4$ deg.

N-Ac-(L)-Phe-Acrylate

This compound was synthesized using the same experimental protocol outlined for N-Ac-(D)-Phe-Acrylate above, except that the starting material here was (L)-Phe-OMe, whereas the ethyl ester was the reagent in the synthesis of N-Ac-(D)-Phe-Acrylate. Yields were similar to that of the (D)-enantiomer in all cases.

N-Ac-(L)-Phe-OEt

Briefly, 5 g (L)-Phe-OEt was dissolved in a solution of 11.0 mL acetic anhydride and 9.5 mL pyridine at 4° C. The reaction was allowed to proceed overnight and was quenched by the addition of 100 mL cold water. The resulting solution was extracted four times with 25 mL methylene chloride. The aqueous phase was discarded. The combined organic extracts were then washed three times each with 25 mL 0.1 M HCl, water, and saturated sodium bicarbonate solution. The organic phase was dried over magnesium sulfate, filtered, and evaporated to dryness under reduced pressure, yielding 4.7 g of N-Ac-(L)-Phe-OEt as a white solid. ^{1}H NMR ([^{2}H]chloroform, TMS = 0.0

p.p.m.): δ 1.25 (t, 3H), δ 1.97 (s, 3H), δ 3.13 (q, 2H), δ 4.16 (q, 2H), δ 4.87 (m, 1H), δ 5.90 (broad, 1H), δ 7.09 (m, 2H), δ 7.27 (m, 3H).

N-Ac-(L)-Phe-α-ketophosphonate

Initially, 4.7 g N-Ac-(L)-Phe-OEt was dissolved in 50 mL THF dried over sodium metal. Separately, 4.4 mL dimethylmethylphosphante was added to 50 mL THF dried over sodium, under an argon atmosphere at -78° C. Dropwise, 16.5 mL of n-BuLi (2.5 M in hexanes) was added to the dimethylmethylphosphonate solution over the course of 30 minutes. A white precipitate formed, which disappeared over 15-30 minutes. The N-Ac-(L)-Phe-OEt solution was added all at once. The reaction was allowed to proceed overnight and come to room temperature. The reaction was quenched via the addition of 100 mL cold water and rinsed twice with diethyl ether. The aqueous phase was acidified to pH 1.0 with dilute HCl, and extracted four times with 50 mL methylene chloride. The pooled organic extracts were dried over magnesium sulfate, filtered, and evaporated under reduced pressure to yield a pale yellow oil. The oil was purified by silica gel chromatography from chloroform/methanol (20:1 v/v), yielding 6.0 g of yellow oil. ^{1}H NMR ([^{2}H]chloroform, TMS = 0.0 p.p.m.): δ 1.98 (s, 3H), δ 2.99-3.15 (m, 4H), δ 3.75 (m, 6H), δ 4.85 (q, 1H), δ 6.53 (d, 1H), δ 7.25 (m, 5H).

Methyl-N-Ac-(L)-Phe-Acrylate

First, 6.0 g N-Ac-(L)-α-ketophosphonate was placed in a round-bottomed flask over an ice bath. Next, 10 mL water and 2.5 mL methyl glyoxylate were added and the solution was allowed to equilibrate for 5 minutes. Then, 20 mL potassium carbonate (0.25 g/mL) was added to initiate the reaction. A white precipitate formed immediately and the reaction was allowed to proceed for 30 minutes. The white precipitate was collected by vacuum filtration, washed with cold ethyl ether, recrystallized from ethanol/water, collected again by vacuum filtration, and dried over phosphorous pentoxide in a vacuum desiccator (1.3 g). ^{1}H NMR ([^{2}H]chloroform, TMS = 0.0 p.p.m.): δ 1.99 (s, 3H), δ 3.00-3.24 (o, 2H), δ 3.81 (s, 3H), δ 5.09 (q, 1H), δ 6.03 (d, 1H), δ 6.78 (d, 1H, J = 15.9 Hz), δ 7.06 (m, 2H, J = 15.9 Hz), δ 7.15 (m, 2H), δ 7.25 (m, 3H).

N-Ac-(L)-Phe-Acrylic Acid

First, 100 mg Methyl-N-Ac-(L)-Phe-Acrylate was dissolved in 8 mL EtOH, and slowly added to 40 mL 100 mM Tris buffer. Then, 6 mg of reconstituted Pig Liver Esterase (E.C. 3.1.1.1, 15 U/mg) in 1 mL Tris buffer was added to initiate the reaction. The reaction was maintained at 37° C and monitored by RP-HPLC at 260 nm as described above. After 24 hours, the reaction had gone to greater than 99% completion. The reaction mixture was then ultrafiltered through a YM-10 membrane to remove the enzyme. The filtrate was acidified to pH 2.0 with dilute HCl, extracted four times with 10 mL EtOAc, dried over magnesium sulfate, and evaporated under reduced pressure to

yield 70 mg of white powder, pure by HPLC. ^{1}H NMR ([^{2}DMSO-d_6, DMSO = 2.9 p.p.m.): δ 1.78 (s, 3H), δ 2.71-3.07 (m, 2H), δ 4.70 (m, 1H), δ 6.56 (d, 1H, J = 15.9 Hz), δ 7.10 (d, 1H, J = 15.9 Hz), δ 7.22 (m, 5H), δ 8.42 (d, 1H); mass spectrum (ESI) m/e = 262.1 (M + 1). Polarimetry: $[\alpha]_D^{25}$ = -14.3 ± 2.9 deg.

Methyl-4-Phenyl-3-Butenoate

Initially, 2.0 g recrystallized 4-Phenyl-3-Butenoic acid (from boiling hexanes) was added to 20 mL MeOH. Reaction was initiated by the addition of 2 drops concentrated HCl and heated under reflux overnight. Then, 100 mL water was added, the reaction mixture was brought to pH 7.0 by addition of 0.01 M NaOH and extracted four times with 25 mL CH_2Cl_2. The methylene chloride solution was dried over $MgSO_4$ and evaporated under reduced pressure to yield a yellow liquid, pure by HPLC. Typically, yields were greater than 90%. ^{1}H NMR ([^{2}H]chloroform, TMS = 0.0 p.p.m.) δ 3.23 (d, 2H), δ 3.74 (s, 3H), δ 6.22-6.38 (m, 1H), δ 6.44 (d, 1H), δ 7.20-7.38 (m, 5H).

***Spodoptera Frugiperda* Cell Culture**

Spodoptera Frugiperda (Sf9) cells were maintained in monolayer cultures with TNM-FH medium supplemented with 10% v/v fetal bovine serum (FBS) and 1% v/v antibiotic/antimycotic solution (10,000 U/mL penicillin G (sodium salt), 10 mg/mL streptomycin sulfate, and 25 μg/mL amphotericin B) in Falcon T-flasks at 27º C. Monolayer culture was employed for cell maintenance. Prior to transfection, cells were

transferred to suspension culture in 500 mL Bellco Spinner flasks, and conditioned over two cell passages from 100% TNM-FH media to 100% serum-free Ex-Cell 401 containing 1% v/v antibiotic/antimycotic solution. Prior to use, 0.1% w/v Pluronic F-68 was added to suspension cultures to prevent cell aggregation. Cells were subcultured every 84 hours.

Expression of *X. Laevis* Skin AE-1

Suspension cell cultures were treated with a Baculovirus Expression Vector (BEV) containing the gene for AE-1 created by Nishikawa et al. Cells were counted via hemocytometer and infected at 10 plaque-forming units per cell. Briefly, the cell suspension was centrifuged at low speeds to pellet the Sf9 cells, which were then resuspended with the appropriate volume of virus solution. Cells were incubated for one hour with end-over-end rocking and Ex-Cell medium was added such that the final cell concentration was approximately 1 X 10^6 cells/mL Cells were incubated in suspension culture for five days and then harvested by Fast Protein Liquid Chromatography (FPLC).

Enzyme Isolation

AE-I was isolated from Sf9 suspension-cultured medium using a procedure developed by Suzuki (Suzuki 1990) and modified by Feng (Feng 2000). Typical starting volumes were 500 mL to 1 L. Cells were pelleted by low-speed centrifugation. The supernatant was loaded onto an SP-Sepharose Fast Flow cation-exchange column (2.6 x 40 cm,

Pharmacia) equilibrated with 50 mM MES-sodium, pH 6.2. After the medium was loaded, the column was eluted for 120 min at a flow-rate of 1.5 mL/min to remove non-adsorbed material. The column was then eluted with a stepwise NaCl gradient: 0-150 mM NaCl over 30 min, 150-250 mM NaCl over 200 min, 250-500 mM NaCl over 50 min, and 500 mM NaCl for 300 min. Fractions were assayed for activity using the standard PAM Assay solution. Fractions with activity were pooled and concentrated over a 10,000 molecular-weight Amicon YM-10 membrane, and the buffer was exchanged to 50 mM TRIS-Cl, pH 8.5 buffer.

The concentrated AE-1 solution was then applied to a MonoQ HR 10/10 column (Pharmacia) equilibrated with 50 mM TRIS-Cl, pH 8.5 buffer. The column was washed for 30 min at 1.0 mL/min with starting buffer, and then eluted with a step-wise NaCl gradient: 0-50 mM NaCl for 15 min, 50-200 mM NaCl over 90 min, 200-500 mM NaCl over 30 min, and 500 mM NaCl for 30 min. Fractions with PAM activity were pooled and concentrated over an Amicon YM-10 membrane and applied to a Superose-12 HR 10/30 gel-filtration column (Pharmacia). Activity was eluted with HEPES pH 7.0 at a flow-rate of 0.5 mL/min for 90 minutes. Purified AE-1 eluted as a single peak over several fractions. Activity was pooled and concentrated, and stored as a 1:1 buffer/ethylene glycol solution at -20º C. Activity is expressed in mU/mL, where 1 U is the amount of enzyme required to produce 1 μM TNP-YV(OH)G per minute at 37º C.

Standard PAM Activity Assay

The assay conditions for PAM activity are similar to those described in the enzymatic synthesis of TNP-YV(OH)G above. Briefly, the assay solution contains 1 mg/mL catalase, 4 mM ascorbic acid, 4 μM copper sulfate, and 35 μM TNP-YVG in 250 μL 50 mM MES-Na, pH 6.5 at 37º C. The conversion of TNP-YVG to TNP-YV(OH)G was kept to under 30% in order to obtain consistent initial rates. The reaction was quenched by the addition of 10% v/v 3M $HClO_4$. Samples were centrifuged at 10,000 g for 30 min and the supernatant was assayed by RP-HPLC. Product concentrations were determined by RP-HPLC analysis on an Alltech Allsphere C8 column (250 mm x 4.2 mm, 5 μm particle size) with an authentic product standard curve. Mobile phase was 44.0/55.9/0.1 acetonitrile/water/trifluoroacetic acid at a flow rate of 1.5 mL/min. Absorbance was measured at 344 nm.

Dilution Assay

Purified PAM was initially incubated in the above assay solution (37º C) at various concentrations of inactivator, also containing 0.1% v/v Triton X-100 and 80 mM KI. Inactivation reactions were initiated by the addition of purified PAM. Aliquots of 10 μL were withdrawn over an appropriate time course and reincubated in the standard PAM assay solution described above, containing saturating concentrations of TNP-YVG (50 μM), 0.1% v/v Triton X-100, and 80 mM KI. The reactions were quenched after 30 min

and analyzed as described above. Residual PAM activity was measured as % initial activity of untreated control enzyme.

Progress Curve Assay

Purified PAM was incubated in the presence of varying concentrations of TNP-YVG (2.0 – 15 μM) and the appropriate inactivator species (20 – 100 μM) in 5 mL of the standard PAM assay solution containing 0.1% v/v Triton X-100 and 80 mM KI. Reaction was initiated by the addition of enzyme and 250 μL aliquots were removed every minute, quenched with 10% v/v 3M $HClO_4$, centrifuged, and the supernatant was analyzed for product concentration according to the chromatographic conditions described above.

Circular Dichroism Spectropolarimetry

Circular Dichroism (CD) spectropolarimetry measurements were acquired on a Jasco J-810 150-S spectropolarimeter. The measurement range was from 190 nm to 350 nm, and all measurements were collected at room temperature. Resolution and bandwidth were 1 nm; scanning speed was 50 nm/min; sensitivity set at 10 mdeg. N-Ac-(L)-Phe-Acrylate and N-Ac-(D)-Phe-Acrylate were dissolved in pure acetonitrile. The Cotton effect was evident from 190-197 nm.

HPLC Chiral Chromatography

Chiral separations of Methyl-N-Ac-(L)-Phe-Acrylate and Methyl-N-Ac-(D)-Phe-Acrylate were carried out on a Phenomenex D-Penicillamine column. Compounds were dissolved in methanol prior to injection. Absorbance was monitored at 260 nm on a Waters LC-Module 1 Plus. Flow rate was 1.0 mL/minute. Mobile phase was 74.5/25/0.5 3M $CuSO_4$/methanol/trifluoroacetic acid.

PAM/Ligand Docking

All simulations were run using Molecular Operating Environment (MOE) software, Chemical Computing Group, Inc. (Montreal, Canada). Additional code "more_dock.svl" was obtained from the SVL Exchange website (http://syl.chemcomp.com).

All ligands were constructed using the MOE Builder module and built from the coordinates of the side chain phenyl ring of the crystal structure ligand IYG (Prigge, 1998), thereby placing the side chains of all ligands in the hydrophobic pocket of the enzyme at the start of each docking run. Polar hydrogens were added to the ligands (including sp_2 hydrogens) and each ligand was minimized using the Engh-Huber force field with default parameters and "solvation" enabled. Non-bonded and bonded cutoffs were changed to 5.5 and 4.5 Å, respectively.

The receptor used for molecular docking was the oxidized PAM crystal structure (Prigge 1998). All water molecules, carbohydrates, and metal ions except for Cu_H and Cu_M were deleted from the receptor prior to molecular docking. Polar hydrogen atoms

were added to the PAM crystal structure receptor, heavy atoms were locked, and the structure was energy-minimized using the Engh-Huber force field. Default energy parameters were used for the minimization and "solvation" was enabled. Non-bonded and bonded cutoffs were changed, as for the ligand minimization, to 5.5 and 4.5 Å, respectively.

Docking simulations were performed using the Simulated Annealing algorithm (Engh-Huber force field), with all default parameters except that "solvation" was enabled and the non-bonded and bonded cutoffs were changed to 5.5 and 4.5 Å, respectively. The docking box was centered at 40.4032 x 25.3060 x 40.4527 (x,y,z) of the crystal structure receptor and had arbitrary dimensions of 60 x 60 x 60 (x,y,z). All residues that were at least partially within the confines of the docking box were selected, and then all residues within 5.5 Å (the non-bonded cutoff) of those residues were selected. All other atoms were deleted.

Minimized ligands were then subjected to a non-random start simulation, and all bonds that are able to undergo rotation were allowed to deviate continuously ± 30º from the minimized configuration. Initial temperatures were 1,000 K. Typically, twenty-five runs were performed for each ligand, resulting in 25 docked conformations per ligand. Each run included 6 cycles of decreasing initial temperature, with 8,000 iterations per cycle. Top scorers were determined from the electrostatic and van der Waals' energy contributions.

Flexible Alignment

The three atoms of the carboxylate group were fixed in each ligand. Flexible Alignment module was used to determine the optimum energy-minimized overlay of each pair of ligands tested. Default parameters were used in all cases. MMFF94 force field, typical for small molecules, was used for the simulations.

Chapter 3: Results

PAM Isolation

The conditions of this protein isolation were initially those of Suzuki (Suzuki, 1990), and include optimizations developed by Dr. Jun Feng (Feng, 2000), as described in Methods. The results of a typical *X. Laevis* AE-1 isolation are presented in Table 3.1.1 below. The specific activity increases from 64.0 mU/mg protein in the initial cell-free extract to 13,500 mU/mg protein after the Superose-12 gel-filtration column, a 211-fold purification. The only other point which requires explanation is the increase in total activity from the MonoQ pool to the Superose-12 pool, which should necessarily decrease rather than increasing. One possible explanation for this paradoxical phenomenon is the presence, in the less pure Mono-Q pool, of proteins which interfere with either the substrate, copper, or ascorbate in the assay mix (by decreasing their effective concentration). It is evident from the chromatograms that the concentration of substrate does not decrease from the "blank" (no added fractionated enzyme) to those assays where protein solution from the isolation fractions is included for assay. Therefore, no proteolytic degradation of substrate from contaminating enzymes occurs. The most likely explanation is the presence of a chelator (proteinaceous or not) which sequesters copper and thus reduces the rate of PAM hydroxylation in the less pure column pools relative to those with a purer enzyme sample.

Table 1. Isolation table of PAM (AE-1) expressed from *Sf9* cells. Total protein concentrations calculated from bovine serum albumin standard curves using Coomassie Brilliant Blue spectrophotometric assay. "Volume" refers to the total sample volume after the purification step was completed (e.g. after centrifugation and pelleting of cells in "Cell Free"). mU are defined as the amount of PAM required to convert 1 nmol of TNP-YVG substrate to TNP-YV(OH)G per minute at 37 °C. Yield refers to percent activity (mU) which remains after each purification relative to initial activity (mU) in Cell Free solution.

Samples	**Volume (mL)**	**PAM Activity (mU/mL)**	**Units (mU)**	**[Protein] (ug/mL)**	**Protein (mg)**	**Spec. Activity (mU/mg)**	**%Yield**	**Pur. Factor**
Cell Free	715	6.36	4560	99.5	71.2	64.0	100	1.000
SP-Sepharose	41.0	38.7	1590	106	4.34	365	34.8	5.712
MonoQ	4.50	135	609.0	80.0	0.360	1690	13.4	26.5
Superose-12	0.960	1670	1601	124	0.119	13500	35.1	211

Synthesis and Characterization of N-Ac-(L)/(D)-Phe-Acrylate

Figures 5 shows the structures of the various reagents and products of the several steps of the syntheses of N-Ac-Phe-Acrylate. In the case of N-Ac-(D)-Phe-Acrylate, the starting material is (D)-Phe-OMe, whereas (L)-Phe-OEt was the initial starting material in the case of N-Ac-(L)-Phe-Acrylate. In some instances, the initial ester starting material was synthesized from (L)-Phe or (D)-Phe employing a simple Fisher esterification. Briefly, proceeding from the starting material, the initial reaction acetylates the free amine using pyridine and acetic anhydride, yielding N-Ac-(L)-Phe-OEt or N-Ac-(D)-Phe-OMe. The pyridine acts as a catalyst, and has been suggested to activate the acetic anhydride via nucleophilic attack, yielding a pyridinium acetate which is then subjected to nucleophilic attack by the free amine of the amino acid ester. The next reaction involves the deprotonation of methyl dimethylphosphonate by n-BuLi, creating a nucleophilic carbanion which displaces the ester group from the carboxylate of the N-Acetyl ester, yielding an α-ketophosphonate. The following reaction, a Wadsworth-Emmons, deprotonates the ketophosphonate to again yield a carbanion, which then reacts with the aldehyde functionality of methyl glyoxylate to yield Methyl-N-Ac-Phe-Acrylate. Lastly, Pig Liver Esterase is used in MES buffer, pH 7.1, to hydrolyze the ester, yielding the final product N-Ac-Phe-Acrylate. Yields, NMR and MS data, and optical rotation data are related in Methods. The circular dichroism (CD) spectrum of N-Ac-(D)-Phe-Acrylate and N-Ac-(L)-Phe-Acrylate is shown in Figure 6., with the Cotton effect evident at very low wavelengths (190-197 nm).

Finally, chiral chromatography was employed to resolve the enantiomeric pair. Unfortunately, the free acid enantiomers could not be resolved on the (D)-penacillamine column which was employed. However, the enantiomeric Methyl-N-Ac-Phe-Acrylate enantiomeric pair was able to be resolved by this column, with the (D)-enantiomer eluting at 21 minutes and the (L)-enantiomer at 28 minutes under the conditions described in Methods (Figures 7 and 8, respectively). The CD results indicate that the compounds are enantiomerically pure prior to the enzymatic hydrolysis, and the polarimetry and circular dichroism data indicate that the compounds are enantiomerically pure subsequent the Pig Liver Esterase-catalyzed hydrolysis. As expected, both enantiomers had identical NMR spectra and mass spectral analysis (ESI) indicated a molecule mass of 261.2 for both compounds. Both the ester and free acid enantiomeric pairs coeluted under multiple different compositions of mobile phase on achiral RP-HPLC (C8), as expected for an enantiomeric pair (data not shown).

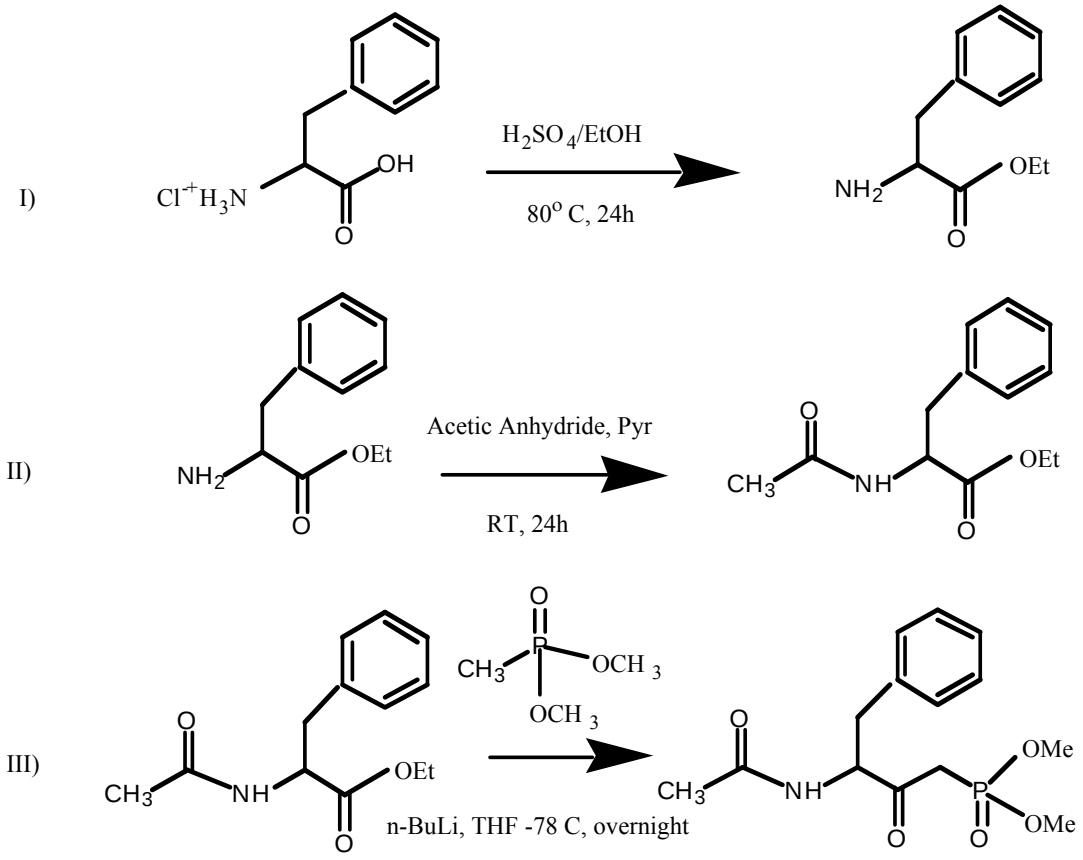

Figure 5. Synthesis of N-Ac-Phe-Acrylate

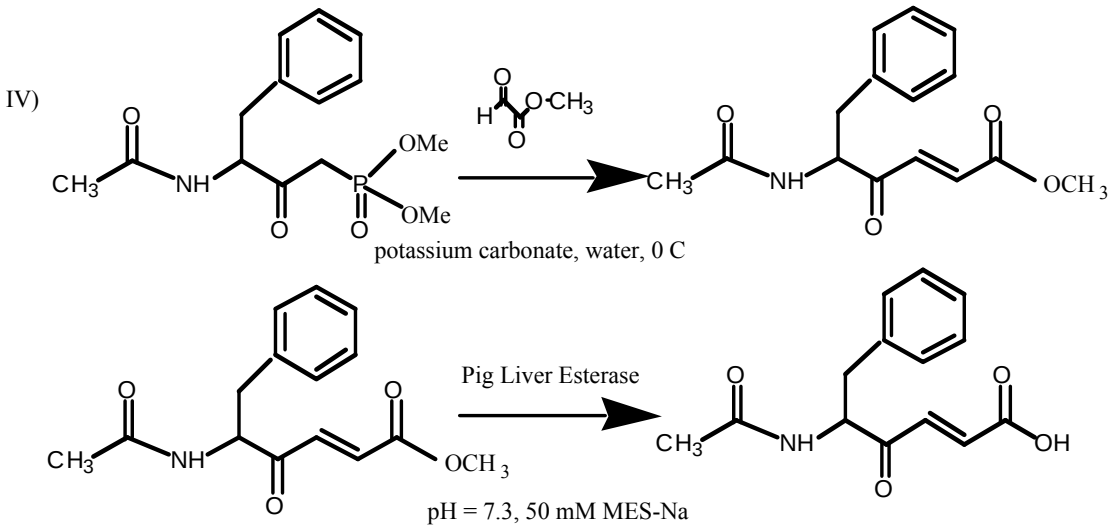

Figure 5 (continued).

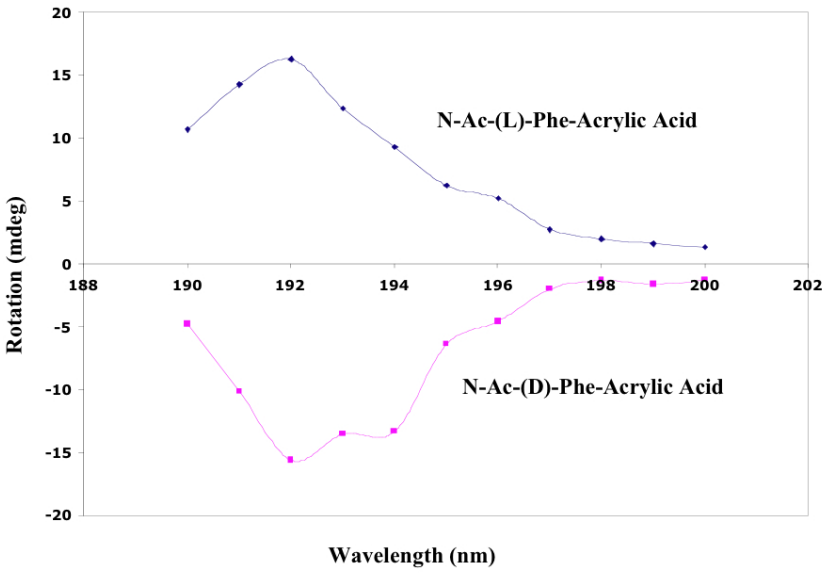

Figure 6. Overlaid Circular Dichroism spectra of N-Ac-(L)-Phe-Acrylate and N-Ac-(D)-Phe-Acrylate in acetonitrile. The Cotton effect is evident from 190 nm (the UV-cutoff of acetonitrile) to 197 nm. No further effect is evident at longer wavelengths, tested up to 350 nm.

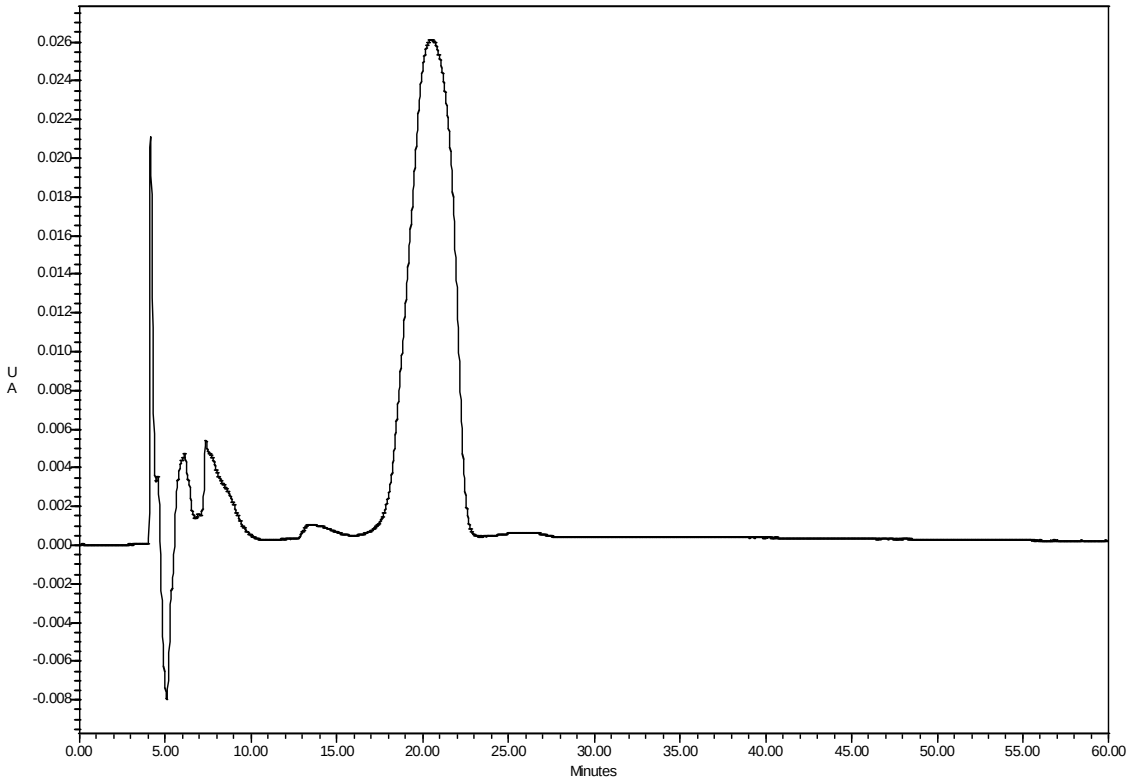

Figure 7. Chromatogram of Methyl-N-Ac-(D)-Phe-Acrylate in MeOH, applied to a (D)-penacillamine chiral column. The (D)-enantiomer elutes at 21 minutes. Monitored at 260 nm, 1 mL/minute. Mobile phase 24.5/75.0/0.5 3M $CuSO_4$ (aq)/MeOH/TFA

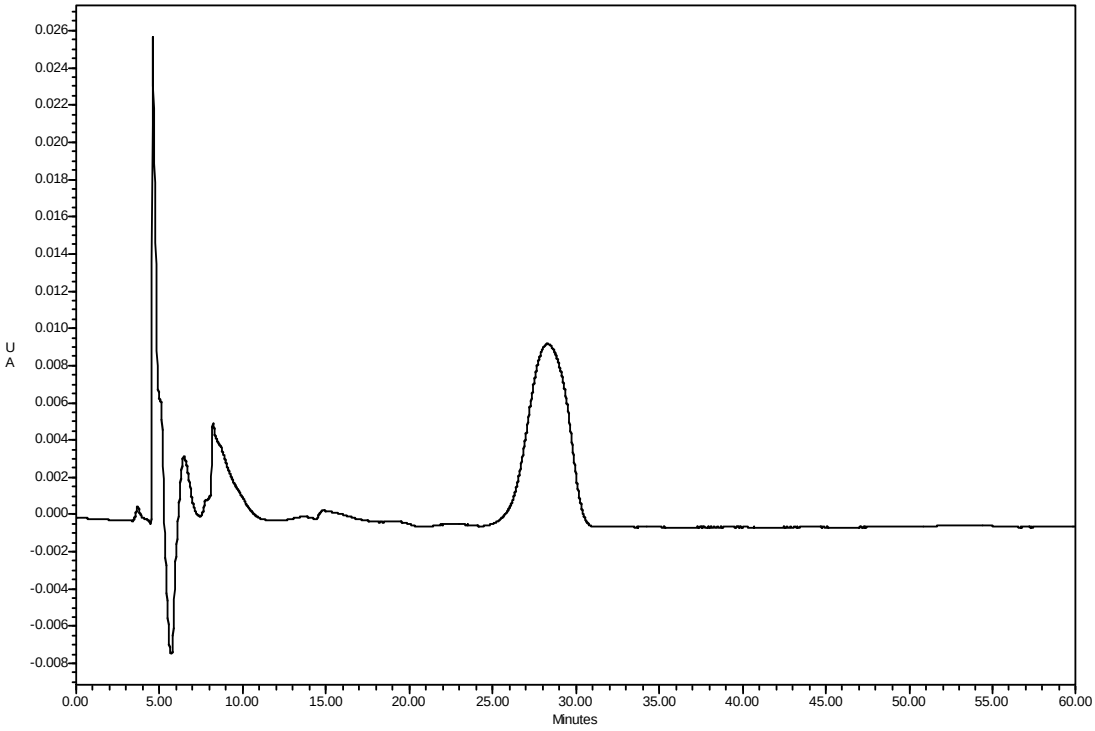

Figure 8. Chromatogram of Methyl-N-Ac-(L)-Phe-Acrylate in MeOH, applied to a (D)-penacillamine chiral column. The (L)-enantiomer elutes at 28 minutes. Monitored at 260 nm, 1 mL/minute. Mobile phase 24.5/75.0/0.5 3M $CuSO_4$ (aq)/MeOH/TFA

Inactivation Kinetics

The efficacy of a mechanism-based irreversible inactivator may be fully described, in the simplest mechanistic case, by both the dissociation constant (K_I) which represents the binding affinity, and by k_{inact} which represents, in this case, the second-order rate constant of inactivation. Figure 9 graphically depicts all possible mechanistic events, both reversible and irreversible, which may occur along the inactivation/inhibition pathway. The simple case above corresponds to an inactivation pathway which involves only the inhibitor species and the free enzyme, either in the complete absence of substrate, or in the presence of a relatively poor substrate where $K_m >> K_I$. In the latter case, one may reasonably assume that the concentration of the ES complex is negligible in comparison to the concentration of the EI complex, if the working concentrations of substrate and inhibitor are fairly close to the K_m and K_I values, and that the system can be mathematically treated as a "single substrate" system. The former case, inactivation occurring in the complete absence of substrate, will be explored via the performance of the "Dilution Assay", to be discussed below.

In contrast, when utilizing a kinetic assay where both substrate and inactivator are present, and are at concentrations relative to their binding constants which are not representative of the limiting case discussed in the above paragraph, it is important to recognize the possibility that several competing pathways may exist besides the direct inactivation reaction involving only inactivator and enzyme. Obviously, so long as the concentrations of substrate and inhibitor are reasonably close to their K_m and K_I values, respectively, any enzyme which has yet to be inactivated will continue to engage in catalysis of substrate to product. Therefore, we have now described two possible

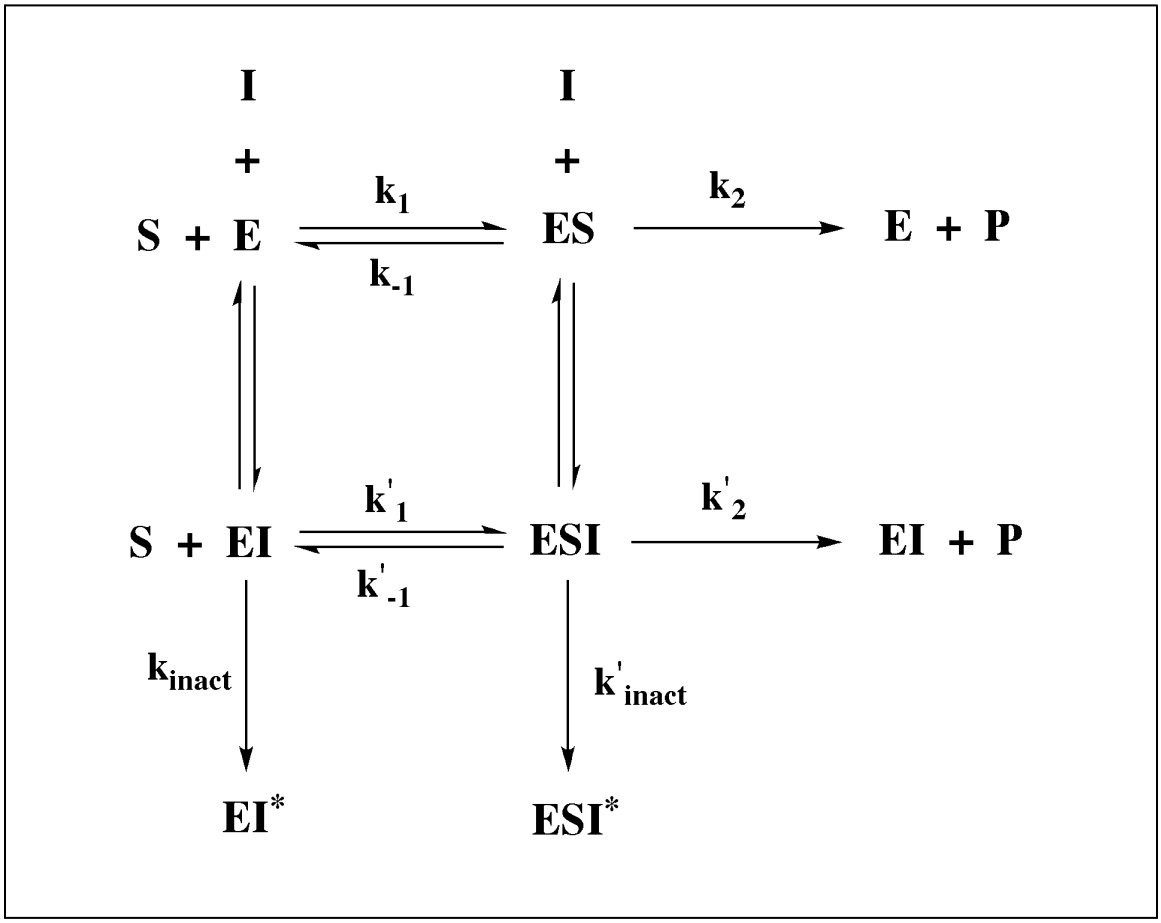

Figure 9. Possible Mechanistic Pathways For Mechanism-Based Inactivators

pathways which may occur when enzyme is incubated in the presence of both substrate and inactivator, represented by the top horizontal reaction in Figure 9 and the leftmost vertical reaction, respectively. Briefly, these reactions provide for free enzyme to bind with either product or inactivator to reversibly form the ES and EI complexes. The ES complex may then either dissociate back to free enzyme and substrate or undergo catalysis to yield an EP complex which subsequently dissociates to yield product and free enzyme. If product dissociation is fast relative to k_{cat} or k_1, then [EP] will be negligible and will not measurably affect the concentrations of either free enzyme ([E]) or the enzyme-substrate complex ([ES]). As will be explained in the Progress Curve Assay section to follow, the values of k_2 and K_m will be derived from a separate enzyme-substrate assay (generated from a Michaelis-Menten plot of initial velocities at various substrate concentrations in the ABSENCE of inhibitor) where the actual value of k_2 represents the contributions of both the catalytic step AND the product dissociation step. Hence, the product dissociation rate is not explicitly included in these figures/calculations although, theoretically, the rate of product release may in fact be equivalent to or slower than the actual catalytic step. However, the fact that the rate of product formation remains linear with respect to time, even at exceedingly high substrate concentrations (e.g. 20-fold greater than K_m) and high conversion percentages (i.e. when [P] becomes equal or greater than [S]) strongly suggests that there is no change in [ES] or any significant product inhibition of the enzymatic reaction, even at these exceedingly high concentrations of substrate. Therefore, the rate of product release is greater than the rate of ES formation. Moreover, the association of E and P to the EP complex does not occur

indicating that the K_d value for EP formation is much greater than the K_m value for the ES complex or that the rate of association of E and P is very, very slow (or both).

Logically, there are two different methods by which to perform an enzyme inactivation study: first, by incubation of the inactivator with the enzyme, substrate, and all requisite catalytic cofactors; and secondly, by a preincubation of the inactivator with the enzyme and cofactors in the absence of substrate, followed by a measurement of residual activity. The first case describes the procedure of the Dilution Assay, while the second is descriptive of the Progress Curve Assay, both of which were utilized in this thesis work.

Dilution Assay

As stated above, the dilution assay involves the preincubation of enzyme with inactivator and cofactors in the absence of substrate. The inactivation reaction was initiated by the addition of enzyme to several preincubation solutions containing different concentrations of the inactivator. Aliquots were taken at various time points and "diluted" into an assay solution identical in all regards to the preincubation solution, save for the inclusion of saturating concentrations of substrate and lack of inactivator. Obviously, there is no way to discriminate between inactivator and enzyme in drawing these aliquots from the preincubation solution and, therefore, there is some trivial (although nonzero) concentration of the inactivating species present in the assay solution. In all cases in this thesis, the "dilution" results in at least a 50-fold decrease in the concentration of enzyme and inactivator relative to the preincubation solution. The highest concentrations of inactivator in the preincubation solution never exceeded, in

relative magnitude, 3-fold that of the resultant K_I value. Therefore, the highest possible concentration of inactivator in the assay solution would be 3/50 the value of K_I. In addition, the concentration of substrate in the assay solution was 10-fold greater than its measured K_m value and the final conversion of substrate to product never consumed more than 30% of the initial substrate present. Moreover, the K_m of the substrate, TNP-YVG, is approximately 1/5 of the K_I value for any of the inactivators tested. So under the saturating concentrations of substrate present in the assay solution, it is highly unlikely that the inactivator will be bound to the active site of the enzyme to any appreciable extent. All of these factors indicate that although some nominal concentration of the inactivating species is present in the assay for residual enzymatic activity, the rate of inactivation is likely to be immeasurably small.

The olefinic peptide (N-Ac-Phe-Gly) analog, N-Ac-(L)-Phe-Acrylate, has been shown previously by this laboratory to be a potent, time-dependent, turnover-dependent inactivator of PAM via the Dilution Assay. As stated above, this assay is performed by preincubating enzyme and inhibitor in the presence of all cofactors, and then removing aliquots at allotted time points and "diluting" them into an assay solution containing saturating concentrations of substrate and all requisite cofactors followed by incubation for a set time and measurement of residual activity via the amount of product formed. However, the use of this assay with different inhibitor preparations or different enzyme preparations, or simply in the hands of different experimenters, has yielded significantly different results with regard to both the K_I and k_{inact} values from assay to assay. However, the Dilution Assay is typically much more reproducible in specifying the k_{inact}/K_I value (rather than the individual components) for the following two reasons.

First, the values of K_I and k_{inact} are represented by -1/x-intercept and 1/y-intercept, respectively. Therefore, as the k_{inact} value approaches one or greater the error in the value of $1/k_{inact}$ (the y-intercept of the double-reciprocal plot) may begin to approach to value of the y-intercept itself. This error in the y-intercept translates to a correspondingly high error in the x-intercept, from which the value of K_I is determined. Secondly, when the points of the double-reciprocal plot are fitted by regression analysis to the equation of a line the slope and the y-intercept (and the x-intercept) are covariant. However, the slope of the fitted line (equal to the reciprocal of k_{inact}/K_I), because of its hugely greater magnitude relative to the values of the x- and y-intercepts, is affected to a much lesser degree by fluctuations in the data introduced via experimental error. Indeed, the slope is greater than 100 in all cases here while the y-intercepts are all approximately one and the x-intercept values are each less than 0.01.

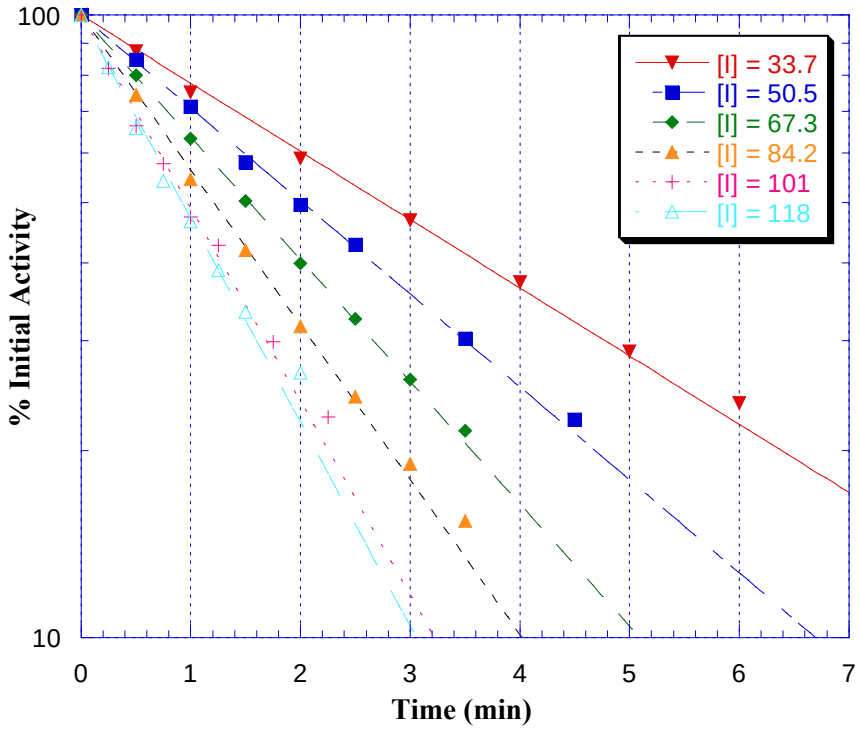

Figure 10. Semi-log Plot of Percent Initial Activity *versus* Time Following Preincubation of PAM with Various Concentrations of N-Ac-(L)-Phe-Acrylic Acid. The slope of each line represents the value for kobs at that inactivator concentration. The reaction is strictly first-order from 30%-100% initial activity and concentration-dependent.

Figure 10 is a plot of log (% initial activity) vs. time, showing that N-Ac-(L)-Phe-Acrylate is a potent concentration and time-dependent inactivator of PAM. The inactivation was strictly first-order, as evidenced by the linearity of the data points, until residual activity dropped below approximately 30%. As the residual activity fell below 30% the plots began to deviate significantly from linearity indicating the possibility that complete elimination of enzyme activity is not possible under the conditions used for these assays. It is, naturally, not reasonable to speculate that as enzyme is inactivated and/or inhibitor is consumed, that the observed rate of inactivation would remain constant

over the entire range of residual activities. Interestingly, the departure from linearity (i.e. a change in the observed rate constant of inactivation) is more marked at higher inhibitor concentrations and begins to develop when residual activities are much higher relative to lower inactivator concentrations.

While this assay (as performed) cannot provide information as to the type of inhibition (competitive, uncompetitive, mixed), previous work in this laboratory (Feng, 2000) has shown that when substrate is present along with inhibitor in the preincubation solution the enzyme is in fact protected from inactivation by the various acrylate derivatives described previously. In addition, inactivation does not occur in the absence of either copper ions (as copper (II) sulfate) or ascorbate, both of which are absolutely required for substrate turnover. These effects, along with others to be described in Progress Curve Assay section, are strongly indicative of competitive inhibition.

A Kitz and Wilson plot of $1/k_{obs}$ vs. 1/[N-Ac-(L)-Phe-Acrylate] (Figure 11) with a weighted linear fit provides the values of both k_{inact} and K_I. All kinetic parameters of each compound are summarized in (Table 1.3.2).

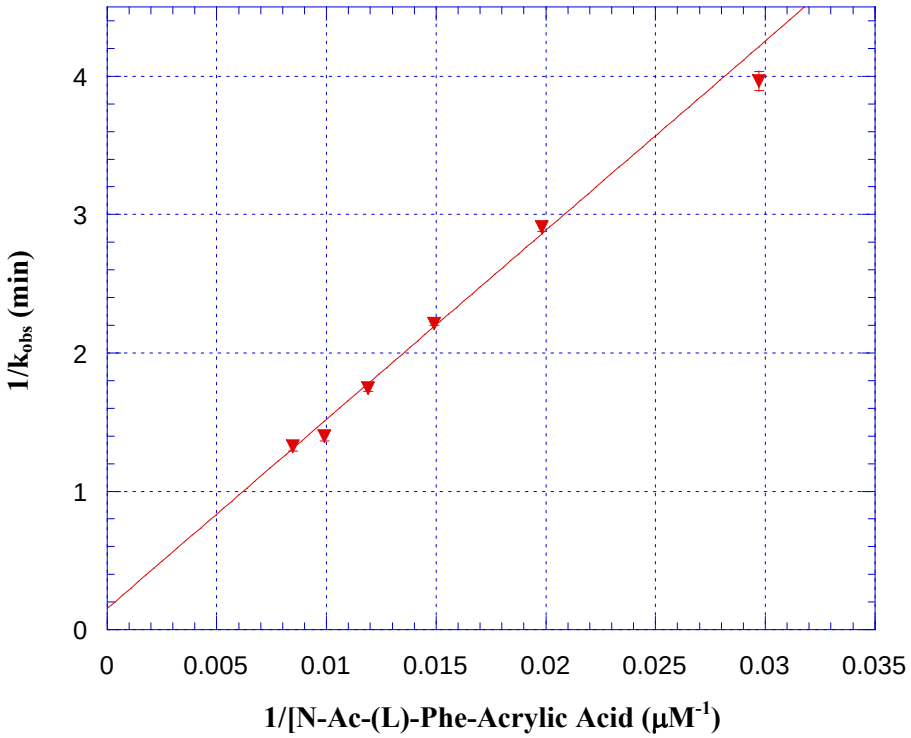

Figure 11. Kitz and Wilson Double-Reciprocal Plot of $1/k_{obs}$ *Vs.* 1/[N-Ac-(L)-Phe-Acrylate. The reciprocal of the slope is equal to k_{inact}/K_I (7.32 ± 0.14 X 10^3 M^{-1} min^{-1})

Previous studies by this lab have demonstrated the absolute stereospecificity of PAM with regard to the spatial orientation of its glycine-extended peptide substrates. Since glycine is prochiral, the stereospecificity with regard to peptide substrates is only material with regard to residues in the P2, P3, etc. positions. Only amino acid residues of absolute (L)-configuration at the P2 position are accepted as substrates by PAM. (Ping, 1992; Ping, 1995) Just as N-Ac-(L)-Phe-Acrylic Acid is an analog of N-Ac-(L)-Phe-Gly, its enantiomer has the same stereoconfiguration as N-Ac-(D)-Phe-Acrylic Acid. Although we assumed that (D)-enantiomer would not be able to bind productively to PAM and result in enzyme inactivation, pure N-Ac-(D)-Phe-Acrylic Acid was

synthesized and incubated with PAM in both the Progress Curve and Dilution assays in order to determine if the trans-alkene functionality and/or lack of the amide nitrogen in the acrylate inactivators would serve to maintain or degrade this stereospecificity.

Contrary to expectations, the (D)-enantiomer not only evinced measurable inactivation but did so on a level comparable to that of the (L)-enantiomer. Percent initial activity versus time is plotted in Figure 12. The Kitz and Wilson plot is shown in Figure 13. The k_{inact}/K_I values for the (L) and (D)-enantiomers, respectively, are 7,300 and 4,100 μM^{-1} min^{-1}, less than a 2-fold difference in efficacy. Compare the above results with the Phe-Acrylate enantiomeric pair with previous results for the N-Ac-Phe-Gly enantiomeric pair and, because N-Ac-(D)-Phe-Gly is not a substrate at all, the measured apparent K_I values for both N-Ac-(L)-Phe-Gly and N-Ac-(D)-Phe-Gly when tested in the presence of another substrate, differed by nearly three orders of magnitude.

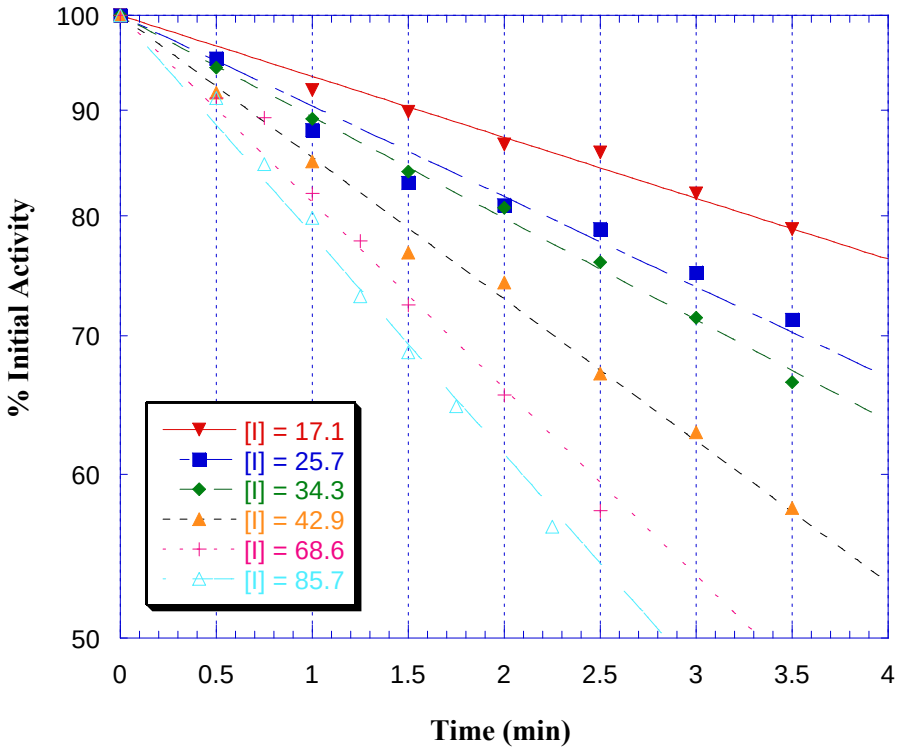

Figure 12. Semilog Plot of Percent Initial Activity *versus* Time Following Preincubation of PAM with Various Concentrations of N-Ac-(D)-Phe-Acrylic Acid. The slope of each line represents the value for k_{obs} at that inactivator

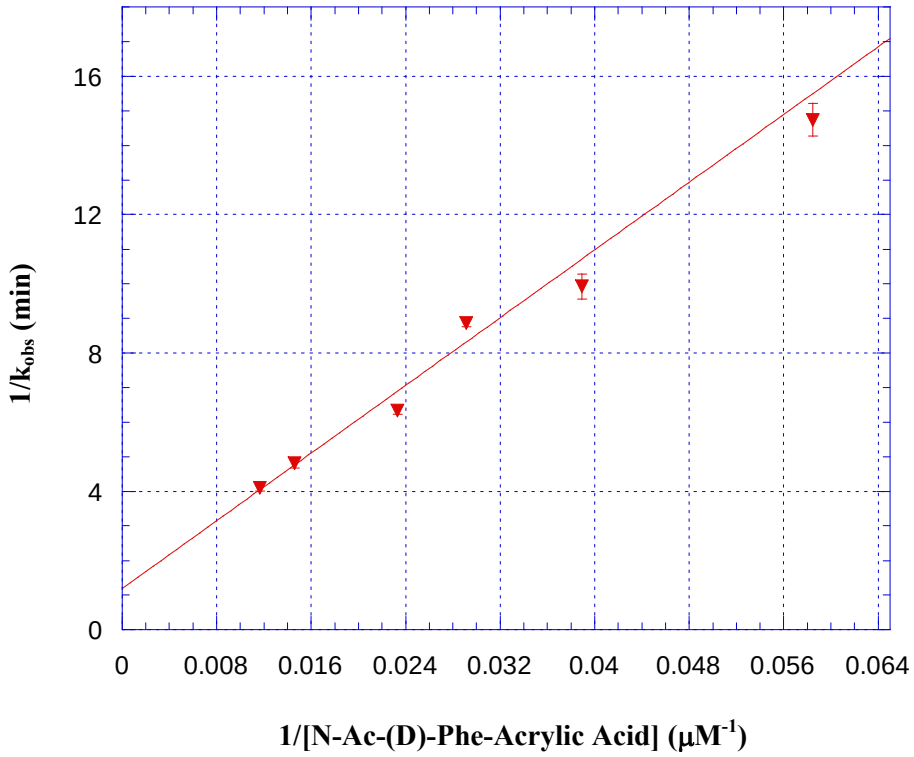

Figure 13. Kitz and Wilson Double-Reciprocal Plot of $1/k_{obs}$ *Versus* 1/[N-Ac-(D)-Phe-Acrylate]. The reciprocal of the slope is equal to k_{inact}/K_I (4.09 ± 0.10 X 10^3 M^{-1} min^{-1}).

Previous work in this lab with the pure enantiomer N-Ac-(L)-Thienyl-Acrylate indicated that sulfur-containing analogs were able to bind more avidly to the PAM active site than derivatives lacking a potential copper-binding sulfur-containing moiety. K_I values for the (L)-Thienyl derivative were approximately 3-fold lower than that of the (L)-Phe derivative (32 and 90 μM, respectively). On the other hand, the k_{inact} values for the (L)-Thienyl compound were approximately one-half those of the (L)-Phe derivative (1.1 and 0.56 min^{-1}, respectively), suggesting that while the potential copper-ligating (L)-Thienyl compound may indeed bind more avidly to PAM, a concomitant slowdown in the

rate of inactivation may indicate that the very act of copper ligation, unsurprisingly, interferes in some regard with the inactivation mechanism. It is evident from the PAM crystal structure (Prigge, 1997) that any ligand which does engage and ligate to Cu_B cannot concurrently occupy the space in the hydrophobic picket of the enzyme which the benzyl moiety of N-Ac-(L)-Phe-Gly occupies. The amino acid methionine contains a sulfur atom which is γ–positioned relative to Cα, and as such is in the same relative position as the sulfur atom in the Thienyl derivatives, but which lacks the aromaticity of the thienyl derivative. Moreover, the terminal methyl group of the methionyl side chain would correspond to the 3' carbon of the thienyl ring. Therefore, with regard to sterics, the two compounds should behave in much the same regard. Electronically, thiophene is an electron-rich aromatic compound and the sulfur therein is a "harder" ligand than the sulfur in the thioether moiety of methionine. All else being equal, the (L)-Thienyl derivative should bind more strongly to Cu_B (if in fact it ligates the copper atom at all) than the (L)-Met derivative. As such, we reasoned that any loss in binding affinity for the (L)-Met derivative might be compensated via an increase in the k_{inact} value.

Percent initial activity *versus* time is plotted in Figure 14. The Kitz and Wilson plot is shown in Figure 15. As the results indicate, the (L)-Met derivative was the most potent PAM inactivator of the three derivatives tested in the present dilution assays (k_{inact}/K_I = 8.14 M^{-1} min^{-1}), intermediate in potency between the (L)-Phe derivative and the previously investigated (L)-Thienyl derivative (Feng, 2000). Insofar as the (L)-Thienyl analog has a bulkier side chain (than Met) and is aromatic to boot (very similar in these regards to the (L)-Phe derivative), one could reason that the energy difference between the (L)-Thienyl and the (L)-Phe analogs may be due almost entirely to the gain in binding

energy of the sulfur/copper ligation less the loss of the aromatic hydrophobic associations in the P2 enzyme pocket. Owing to previously mentioned difficulties in separating the individual kinetic components in the Dilution Assay (K_I and k_{inact}), one cannot really make any pertinent observations regarding the actual effects of any sulfur ligation or changes in side chain composition on the relative binding strengths or inactivation rates of the individual kinetic components. The Progress Curve Assay, which allows all possible kinetic elements of the inactivation process to be determined in one assay, will be described next and serve to elucidate the individual component values of k_{inact}/K_I.

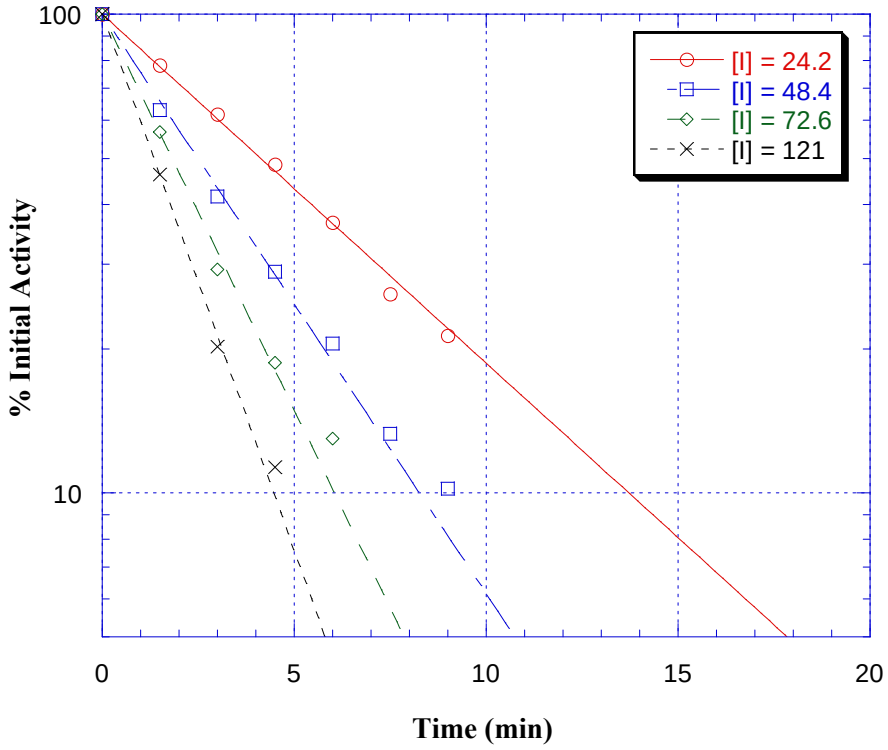

Figure 14. Semi-log Plot of Percent Initial Activity *versus* Time Following Preincubation of PAM with Various Concentrations of N-Ac-(L)-Met-Acrylic Acid. The slope of each line represents the value for kobs at that inactivator concentration. The reaction is strictly first order from 30%-100% initial activity and concentration-dependent.

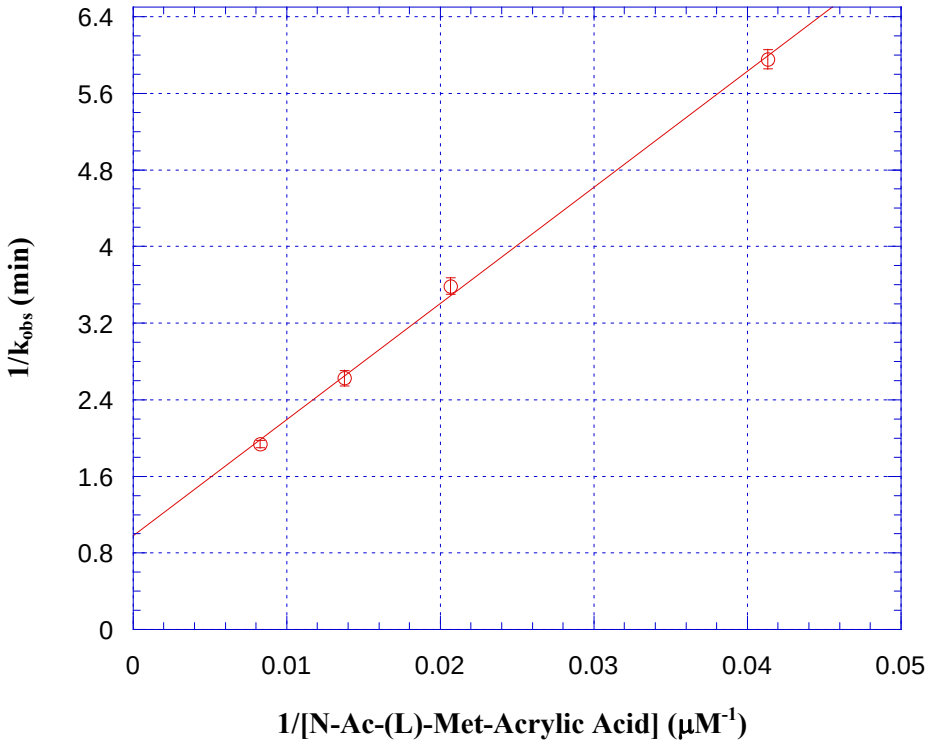

Figure 15. Kitz and Wilson Double-Reciprocal Plot of 1/kobs *Versus* 1/[N-Ac-(L)-Met-Acrylate]. The reciprocal of the slope is equal to k_{inact}/K_I (8.14 ± 0.21 X 10^3 M^{-1} min^{-1}).

Progress Curve Assay

The Progress Curve Assay (PCA), also known, *inter alia*, as the Product Formation Assay, has several benefits over the Dilution Assay, along with one glaring deficiency. Firstly, the PCA is performed in the presence of varying concentrations of both substrate and inhibitor which allows for a more reasonable approximation of the environment that would be seen with the drug candidate in *in vivo* experiments (recall that the inactivation process in the Dilution Assay takes place in the ABSENCE of substrate). Secondly, ALL kinetic parameters (save for the enzyme/substrate constants k_2 and K_m) may be obtained

via the PCA, including K_I', k'_2 and k'_{inact}, which represent inactivator binding to the ES complex (to form the ternary ESI complex), conversion of the ESI complex to the inactivator/enzyme complex and product (EI + P), and the conversion of the ESI complex to an inactivated enzyme complex (ESI^*), respectively (Figure 9). The rate constant k_2 and the Michaelis constant K_m must be obtained from a separate assay involving only enzyme, substrate, and requisite cofactors. The downside to the PCA *vis-à-vis* the Dilution Assay lies in the potential magnification of experimental error throughout all of the replots of the original data. Furthermore, owing to the discontinuous nature of this assay, it is simply not possible to perform the entire assay on any given day with one enzyme substock. Instead, the assay is typically broken up over the course of 5 days (one day for each substrate concentration) which requires the use either of a freshly prepared enzyme substock or the use of the previous day's substock less any activity lost overnight. Either way, extra error is introduced into this assay relative to the dilution assay which is performed all at once with a given substock of enzyme solution and under identical environmental (laboratory) conditions (temperature, relative humidity, ambient molecular oxygen concentration, pressure, etc.). That having been said, a well-performed PCA returns more precise results with a smaller associated degree of error, and with a more exhaustive treatment of all possible inactivation events in the enzyme/substrate/inactivator system, than does the Dilution Assay.

The N-Ac-Phe-Gly substrate analog N-Ac-(L)-Phe-Acrylate had previously been synthesized and assayed by both the PCA and Dilution Assays in this laboratory. However, because we were seeking to compare the kinetic parameters of the enantiomeric pair of the N-Ac-Phe-Acrylates the L-enantiomer was resynthesized and subjected to both kinetic assays (PCA and Dilution) such that all compounds tested could be analyzed with the same enzyme preparation.

The PCA is initiated when an enzyme aliquot is added to a solution of assay mix containing varying levels of substrate and inactivator and fixed concentrations of the cofactors ascorbic acid and Cu(I). Aliquots are then removed periodically from the assay mix, quenched with 10% v/v 3M $HClO_4$, and the product concentration at each time point quantified by RP-HPLC based on previously performed standard curves. Each initial plot (Figure 16) of product concentration vs. time is representative of one fixed concentration of substrate, with each of the progress curves representing a varying concentration of N-Ac-(L)-Phe-Acrylate. When the data are fit to the equation ($[P] = [P]_{inf}(1-e^{-kt})$), both k_{obs}, the observed rate constant of inactivation at a given concentration of substrate and inactivator, and $[P]_{inf}$, the product concentration at time infinity, are obtained.

What follows mathematically is a divergent series of replots and secondary replots, one stemming from the $[P]_{inf}$ values to ultimately yield the value of k_{inact}/K_I and the other stemming from the k_{obs} values to ultimately yield the value of K_I. Although the slope of the line which provides the k_{inact}/K_I value is, like that in the Kitz and Wilson plot of the Dilution Assay, covariant with regard to those two kinetic parameters, the gamma plot provides the value of K_I directly (reciprocal slope) with a very small relative error. Therefore, since both k_{inact}/K_I and K_I itself are expressed as parameters independent of

each others values, and obtained from different data transformations (from P_{inf} and k_{obs}, respectively), we can state with confidence the value of k_{inact}, even though unlike K_I it is not specifically enumerated as "its own value" by this assay.

As mentioned above, replots involving the P_{inf} values obtained from curve-fitting of the initial HPLC data ultimately lead to the value of k_{inact}/K_I. The first replot is of P_{inf} vs. 1/[I] (Figure 17). Each line is representative of a constant substrate concentration with varying concentrations of inactivator. Immediately evident is the convergence of all lines at the origin indicating that, at any given substrate concentration, as the concentration of N-Ac-(L)-Phe-Acrylic Acid approaches infinity the final product concentration will approach zero, let the reaction be allowed to continue so long as it will. So, as the concentration of inactivator becomes sufficiently high no product will ever be formed at finite substrate concentrations. The y-intercept of this plot is, when numerator and denominator are multiplied through by K_I*K_I', represented by the following expression:

$$\text{y-intercept} = (k_2'/K_I'[E]_o[S])/(k_{inact}K_m/K_I') + (k'_{inact}[S]/K_I')$$

Since the y-intercepts of all of the lines are clearly equal to zero, that means that either the numerator of the above expression is equal to zero, or the denominator approaches infinity, or both. In the first case, supposing the numerator of the above is equal to zero provides the following equation:

$$0 = (k_2'/K_I'[E]_o[S])$$

Since $[E]_o$, and [S] are both, obviously, representative of nonzero values, the value of k_2' must either approach or equal zero or the value of K_I' must approach infinity, or both. In the second case, were the denominator to approach infinity the expression would read:

$$\infty = (k_{inact}K_m/K_I') + (k'_{inact}[S]/K_I)$$

So, either the expression $k_{inact}K_m/K_I'$ or $k'_{inact}[S]/K_I$ must approach infinity, or both. Clearly the terms k_{inact}, K_m, K_I, and [S] are not infinite. That means that either k'_{inact} must approach infinity or K_I' must approach zero, or both. It is obvious from the assays that k'_{inact} does not approach infinity because product is formed at each concentration of substrate and inactivator. If k'_{inact} approached infinity, no product would be formed under any of the assay conditions described herein. Since k'_{inact} is not infinite, then for the above expression to approach infinity, K_I' must approach zero. This would obviously lead to a nonsensical situation where the EI complex would not be formed at all and all inactivation would take place via the ESI intermediate complex alone (with a rate constant of k'_{inact}.. But from the Dilution Assay, we know clearly, since substrate is absent from that reaction mixture, that any inactivation which occurs must proceed through the EI complex. Moreover, previous research has shown, and the research presented herein clearly demonstrates, that increasing the concentration of substrate in the Progress Curve Assay actually reduces the observed rate constant of inactivation (k_{obs}), and the inclusion of substrate in the incubation mixture of the Dilution Assay protects PAM from inactivation by the various acrylate compounds. All of these lines of argument show clearly that the denominator of the above equation cannot approach

infinity. Therefore, the numerator must be equal to zero and the value of k_2'/K_I' must approach zero. In this case, it is very likely that k_2' is equal to zero and that the value of K_I' approaches infinity. In terms of mechanistic implications, this means that even if the ESI complex forms to some infinitesimal concentration no product will be formed and the concentration of substrate would remain unchanged.

The subsequent replot of reciprocal slope from Figure 17 vs. reciprocal substrate concentration (TNP-YVG) is shown in Figure 18. As with the lines in the previous plot, it is immediately evident that the line passes through the origin, with a y-intercept value of zero. The y-intercept of the plot is represented by the following expression:

$$\text{y-intercept} = k'_{inact}/K_I'k_2[E]_o$$

Since the line passes through the origin and the y-intercept is thusly zero, it is clear from the above expression that either k'_{inact} approaches zero or that the denominator approaches infinity, or both.. If the denominator approaches infinity, then since, experimentally, neither k_2 nor $[E]_o$ is infinite, it must be K_I' which is infinite. Again, as shown above with the previous replot, all lines of reasoning indicate that k'_{inact} approaches zero and K_I' approaches infinity. So, since k_2' and k'_{inact} are both zero and K_I' approaches infinity (or is extremely large relative to K_I) the ESI complex does not form to any appreciable extent. To the limited extent that it may form, no product formation or enzyme inactivation may take place from the ESI complex. The slope of the line in this figure is represented by the following equation:

Slope = $k_{inact}K_m/K_Ik_2[E]_o$

Recall that $k_2[E]_o$ is equal to V_{max}. The values of K_m and V_{max} are known from a prior experiment plotting rate vs. concentration of substrate. Since the ratio of enzyme used in the progress curve assay vs. that used in performing Michaelis-Mentin kinetics is known, we can use this ratio and the value of V_{max} (along with the K_m value) to determine the value of k_{inact}/K_I. Further below, the replots involving k_{obs} values obtained from the original data will yield a value for K_I alone. Once K_I is known, the value of k_{inact} can be obtained from k_{inact}/K_I given here.

A plot of $1/k_{obs}$ vs. 1/[N-Ac-(L)-Phe-Acrylic Acid] is shown in Figure 19. Each line represents various inactivator concentrations at a fixed concentration of substrate. The slope of each line varies, but all lines converge at the same positive y-intercept value. This indicates that the observed rate constants of inactivation (k_{obs}), for all substrate concentrations around the K_m value, will converge at the same value as inactivator concentrations are increased toward infinity. Also, the denominator for the y-intercept in this figure is identical to that of the denominator from Figure 18. Since the y-intercept value for the $1/k_{obs}$ vs. 1/[N-Ac-(L)-Phe-Acrylic Acid] plot is not zero, this indicates that the expression k'_{inact}/K_I' approaches zero AND NOT INFINITY as was a possibility from the evaluation of the y-intercept from Figure 18. Therefore, this proves that k_2' is zero and indicates that k'_{inact} is also zero. Again, there is no indication that K_I' has a finite value. Therefore, either the ESI complex is not formed at all or if it is formed to some trivial extent, no product formation or inactivated ESI^* complex is formed. This eliminates all possible pathways of mechanistic inactivation save for via the EI complex.

Finally, the ratio γ, of y-intercept/slope from Figure 19**,** is plotted vs. [S]/[S] + K_m in Figure 20 where the value of K_m has been determined via Michaelis-Mentin kinetics performed in a separate assay (the same used to obtain V_{max} above). The y-intercept of this line is equal to $1/K_I$ and the slope is equal to $1/K_I' - 1/K_I$. Since we have shown that the value of K_I' likely approaches infinity, the value of $1/K_I'$ should approach zero and therefore the slope of the line of this figure should be equal in absolute value to that of the y-intercept. Although some small deviation is evident between the absolute values of the slope and the y-intercept, this is likely more indicative of experimental error propagating though the replot and secondary replot than of an actual non-infinite value for K_I'. The inverse of the y-intercept, since it represents K_I alone, was used to determine the value of K_I for N-Ac-(L)-Phe-Acrylic Acid.

In addition to N-Ac-(L)-Phe-Acrylic Acid, the two derivatives N-Ac-(D)-Phe-Acrylic Acid (the enantiomer) and N-Ac-(L)-Met-Acrylic Acid were subjected to kinetic analysis via the Progress Curve Assay. Both followed the well-behaved kinetics seen above with the L-enantiomer and proceed through the same inactivation mechanisms. In neither case do any of the kinetic parameters of the results indicate that the inhibition is anything other than strictly competitive, and does not proceed via any other mechanism than direct inactivation of the EI complex. The Progress Curve Assay plots for N-Ac-(D)-Phe-Acrylate are displayed in Figures 21 through Figure 25 below, and for N-Ac-(L)-Met-Acrylate in Figures 26 to 30. All pertinent kinetic parameters and values are collected for comparison in Table 1.2.1.

A Hanes-Woolf plot of [S]/v *versus* [S], under the same conditions of cofactors and buffers as used in the Progress Curve Assays, is presented in Figure 31**.** In this

experiment, both potassium iodide (KI) and Triton X-100 were included in the incubation mixture. Figure 32 is a Hanes-Woolf plot of [S]/v *versus* [S] where neither potassium iodide (KI) nor Triton X-100 were added to the assay mixture. It is evident from the results of both of the above that the inclusion of these two components results in a significantly lower K_m value (1.34 μM vs. 10.1 μM without KI or Triton X-100) with a concomitant, and proportional, decrease in the value of V_{max} (0.074 μM/min vs. 0.84 μM/min without), each value changed by approximately a factor of ten. Owing to the fact that $V_{max} = k_2[E]_o$, and that the portion of the expression $k_{inact}K_m/K_Ik_2[E]_o$ which must be obtained via the separate Michaelis-Menten assay is $K_m/k_2[E]_o$, and substituting V_{max} for $k_2[E]_o$ yields K_m/V_{max}, the resulting value of k_{inact}/K_I is not significantly different (factor of 1.5) whether these parameters are used from the results of one K_m determination vs. the other. The results presented herein use the data from the K_m assay which includes potassium iodide (KI).

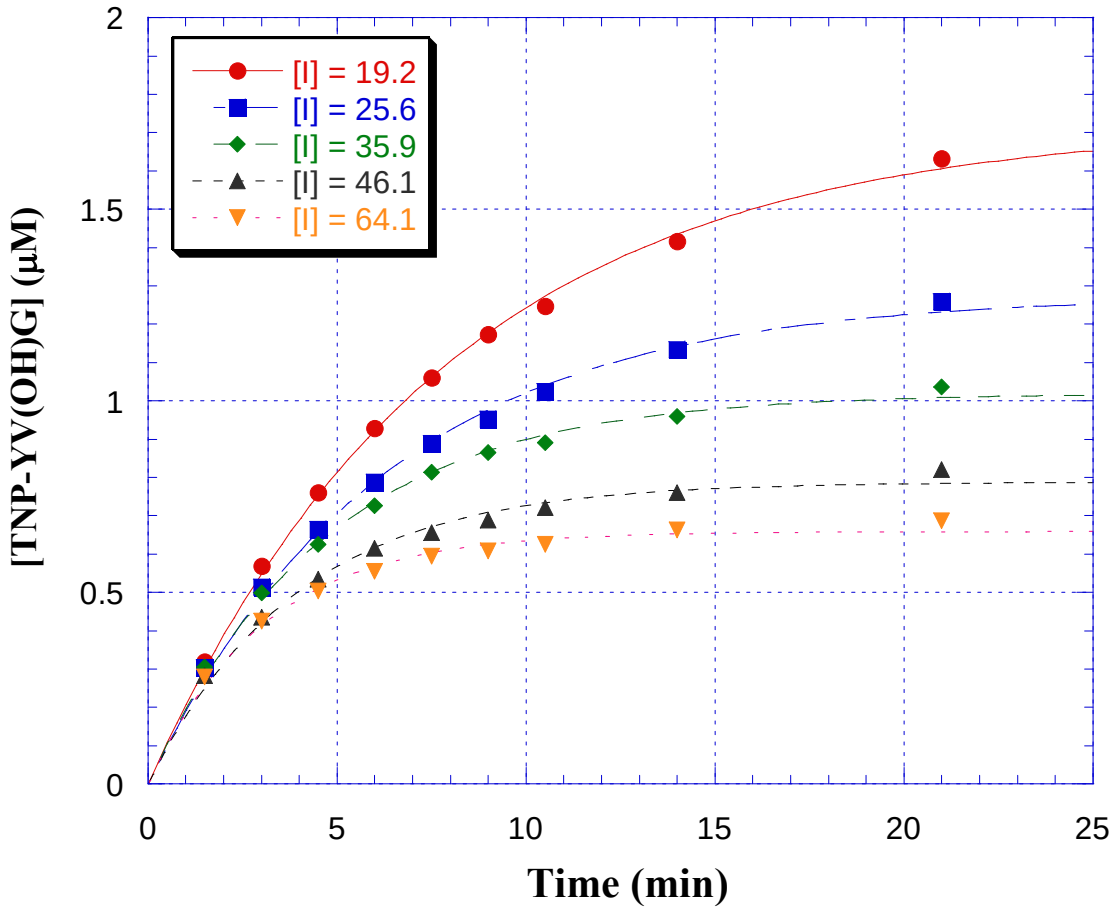

Figure 16. Product Concentration *versus* Time At Various Concentrations of N-Ac-(L)-Phe-Acrylate at Fixed [TNP-YVG] (5.86 µM). The values of $[P]_{inf}$ and k_{obs} were obtained using iterative computer analysis to fit data to the equation $[P] = [P]_{inf}(1-e^{-kt})$ where $k = k_{obs}$.

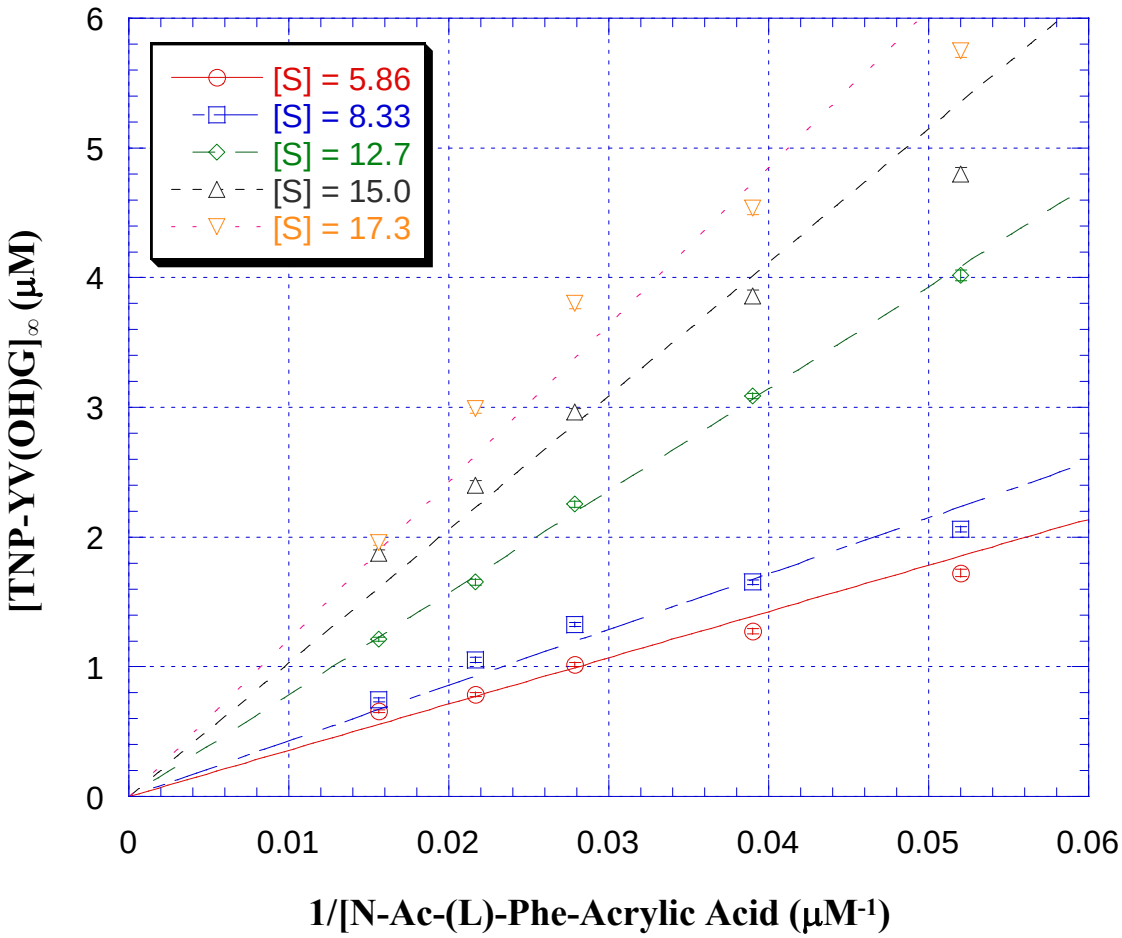

Figure 17. Plot of $[TNP\text{-}YV(OH)G]_{\infty}$ *versus* 1/[N-Ac-(L)-Phe-Acrylate] at Various [TNP-YVG]. Linear regression of the data yields five lines passing through the origin.

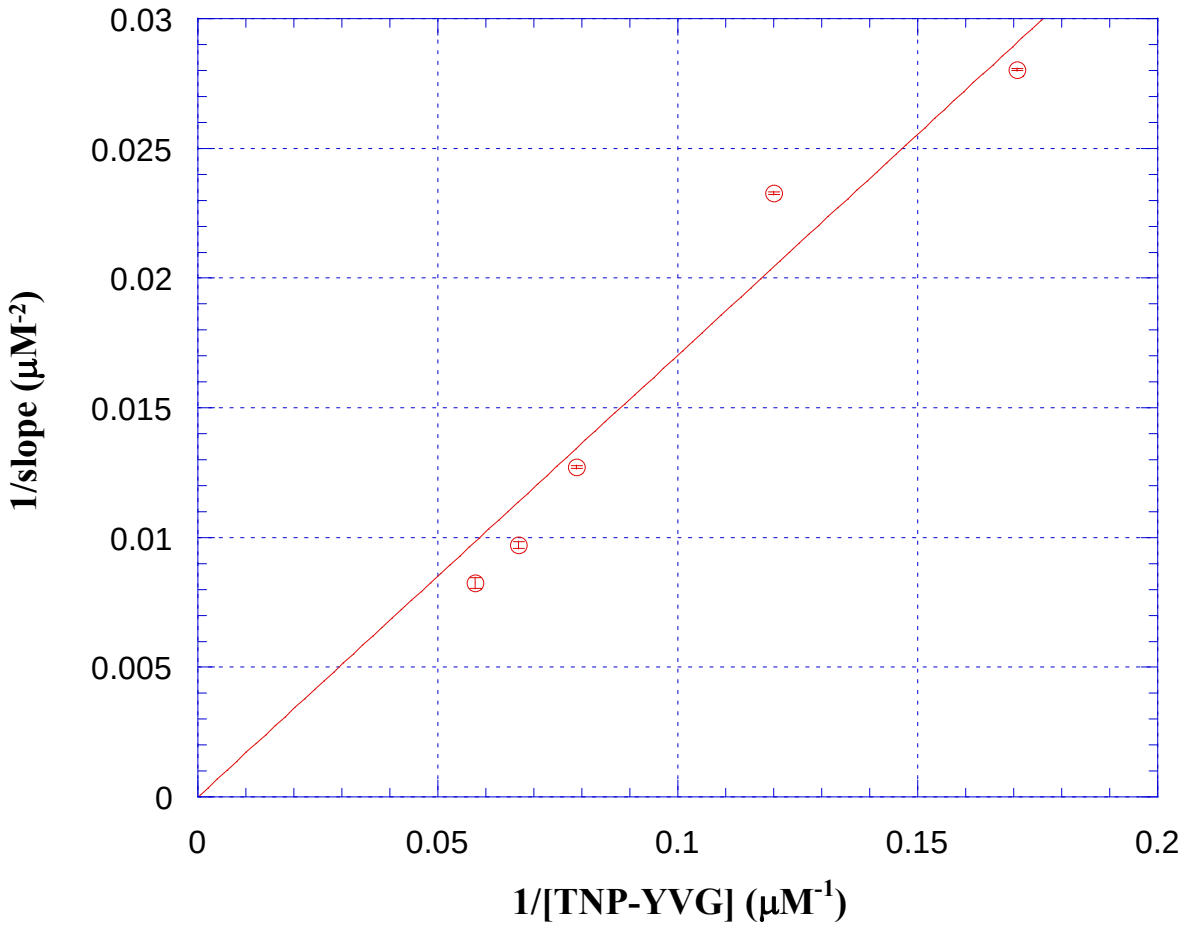

Figure 18. Plot of 1/slope (from Figure 1.3.14) *versus* 1/[TNP-YVG]. Linear regression yields a straight line which passes through the origin. The slope of the line is equal to $k_{inact}K_m/K_Ik_2[E]_0$. k_{inact}/K_I = 7080 M-1 min-1.

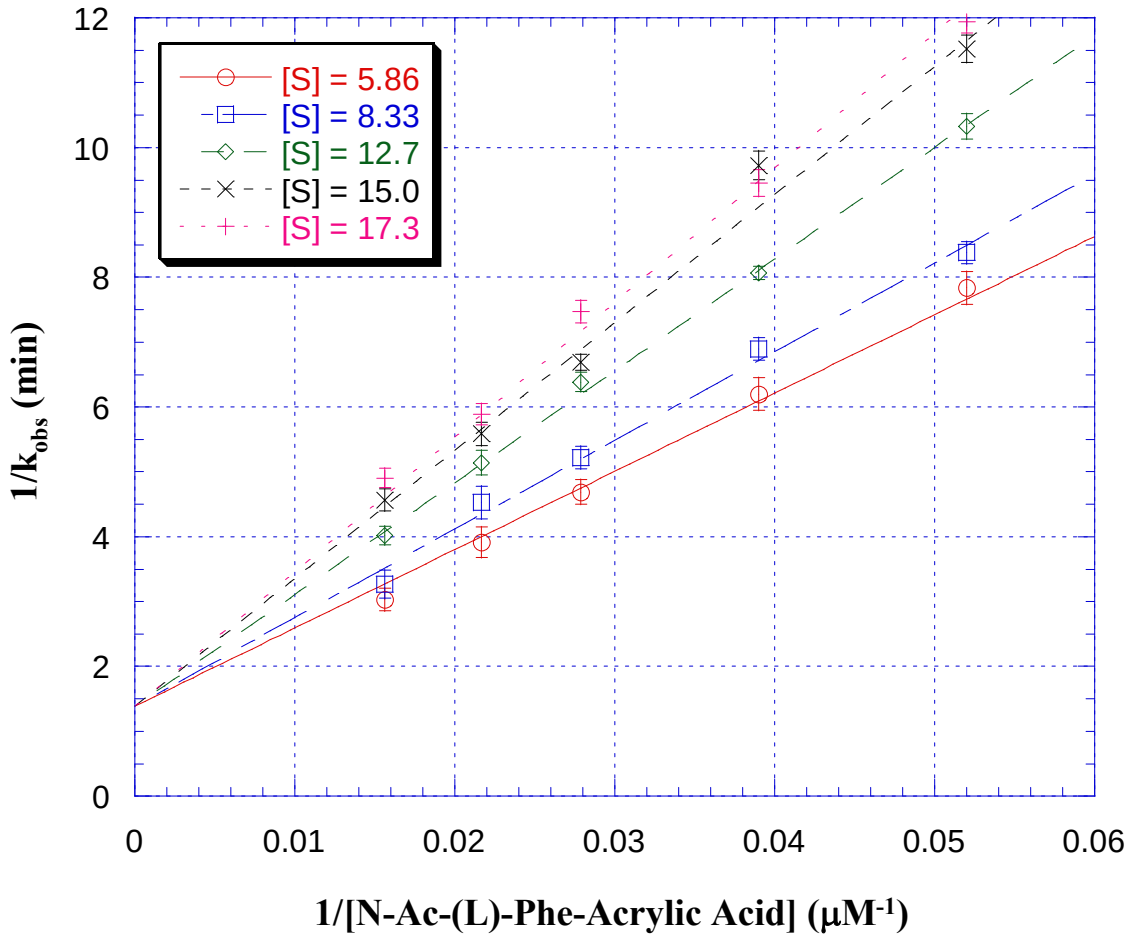

Figure 19. Plot of $1/k_{obs}$ *versus* 1/[N-Ac-(L)-Phe-Acrylate] at Various Fixed Substrate Concentrations. Linear regression yields five straight lines with the same y-intercept value.

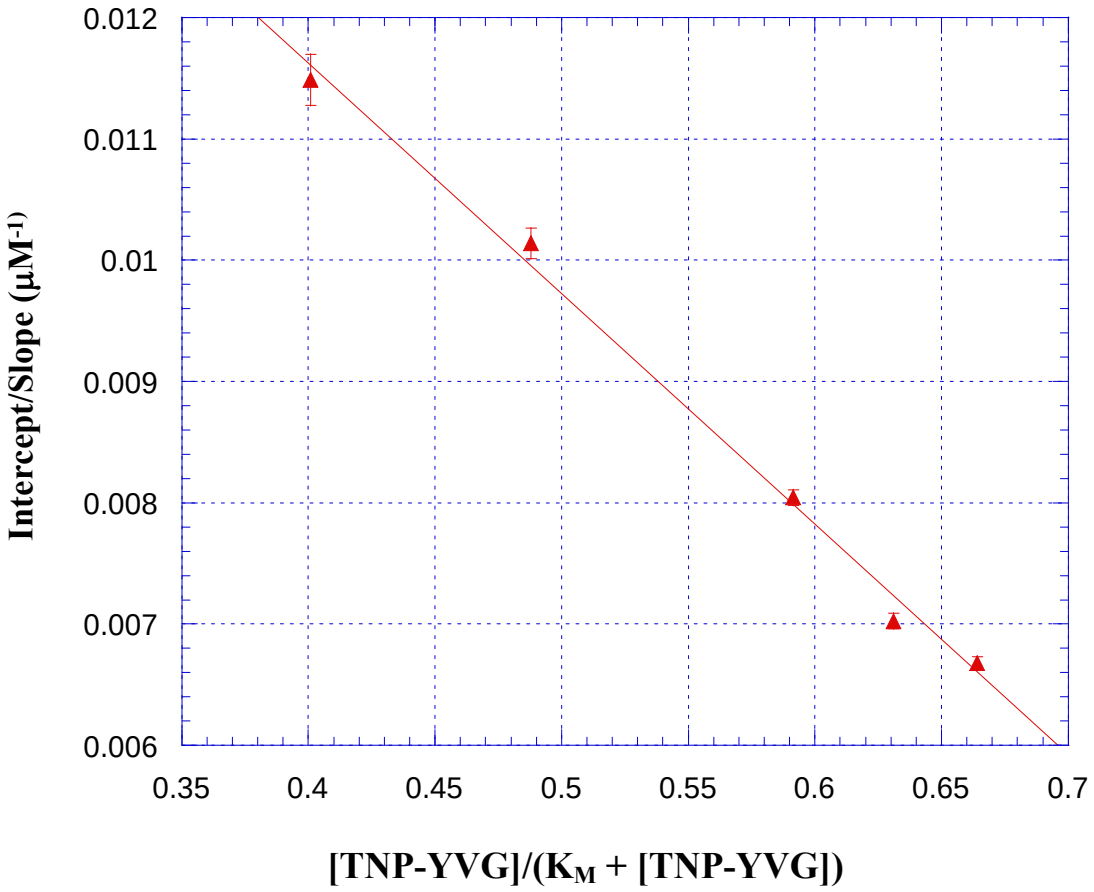

Figure 20. Ratio of Intercept/Slope from Figure 1.3.16 *Vs.* [TNP-YVG]/(K_m + [TNP-YVG]). Assuming K_I' approaches infinity, K_I = 1/y-intercept = 53.7 μM.

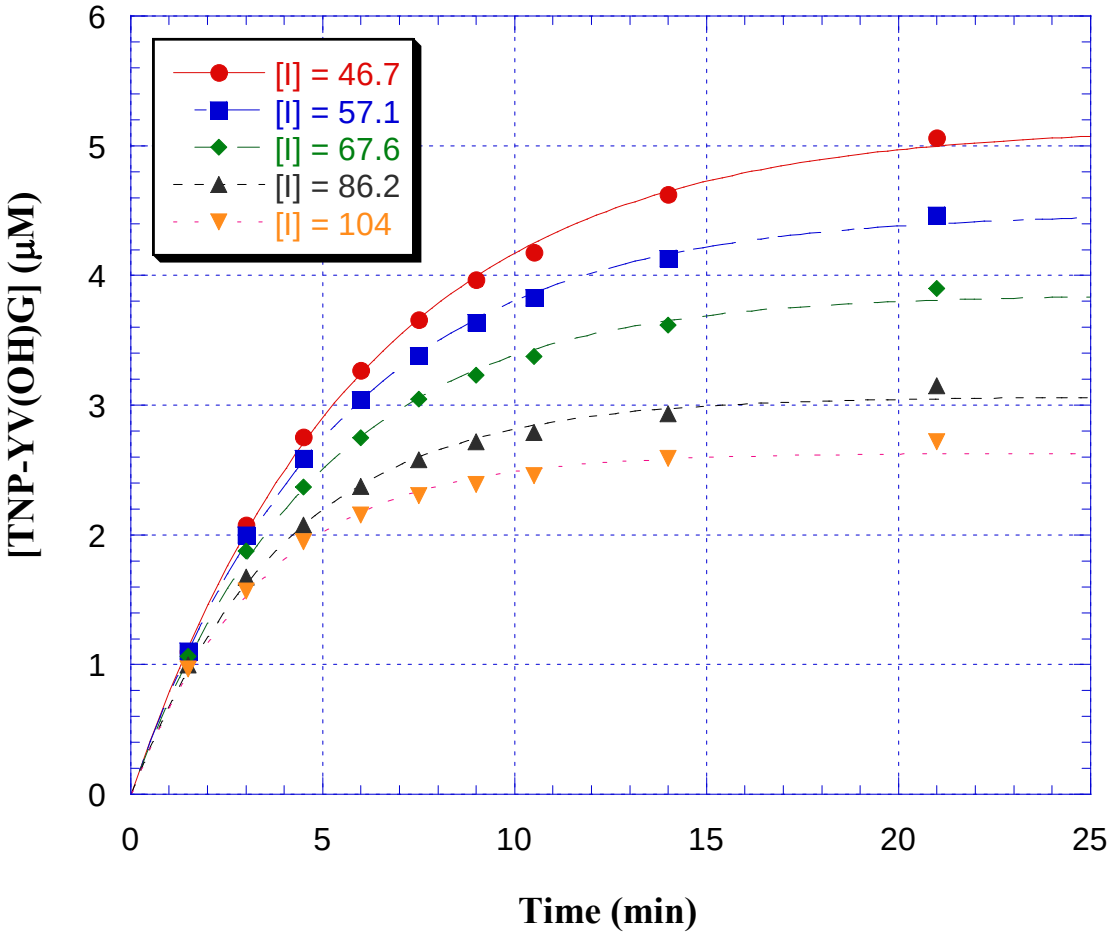

Figure 21. Product Concentration *versus* Time At Various Concentrations of N-Ac-(D)-Phe-Acrylate at Fixed [TNP-YVG] (18.4 µM). The values of $[P]_{inf}$ and k_{obs} were obtained using iterative computer analysis to fit data to the equation $[P] = [P]_{inf}(1-e^{-kt})$ where $k = k_{obs}$.

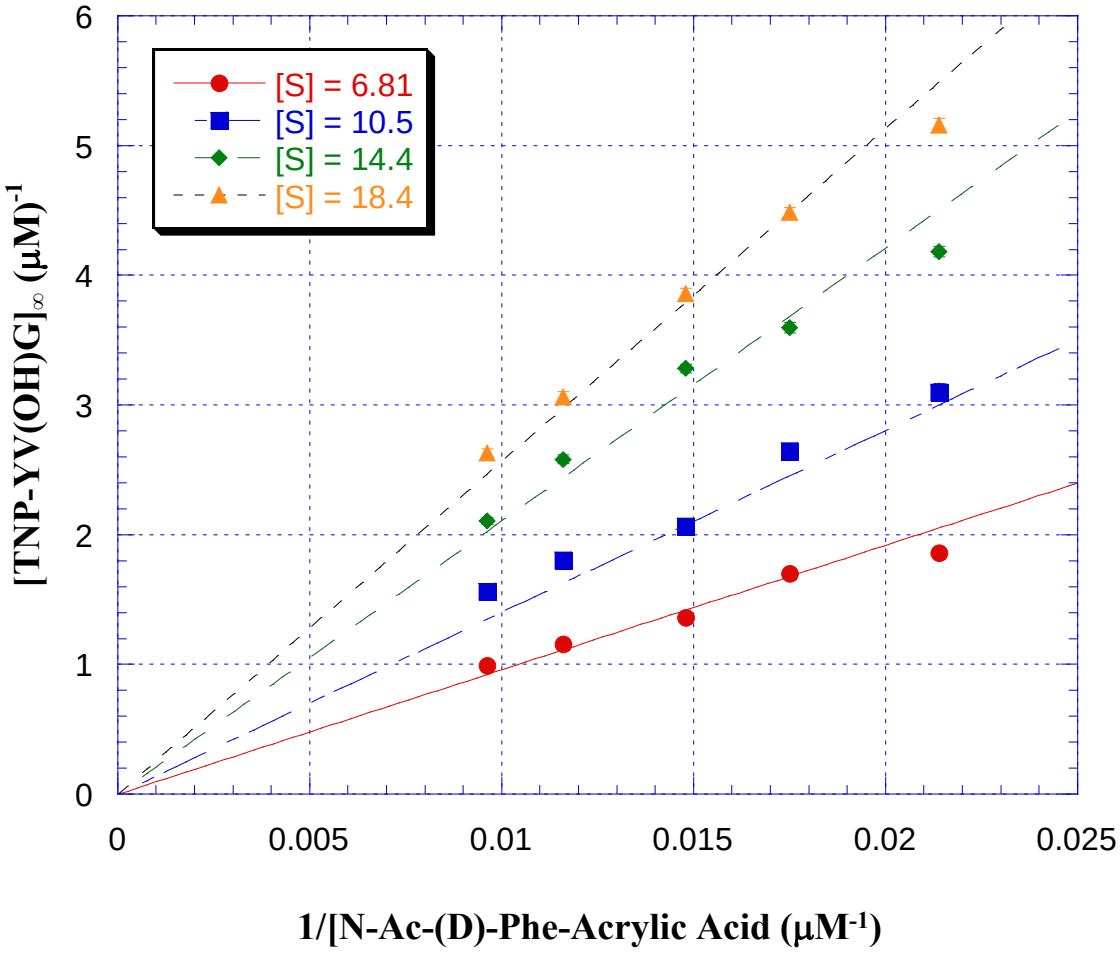

Figure 22. Plot of $[TNP\text{-}YV(OH)G]_{\infty}$ *vs.* 1/[N-Ac-(D)-Phe-Acrylate] at Various [TNP-YVG]. Linear regression of the data yields four lines passing through the origin.

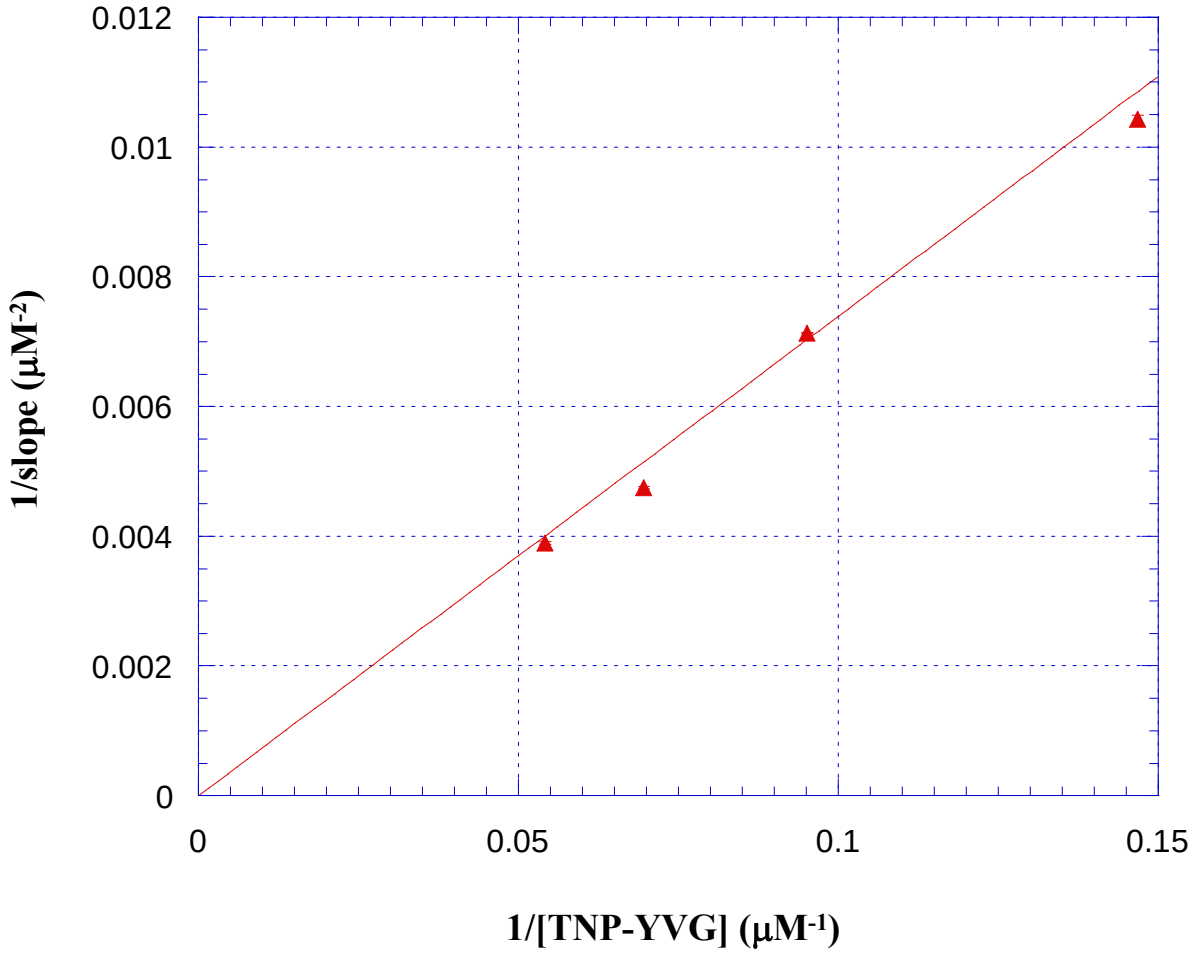

Figure 23. Plot of 1/slope (from Figure 1.3.19) *versus* 1/[TNP-YVG]. Linear regression yields a straight line which passes through the origin. The slope of the line is equal to $k_{inact} K_M/K_I k_2[E]_o$. k_{inact}/K_I = 3090 $M^{-1}min^{-1}$

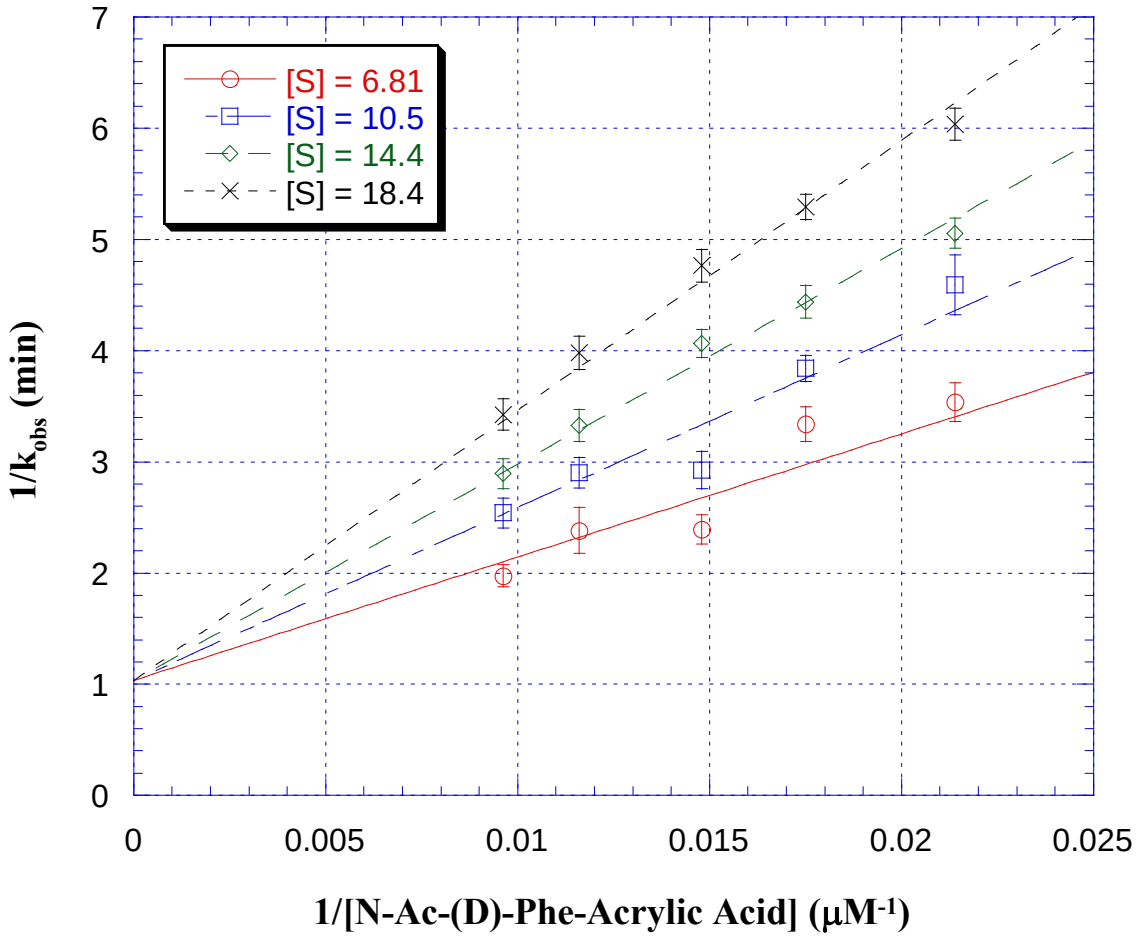

Figure 24. Plot of $1/k_{obs}$ *versus* 1/[N-Ac-(D)-Phe-Acrylate] at Various Fixed Substrate Concentrations. Linear regression yields four straight lines with the same y-intercept value.

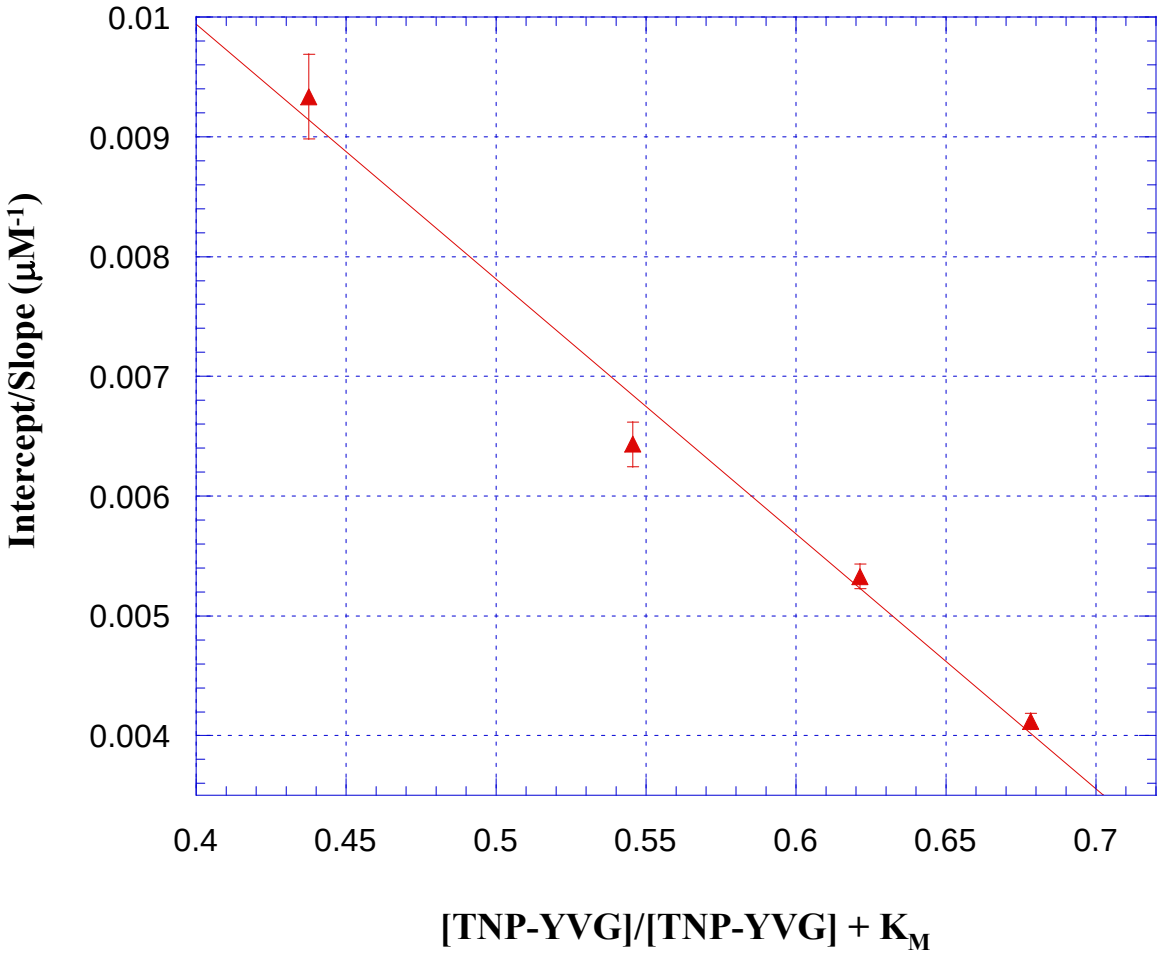

Figure 25. Ratio of Intercept/Slope from Figure 1.3.22 *Versus* [TNP-YVG]/(Km + [TNP-YVG]). Assuming K_I' approaches infinity, K_I = 1/y-intercept = 60.0 μM.

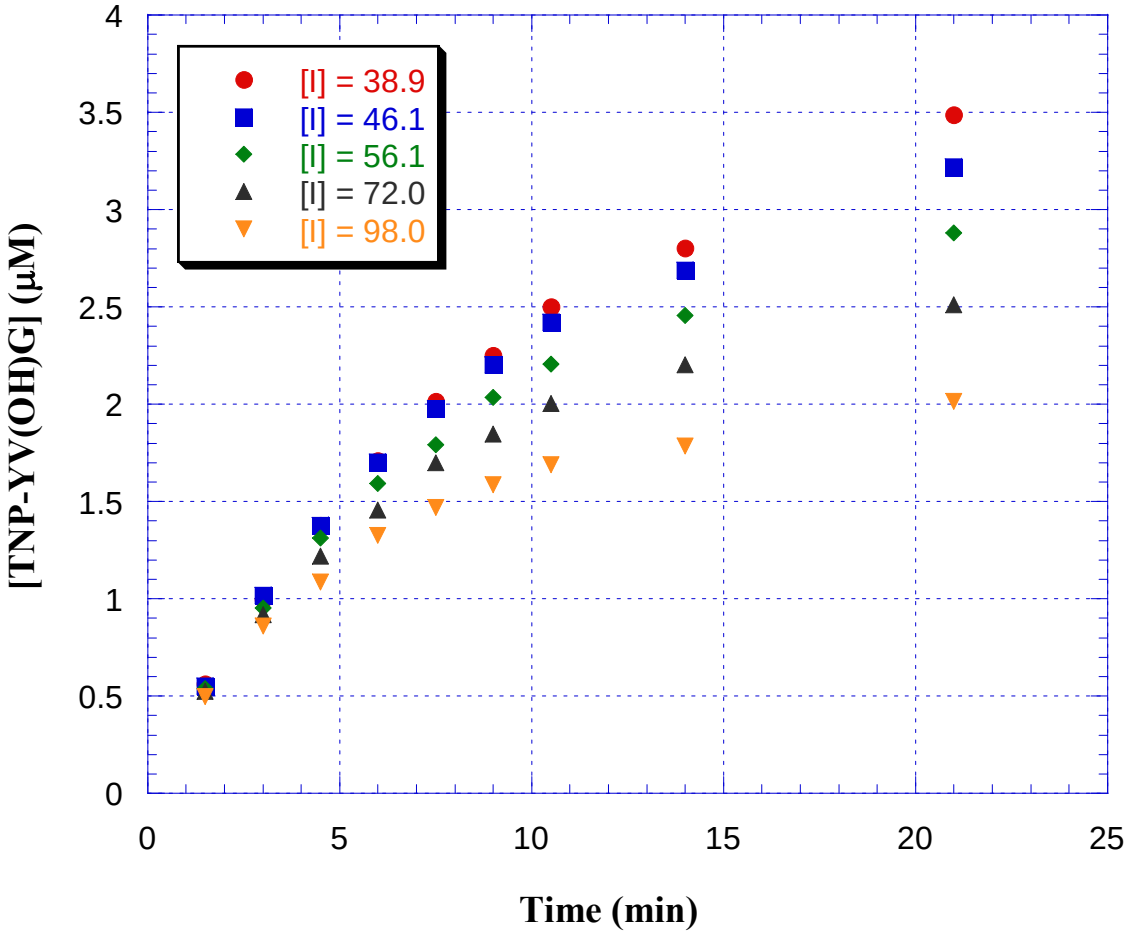

Figure 26. Product Concentration *versus* Time At Various Concentrations of N-Ac-(L)-Met-Acrylate at Fixed [TNP-YVG] (8.82 µM). The values of $[P]_{inf}$ and k_{obs} were obtained using iterative computer analysis to fit data to the equation $[P] = [P]_{inf}(1-e^{-kt})$ where $k = k_{obs}$.

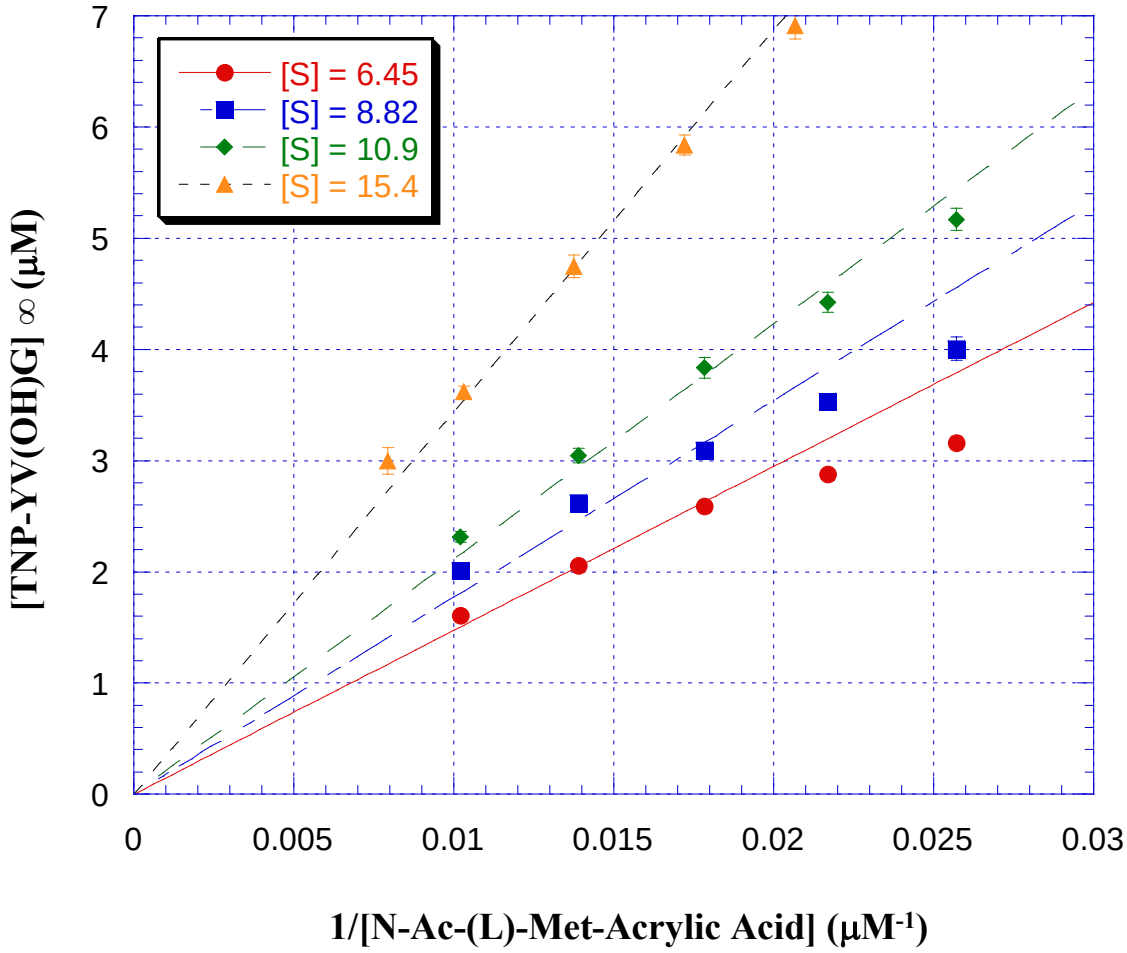

Figure 27. Plot of $[TNP\text{-}YV(OH)G]_{inf}$ *versus* 1/[N-Ac-(L)-Met-Acrylate] at Various [TNP-YVG]. Linear regression of the data yields four lines passing through the origin.

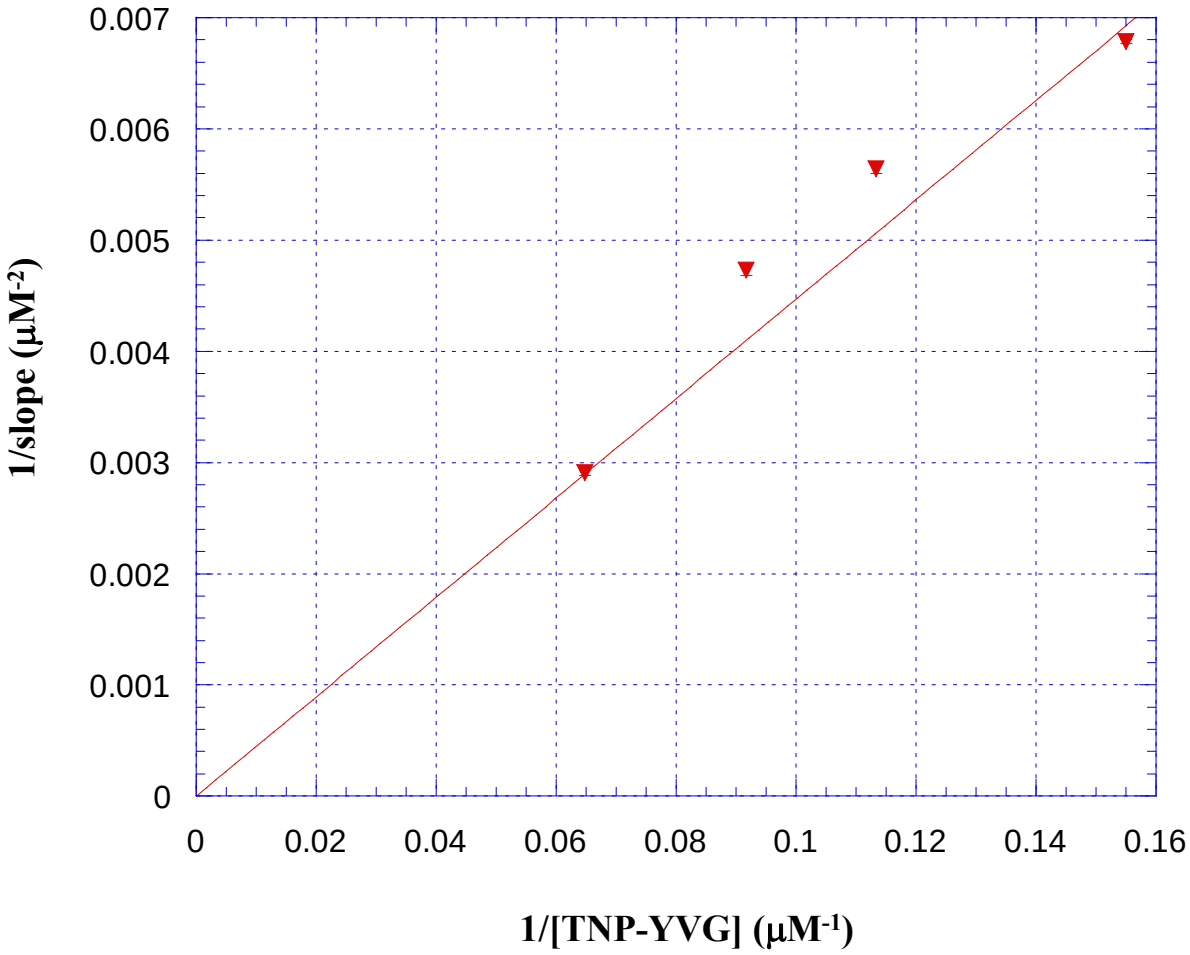

Figure 28. Plot of 1/slope (from Figure 1.3.25) *versus* 1/[TNP-YVG]. Linear regression yields a straight line which passes through the origin. The slope of the line is equal to $k_{inact}K_m/K_Ik_2[E]_o$. K_{inact}/K_I = 2440 M^{-1} min^{-1}.

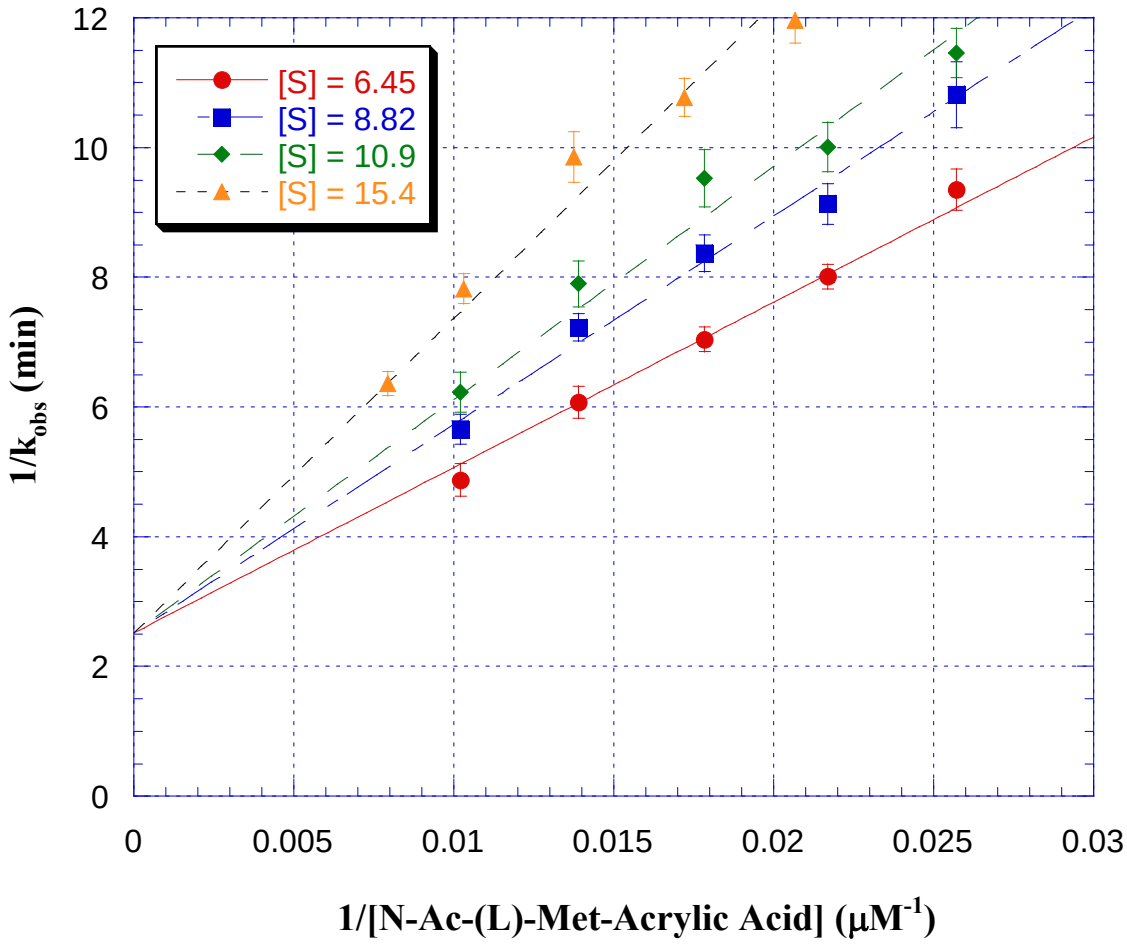

Figure 29. Plot of $1/k_{obs}$ *versus* 1/[N-Ac-(L)-Met-Acrylate] at Various Fixed Substrate Concentrations. Linear regression yields four straight lines with the same y-intercept value.

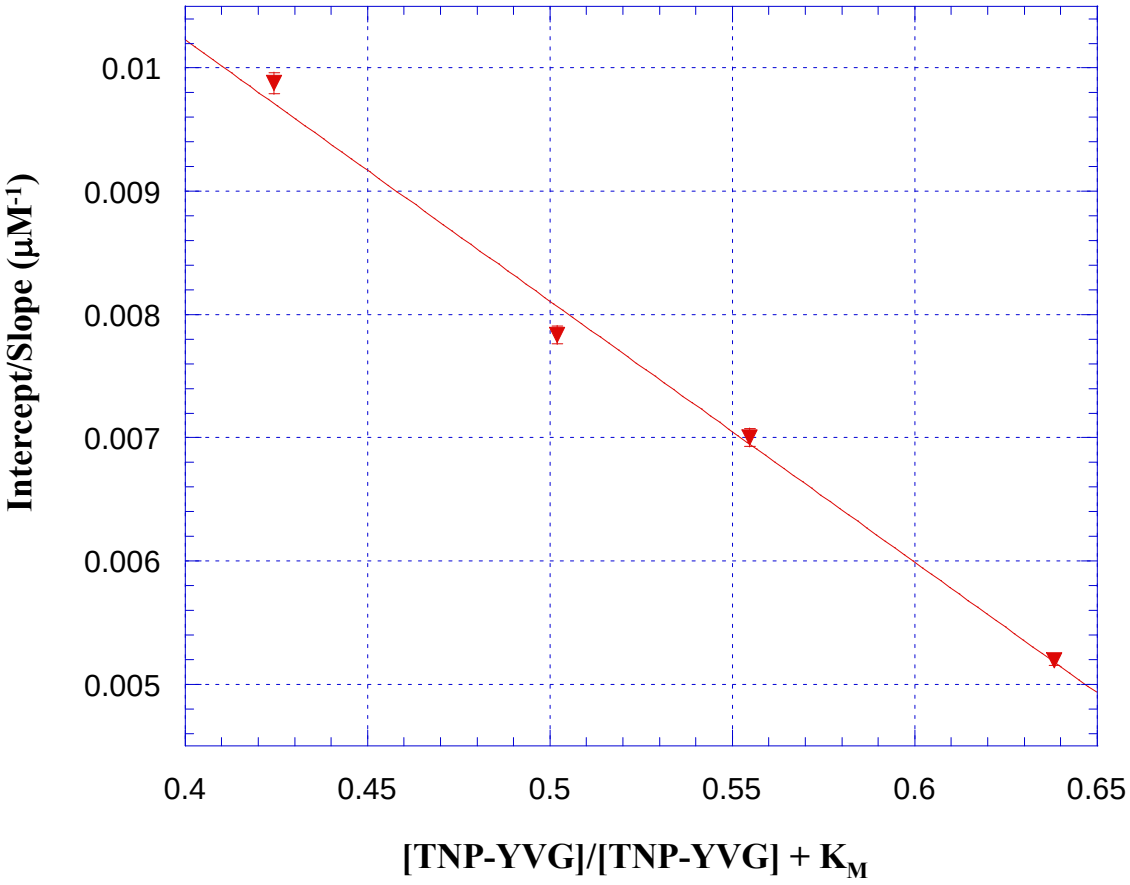

Figure 30. Ratio of Intercept/Slope from Figure 1.3.27 *Versus* [TNP-YVG]/(K_m + [TNP-YVG]). Assuming K_I' approaches infinity, K_I = 1/y-intercept = 56.5 μM.

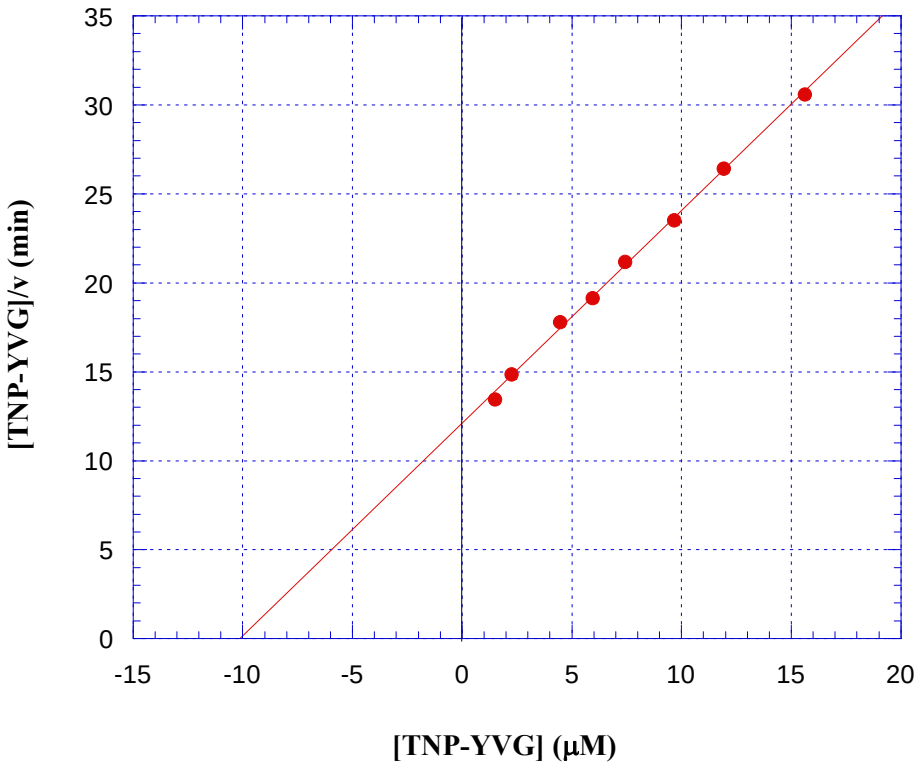

Figure 31. Hanes-Woolf Plot of [TNP-YVG]/v *vs.* [TNP-YVG] in the Presence of Potassium Iodide and Triton X-100. K_m = -x-intercept = 10.1 μM and V_{max} = 1/slope = 0.0740 μM/min.

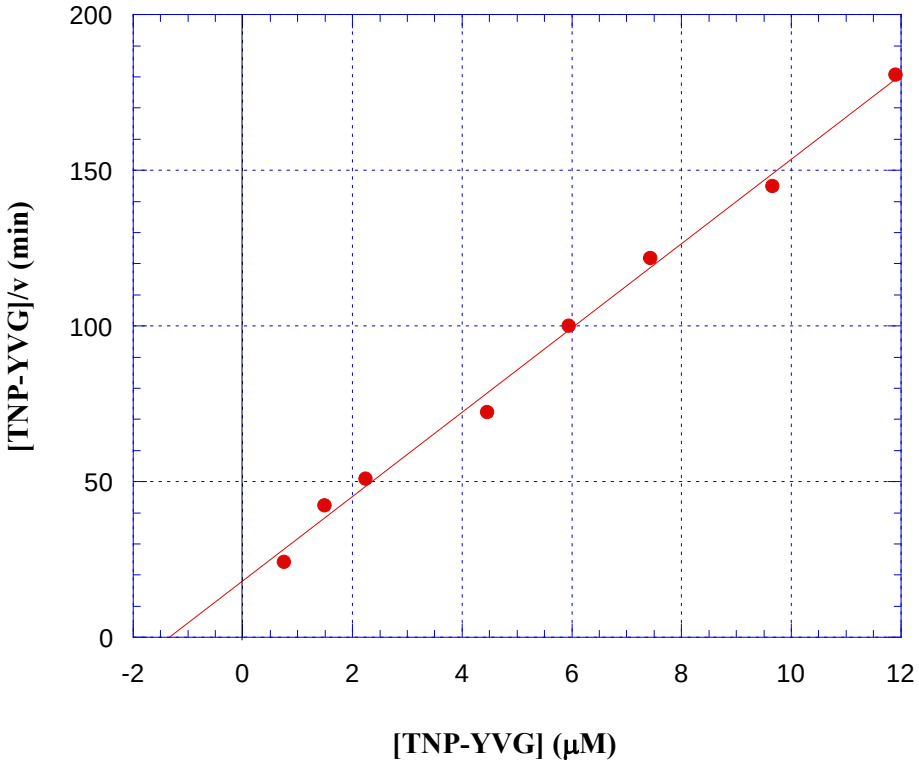

Figure 32. Hanes-Woolf Plot of [TNP-YVG]/v *vs.* [TNP-YVG] in the Absence of Potassium Iodide and Triton X-100. K_m = -x-intercept = 1.34 μM and V_{max} = 1/slope = 0.837 μM/min.

Table 2. Collected kinetic parameters from dilution and progress curve assays.

Inactivator	N-Ac-(L)-Phe-Acrylate		N-Ac-(D)-Phe-Acrylate		N-Ac-(L)-Met-Acrylate	
Assay Method	Dilution	Progress Curve	Dilution	Progress Curve	Dilution	Progress Curve
K_I (μM)		53.7 ± 1.0		60.0 ± 2.3		56.5 ± 0.5

PAM/Ligand Docking

When performing molecular simulations using a given module, it is important that a reliable system is created that maximizes the consistency of results. After testing several modeling programs, we found that the program Molecular Operating Environment (MOE) provided results consistent with the expectations of various potential ligands, whether they are known to be substrates, inhibitors, or neither. The first consideration is the selection of an appropriate force field, of which, in the case of protein/ligand docking, the consensus choice is the Engh-Huber force field. Engh-Huber uses empirical crystallographic radii from various proteins, and requires the addition of polar hydrogen atoms to the both the ligand and the receptor. Polar hydrogens include those bound to heteroatoms (S, N, O, etc.) and also sp2 hydrogen atoms (as found in many of the ligands tested in these docking simulations). The following is a brief recapitulation of the procedure for the preparation of the receptor and ligands involved in a docking simulation (see Materials section). First, all non-essential molecules/ions (e.g. heavy metals not involved in catalysis or bound nonspecifically to the enzyme, carbohydrates, glycerol, waters, etc.) are deleted from the protein structure, including any bound active-site ligands (i.e. N-Ac-Diiodo-Tyr-Gly in 1OPM). Second, appropriate charges are assigned to metal ions (i.e. +2 for copper ions in 1OPM). Third, all heavy atoms (i.e. non-hydrogens) are "fixed" such that they will not engage in translational movement in the course of any minimizations or simulations. The receptor is then subjected to a "tethered minimization," under the appropriate force field. The Energy Minimization module adds polar hydrogens (because they are not present in the X-Ray crystal structure,

but are required elements of the docking simulation using the Engh-Huber force field) where applicable and calculates the partial charges on all of the atoms in the crystal structure receptor. The result is a receptor where all heavy atoms have the same coordinates as in the published crystal structure, with the addition of polar hydrogens whose orientations and coordinates are determined via the tethered energy minimization. At this point, the receptor is completely ready for use in docking simulations.

The desired ligand is constructed using the "Builder Module." Appropriate charges are added (i.e., carboxylate oxygen assigned a charge of –1) and the ligand molecule is energy-minimized, during the course of which the non-polar hydrogen atoms are deleted (the builder constructs the ligand such that ALL hydrogen atoms expected in the structure are initially present). At this point, the ligand is fully prepared for use in docking simulations.

The docking run is then performed using the Simulated Annealing method, in conjunction with the more_dock.svl module. This module was written to supplement the default docking code with various parameters which allow for recognition of transition series metal ions, such as copper. Briefly, a database of 25 docking "runs" is generated. A "run" involves a specified number of temperature cycles (six, in all cases here), each with a specified number of iterations/cycle (6,000, in all cases here). Each cycle involves a temperature gradient (high to low, from beginning to end of the cycle, starting at 1,000 K for the first cycle) and each subsequent cycle utilizes a lower starting temperature than the previous one. In this way, the ligand is "annealed" into the active site of the receptor. At the beginning of a cycle, when the temperature is high, it is relatively easy for the ligand to escape from local energy minima. As the cycle progresses and the temperature

drops, the ligand settles (ostensibly) into a "more global" energy minimum. Typically, one sees radical changes in the orientation of the ligand only in the first one or two cycles as local minima are explored in search of a global energy minimum. Subsequent cycles are for "fine-tuning" of conformations as the lower initial temperatures prevent the ligands from escaping global energy wells they have entered. Typically, any significant translational motion of the ligand through the active site ends after the first or second cycle and rotational movements predominate as the cycles progress toward the end of the "run."

During a docking run, ONLY the atoms of the ligand molecule are allowed to move. Translational and rotational movement of receptor atoms is explicitly forbidden. The ligand is allowed complete translational and rotational movement, the latter within constraints set by the user. Indeed, via the Ligand Flexibility tool, the user may specify to what degree the ligand conformations may deviate from the initial minimized ligand structure. In all cases in this thesis, a ± 30-degree freedom of movement about rotatable bonds was allowed (maximum allowed by the software). Even if no freedom of rotational motion is allowed with this module, the ligand remains unconstrained with respect to translational movement, as a rigid body in this limiting case.

A "docking box" must be created which limits the translational freedom of movement of the ligand throughout the active site of the enzyme. In the interests of minimizing computational time, the box should encompass only those residues directly involved in binding and catalysis of substrates and/or competitive inhibitors/inactivators of the enzyme, to the exclusion (as possible) of all others. The box, using the coordinates from the 1OPM (oxidized PAM) crystal structure, was centered at (40.4032, 25.3060, 40.4527)

and formed a cube of 60 x 60 x 60 (arbitrary units). The user may specify the 3-coordinate origin of the docking box, and the width, depth, and height of the box in each of the x, y, and z axes. Although the ligand may not escape the box during the simulation, receptor residues outside of the box still influence the docking, in a manner determined by the setting of the bonded- and non-bonded cutoffs specified in the Engh-Huber force field parameters. In all cases in this thesis, the bonded cutoff was set "on" at 4.5 Å and "off" at 5.5 Å. These cutoffs were selected empirically to minimize computation time while still allowing for the effects of van der Waals' contacts (typically 4.0 Å maximum). After the Docking Box is delineated, all residues toward the periphery of the receptor which lie outside of the "off" cutoff are deleted and, as such, do not contribute at all to the docking simulation.

The last consideration prior to the initiation of the docking run is whether to bias the initial location of the ligand (or any particular part thereof) in the active site of the enzyme within the docking box. To this end, the user may either enable a "random start" or not. If enabled prior to the initiation of the docking simulation, a number of initial conformers (based on quick calculations by the docking module which seek to exclude nonproductive, high-energy conformers) will be generated which are equal to the number of specified "runs" in the simulation. If "random start" is disabled, all runs will originate with the ligand in the coordinates specified by the user. In all cases in this thesis, "random start" was NOT used and the ligands were biased with regard to the placement/orientation of the P2 residue in the protein. In other words, all of the ligands used in the docking simulations herein were constructed from the coordinates of the phenyl ring of IYG found in the 1OPM (oxidized PAM with bound IYG) crystal structure

and, as such, their P2 side chains share coordinates with the crystal structure ligands, to the maximum extent possible. This was based empirically on the quality of the results of initial docking runs with a variety of different ligands. The reason that we chose to use this bias is as follows: the Engh-Huber force field lends more weight to electrostatic and van der Waal's contributions than to energetically favorable desolvations of hydrophobic groups located in hydrophobic enzyme pockets. It is important to note that this bias will NOT lead to energetically unfavorable conformations being generated and DOES NOT serve to "lock" the P2 residue in the hydrophobic P2-binding site of the PAM active site. The ligand is allowed to migrate freely about the docking box, the initial coordinates of the ligand at the outset of the run notwithstanding. Indeed, in the case of several of the ligands with D-amino acids at the P2 position, the ligand P2 side chain is expelled completely from the hydrophobic pocket of the active site, regardless of this initial bias.

After the completion of all "runs" in the docking simulation, an output database of conformers is generated. Individual contributions of the energy of electrostatics, van der Waal's, the inherent energy of the ligand conformer, and solvation are included and serve, *in toto*, to provide the total energy of the ligand/receptor interaction. Taken together, the energy contributions of the electrostatics and van der Waal's fields represent the "energy of binding." Top scorers from the output database are identified by the total energy of these two components. Finally, the top scorers are subjected to a final energy minimization in the active site of the receptor. In these minimizations the coordinates of all the atoms of the receptor (including polar hydrogens) are fixed. No atoms of the top-scoring ligand are fixed, but a weighted heavy-atom tether is used such that gross translational movements of non-hydrogen ligand atoms are not observed. The

conformation/orientations generated from this final minimization represent those shown in the results section to follow.

IYG (2,4-diiodotyrosylglycine)

In order to compare the orientations and conformations of various docked ligands of interest in a meaningful manner, it is exceedingly important that the Docking module is able to reasonably reproduce the conformation of a ligand that has been crystallized with the protein of interest. Obviously, if no such reproduction is possible the importance, reliability, and conclusions from protein/ligand docking simulations are obviated. To this end, we initially performed a docking simulation on the ligand/substrate which is cocrystallized with the oxidized PAM catalytic core (PDB ID: 1OPM), namely N-Ac-Diiodo-Tyr-Gly.

In Figure 33, the IYG molecule in red represents the minimized crystal structure ligand in which all heavy atoms were fixed such that only the added polar hydrogens were subjected to energy minimization. Therefore, all heavy atoms are in positions identical with the coordinates of the corresponding published crystal structure ligand. The IYG molecule in green represents the tethered minimization of the crystal structure ligand where both the heavy atoms and the polar hydrogens were allowed to alter their positions. Note the excellent agreement between the two structures, indicating that the final energy minimization, performed also upon the best scorers of each ligand subsequent to the docking simulation, does not significantly alter the heavy atom coordinates in the case of the crystal structure ligand. Finally, the IYG molecule in blue

represents the best scorer provided by an actual docking simulation using the crystal structure ligand. Note, again, the good agreement between the docked IYG (in blue) and the original crystal structure IYG (in red), especially the atoms of the terminal glycine residue. Some very minor deviations are noted between the diiodophenol side chains of the docked and crystal structure ligands. The deviations between the N-Acetyl groups are slightly more significant, but as the specificity of binding is driven by the P2 side chain and the terminal glycine residue, the deviation at the N-terminus of this dipeptide is relatively inconsequential, especially in light of the fact that physiological PAM substrates, such as SP-Gly, contain ten or more amino acid residues. This space in the active site pocket must accommodate the main chain atoms of the P3 residues of these peptides, so there is a great deal of space available in this vicinity.

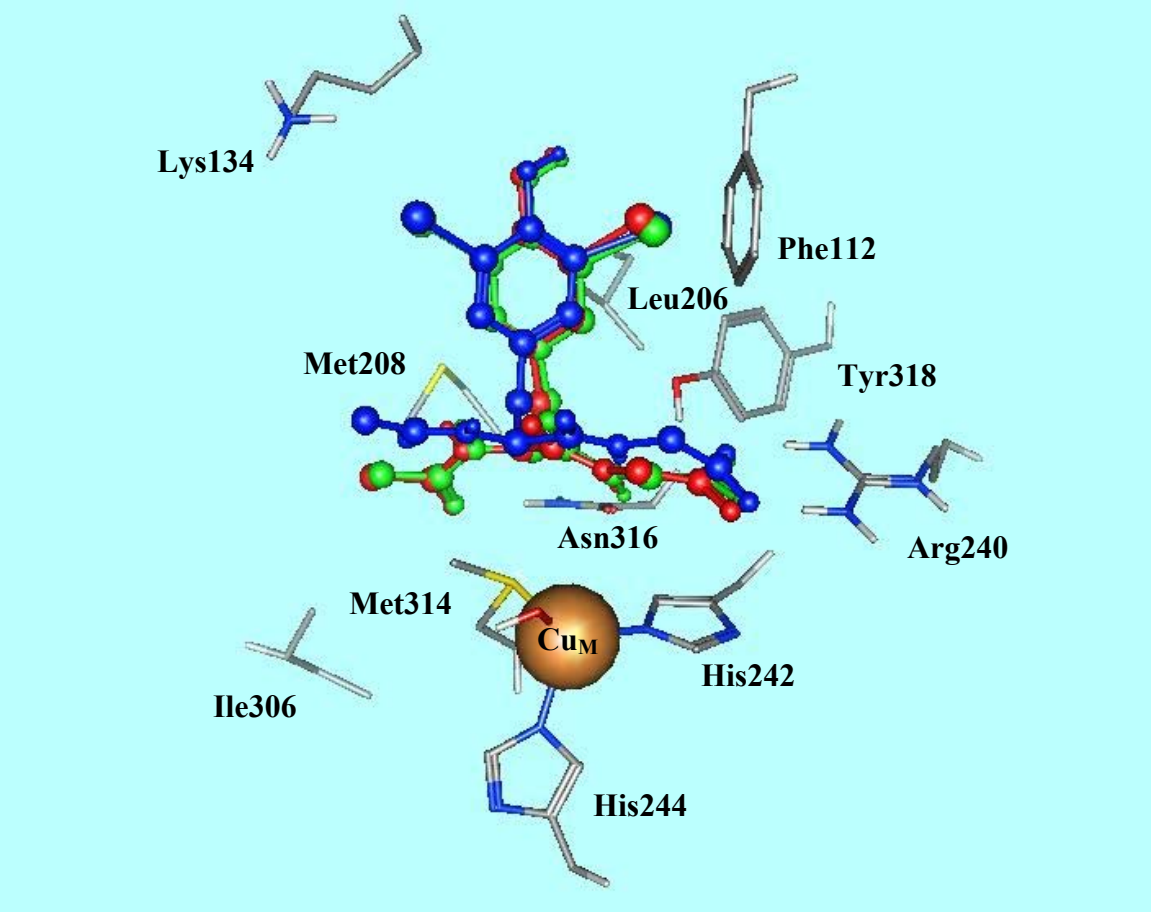

Figure 33. IYG docked to PAM active site Red: Crystal Structure IYG with polar hydrogens added, only hydrogens minimized into active site. Green: Crystal structure IYG with polar hydrogens added, entire molecule minimized into active site. Blue: Best docked scorer of IYG, with subsequent minimization into the PAM active site.

Based on the crystal structure IYG orientation, the three main residues involved in the binding of the glycyl residue are R240, N316, and Y318. The carboxylate of the ligand forms a tight salt bridge to the guanidinium moiety of R240. The phenolic hydrogen of Y318 forms a hydrogen bond to an oxygen atom of the ligand carboxylate, and the hydrogen atom of the glycyl amide bond forms a hydrogen bond with the amide oxygen of the side chain of N316. These three interactions are necessary to orient the ligand such that the pro-S glycyl hydrogen is directed toward the copper center. The P2 diiodophenol side chain of IYG makes close contacts with a number of residues in the hydrophobic pocket of the receptor, including (but not limited to) F112, K134, L206, M208, I306, M314, and Y318.

For comparison, the carboxylate oxygens of the crystal structure IYG lie within 1.8 and 1.7 Å of the R240 guanidinium hydrogen atoms whereas the oxygens of the docked IYG molecule lie within 1.6 and 1.5 Å of R240. The hydrogen bond between the glycyl amide and N316 has a length of 2.0 Å in the crystal structure IYG, with the bond lengthening to 3.2 Å in docked IYG. The hydrogen bond length between Y318 and the ligand carboxylate is 1.8 Å for both the crystal structure and docked IYG. Subsequent (post-docking) addition of the nonpolar glycyl methylene hydrogen atoms (not shown) shows the pro-(S) hydrogen directed toward the reactive copper center. On the basis of the close similarity between the positions of the docked IYG ligand and the crystal structure ligand, a number of further docking simulations were performed with various substrates, competitive inhibitors, and competitive inactivators.

N-Ac-(L)-Phe-Gly and N-Ac-(D)-Phe-Gly

PAM is known to be only reactive toward glycine-extended peptides with penultimate residues of the L-configuration. The corresponding peptides with P2 residues in the D-configuration are not substrates, and are, moreover, exceedingly poor competitive inhibitors. To see if our MOE docking protocol could distinguish between enantiomeric pairs, both enantiomers of N-Ac-Phe-Gly were docked to the 1OPM active site.

Figure 34 depicts N-Ac-(L)-Phe-Gly docked to 1OPM. The similarity of the orientation of docked N-Ac-(L)-Phe-Gly to that of the crystal structure ligand IYG is quite striking. The two ligand carboxylate oxygens are both 1.5 Å from the corresponding guanidinium hydrogen atoms of R240, again forming a tight salt bridge. The hydrogen bond length between Y318 and ligand carboxylate is 1.8 Å, and the hydrogen bond length between N316 and the glycyl amide is also 1.8 Å. Again, the pro-(S) hydrogen is oriented toward the copper center (the Engh-Huber force field does not explicitly include non-polar hydrogen atoms, so the pro-(S) and pro-(R) hydrogen atoms are not shown). The phenyl ring of N-Ac-(L)-Phe-Gly is directed into the same hydrophobic pocket as was the corresponding diiodophenol moiety of IYG and is packed near the aromatic hydrophobic residues F112 and Y318.

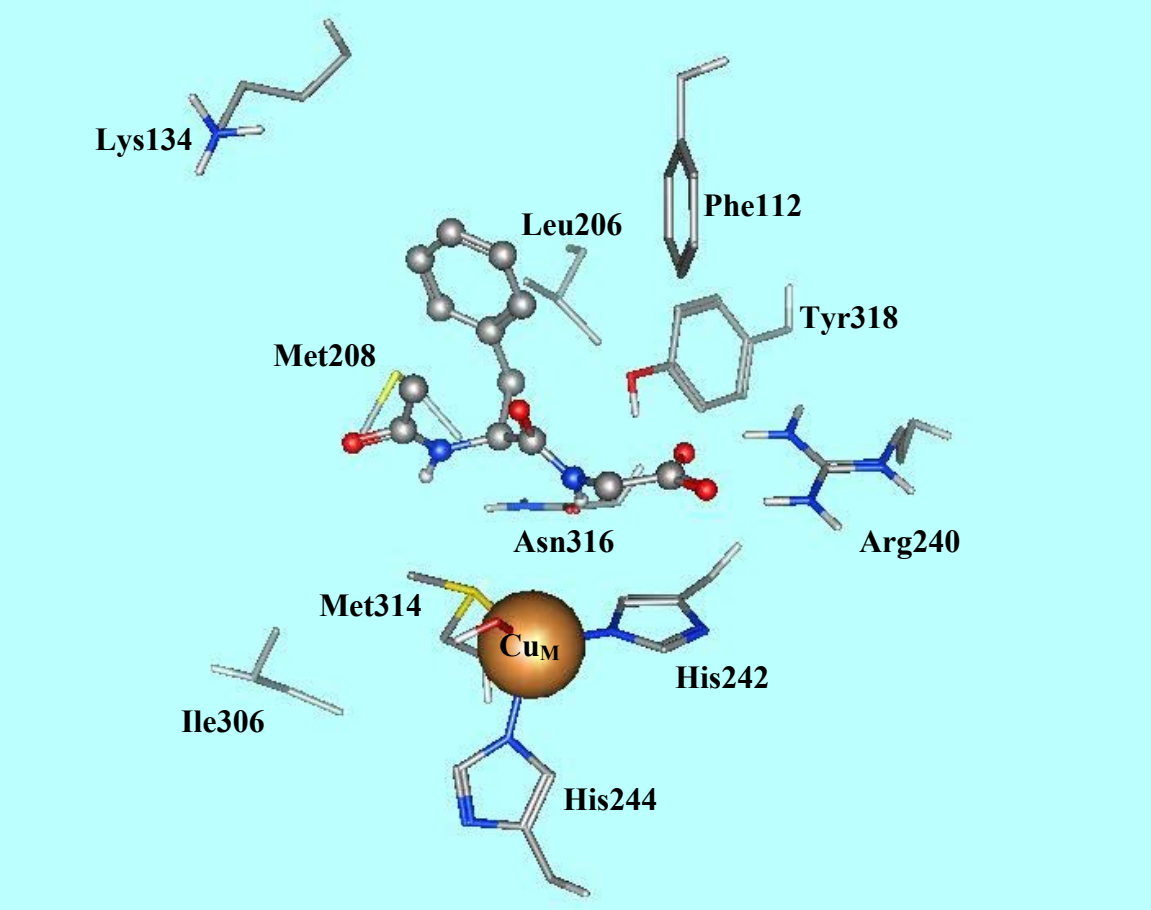

Figure 34. N-Ac-(L)-Phe-Gly docked to PAM active site.

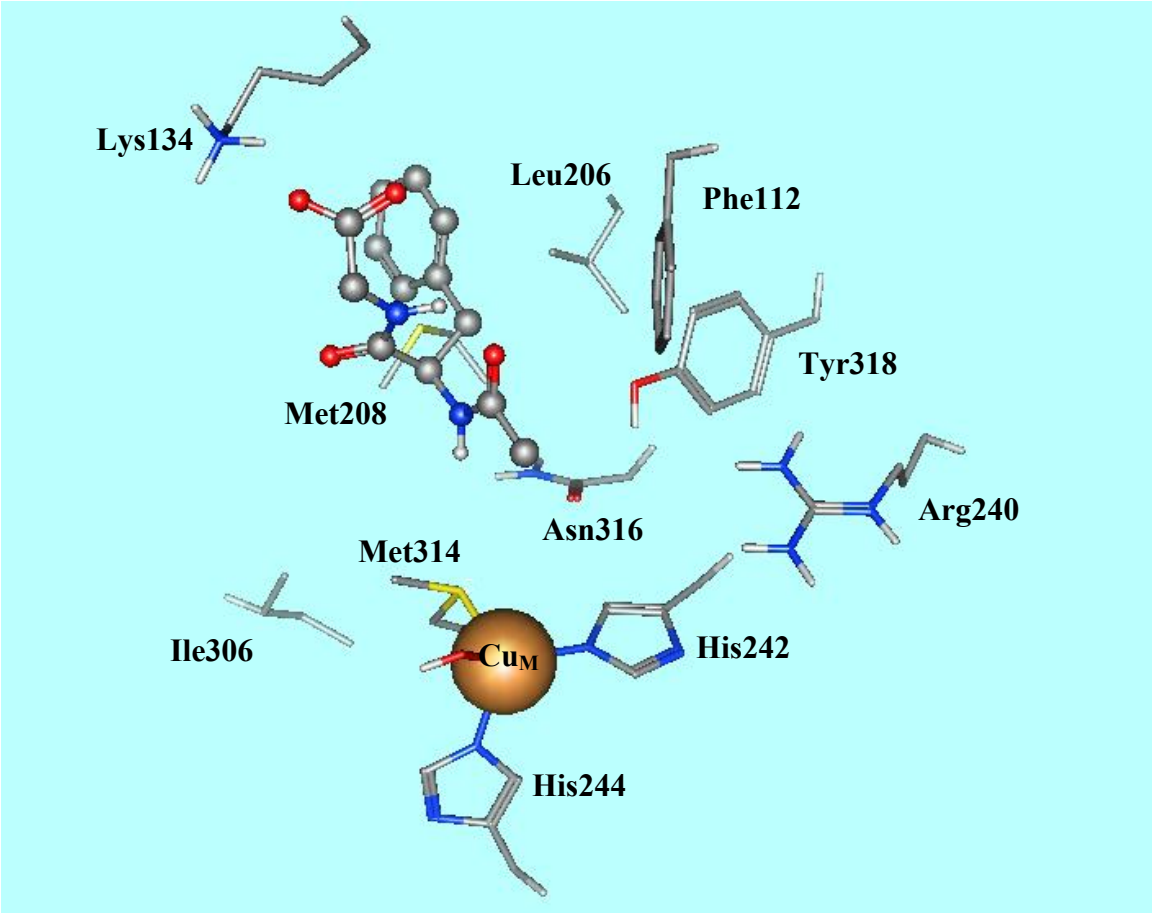

Figure 35. N-Ac-(D)-Phe-Gly docked to PAM active site

Figure 35 shows the results of the nonsubstrate ligand N-Ac-(D)-Phe-Gly docking simulation. This molecule binds in a very different manner from its enantiomeric substrate counterpart. At this point, it is important to point out the following: because of the restrictions placed on these simulations by the use of the Docking Box, ligands which do not in actuality bind at the active site of the enzyme will nevertheless remain within the confines of the Box. This is not to be assumed to imply that they would, as a result of the conformation given by the best scorers of the simulation, occupy this space in an *in vivo* or *in vitro* situation and, importantly, should not lead the reader to believe that they would be competitive inhibitors in the active site with respect to substrate. Significant deviations from the orientation of IYG, such as lack of salt bridge formation between ligand carboxylate groups and R240 guanidinium moieties, are assumed to be hallmarks of poor substrates/inhibitors. All docked ligands in these simulations which fail to form a salt bridge with R240 or a hydrogen bond with Y318 are known, *in vitro*, to fail to act as PAM substrates or competitive inhibitors.

Here, the carboxylate is oriented toward the positively charged side chain of K134. No salt bridge is formed with R240 and there are no interactions with either N316 or Y318. The phenyl ring remains in the hydrophobic pocket. Again, this conformation, with so few active site interactions, is not necessarily indicative of a "true" binding site for this compound, but simply its most favored conformation within the confines of the Docking Box.

N-Ac-(L)-Leu-O-CH_2-COOH and N-Ac-(D)-Leu-O-CH_2-COOH

In addition to catalyzing the α-hydroxylation of glycine-extended peptides, PAM has been shown by this laboratory to undergo competitive inhibition by the corresponding O-glycolate esters. The N-Ac-Leu-O-CH2-COOH enantiomeric pair was found to exhibit the same stereochemical requirements as corresponding N-acetyl dipeptides terminating in glycine, namely that the L-leucyl compounds are competitive PAM inhibitors whereas D-Leucyl compounds are not (P2 subsite stereospecificity).

By modeling this enantiomeric pair, we are able to further probe the ability of our model to distinguish between pairs of enantiomers where the (L)-enantiomer is a PAM substrate and the (D)-enantiomer is not. Figure 36 displays N-Ac-(L)-Leu-O-CH_2-COOH docked to the active site of 1OPM.

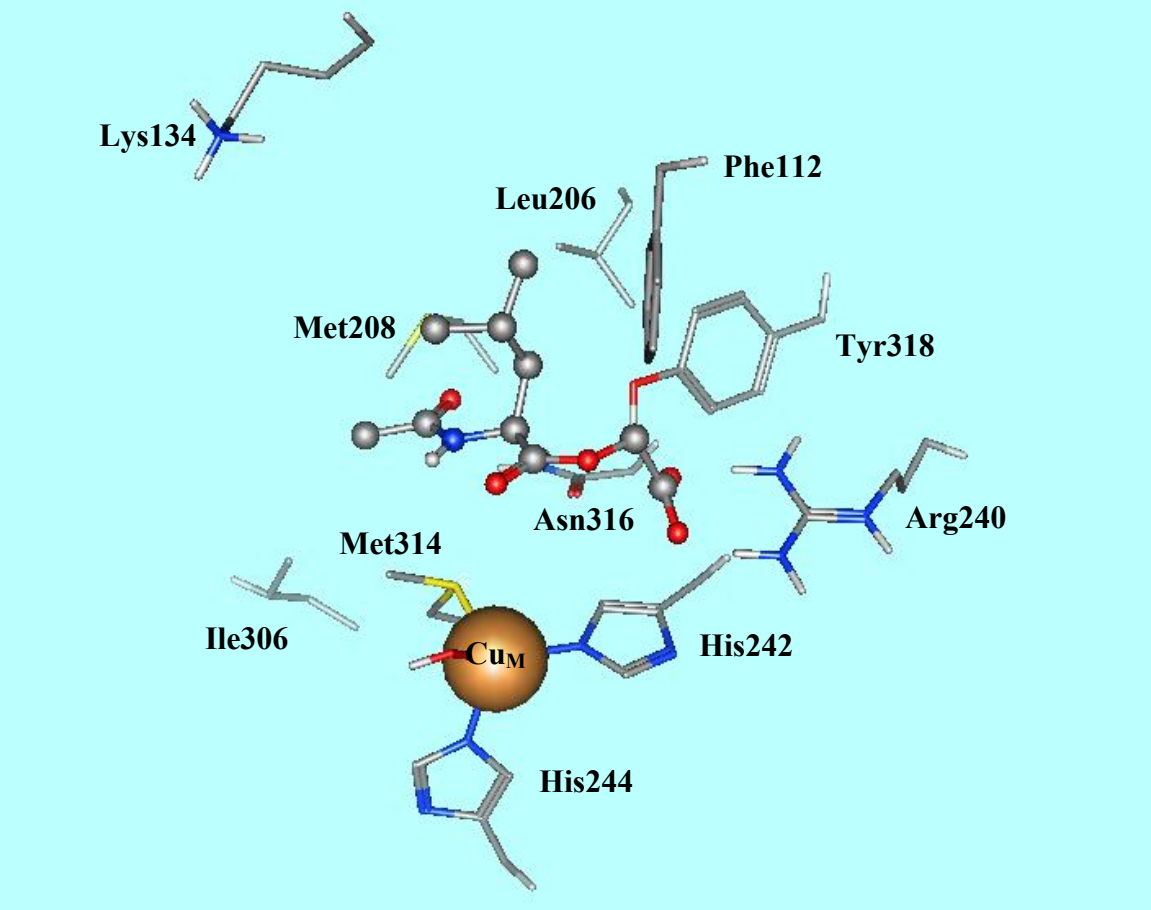

Figure 36: N-Ac-(L)-Leu-OCH_2-COOH docked to PAM active site.

There are two major differences between glycine-extended dipeptides and these O-glycolate esters. Firstly, the glycyl esters are able to rotate freely about the carbonyl-oxygen bound whereas the corresponding carbonyl-nitrogen bond of the dipeptide compounds is constrained in its rotation due to the partial double-bond character of the amide. Secondly, the amide nitrogen of the dipeptides has a hydrogen bond donor that forms a hydrogen bond with the side chain amide of N316. Instead, the ester compounds have a hydrogen bond acceptor oxygen in the corresponding position and therefore cannot form a hydrogen bond with N316 in the same manner as the dipeptides with (L)-configuration at the P2 position.

As evident from Figure 36, the L-Leucyl compound binds to the active site of 1OPM in much the same way as does N-Ac-(L)-Phe-Gly. The carboxylate is oriented towards and forms a salt bridge with the guanidinium side chain of R240, with the two oxygen atoms of the carboxylate at a distance of 1.5 Å from the guanidino hydrogens. Y318 forms a hydrogen bond (1.8 Å) with the carboxyl oxygen of the ligand, again similar to the docked dipeptide N-Ac-(L)-Phe-Gly. The sec-butyl side chain of the L-Leucyl compound is found, as expected, in the hydrophobic pocket of 1OPM. As discussed above, there is no hydrogen bond formed between the ligand and N316. Furthermore, the methylene glycyl carbon is oriented outward toward the viewer rather than inward toward N316 as was the case for N-Ac-Phe-Gly. This may help to explain why these compounds do not undergo PAM-catalyzed hydroxylation, and instead behave as potent competitive inhibitors.

Figure 37 below displays N-Ac-(D)-Leu-O-CH_2-COOH bound to the active site of 1OPM. The carboxylate moiety of the ligand does not interact with R140 or form a hydrogen bond with Y318. In addition, no hydrogen bond is formed between the amide of the ligand and N316. Indeed, the entire glycyl portion of the molecule is oriented completely away from the PAM glycine-binding site. The hydrophobic leucyl side chain remains in the hydrophobic pocket of the enzyme. None of the interactions indicative of substrate or inhibitor binding are evident with the D-enantiomer of this compound. Indeed, *in vitro,* this compound is a poor substrate/competitive inhibitor of PAM.

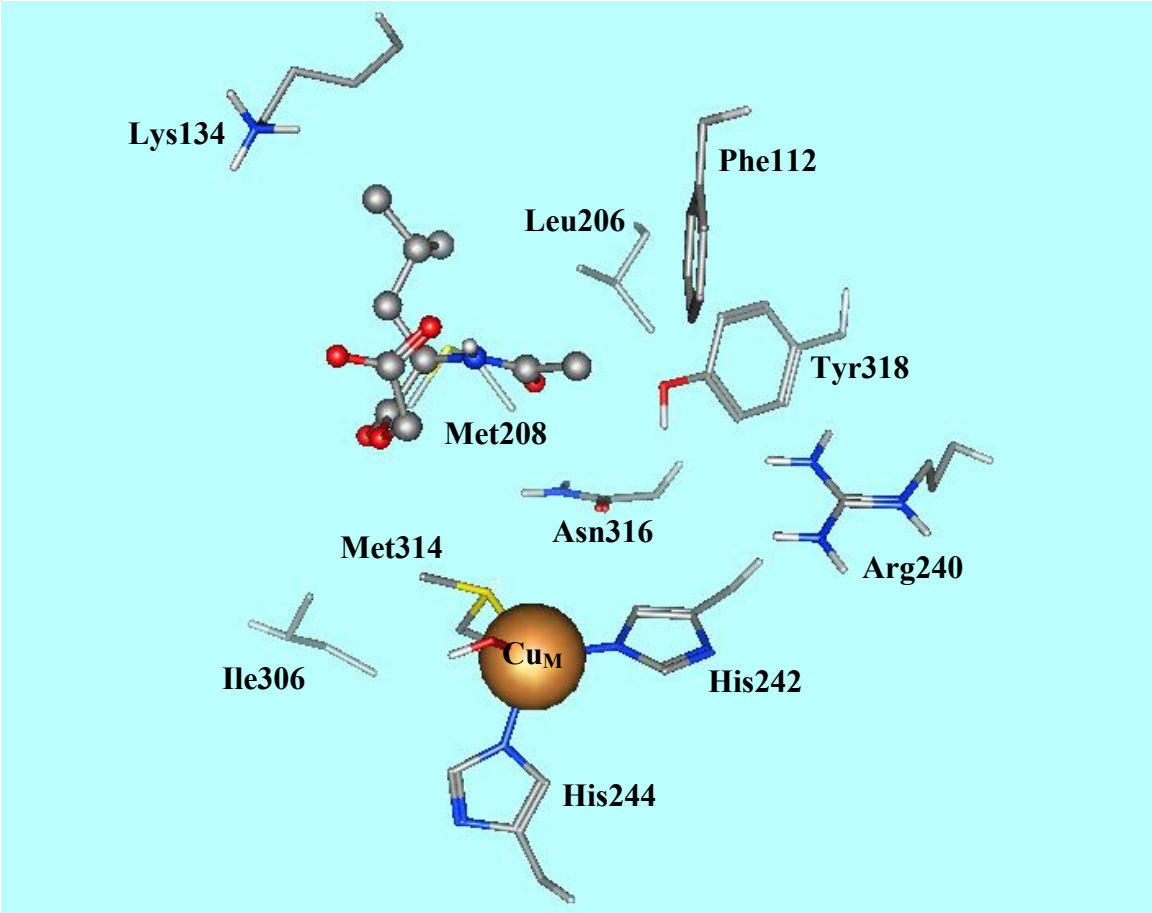

Figure 37. N-Ac-(D)-Leu-OCH_2-COOH docked to PAM active site.

N-Ac-(L)-Phenylglycine-Gly and O-Ac-(R)-Mandelyl-Gly

These compounds have been tested *in vitro* as PAM substrates/inhibitors by our laboratory. Stereotopically, the (L)-derivative is the same as (L)-phenylalanyl and the (R)-mandelyl derivative is stereotopically the same as (D)-phenylalanyl compounds. They differ only in that the mandelyl compound has an O-acetyl, rather than an N-acetyl, group. Keeping to the trends established above, the (R)-mandelyl derivative is neither a substrate nor inhibitor of PAM, whereas the (L)-derivative is indeed a PAM substrate. The fact that the mandelyl compound possesses an O-Acetyl group at the "N-terminus" whereas the Phe-Gly compounds and the Leucine compounds are N-acetylated at the N-terminus is expected to have little effect on receptor binding. The N-acetyl group does not contribute to ligand binding to any appreciable extent in the cases studied herein.

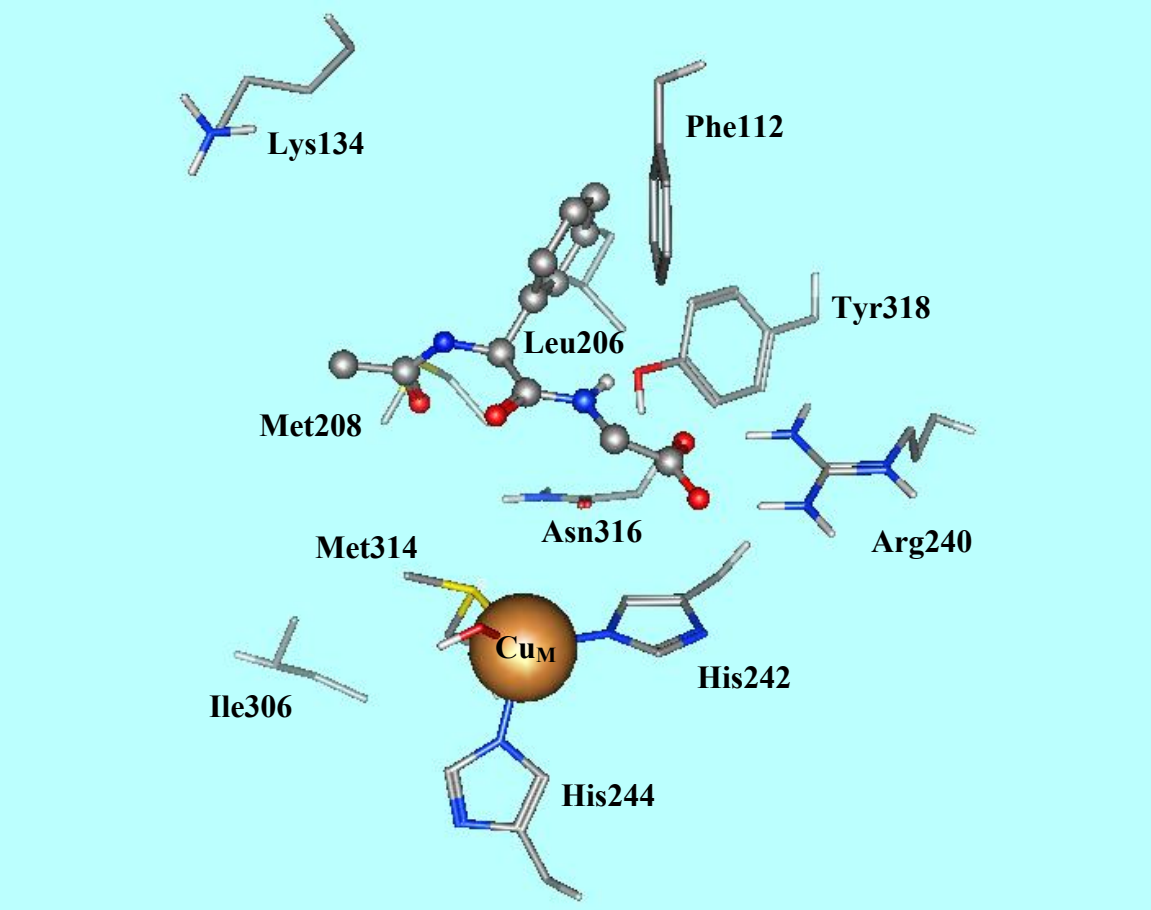

Figure 38. N-Ac-(L)-Phenylglycine-Gly docked to PAM active site.

Figure 38 below displays N-Ac-(L)-Phenylglycine-Gly bound to the active site of 1OPM. As can be seen in the figure, this compound binds in the manner typical of a known PAM substrate. The salt bridge with R240 is evident with both carboxylate oxygen atoms at a distance of 1.5 Å from the guanidinium hydrogens. Y318 forms a hydrogen bond with one of the carboxylate oxygens (1.8 Å). The mandelyl phenyl group is directed into the hydrophobic active site pocket, but appears to have been pulled upward and to the right in the active site, relative to the phenyl ring of N-Ac-(L)-Phe-Gly, bringing it into closer proximity with F112 and Y318. It appears likely that the lack of the methylene spacer between the α-carbon and the phenyl ring of the (L)-phenylglycine derivative is the cause

of this effect (such that aromatic hydrophobic interactions between ligand and receptor are maximized). This results in a much greater distance (4.4 Å) between the amide hydrogen bond donor of the ligand and the amide hydrogen bond acceptor of the side chain of N316, and therefore the hydrogen-bonding interaction is lost in the case of the (S)-mandelyl compound. Again, a rendering of all hydrogens (rather than just polar hydrogens) places the pro-(S) hydrogen atom of glycine in closer proximity to the copper center than the pro-(R) hydrogen atom.

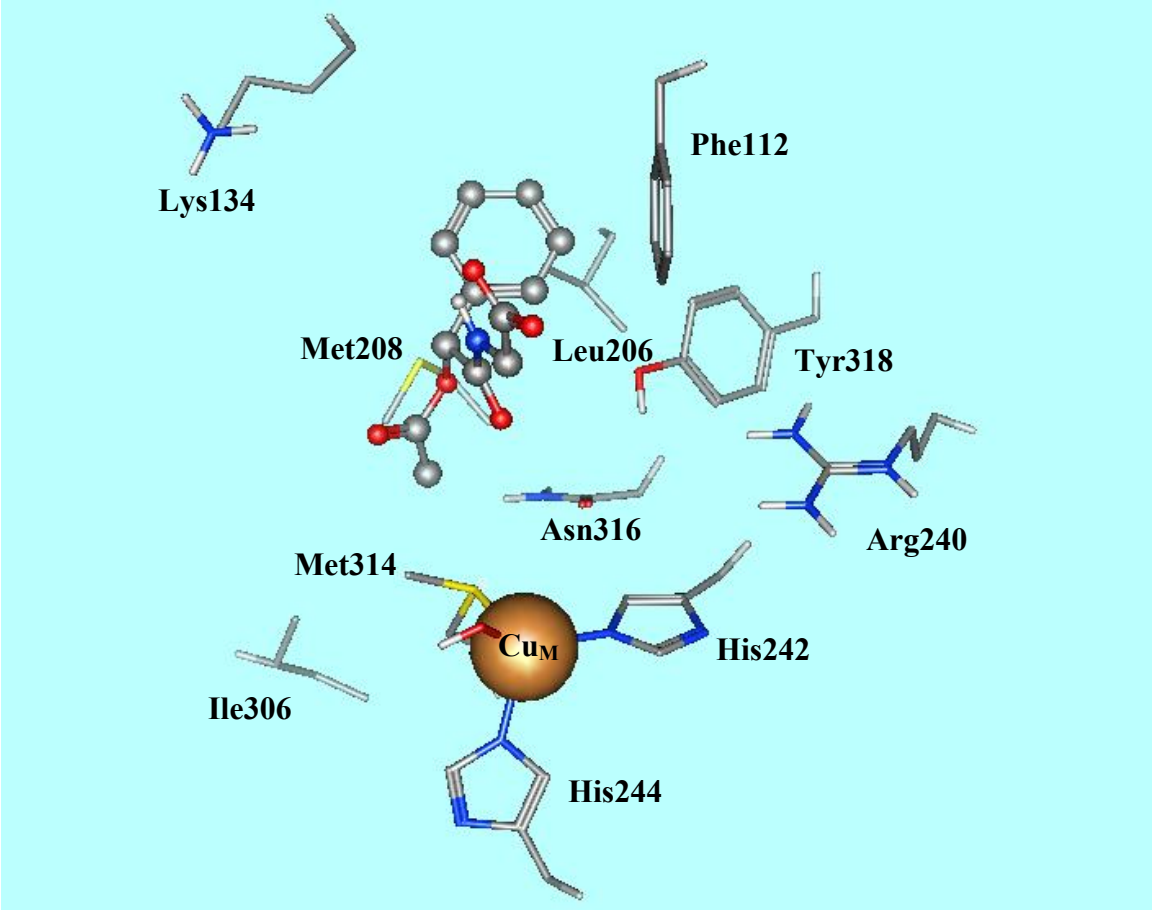

Figure 39. O-Ac-(R)-Mandelyl-Gly docked to PAM active site.

O-Ac-(R)-Mandelyl-Gly docked to 1OPM is shown in Figure 39. This compound was neither a substrate nor inhibitor of PAM in our *in vitro* studies, and the docking result below is consistent with this fact. The molecule floats freely in the active site of the enzyme and displays no specific interactions whatsoever. The glycyl end of the molecule does not associate with R240, Y318, or N316 and is in no position to undergo catalysis.

N-Ac-(L)-Phe-Acrylate and N-Ac-(D)-Phe-Acrylate

As related in the kinetics results section, N-Ac-(L)-Phe-Acrylate is the most potent turnover-dependent inactivator of PAM currently known (based on k_{inact}/K_I values) and is isoelectronic with N-Ac-Phe-Gly. Two major structural differences exist; first, rather than the glycyl sp2-nitrogen, the acrylate compound possesses an sp2-carbon and, as such, cannot form a hydrogen bond with the side chain of N316. Secondly, the N-Ac-Phe-Gly sp3-glycyl carbon is replaced with a second sp2-carbon atom. These changes result in a molecule containing an α,β-unsaturated ketone functionality. Because of this conjugation, rotational freedom is likely limited about the C3-C4 bond, whereas N-Ac-Phe-Gly is able to freely rotate about this bond. Moreover, freedom of rotation is also restricted, obviously, about the alkenyl double bond of N-Ac-(L)-Phe-Acrylate. It is unclear whether or not the carboxylate functionality can be considered to be conjugated to the α,β-unsaturated ketone, especially in the negatively-charged deprotonated state at physiological pH (and at the pH of the buffer system used to perform PAM inactivation assays.

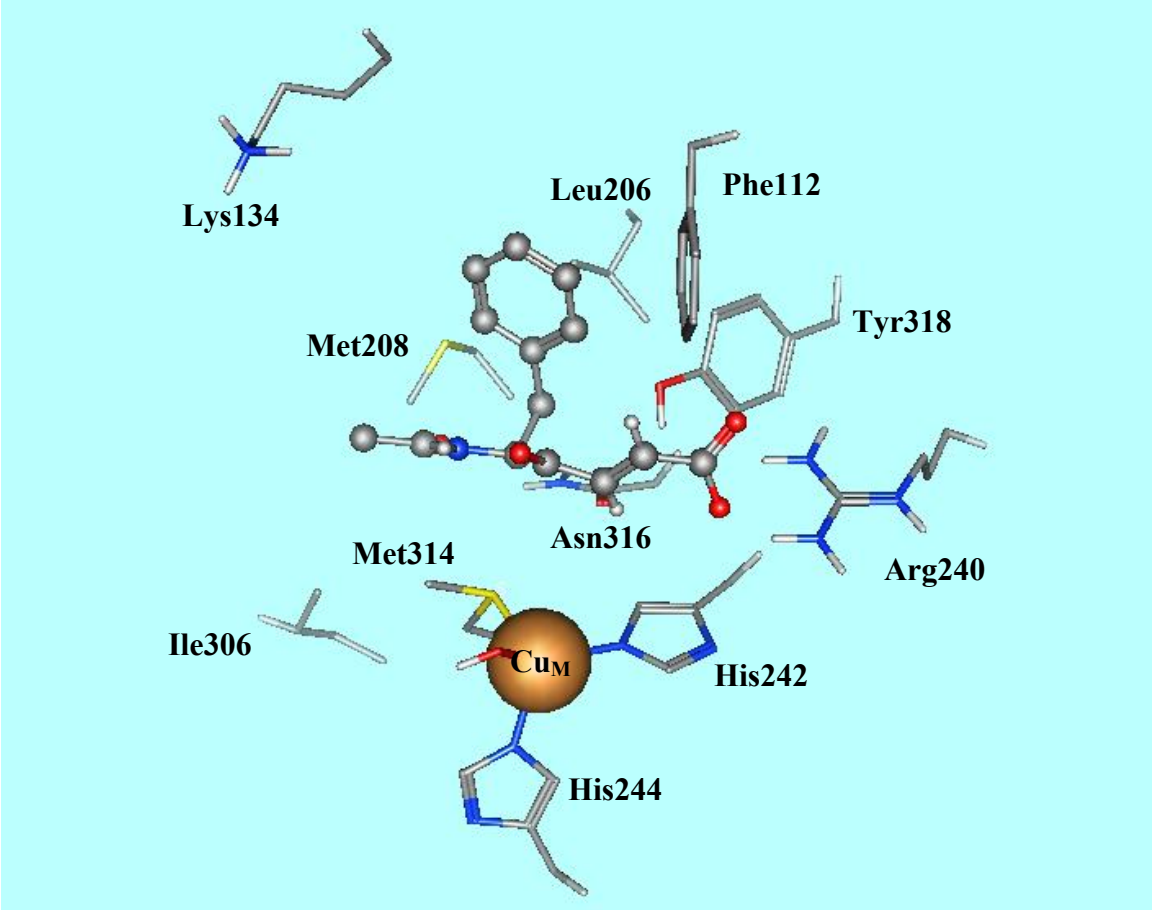

Figure 40. N-Ac-(L)-Phe-Acrylate docked to PAM active site.

The best scoring conformer of N-Ac-(L)-Phe-Acrylate docked to 1OPM is shown in Figure 40. Immediately, it is evident that this compound binds in a manner quite similar to N-Ac-(L)-Phe-Gly, with the benzyl group of the phenylalanine residue protruding into the PAM hydrophobic pocket and its carboxylate group directed towards the guanidinium moiety of R240. Interestingly, the negatively charged carboxyl group of the ligand is no longer coplanar with the positively charged guanidinium moiety of R240, although the two ligand oxygens remain in close proximity (1.6 and 1.8 Å). The phenolic hydrogen of Y318 again forms a hydrogen bond with the carboxylate (3.0 Å). One further interaction

of interest is the appearance of a weak hydrogen bond (3.2 Å) between the N-acetyl oxygen of the ligand and the terminal amide of the N316 side chain.

Surprisingly, the N-Ac-(D)-Phe-Acrylate enantiomer appears to bind in a manner very similar to N-Ac-(L)-Phe-Acrylate and N-Ac-(L)-Phe-Gly, with respect to the carboxylate end of the molecule. Recall that N-Ac-(D)-Phe-Gly was not able to bind in a productive manner to the 1OPM active site and bore no similarities in binding to N-Ac-(L)-Phe-Gly. Figure 41 depicts N-Ac-(D)-Phe-Acrylate bound to the active site of 1OPM.

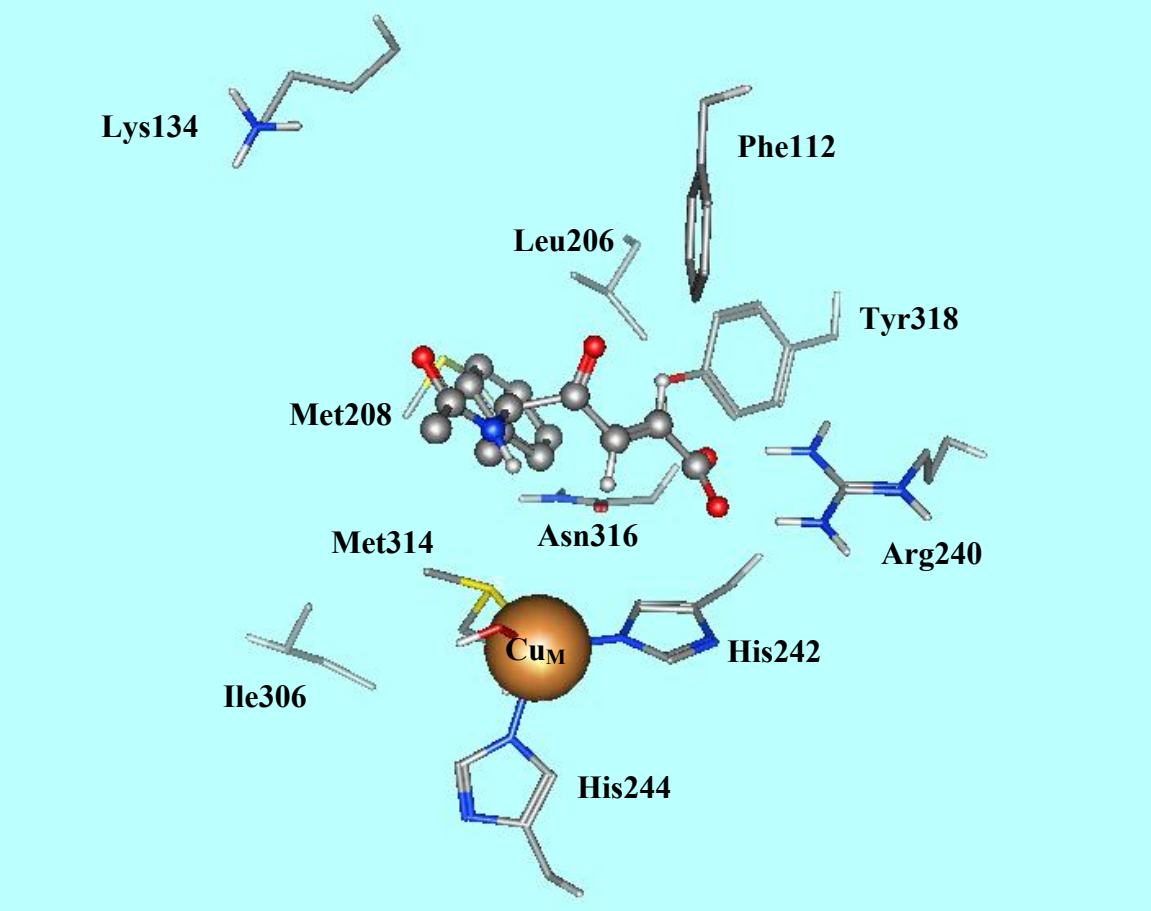

Figure 41. N-Ac-(D)-Phe-Acrylate docked to PAM active site.

The C-terminus of the ligand is oriented in the same manner in the active site as was seen for both N-Ac-(L)-Phe-Acrylate and N-Ac-(L)-Phe-Gly, forming a tight salt bridge with R240 (1.5, 1.6 Å), and a hydrogen bond with Y318 (1.9 Å). The phenyl ring still protrudes into the enzyme's hydrophobic pocket but a comparison with its enantiomeric counterpart shows some differences in orientation. The N-acetyl group is directed outward (i.e. toward the viewer in the figure) in the case of N-Ac-(D)-Phe-Acrylate.

Sulfur-Containing Acrylates

The two sets of enantiomeric pairs of N-Ac-Thienyl-Acrylate and N-Ac-Met-Acrylate were evaluated with our MOE docking protocol. These molecules differ from the ligands evaluated above because the sulfur atoms in their side chains have the potential to ligate to the copper(II) ion in the active site. Obviously, however, transition metal chemistry and ligation are extremely complicated processes (relative to simple electrostatics and van der Waal's calculations) and we are uncertain as to whether such interactions can be effectively modeled by this software. Moreover, the active site copper depicted in these results is already 4-coordinate (M314, HIS242, HIS244, hydroxide) and, because all receptor atoms/residues are static in these modeling simulations, it is impossible to create a situation where a ligand sulfur moiety (whether a thiophene or a thioether) would displace one of the coordinating ligands. That being said, it certainly remains appropriate to run docking simulations to see if the various enantiomeric ligands are able to bind in a manner similar to known substrates and inactivators.

N-Ac-(L)-Met-Acrylate and N-Ac-(D)-Met-Acrylate

These compounds are very interesting in that their side chains are identical to one of the ligands for Cu^{+2}, namely M314. Both contain a thioether functionality, and the possibility exists that these compounds, in the proper orientation, could theoretically displace M314 as a ligand to CuB. Again, this would require the movement of atoms and residues in the receptor itself, which is not possible in these docking simulations. However, it is certainly possible to investigate whether or not these sulfur-containing compounds can dock in a manner similar to the Phe-acrylates and other PAM substrates and competitive inhibitors.

N-Ac-(L)-Met-Acrylate is shown docked to the active site of 1OPM in Figure 42. It is evident that this compound binds similarly to other known PAM substrates and inactivators. The carboxylate functionality of the ligand forms a salt bridge with R240 (1.7 and 1.8 Å), although a slight departure from coplanarity with the guanidinium group is evident. Y318 forms two hydrogen bonds, one with each carboxylate oxygen (2.9 and 3.1 Å). The methionyl side chain rests in the PAM hydrophobic pocket, with the thioether sulfur atom over 9.0 Å distant from the reactive copper center. There is no evidence in these simulations of the sulfur atom of N-Ac-(L)-Met-Acrylate engaging in any type of interaction with the Cu^{+2} ion, although the limitations described above must be kept in mind.

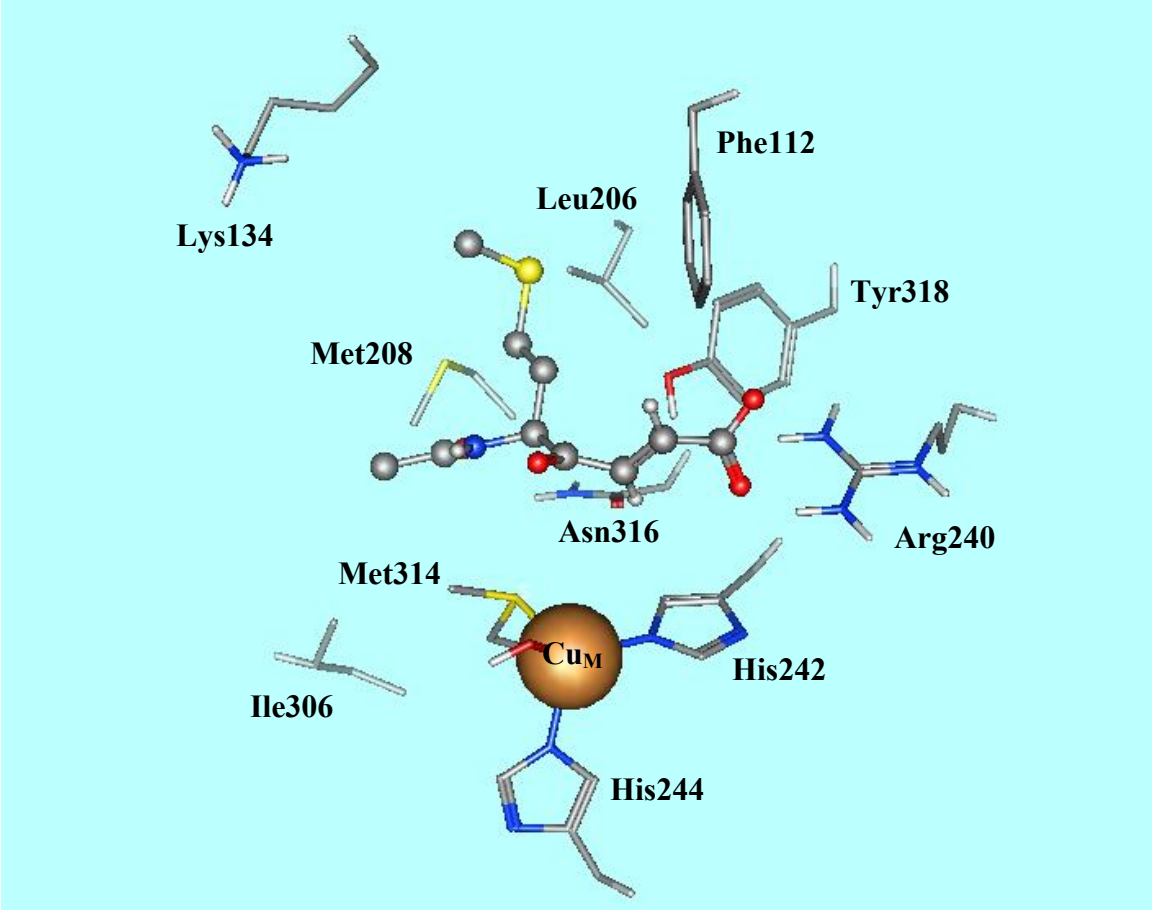

Figure 42. N-Ac-(L)-Met-Acrylate docked to 1PAM active site.

The top scoring N-Ac-(D)-Met-Acrylate candidate docked to 1OPM is shown in Figure 43. Again, the orientation is indicative of the productive binding of a substrate, competitive inhibitor, or inactivator. However, the carboxylate of the ligand does not associate as strongly with the R240 guanidinium moiety (oxygen atoms 1.5 and 2.6 Å distant). A hydrogen bond between the ligand carboxylate and Y318 is also present (3.0 Å). Although the methionyl side chain is again found in the active site hydrophobic pocket, the orientation is different than that seen in N-Ac-(L)-Met-Acrylate, and is directed toward the positively charged amine of K134 (4.0 Å). As this compound

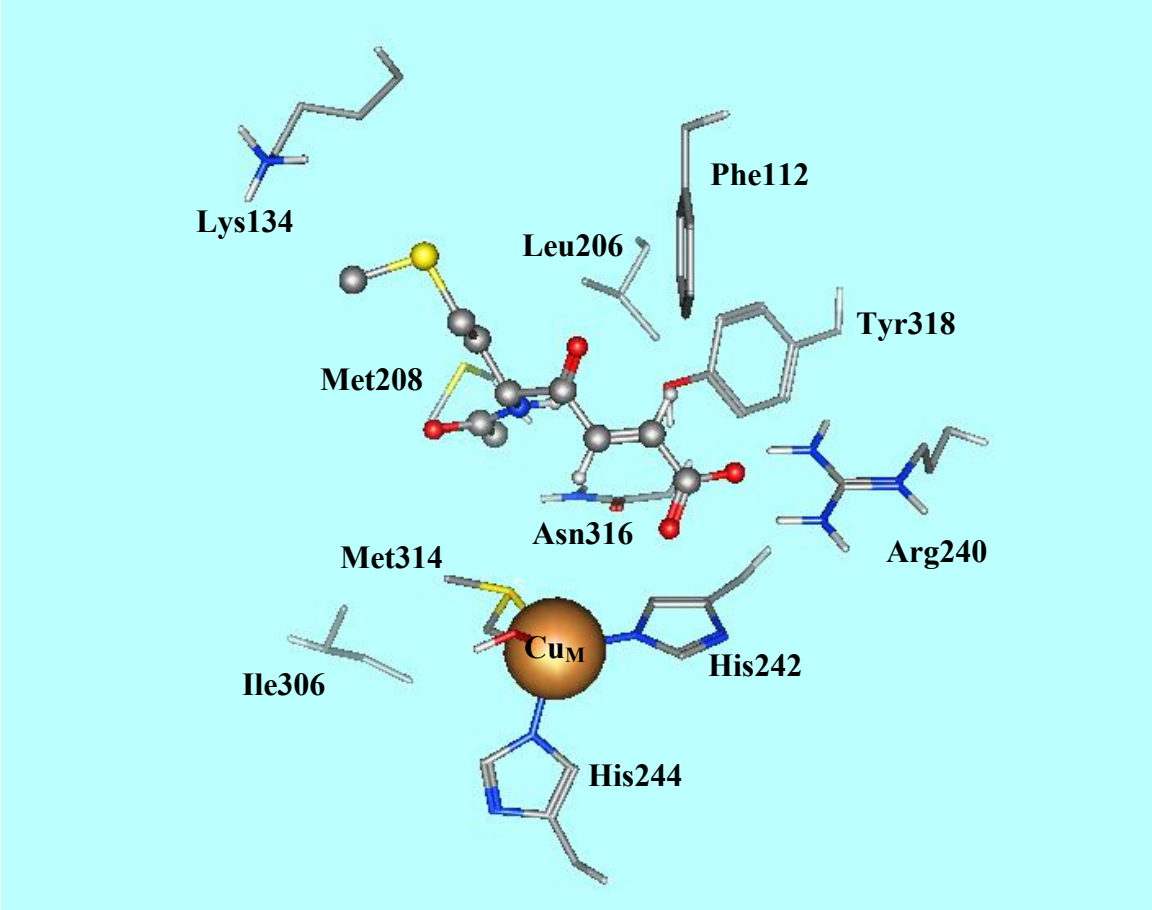

Figure 43. N-Ac-(D)-Met-Acrylate Docked to PAM active site.

was not synthesized, it is difficult to declare definitively whether or not it would behave as a PAM inactivator *in vitro* as does its enantiomer, N-Ac-(L)-Met-Acrylate.

N-Ac-(L)-2'-Thienyl-Acrylate and N-Ac-(D)-2'-Thienyl-Acrylate

Spatially, the thienyl compounds are very similar to the Phe-Acrylate compounds as both groups contain an aromatic ring of similar size (5-membered in the case of the thienyl derivatives and 6-membered in the case of the phenyl derivatives) and a

methylene side chain group. Electronically, however, both classes of compounds differ significantly in that the thiophene ring is classified as "electron-rich" in that there are six p-orbital electrons in a five-membered aromatic ring, where the phenyl ring has six p-orbital electrons in a six-membered ring. As a result of the electron-rich nature of the thiophene ring, any pi-cation interactions will be more pronounced than for a corresponding phenyl group. Moreover, the sulfur contains an extra lone pair of electrons (which are not part of the aromatic pi-system) which, theoretically, could participate in metal cation ligation. Indeed, ligation of a Cu+2 cation could proceed with either a direct coordination to the thienyl sulfur atom, or via a pi-system/cation interaction. We reasoned (Feng 2000) that if the thienyl side chain were able to coordinate the active site copper ion which is responsible for dioxygen activation, this inhibitor would bind more tightly and yield a lower K_I value than the corresponding phenyl compounds, even though this coordination would likely result in an orientation different from that seen for the N-Ac-(L)-Phe-Gly compound. The (L)-thiophene compound is indeed a potent mechanism-based PAM inactivator, but any direct interaction with the active site copper cannot be proven or discounted based solely on the kinetic data.

The top-scoring N-Ac-(L)-Thienyl-Acrylate orientation is shown in Figure 44.

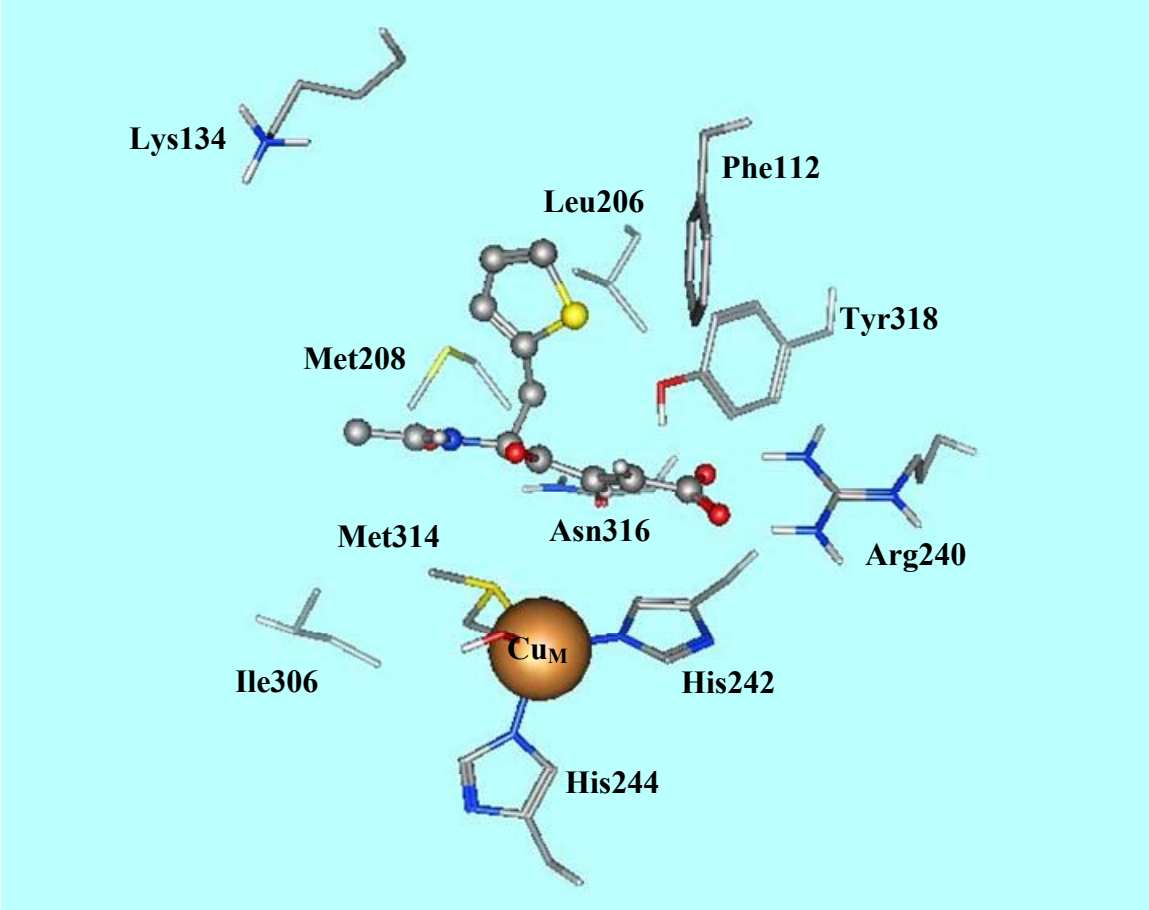

Figure 44. N-Ac-(L)-Thienyl-Acrylate docked to PAM active site.

Strikingly evident is the similarity in binding of N-Ac-(L)-Thienyl-Acrylate to that of N-Ac-(L)-Phe-Acrylate. The docked conformation yields a side chain in the active site hydrophobic pocket, a salt bridge between the inactivator carboxylate and the R240 guanidinium moiety (each oxygen 1.5 Å distant from the corresponding guanidinium hydrogen atoms), and a hydrogen bond between a carboxylate oxygen and Y318 (2.0 Å). Again, it is not possible in these simulations to allow for a displacement of an active site ligand (H242, H244, or M314) since all enzyme residues/atoms must remain static.

Oddly, N-Ac-(D)-Thienyl-Acrylate, shown in Figure 45, deviates significantly from the orientation seen with N-Ac-(D)-Phe-Acrylate.

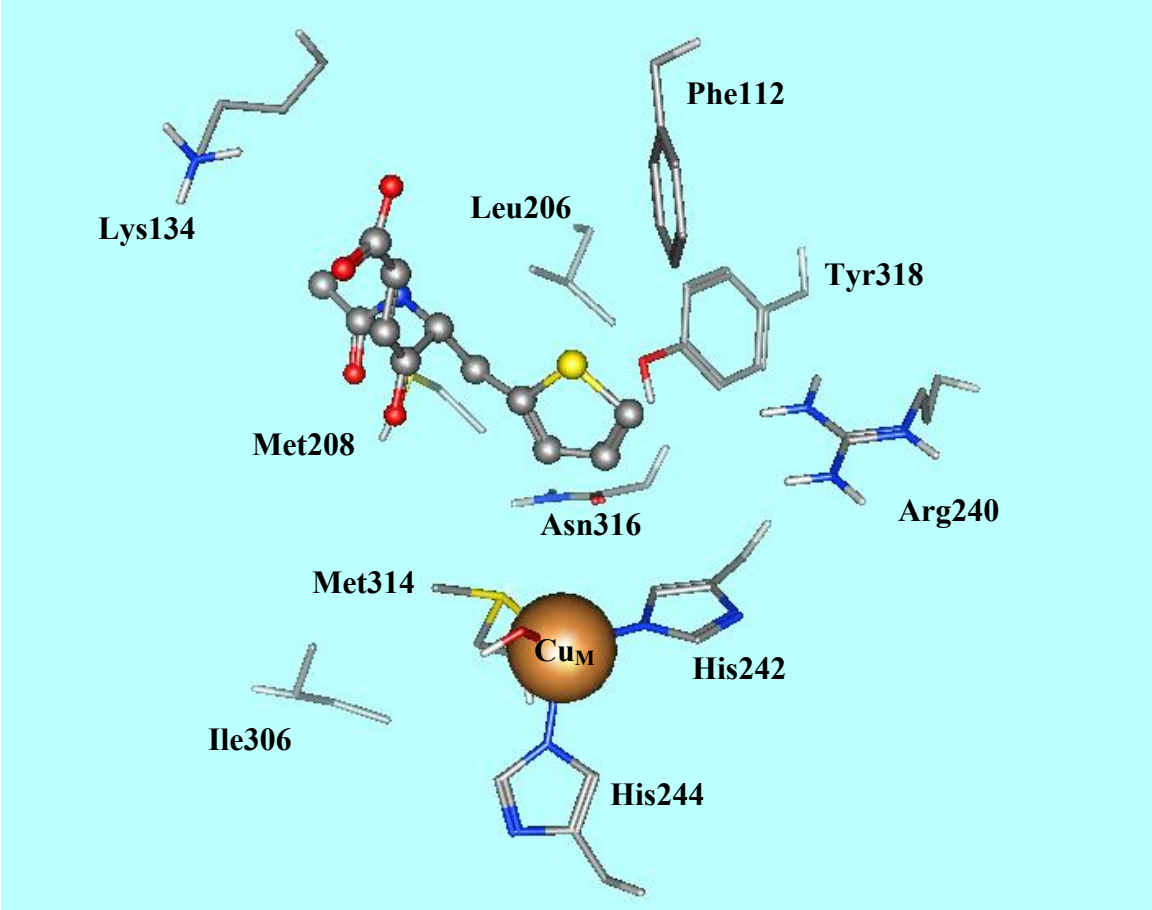

Figure 45. N-Ac-(D)-Thienyl-Acrylate docked to 1PAM active site.

Instead of adopting the conformation of the corresponding enantiomer of N-Ac-Phe-Acrylate, N-Ac-(D)-Thienyl Acrylate deviates completely from the orientations shown for all actual (and hopefully potential) substrates, inhibitors, and inactivators. There is no interaction between the carboxylate of the ligand and R240; instead, the carboxylate moiety interacts with the positively-charged side chain of K134. The thienyl ring, instead of being directed into the hydrophobic pocket of the enzyme, projects toward the space normally reserved for the substrate/inhibitor carboxylate and C_α. As mentioned previously for N-Ac-(D)-Phe-Gly, a failure to bind in the productive conformation,

including salt-bridge formation and the side chain in the hydrophobic pocket of the enzyme, implies that this compound will either not be an inhibitor/inactivator at all, or an exceedingly poor one relative to those compounds which bind productively.

N-Ac-(L)-Phe-Crotonate and N-Ac-(D)-Phe-Crotonate

These compounds differ from the Phe-acrylates via the inclusion of a methylene spacer between the carbonyl group and the proximal carbon atom of the alkenyl functionality. The effects of this inclusion are three-fold. First, the compound no longer contains an α,β-unsaturated ketone. Secondly, the location of the methylene group results in the addition of two freely rotatable bonds, one on each side of the new methylene group. Finally, the carbon bearing the benzyl functionality is one carbon further distant from the terminal carboxylate, which would disturb the position of the phenyl ring in the hydrophobic pocket of the enzyme if these compounds bind in a productive fashion similar to the Phe-Acrylates (requiring, or course, the salt bridge formation between the ligand carboxylate and R240 of the enzyme).

The top scorer of N-Ac-(L)-Phe-Crotonate in the 1OPM active site is shown in Figure 46. The first striking feature of this association is the orientation of the ligand carboxylate downward toward CuB, rather than being directed toward R240. The second striking feature is that the phenyl ring of N-Ac-(L)-Phe-Crotonate occupies virtually the same space as the phenyl ring of N-Ac-(L)-Phe-Acrylate and N-Ac-(L)-Phe-Gly. This hydrophobic interaction appears to predominate, from a binding standpoint, over the ionic effects of ligand/receptor interactions, as the ligand carboxylate did not form a salt

bridge with R240 and drive the phenyl ring further "to the left" in the hydrophobic pocket. This results in a compound which appears to be tightly bound to the active site. Since the compound has not been investigated experimentally, it is uncertain whether or not it would be a competitive PAM inhibitor or inactivator, but it appears to be a promising candidate. The possibility of maintaining the phenyl/hydrophobic pocket interaction while exchanging the carboxylate/R240 ionic interaction with a Cu+2/carboxylate interaction makes this a very intriguing compound.

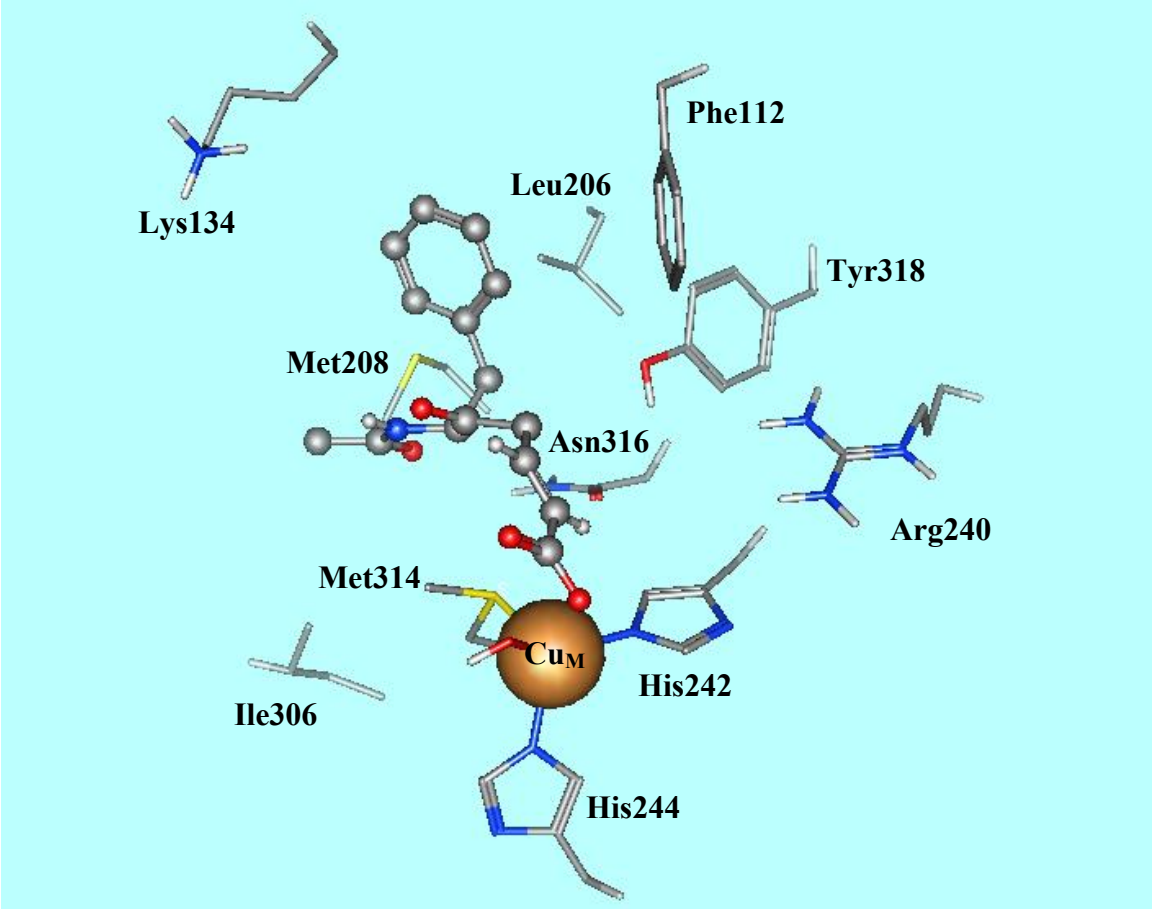

Figure 46. N-Ac-(L)-Phe-Crotonate docked to PAM active site.

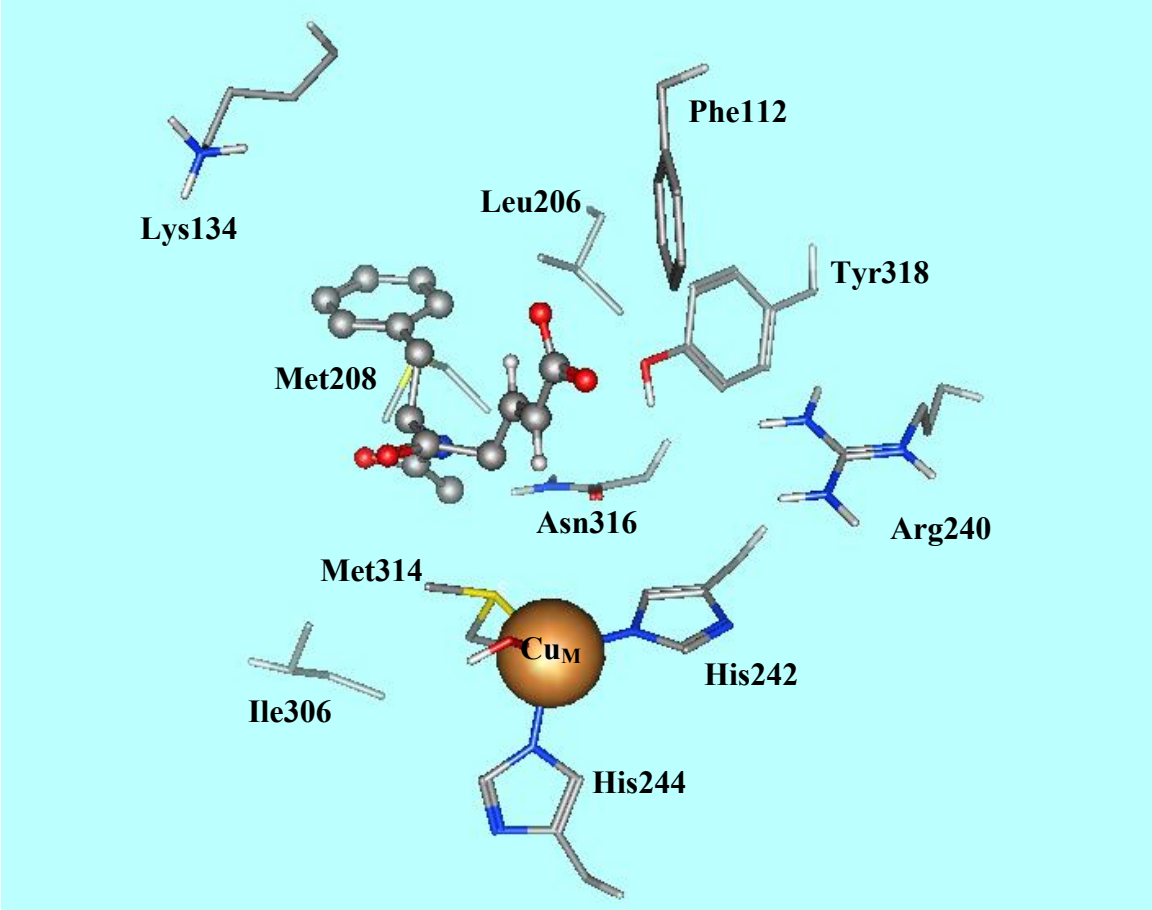

Figure 47. N-Ac-(D)-Phe-Crotonate docked to PAM active site.

By contrast, N-Ac-(D)-Phe-Crotonate appears to bind unproductively or not at all to the PAM active site (Figure 47). This enantiomer not only fails to form a salt bridge with R240 but no interactions between the ligand carboxylate and the copper ion are evident. Furthermore, the favorable association of the phenyl ring seen for the L-enantiomer in the active site hydrophobic pocket has been altered. Based on these factors, it is unlikely that the D-enantiomer would be an effective PAM inhibitor.

N-Ac-(L)-Phe-Propiolate and N-Ac-(D)-Phe-Propiolate

These compounds differ from the N-Ac-Phe-Acrylates in two concrete ways. First, from an electronic standpoint, the α,β-alkenyl group is oxidized to an α,β-alkynyl group. Secondly, the structure of the C-terminal end of the inactivator has been altered spatially from a trans-alkene to a linear moiety across the triple bond and carboxylate. Obviously, the two sp2 hydrogens of the N-Ac-Phe-Acrylates are gone altogether, which results in a smaller molar volume at the C-terminus for the Phe-Propiolate compounds. These compounds have not been investigated experimentally.

Figure 48 displays the top scorer of N-Ac-(L)-Phe-Propiolate bound to the PAM active site. Here, we see the carboxylate/R240 salt bridge characteristic of PAM substrates/inhibitors (carboxylate oxygens 1.6 and 1.7 Å distant from the terminal guanidinium hydrogen atoms) and the typical hydrogen bond between the carboxylate oxygen and the phenolic hydrogen of Y318. The phenyl moiety appears to be offset slightly relative to that seen for N-Ac-(L)-Phe-Gly and N-Ac-(L)-Phe-Acrylate, but lies in essentially the same position. The β-carbon of the N-Ac-(L)-Phe-Propiolate, owing to the linear nature of the alkynyl moiety, is pushed "upward" relative to the corresponding carbon in the N-Ac-(L)-Phe-Acrylate, resulting in a greater distance between the copper (which ligates dioxygen in the reduced form of the enzyme) and this carbon atom. If this compound is found to be an inactivator of PAM, this increased distance from CuB may have interesting mechanistic implications, which will be examined further in the Discussion section.

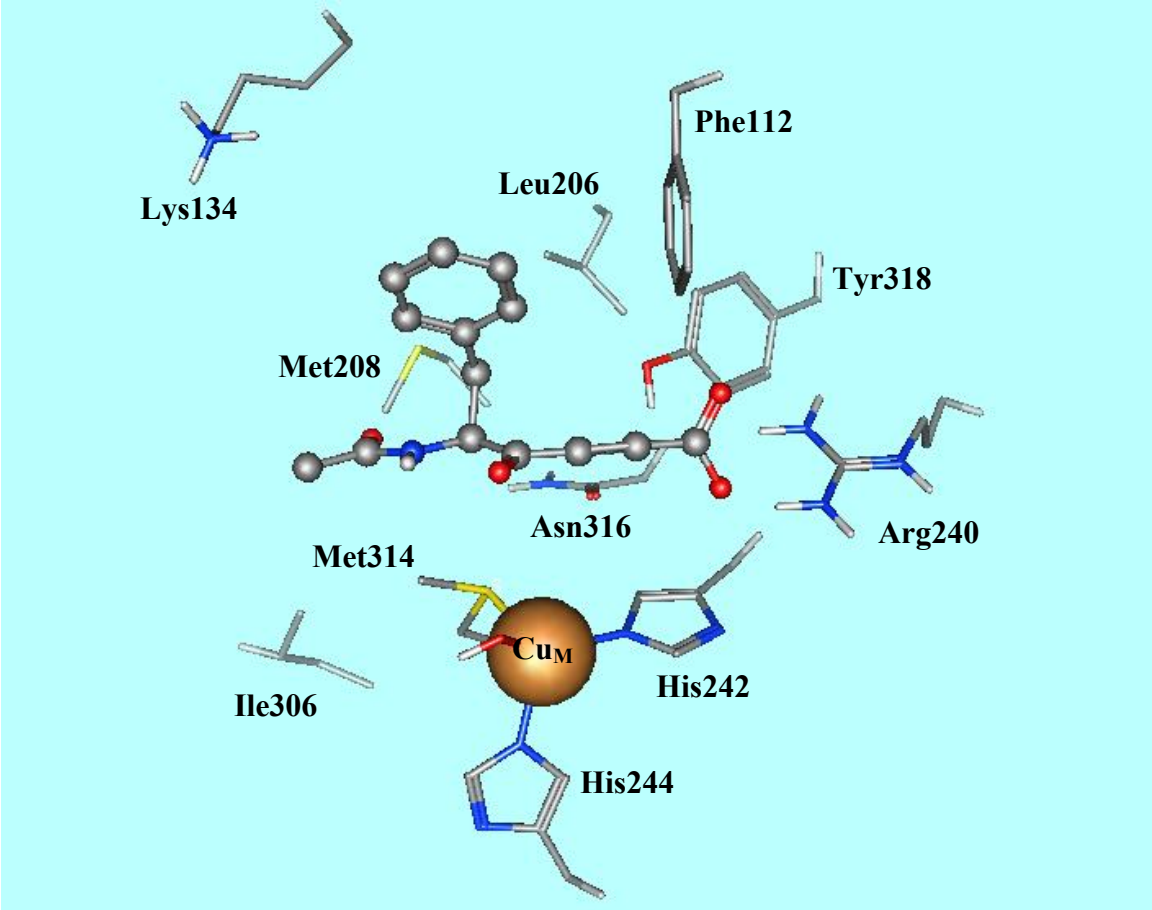

Figure 48. N-Ac-(L)-Phe-Propiolate docked to the PAM active site.

The N-Ac-(D)-Phe-Propiolate enantiomer is shown bound to 1OPM in Figure 49. Here, we see that the carboxylate has disengaged from R240 and the phenyl ring of the ligand has been displaced "to the left" relative to the (L)-enantiomer. This results, overall, in a conformation/location which would be expected to be unfavorable with regard to affinity to the PAM active site, relative to the (L)-enantiomer. N-Ac-(D)-Phe-Propiolate appears to be a poor inhibitor/inactivator of PAM based upon its active site location.

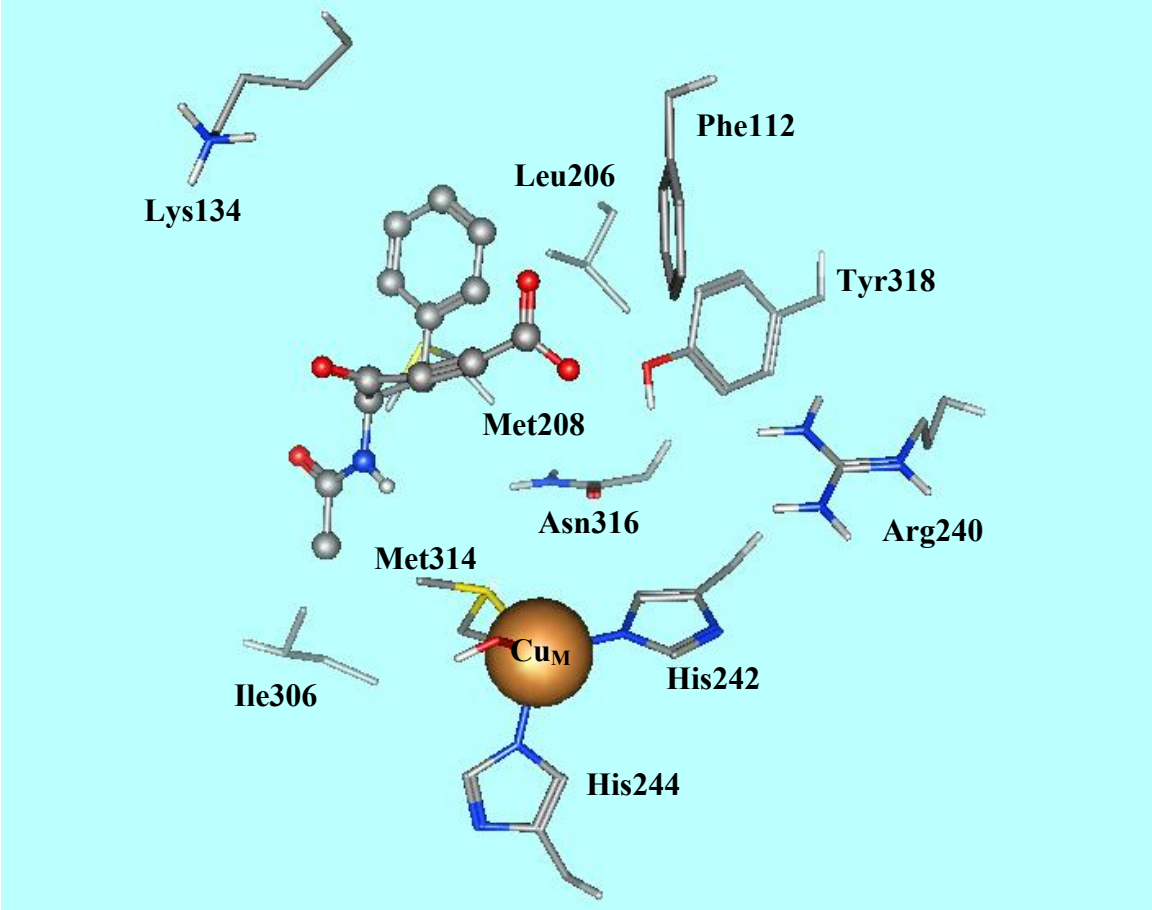

Figure 49. N-Ac-(D)-Phe-Propiolate docked to PAM active site.

PBA (4-Phenyl-3-Butenoic Acid)

PBA differs from the other inactivators/inhibitors (potential and theoretical) modeled above in that it is an analog of hippuric acid (N-Benzoylglycine) rather than N-Ac-X-Gly. It lacks the carbonyl group common to all of the other compounds, and is not isoelectronic with regard to other peptide-based substrates and inhibitors. Furthermore, unlike the Acrylates, Crotonates, and Propiolates, PBA IS analogous to glycine at the C-terminus, containing an sp3-hybridized acetate functionality. Also, PBA contains a 3-

alkene whereas the others contain a 2-alkene (or alkyne). PBA is an inactivator of PAM under standard assay conditions, although one with a high partition ratio, and therefore was expected to dock in the same manner as other PAM substrates/inhibitors/inactivators. The top-scoring conformer of PBA docked to 1OPM is shown in Figure 50.

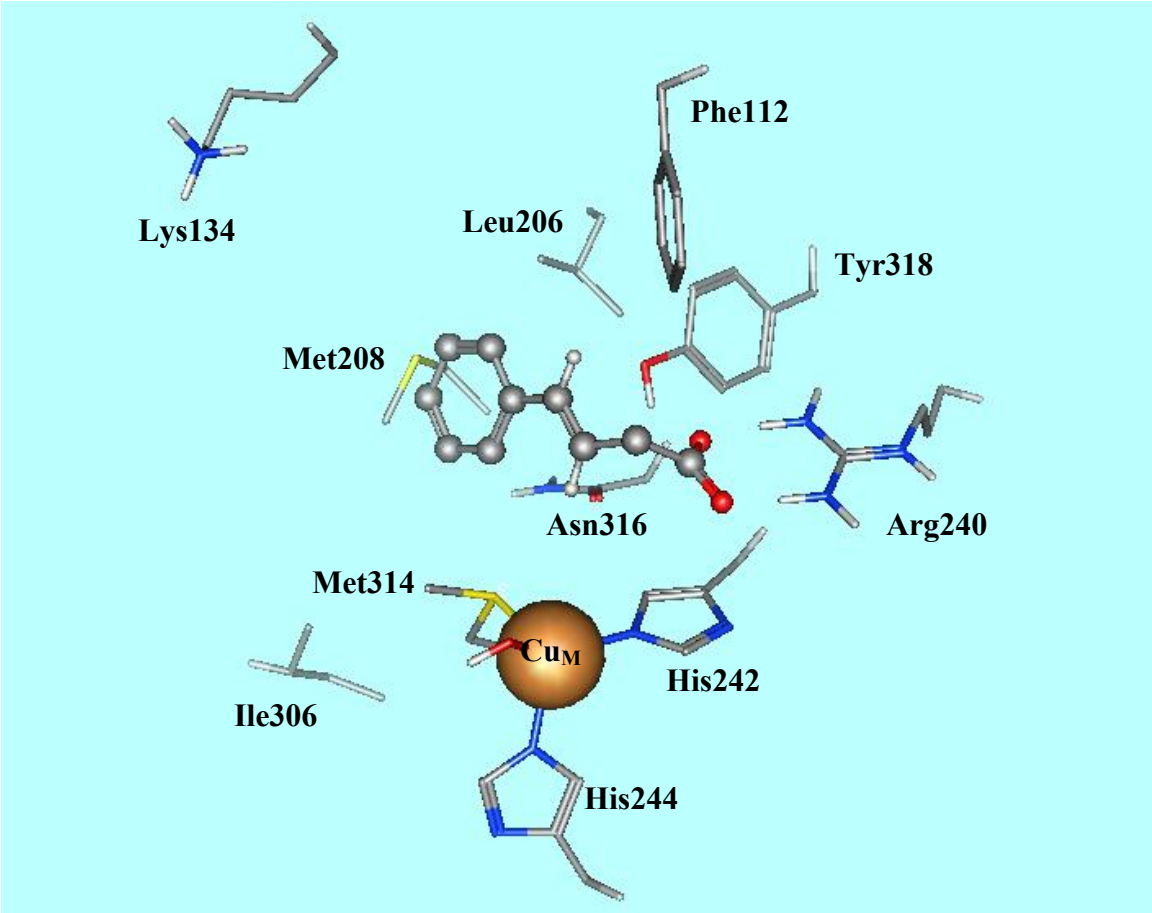

Figure 50. PBA docked to PAM active site.

Indeed, PBA bound to the active site in the expected manner. The two carboxylate oxygens of PBA are both 1.5 Å distant from the R240 guanidinium nitrogens, and Y318 forms a hydrogen bond (2.0 Å) with a carboxylate oxygen. The phenyl ring, however, is

not oriented into the same site of the enzyme's hydrophobic pocket as other known substrates/inactivators. This is due to the fact that PBA is "short" two carbons relative to N-Ac-(L)-Phe-Gly and N-Ac-(L)-Phe-Acrylate; because of this, the PBA phenyl ring is bound to the carbon atom which would correspond to the carbonyl carbon of both of the above compounds and cannot be expected to bind in a similar manner.

Chapter 4: Kinetics and Modeling Discussion

Kinetic analyses and molecular modeling studies of the three acrylate compounds reinforced certain known aspects about PAM substrate/inhibitor specificity, while illustrating a number of important new aspects to the discussion of the active site residues involved in catalysis and stereospecificity. First, the sulfur-containing N-Ac-(L)-Met-Acrylic Acid was shown to bind slightly less favorably to the enzyme's active site than the hydrophobic N-Ac-(L)-Phe-Acrylic Acid (K_I = 53.7 μM vs. 56.5 μM, respectively). Previous work in this laboratory had demonstrated a 3-fold lower K_I value for the (L)-thienyl derivative relative to the (L)-phenylalanyl derivative (Feng, 2000). The thienyl compound is both aromatic and sulfur-containing, and was expected to bind potently to the PAM active site by virtue of both characteristics. The methionyl compound, on the other hand, while hydrophobic, lacks the aromaticity of both the phenylalanyl and thienyl derivatives. As mentioned previously, the P2 residues of peptide substrates tend to contribute most heavily to the overall binding affinity of dipeptide or tripeptide substrates, and sulfur-containing and hydrophobic residues at this position tend to result in the most tightly-bound compounds. Although both the (L)-thienyl and (L)-methionyl acrylates bind tightly to the active site, in both cases the rate constant of inactivation is depressed relative to the (L)-phenylalanyl derivative (by approximately 50% in both cases). The most obvious interpretation of these lower inactivation rates would be a disturbance of the Cu_M ligand environment by the sulfur compounds, indicating that these side chains are able, at least transiently, to ligate Cu_M. Any disturbance of the catalytic complex would be presumed, *a priori*, to prevent the electron transfer requisite for

enzyme inactivation. On the other hand, the lowered rate constants of inactivation could be the result of an electronic effect, rather than an effect of copper ligation. Relative to the benzyl side chain of the phenylalanyl derivative, both the thioether of methionine and the 5-membered aromatic sulfur-containing ring of the thienyl derivative are clearly less electron-withdrawing and, as such, may be less effective regarding the generation of the inactivating intermediate, compared to the phenylalanyl derivative. Nevertheless, the relatively equipotent binding affinities of the (L)-Met and (L)-Phe acrylates was not unexpected, especially since the corresponding glycine-extended peptides with Met or Phe in the P2 position exhibit much the same behavior.

Unexpectedly, and in contrast to the earlier analyses of both peptidyl substrates and competitive inhibitors, both N-Ac-(L)-Phe-Acrylate and N-Ac-(D)-Phe-Acrylate have nearly identical K_I values, with the (D)-Phe actually binding more avidly than the (L)-Phe derivative (60.0 μM vs. 53.7 μM, respectively). All previously explored dipeptide enantiomers with glycine at the C-terminus have consistently shown that only the (L)-compounds are either substrates or competitive inhibitors. In contrast, the rate constant of inactivation for the (L)-Phe acrylate was 2-fold greater than for the (D)-Phe acrylate (0.383 min^{-1} vs. 0.185 min^{-1}, respectively). These results imply that the structure of the acrylates is sufficiently different from that of their corresponding dipeptide analogs that the established stereochemical requirements for peptide substrates do not apply to the acrylates. Structural differences, between N-Ac-(D)-Phe-Gly and N-Ac-(D)-Phe-Acrylate, for instance, can explain this abolition of binding stereospecificity with regard to the acrylates and will be explored more fully when the modeling results are discussed below. It is interesting that, while the binding constants for the (L) and (D)-Phe acrylates

are nearly identical, the (D)-enantiomer is only ½ as potent insofar as the rate constant of inactivation is concerned. This implies that while both compounds are able to bind equipotently to the PAM active site, they may indeed bind differently, such that, once bound, the (D)-enantiomer is in a less favorable orientation for mechanistic inactivation. This difference will also be explored in the modeling discussion.

All of the above kinetic parameters were derived from the Progress Curve Assay, in which varying concentrations of substrate and inactivator are simultaneously incubated with enzyme and product formation is measured with respect to time of incubation. The k_{inact}/K_I values for the (L)-Phe, (D)-Phe, and (L)-Met compounds were found to be 7130 ± 240, 4750 ± 100, and 2440 ± 80 M^{-1} min^{-1}, respectively. In contrast, the same results from the Dilution Assay, where enzyme is preincubated with inactivator for varying times prior to transfer into assay mix with saturating substrate concentrations, yielded the following values: 7320 ± 140, 4090 ± 100, and 8140 ± 210 M^{-1} min^{-1} for (L)-Phe, (D)-Phe, and (L)-Met, respectively. The specificity constants from both assays are either within or very close to the margin of error in the cases of both the (L)-Phe and (D)-Phe acrylates, but is inflated by 3-fold in the case of the (L)-Met compound in the Dilution Assay. This was also the case for the sulfur-containing (L)-thienyl acrylate derivative analyzed by Feng (Feng 2001) using the Progress Curve and Dilution assays, although in her hands, the (L)-thienyl derivative was only twice as potent in the Dilution assay; the (L)-Phe derivative, on the other hand, yielded approximately the same values in both types of assay. These differences in results for the different assays employed, in both cases involving a sulfur-containing inactivating molecule, suggests that the absence of substrate during the incubation of enzyme with acrylate somehow renders the enzyme

subject to a more efficient inactivation. As mentioned in the Results section, analysis of kinetic data from the Dilution assay for compounds which yield an individual value for k_{inact} of less than one, and owing to the covariance of the k_{inact} and K_I values, yields individual values for both of these parameters associated with very high error values. In other words, repetition of the Dilution assay will yield consistent values of k_{inact}/K_I but often very different values, from assay to assay, for the individual components of that parameter. Nevertheless, it appears that the value for k_{inact}, and not so much K_I, is the parameter that prompts such a drastic change in the value of k_{inact}/K_I between the Progress Curve and Dilution assays. So, the binding of these compounds to the active site, and their relative affinities, do not change dependent upon the presence or absence of substrate; however, the rate constant of inactivation does change, implying that the presence of substrate somehow affects the mechanism of inactivation, but only in the case of the sulfur-containing (and potentially copper-ligating) acrylates. Likely, taking into account the generally lower rate constant of inactivation of the sulfur-containing acrylates (in both assay types) relative to the phenylalanyl acrylates, the substrate in the Progress Curve assay is able to displace the sulfur-containing inactivators before the inactivation event occurs, thereby reducing the number of productive binding events between the acrylate and the enzyme, thereby selectively reducing the inactivation rate relative to the Dilution assay. This would be best expressed as $E + I \rightarrow E\text{-}I \rightarrow E\text{-}I' \rightarrow E\text{-}I^*$, where an initial enzyme-inhibitor complex (E-I) forms quickly, followed by a slower step where the enzyme and inhibitor adopt the productive inactivation complex (E-I'), followed by the inactivation event itself to yield the ($E\text{-}I^*$) inactivated enzyme. If the conformational change required to adopt a productive complex is slow, relative to the other steps,

substrate in solution may be able to displace the sulfur-containing acrylate prior to the inactivation event. In this case, k_{inact} would be representative of the rate of this conformational change if indeed that step is slower than the inactivation event itself. Disruption and reorganization of the active site via copper ligation may be expected to take place on a relatively slower time-scale than electron transfer or reaction with the ROS at Cu_M, and would explain the discrepancy in results between these two assay methods, for the sulfur-containing acrylates. In addition, it would be expected that copper ligation by the thioether moiety of N-Ac-(L)-Met-Acrylate would be less favorable than for the more potently-ligating thiophene of N-Ac-(L)-Thienyl-Acrylate. The greater discrepancy (3-fold) in k_{inact}/K_I values between the Dilution and Progress Curve assays in the case of (L)-Met-Acrylate may reflect this slower rearrangement of the E-I complex to the productive inactivating complex; the discrepancy is only 2-fold in the case of the potentially more powerful copper ligator (L)-Thienyl-Acrylate.

Once the crystal structure has been solved and the nature and orientation of residues in the active site have been determined, a much better understanding of substrate and inhibitor binding may be derived from computer-assisted molecular docking of ligands to the protein of interest. Certainly, it is even more instructive when the enzyme is co-crystallized with substrate bound to the active site, and the nature of the residues responsible for binding and catalysis are delineated. In 1998, Prigge et al. solved the structures for PAM in the oxidized and reduced forms of the enzyme (Cu^{+2} and Cu^{+1}, respectively), and the oxidized form with the substrate N-acetyl-diiodotyrosylglycine (IYG). The residues Arg240, Tyr318, and Asn316 are the most important residues for binding this substrate, with Arg forming a bidentate salt bridge with the carboxylate of

the substrate, Tyr forming a hydrogen bond with the substrate carboxylate, and Gln forming a hydrogen bond with the peptide bond of the substrate. Many hydrophobic contacts are formed with the active site residues Phe112, Lys134, Leu206, Met208, Ile306, Met314 (a Cu_M ligand), and Tyr318. A modeling simulation run with IYG resulted in a placement and conformation of the molecule that was nearly superimposable upon the crystal structure ligand, with only a slight deviation in placement of the N-acetyl group. The active site environment around the N-acetyl group is a relatively open space, so this slight deviation is not surprising. All of the polar and electrostatic contacts present in the IYG-bound crystal structure were present in the case of docked IYG. The close agreement of the two structures provides evidence that this simulation, and by extension simulations run with other similar molecules, is capable of closely approximating the orientations and placement of glycine-extended dipeptides and the corresponding acrylate-containing inhibitors.

The known PAM substrate N-Ac-(L)-Phe-Gly is very similar in structure to the IYG substrate bound in the oxidized PAM crystal structure. Indeed, the molecules are identical save for the substitutions on the phenyl ring, with IYG containing two iodine atoms and a hydroxyl group which are oriented toward the side chains of the various residues lining the hydrophobic pocket of the active site. The carboxyl ends of both molecule are identical, and the simulations demonstrated that the three main electrostatic/polar interactions are preserved in the case of N-Ac-(L)-Phe-Gly. The salt bridge between substrate carboxylate, and the hydrogen bonds to Tyr318 and Asn316 are all maintained in IYG-docking simulation. The unsubstituted phenyl ring does not associate as closely with Phe112 as it lacks the large iodine atom of IYG which forms a

close hydrophobic interaction with this residue. The N-acetyl group of N-Ac-(L)-Phe-Gly is rotated slightly with respect to that of IYG, but this does not affect the binding of the C-terminus of the substrate where hydroxylation occurs. In both cases, the glycine C_α is oriented downward toward the copper complex with the pro-(S) hydrogen in a favorable position for abstraction. The pro-(R) hydrogen is directed upwards away from the catalytic complex, in agreement with the substrate stereospecificity studies performed by this laboratory (Ping 1992, Ping 1995).

Previous work in this laboratory (Katopodis 1990) has shown unequivocally that the molecule N-Ac-(D)-Phe-Gly is not a PAM substrate and an exceedingly poor competitive inhibitor, indicating that not only is this enantiomer unable to bind productively for catalysis, but is also effectively unable to bind at all to the PAM active site. Therefore, this molecule was not expected to bind to the active site in a manner at all similar to its enantiomeric substrate counterpart, and this turned out to be the case in the molecular docking simulation. Indeed, this molecule failed to associate with any of the residues critical for catalysis, hydrogen-bonding, or electrostatic interactions seen for IYG or N-Ac-(L)-Phe-Gly. The change in stereochemistry prevents this molecule from adopting a productive conformation complementary to the critical residues of the active site.

The same trends were evident with the enantiomeric pairs N-Ac-(L)-Leu-OCH_2-COOH/N-Ac-(D)-Leu-OCH_2COOH and (S)-O-Ac-Mandelyl-Gly/(R)-O-Ac-Mandelyl-Gly (stereotopically equivalent to (L)-O-Ac-Mandelyl-Gly/(D)-O-Ac-Mandelyl-Gly). In both cases, the (L)/(S)-enatiomers were found to bind in a manner very similar to IYG and N-Ac-(L)-Phe-Gly. N-Ac-(L)-Leu-OCH_2COOH is an ester analog of PAM dipeptide substrates which fails to undergo PAM catalyzed hydroxylation, but was found to be a

potent competitive inhibitor (Ping, 1995). Unlike N-Ac-(L)-Phe-Gly, the (L)-Leu derivative does not possess a hydrogen-bond donor at the position analogous to the peptide bond. Therefore, it cannot form a hydrogen bond with the side chain of Asn316. In addition, rotation about the ester bond is less restricted than that of the amide bond of the corresponding N-Ac-(L)-Phe-Gly. Nevertheless, the carboxylate still associates closely with Arg240 and hydrogen bonds to Tyr318. The leucine side chain occupies the same space in the hydrophobic pocket as the phenyl ring of N-Ac-(L)-Phe-Gly, associating closely with Phe112. The pro-(S) hydrogen is still directed toward the Cu_M catalytic complex, with the pro-(R) hydrogen directed upwards toward Tyr318, but the position of this hydrogen does not appear to lie as closely to the copper complex as was the case for N-Ac-(L)-Phe-Gly, and may indeed exceed the maximum possible distance for catalysis to occur. On the other hand, the electronic effects of the ester bond may be a major contributor to the lack of catalysis. The glycolate ester of 4-methoxybenzoic acid also failed to undergo PAM catalysis where the corresponding amide was indeed a substrate (Katopodis 1990). (S)-O-Ac-Mandelyl-Gly is very closely related, and stereotopically equivalent to N-Ac-(L)-Phe-Acrylate, the only differences being that whereas the side chain of the Phe compound is a benzyl group, that of the mandelyl compound is a phenyl moiety lacking the methylene group. Since the acetyl group is oriented into an open area of the PAM active site, and not associated with any active site residues, it was not expected that this structural change would have much effect on the docking of the (L)-Mandelyl compound in the active site. The phenyl group associates very closely with Phe112, and although the carboxylate end of the ligand still forms a salt-bridge with Arg240, the rest of the molecule is pulled upwards to the extent that the

amide nitrogen of the substrate cannot form a hydrogen bond with Asn316. The loss of this interaction is reflected in the less favorable K_M value of the (L)-Mandelyl derivative relative to the (L)-Phe derivative (170 μM vs. 7.9 μM, respectively). Conversely, neither N-Ac-(D)-Leu-OCH_2COOH nor (R)-O-Ac-Mandelyl-Gly are substrates or inhibitors of PAM. Neither associated closely with any active site residues in the docking simulations.

Initially, the similar potencies of PAM inactivation by N-Ac-(L)-Phe-Acrylate and N-Ac-(D)-Phe-Acrylate were very surprising in light of the previous results. Indeed, the N-Ac-Phe-Acrylates are the only enantiomeric pair corresponding to N-Ac-X-Gly dipeptides in which both species either undergo catalysis or competitively inhibit or inactivate PAM. Exhaustive work with circular dichroism spectroscopy, polarimetry, and chiral chromatography all proved that the N-Ac-(L)-Phe-Acrylate and N-Ac-(D)-Phe-Acrylate preparations used for inactivation kinetics were enantiomerically pure. There exist several possibilities for the enzyme's ability to process both of these enantiomers in an indiscriminant manner. First, the absence of a hydrogen-bond donor or acceptor in a position analogous to the amide bond of peptide substrates eliminates a point of contact with the active site of the enzyme (Asn316). Second, the conjugation of the bonds in the acrylate would be expected to severely restrict the rotational freedom and limit the number of possible conformers at the carboxylate end of the inactivator. For the acrylate, the extra sp^2 center (at the position analogous to C_α in N-Ac-Phe-Gly) influences the geometry of the rest of the molecule, and is coplanar with, at the minimum, the carboxylate carbon atom and C_β.

Docked N-Ac-(L)-Phe-Acrylate and N-Ac-(D)-Phe-Acrylate both form bidentate salt-bridges with Arg240, and both sp^2 C_α and C_β atoms occupy the same space in the active

site. The rest of the docked structures, to the amino side of C_β, diverge significantly from one another. The (L)-enantiomer binds in a manner almost identical to N-Ac-(L)-Phe-Gly and IYG, with a close interaction of the phenyl ring of the inhibitor and Phe112. The (D)-enantiomer has undergone a rotation of approximately 120º about the Phe C_α-C(=O) bond, directing the phenyl ring directly back into the hydrophobic pocket, rather than aligning to interact with Phe112. The N-acetyl group remains generally in the same position for both enantiomers in the free space above and to the left of the Cu_M center. It must be noted that the crystal structure employed for these studies does not contain molecular oxygen ligated to Cu_M. The acrylates lack the sp^3 glycyl methylene groups of standard glycine-extended peptides. It is very likely that the mechanism (discussed below) proceeds differently for acrylate inactivation versus substrate hydroxylation. This would be a function of the difference in bond strength between an sp^2 C-H bond and an sp^3 C-H bond (110 kcal/mol vs. 95 kcal/mol for propene and the secondary C-H bond of propane, respectively (Vollhardt 1994). The PAM reaction, as evidenced by the large (10-12) deuterium kinetic isotope effect, is very sensitive with regard to the nature and strength of the C-H bond at C_α. It is quite possible that PAM is unable to cleave an sp^2 C-H bond. If this is the case, then the mechanism of inactivation would proceed through an alternate pathway (i.e. without hydrogen atom abstraction), possibly involving the initial reduction (by the superoxide generated at CuM) of the Phe-Acrylate to a radical anion, followed by reaction with an active site residue, such as Tyr318. Under these circumstances, the stereochemical requirements may be obviated so long as there is sufficient room to accommodate the molecule in the active site, form the salt-bridge with R240, and place either C_α or C_β in close proximity with molecular oxygen ligated to Cu_M.

A “flexible alignment” simulation is one whereby the conformational space of a pair of related molecules can be explored in order to find the most energetically favorable conformations of each of the two molecules which provide the most favorable overlap of its various hydrophobic, acidic, alkaline, polar, and H-bond donor/acceptor moieties. These simulations were performed on the following pairs of molecules: N-Ac-(L)-Phe-Gly and N-Ac-(L)-Phe-Acrylate, N-Ac-(L)-Phe-Gly and N-Ac-(D)-Phe-Gly, and N-Ac-(L)-Phe-Gly and N-Ac-(D)-Phe-Acrylate. The results of these simulations are presented in Figures 51 – 53, respectively. The carboxylate group of each ligand was “fixed” at the coordinates of the IYG molecule from the crystal structure (restricted from rotational or translational motion) and therefore each alignment pair has an obligate overlap of this functionality. The salt-bridge which forms between the substrate/inhibitor carboxylate and the guanidinum group of Arg240 has been shown above to be present not only in the Prigge crystal structure, but also in every case presented in the docking results above of all *known* substrates and inhibitors tested. This restriction was necessary to allow the evaluation of the orientations of the other portions of the various molecules, under the assumption that the positioning of the carboxylate is necessary but not sufficient in determining whether or not a particular compound will be able to bind

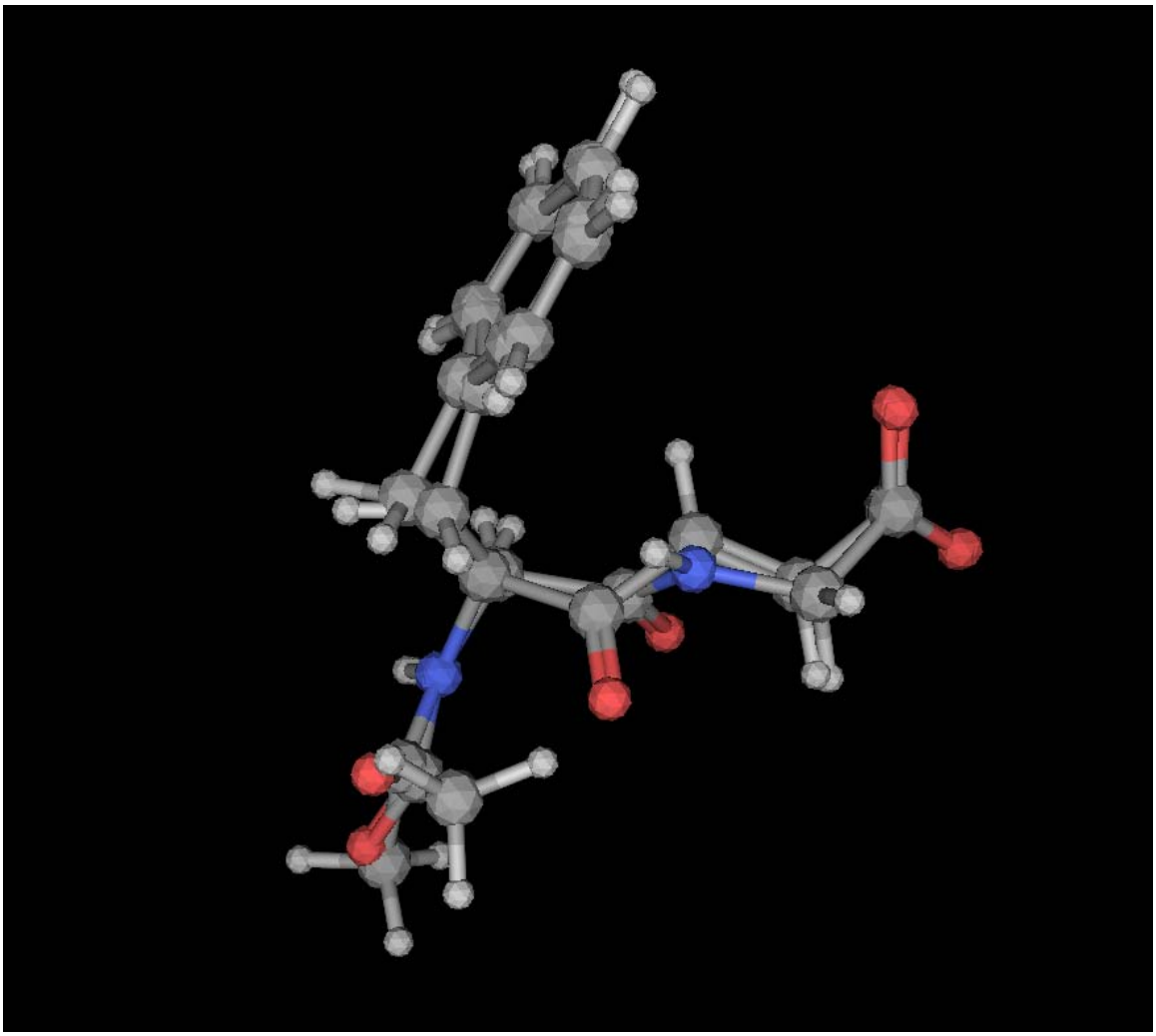

Figure 51. Flexible alignment overlay of N-Ac-(L)-Phe-Gly and N-Ac-(L)-Phe-Acrylate. Deviations in the alignment of the N-acetyl groups are evident. The glycyl portions of the two molecules are well-aligned, with the pro-(S) hydrogen of N-Ac-(L)-Phe-Gly almost perfectly overlaid with the corresponding sp^2 hydrogen atom of the acrylate.

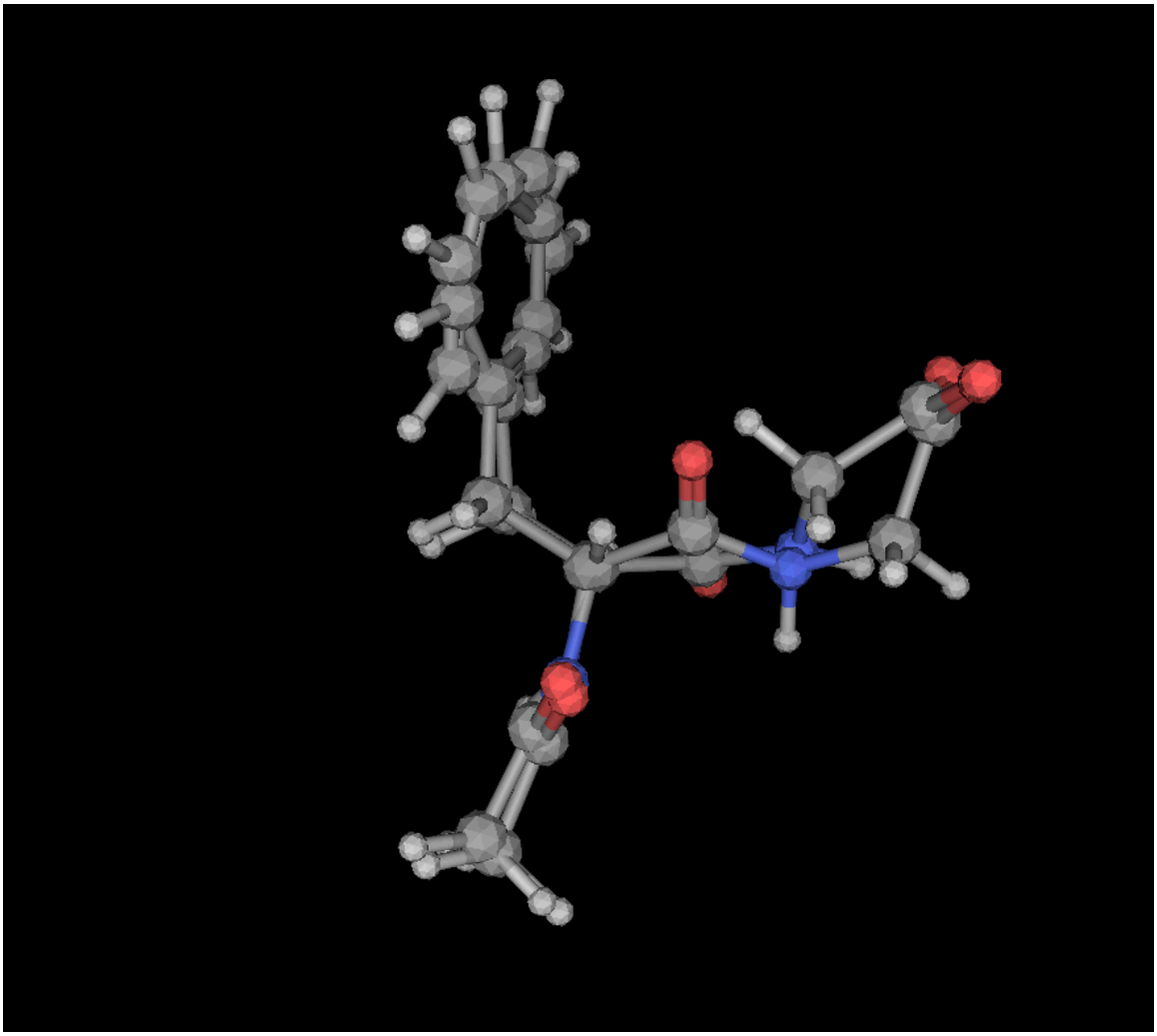

Figure 52. Flexible Alignment overlay of N-Ac-(L)-Phe-Gly and N-Ac-(D)-Phe-Gly. The molecules deviate markedly across the amide functionalities and glycyl residues of the two molecules.

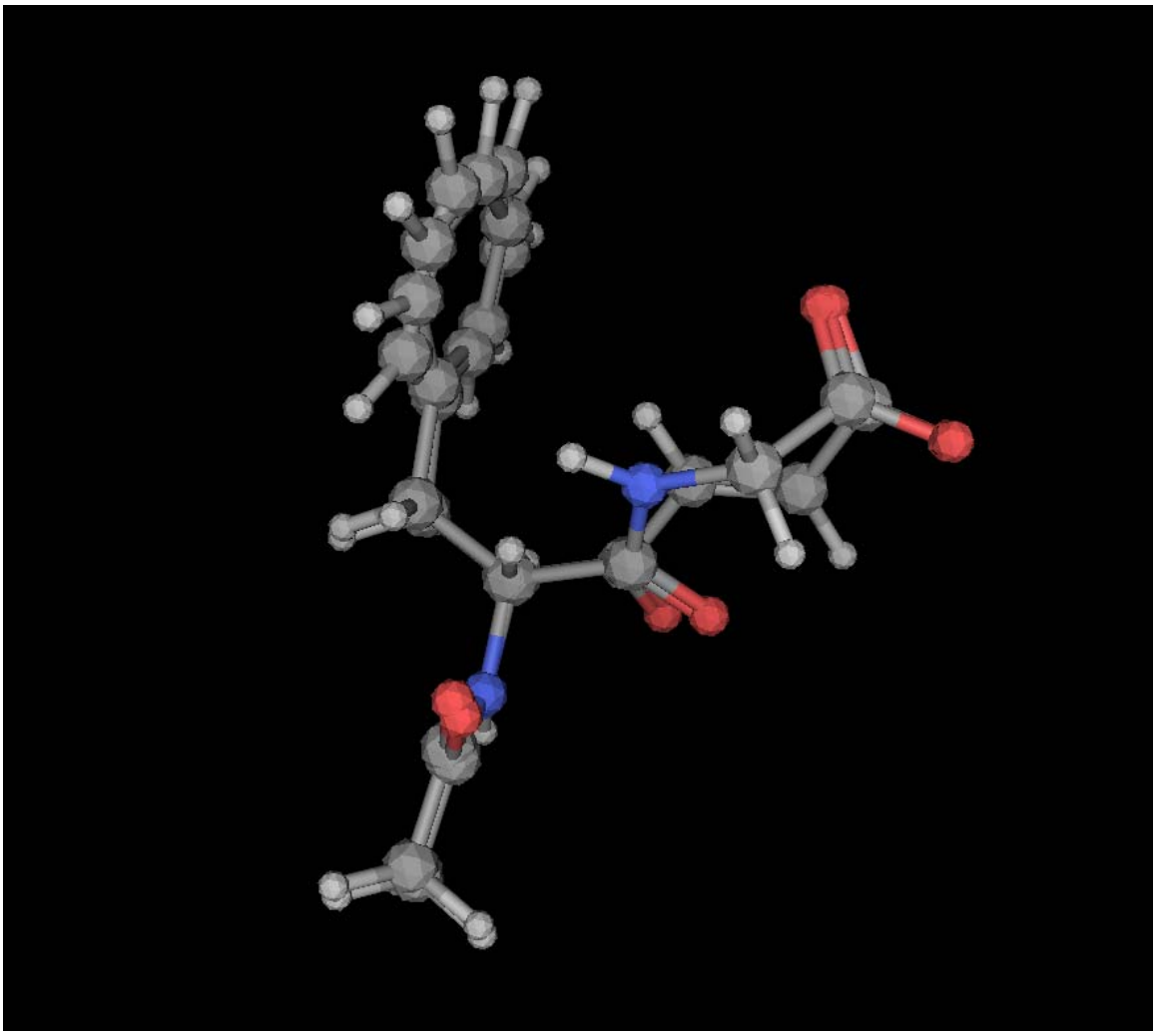

Figure 53. Flexible Alignment overlay of N-Ac-(L)-Phe-Gly and N-Ac-(D)-Phe-Acrylate. The glycyl portions of both molecules are well-aligned, with relatively minor deviations from C2 to C4.

productively as either a substrate or inhibitor. This allows any deviations in overlap to be explored as conditions which may cause a particular enantiomer to fail to bind. While these flexible alignment simulations would likely not be very instructive *in vacuo,* they are useful in the context of the modeling results.

N-Ac-(L)-Phe-Gly and N-Ac-(L)-Phe-Acrylate are both known *in vitro* to bind potently to the PAM active site, the first as a substrate, the second as an irreversible inactivator. The *in silico* results established that both compounds bind to the enzyme in a very similar manner. The results of the flexible alignment simulation shown in Figure 51 indicate a nearly complete overlap of these conformers. The C2 sp^2 hydrogen of the acrylate aligns with the pro-(S) hydrogen of the dipeptide. The benzyl groups and the stereocenters of both molecules overlap with only slight and likely insignificant deviations. The acetyl groups show the most deviation, but results from the modeling indicate that there is sufficient space available in this area of the active site for relatively large deviations in the placement of this functionality. The acrylate C3 and C4 atoms overlap the C and N atoms from the amide bond of N-Ac-(L)-Phe-Gly. There is a slight deviation (less than 30º) between the C3 hydrogen of the acrylate and the amide hydrogen of the dipeptide, and between the C4 carbonyl oxygens of both compounds. Not surprisingly, all of the atoms or the acrylate carboxylate, C2 and C3, and carbonyl group are nearly coplanar, owing to the conjugated nature of the molecule.

The flexible alignment of N-Ac-(L)-Phe-Gly and N-Ac-(D)-Phe-Gly is shown in Figure 52. The N-acetyl groups, benzyl groups, and carboxylate groups are all nearly perfectly aligned. The stereocenters overlap, although the C-H groups point in opposite directions. However, a large deviation occurs between the C1-C4 residues of the

enantiomeric pair and their substituents. The carbonyl groups of the peptide bond point directly opposite from each other (nearly 180º rotation *vs.* approximately 30º between N-Ac-(L)-Phe-Gly and N-Ac-(L)-Phe-Acrylate), and the glycyl methylene carbon atoms are bent away from each other with one of the hydrogens from each molecule also directed 180º from each other. The deviation between the amide hydrogens is less pronounced. It is therefore reasonable to assume that it is the conformation of the glycyl residue, all else being fairly equal, that determines whether a given molecule is able to bind to the active site. It is important to remember that the lack of turnover of N-Ac-(D)-Phe-Gly by PAM could be explained by an unproductive orientation of the C2 hydrogen atoms, such that this enantiomer would be able to bind to the active site but would fail to undergo catalysis. However, in addition to being unable to function as a substrate, the (D)-enantiomer is an exceedingly poor competitive inhibitor (Ping, 1995). This implies that this molecule fails to bind at all to the PAM active site. Therefore, the conformation adopted by the (D)-enantiomer precludes its catalysis *and* binding, and there is insufficient space in the portion of the active site responsible for glycine binding to accommodate the altered positions of C2-C4 and their substituents in the case of N-Ac-(D)-Phe-Gly.

The next step was to investigate the overlap of N-Ac-(L)-Phe-Gly and N-Ac-(D)-Phe-Acrylate (Figure 53). As in the case of the N-Ac-(L)-Phe-Gly/N-Ac-(D)-Phe-Gly flexible alignment pairing, there is nearly perfect overlap between the benzyl groups and N-acetyl groups. The stereocenters again overlap, with the hydrogen atoms oriented in opposite directions. Interestingly, the overlap of C1-C4 and their substituents is in much better agreement in this case than for the Phe-Gly enantiomeric pair. The carbonyl

groups are only about 15º out of plane, and the same is true of the nitrogen of the peptide bond and the C3 hydrogen of the acrylate. Again, for the acrylate, the entirety of the "glycyl" portion of the molecule is coplanar. This planarity allows the acrylate enantiomers to "thread the needle" between the extremes of the positions of the glycyl moieties of the Phe-Gly enantiomeric pair. It seems from these results that the orientation of the carbonyl oxygen of N-Ac-(D)-Phe-Gly, and an unfavorable repulsive electronic interaction with the side chain carbonyl of Asn316 is the condition which explains its failure to act as either a competitive inhibitor or PAM substrate.

The sulfur-containing acrylates are more difficult to discuss in the context of molecular modeling owing to a limitation of the docking methodology. The Molecular Operating Environment docking software requires that all atoms and functionalities of the receptor be static. Only the ligand itself is allowed to undergo translational or rotational movement. Normally, this does not lead to any problems. However, in the cases of N-Ac-Met-Acrylate and N-Ac-Thienyl-Acrylate, where the inactivators were rationally designed in the hopes that ligation of their sulfur atoms to copper would increase their binding affinity, the inability of the software to displace a ligand from Cu_M precludes any detailed analysis of copper-sulfur interactions. Likely, EXAFS or a crystal structure with a bound sulfur-containing acrylate would provide an answer to the question of whether the sulfur atoms indeed ligate active site copper, but those are beyond the scope of this research. Regardless, the modeling shows that N-Ac-(L)-Met-Acrylate, N-Ac-(D)-Met-Acrylate, and N-Ac-(L)-Thienyl-Acrylate bind in a manner consistent with PAM substrates and competitive inhibitors. Only the (D)-Thienyl enantiomer was unable to bind in a manner commensurate with the properties common to substrates. Although the

(D)-Met derivative binds in a manner similar to substrates or inhibitors, it also displays the most significant deviation from a tight salt-bridge formation with Arg240. This compound was not synthesized and therefore no data with regard to its *in vitro* efficacy as a PAM inactivator are available. Likewise, the (D)-Thienyl compound was not synthesized, although a comparison of the kinetic parameters of the pure (L)-Thienyl derivative and the (D,L)-Thienyl racemate indicate that the (D)-enantiomer would be an exceedingly poor inactivator, with the effect more pronounced in the K_I value than the k_{inact} value (Feng, 2001). Because of these limitations, the modeling is likely not as well able to predict the binding of potential copper chelators as it is for other compounds which do not have such a capability.

The time-dependent PAM inactivator PBA is a 3-alkenyl carboxylic acid, whereas the acrylate series are 2-alkenyl carboxylic acid derivatives. The structural difference results in a "glycine-like" $–CH_2COOH$ functionality in PBA, which is lacking in the acrylate series of inactivators. Additionally, incubation of PBA with PAM and the requisite cofactors results in two hydroxylated products (2-hydroxy-4-phenyl-3-butenoic acid and 4-hydroxy-4-phenyl-2-butenoic acid). The partition ratio for PAM inactivation by PBA was found to be approximately 90 (Driscoll 2000). The most reasonable explanation is that PBA, like glycine-extended substrates, undergoes hydrogen-atom abstraction and, 89 times out of 90, hydroxylation; one time out of ninety, however, an inactivation event occurs. The formation of both 2- and 4-hydroxy products implies that PBA, owing to its relatively smaller size and fewer interactions with active site residues, has some freedom of movement in the active site subsequent to hydrogen-atom abstraction. The presence of the 3-alkenyl group (next to an electron-withdrawing phenyl ring) allows for

delocalization of the nascent radical, which explains the ability to form two different hydroxy products, and is presumably dependent upon the ability of C2 and C4 to position themselves in close proximity to bound molecular oxygen.

Docked PBA forms a close bidentate salt-bridge with Arg240 and a hydrogen bond between its carboxylate group and the phenolic group of Tyr318. The C2 atom lies in closer proximity to Cu_M. However, a 180º rotation about the C2-C3 bond of PBA would bring C4 into closer proximity with Cu_M, although relatively unfavorable steric interactions between the phenyl group of PBA and the ligated copper would occur. Somewhere between the two extremes, it would be expected that C4 would approach closely enough to the ROS at Cu_M for 4-hydroxylation to occur, but without the steric hindrance from the phenyl group. Since PBA is relatively small, rotation about the C1-C2 bond could render either the pro-(S) or pro-(R) hydrogen at C2 into a position favorable for hydrogen-atom abstraction. Driscoll's results showed that PBA hydroxylation is stereoselective ((S)-2-hydroxy-4-phenyl-3-butenoic acid is formed at a ratio of 70:30 compared to the (R)-enantiomer), but not stereospecific. The modeling results presented here help to explain this phenomenon.

The enantiomeric N-Ac-Phe-Propiolate pair was also subjected to docking analysis. Attempts to synthesize the (L)-enantiomer with a reaction involving the acid chloride of N-Ac-(L)-Phe and methyl propiolate deprotonated by n-BuLi were unsuccessful, so there is no kinetic data with respect to PAM available for this compound. However, this compound is an interesting prospect for three reasons. First, this alkynyl derivative would likely be more reactive toward ROS generated at Cu_M than the corresponding alkenyl acrylates. Secondly, the linearity of the alkynyl molecule from C1-C4 as

opposed to the planarity and 120º bond angles of the acrylate results in a longer molecule, with perhaps interesting consequences as regards the positioning of the benzyl group, and especially the phenyl ring, in the active site. Thirdly, there are no hydrogen atoms bound to either C2 or C3 in the case of N-Ac-(L)-Phe-Propiolate. Therefore, if this compound were able, experimentally, to inactivate PAM it would be certain that the mechanism could not involve a hydrogen atom abstraction step. As mentioned above, although the acrylates have a hydrogen at C2 which is positioned such that it could conceivably be abstracted by the ROS generated at Cu_M, the alkenyl C-H bond is approximately 15 kcal/mol stronger than the corresponding glycyl C-H bond. The large deuterium KIE noted above implies that hydrogen-atom abstraction is extremely sensitive to changes in bond strength. It is possible, however, that a large part of the KIE is accounted for by tunneling (Francisco 2002); all else being equal it is more problematic to tunnel the proton, neutron, and electron of deuterium than it is the proton and electron of hydrogen. Nevertheless, the change in the strength of the C-D/C-H bond must contribute, at least in part, to the KIE. However, the potential for hydrogen atom abstraction from C2 of the acrylates remains, regardless of the increased difficulty in the homolytic cleavage of the bond. In the case of the alkyne, this possibility can be ruled out, and inactivation, if it occurs, would have to proceed either by an alkynyl radical anion or by a nucleophilic attack by superoxide generated at Cu_M. The docking results for N-Ac-(L)-Phe-Propiolate are indicative of a productive binding to the PAM active site, with a carboxylate/guanidinium salt-bridge in clear evidence. The benzyl group of the ligand is indeed forced further away from Phe112/Tyr318, as the molecule is almost perfectly linear from C1-C5. The (D)-Phe-Propiolate does not appear to bind productively.

The N-Ac-Phe-Crotonates were used to probe the effect of the addition of an additional methylene "spacer" group between the stereocenter and the alkenyl functionality of the molecule. We reasoned that this may provide more flexibility in the conformational space available to the benzyl group of the ligands, and allow, perhaps, for more potent association with the PAM active site, especially since the carbonyl group would be allowed to freely rotate, rather than being constrained by resonance, as is the case for the acrylate/propiolate derivatives. Interestingly, the (D)-enantiomer failed to interact favorably with any part of the active site as was the case for the (D)-propiolate. It appears that the increased distance between the ligand carboxylate and the benzyl groups of both N-Ac-(D)-Phe-Propiolate and N-Ac-(D)-Phe-Crotonate affects the ability of these compounds to bind to the PAM active site. The carboxylate of the (L)-Crotonate interacts closely with the copper ion at Cu_M, rather than the guanidinium of Arg240. This is the only instance in all of the docking simulations where this copper/carboxylate interaction occurs. This is an interesting case, because if this representation is indeed accurate, it is possibly that this would be an extremely potent competitive inhibitor of PAM owing both to this interaction and to the fact that the benzyl and N-acetyl groups seem to occupy a favorable area of the hydrophobic pocket. However, the failure to associate with Arg240 would likely preclude electron-transfer from Cu_H and impede any potential inactivation mechanism, even though this molecule has the exact same C-terminus as the known inactivator N-Ac-(L)-Phe-Acrylate.

The exact mechanism of catalysis by PAM remains elusive. Most difficult to resolve is the question of how two reduced coppers, 11 Å apart, each donate one electron to molecular oxygen/substrate without any decoupling of oxygen consumption from product

formation. While Cu_M is located in close proximity to the glycyl moiety of PAM substrates, Cu_H lies across the solvent-accessible cleft of the enzyme, with no clearly defined or evident path for electron transfer. It has become evident in recent years that a Cu_M(II)-superoxo intermediate is responsible for the abstraction of the pro-(S) hydrogen from glycine-extended peptides and related compounds (Evans 2003, Francisco 2004). A study with oxidized PAM and hydrogen peroxide in the presence and absence of molecular oxygen, yielded some very interesting results (Bauman 2006). Hydrogen peroxide is the protonated form of the peroxo-species formed from a two-electron reduction of molecular oxygen, and if able to bind to Cu_M and hydroxylate PAM, does not absolutely require the input of any additional reducing equivalents from the enzyme. The authors showed that peptide substrate, oxidized PAM, and hydrogen peroxide were sufficient to catalytically yield hydroxylated product. This was true both in the presence and absence of molecular oxygen, and the kinetic parameters were unchanged under aerobic and anaerobic conditions, indicating that hydrogen peroxide is not simply fulfilling a role as a copper reducing agent. The reaction is catalytic in both cases. However, investigations with two histidine mutants, one a Cu_M ligand (H242A) and the other a Cu_H ligand (H172A), both known to reduce PAM activity by more than 99% (Jaron 2002), shows that *neither* mutant was catalytically competent using the hydrogen peroxide system. This clearly indicates that hydrogen peroxide, and by extension a peroxo-bound Cu_M species, is not capable of directly catalyzing the PAM reaction. This implies that the electron transfer from Cu_H is important not only for the PAM reaction as a whole, but also that (at least) a reduced Cu_H center is required for the reaction to occur. It is important, not only that a reducing equivalent actually arrives at the Cu_M/molecular

oxygen complex, but also that the manner in which it is transferred, and its pathway of transfer, is of equal necessity to catalysis.

The authors again suggest a superoxide channeling mechanism, whereby hydrogen peroxide reduces Cu_H(II) to Cu_H(I), and is itself oxidized to superoxide which channels back to Cu_M, and is then reduced back to hydrogen peroxide by the hydrogen peroxide ligated there, yielding a Cu_M(II)-superoxide with Cu_H being in the active reduced form. While this sounds feasible on its face, it conflicts with the $^{18}O_2$ data which necessitates that all oxygen activation steps are reversible until hydrogen atom abstraction occurs. Moreover, why can't hydrogen peroxide reduce Cu_M, form Cu_M(I)-superoxide, and perform the hydroxylation directly? It is possible that this is precluded by the coordination chemistry and reduction potential at Cu_M, relative to Cu_H, but this mechanistic conjecture suffers from a lack of parsimony and again suffers from the requirement of a reversible migration of superoxide across the solvent-accessible cleft. Also, this mechanism leaves a reduced Cu_H and an oxidized Cu_M after each hydroxylation. How is Cu_H(I) then oxidized back to its active (i.e. Cu_H(II)) form in this environment, especially when the system was shown to be catalytic? Cu_H(I) reduction of hydrogen peroxide, if it occurred at all, would upon protonation produce two hydroxyl radicals (and Cu_H(II)), the generation of which would lead to a deleterious radical cascade that would presumably cause enzyme inactivation. Nevertheless, the apparent requirement for a Cu_H(I) species, even in the seeming absence of any necessity for electron transfer in the case of the hydrogen peroxide system, has interesting mechanistic implications which will be elucidated below.

The reduced PAM crystal structure with both bound substrate and molecular oxygen also argues against the necessity for the migration of superoxide from Cu_H to Cu_M. Instead, an electron-transfer pathway exists which involves H108 (a Cu_H ligand), a water molecule, and the substrate carboxylate. The Cu_M system would then, either via a Cu(II)-superoxo or a Cu(I)-peroxo species, abstract the pro-(S) hydrogen from the substrate. This would require only a thermal rotation of the O-O bond and the breaking of a weak VDW contact with M314 (Prigge 2004). The electron from Cu_H is not necessarily obliged to have been transferred prior to the abstraction of the substrate hydrogen atom in this case. The one-electron reduction of molecular oxygen to superoxide is -0.33 V, in the case of horseradish peroxidase, whereas the reduction potential of superoxide to peroxide (with protonation) is a more favorable 0.94 V and could drive the reaction forward (Courteix 1995). However, here the same situation is reached as would be the case if hydrogen peroxide bound to oxidized Cu_M. The Bauman paper shows that Cu_H is required for the hydrogen peroxide-catalyzed hydroxylation of peptide substrate in the case of the oxidized enzyme. So, we have arrived at a paradoxical situation as regards the two explanations for electron transfer, and have two explanations available for this situation. First, the protonation state of hydrogen peroxide is incompatible with hydrogen atom abstraction *unless* it is generated *in situ* at Cu_M. Second, the electron from Cu_H does not arrive properly mechanistically unless it is actually conducted *through* the substrate. This would occur subsequent to hydrogen atom abstraction, and potentially generate a carbanion at C2 of the peptide substrate which would then attack the hydroperoxide at Cu_M(II), generating hydroxylated peptide and a hydroxide anion (seen ligated to Cu_M in the oxidized PAM crystal structure).

The above relates to the potential mechanism of PAM inactivation by the peptidyl acrylates. The paper on α,β-unsaturated ketones by Gibian (Gibian 1984) illustrates both the failure of superoxide to act as a nucleophile towards these compounds, and its ability to generate an anionic radical centered at the carbonyl carbon atom of the unsaturated ketone, with the negative charge carried by the carbonyl oxygen atom. Assuming that superoxide cannot abstract the sp_2 glycyl hydrogen atom of the acrylate, and the fact that it is unable to add productively to the C2 sp_2 carbon via a nucleophilic attack upon this class of compound, it seems reasonable to assume that the radical acrylate anion is formed. The source of the electron could be either Cu_M (via superoxide) or, alternatively, the electron could come from Cu_H. If the latter is the case, instead of the electron being transferred to the ROS at Cu_M via the H108/water/substrate carboxylate, it could be subsumed into the acrylate, yielding the inactivating radical anion inactivating species. This argument is bolstered by the proximity in the active site of Tyr318 to the carbon-centered radical. The activation barrier for tyrosyl radicals is fairly low, and their stability relatively high, so it is possible that a hydrogen atom is abstracted from the tyrosyl phenyl group, leaving a tyrosyl radical in the active site. In addition, the hydrophobic nature of the active site and the neighboring Phe112 and Leu206 residues could contribute significantly to the ease of formation and stability of a tyrosine radical in the PAM active site. Studies on the tyrosyl radical generated in the hydrophobic pocket of the active site of the enzyme Ribonucleotide Reductase clearly indicate that the hydrophobicity of the environment is critical to the stability of the tyrosyl radical. Indeed, mutations of three neighboring amino acids in that enzyme (F208Y, F212Y, and

I234N) to more hydrophilic residues significantly reduced the yield of the tyrosyl radical. (Ormo 1995)

Alternatively, a bond may form between the carbonyl carbon of the acrylate and the phenoxy group of the tyrosine, in which case the enzyme would be labeled by the acrylate suicide substrate. In any event, the incubation of PAM with the alkynyl analog of N-Ac-Phe-Acrylate would certainly be useful in elucidating this mechanism of inactivation, since this molecule lacks any hydrogen atoms bound to C2. Furthermore, it would be expected that the reduction potential of the alkynyl analog would be more favorable as regards formation of an anionic radical species. As such, the alkynyl series could provide greater rates of inactivation than the acrylates. The modeling results above indicate that N-Ac-(L)-Phe-Propiolate has a high probability of binding to the active site, bearing all of the associations with the enzyme that characterize the binding of N-Ac-(L)-Phe-Acrylate, including salt-bridge formation with Arg240, a hydrogen bond between the carboxylate of the ligand and Tyr318, and association of the hydrophobic phenyl group with Phe112 and Tyr318.

Finally, an evaluation of the active site of the enzyme with various docked dipeptide analogs reveals that a great deal of space is available in the hydrophobic pocket of the enzyme beyond that occupied by the various P2 side chains. This suggests that further modifications to the P2 side chain could significantly improve the K_I values of these inhibitors. Notably, it appears that the inclusion of a moiety, such as an additional carboxylate group, sulfonic acid group, or other type of anionic functionality which could form a salt-bridge with Lys134 would be desirable. A two- or three-carbon chain terminating in such a group and attached at the *meta* or *para* positions of the phenyl ring

of N-Ac-(L)-Phe-Acrylate may allow for the formation of this type of salt bridge. Alternatively, bulkier aromatic side chains such as napthylene or anthracene could increase the binding affinity, or such a side chain with an additional carboxylate group which might associate with Lys114 might be appropriate for investigation. The acrylates are the most potent class of inactivators of PAM that are known at the present time. Certainly, any of these modifications to improve their efficacy are worthwhile pursuits.

The major question regarding the acrylate series of compounds was the question of why they appeared to lack the stereochemical requirements at the P2 position which are so stringent for their dipeptide analogs, and from thence, why the inactivation kinetics were so similar for the N-Ac-Phe-Acrylic acid enantiomeric pair. We have shown that our Modeling protocol is effective in identifying those compounds known to be PAM substrates or inhibitors based upon two requirements: first, that the carboxylate of the substrate/inhibitor be able to form a salt bridge with the guanidinium functionality of R240 of the PAM active site, and secondly, that the P2 side chain be oriented upwards (away from Cu_M) into the hydrophobic pocket of the enzyme. In addition, for substrates, it is necessary that a hydrogen (always the pro-(S) in the cases studied herein) atom be directed toward the hydroxyl group ligated to that copper ion. The acrylates lack the glycyl amide bond of corresponding dipeptide substrates, and, as such, are not subject to hydrogen bonding with N316. This bond serves to orient PAM substrates into a position favorable for hydrogen-atom abstraction. While the dipeptides with (L)-amino acids at the P2 position are all PAM substrates, those with (D)-amino acids are not (and poor competitive inhibitors as well). The planarity of the acrylate through the C2-C3 double bond, and the lesser relative molar volume taken up by this group, allow the acrylates to

remain uninfluenced by N316 (the corresponding P2 dipeptides containing (D)-amino acids may be subject to electronic repulsion by this residue) and occupy the space available to dipeptides containing (L)-residues at the P2 position, whether that P2 residue is of (L)- or (D)-configuration. The kinetic interchangeability of these enantiomers could be potentially important in forthcoming *in vivo* studies, especially as the pharmacokinetics of these compounds is concerned. The (L)-acrylates more closely resemble naturally-occurring physiological peptides than the (D)-acrylates, and therefore may be subject to greater proteolytic degradation than the latter. In addition, (D)-acrylates, by the same logic, would be expected to interfere, perhaps, with fewer enzymes than the (L)-acrylates and may manifest, therefore, potentially fewer side-effects upon dosing. This elegant and interesting class of compounds is certainly an exciting new breed of anti-inflammatory compounds with a great deal of potential in further animal experiments.

Part 2

Novel Inhibitors of Substance P Bioactivation as Potential Anti-Inflammatory and Anti-Neoplastic Agents

Chapter 5: Introduction

General Introduction

Substance P (SP) is an 11-residue amidated peptide which is involved in cell-signaling pathways which control the expression and release of pro-inflammatory mediators and various mitogenic growth pathways which have been shown to be involved in the epigenetic progression of a variety of neoplastic conditions. The bioactivation of Substance P from its glycine-extended precursor is catalyzed by the sequential activities of the enzymes peptidylglycine α-amidating monooxygenase (PAM) and peptidoamidoglycolate lyase (PGL). PAM catalyzes the α-hydroxylation of the glycine-extended peptide to stereospecifically form C-terminal (S)-hydroxyglycines, and PGL catalyzes the N-dealkylation of this intermediate to yield the desglycyl C-terminal amidated peptide and glyoxylate (Ping, 1992; Ping, 1995; Katopodis, 1990). Substance P is categorized as a neuropeptide hormone, owing to its discovery (and the discovery of a variety of other neuropeptides) as a modulator of function and activity in the central nervous system (von Euler, 1931). Since the discovery of neuropeptides, many have been found to have a variety of activities throughout the periphery, and have been shown to be released by a variety of non-neuronal cell types and affect the function of a variety of physiological processes. Substance P is classified as a tachykinin (neurokinin), and exerts its effects via activation of the neurokinin-1 receptor (NK-1), a so-called serpentine receptor with seven transmembrane helical domains and an intracellular C-terminal loop and an extracellular N-terminal loop (Masu, 1987; Gerard, 1990; Gerard,

1991). These receptors are also called G-protein-coupled receptors (GPCRs) and their activation results in a cascade of events which lead to a variety of cellular stimulation processes (Hershey, 1990). Most notably, through the activation of the intermediate phospholipase C (PLC) pathway, receptor occupation results in the downstream activation of nuclear transcription factors for a variety of pro-inflammatory mediators and cytokines, especially nuclear factor κB (Li, 1997). Additionally, SP is classified as a mitogen (activator of mitosis), and activates a wide variety of cellular processes which lead to cellular growth and proliferation (Nilsson, 1985; Lotz 1987). The activation of the Ras pathway is of particular concern, as it is well-established that a constituitively-activated Ras pathway is present in a wide variety of cancers and tumor subtypes (Ahmadian, 2002; Hamad, 2002). Therefore, SP has been found to be implicated in both chronic inflammatory diseases such as rheumatoid arthritis, and in neoplastic growth and metastasis (Firestein, 1996; Bresnihan, 1999). Furthermore, chronic inflammation has been shown to potentiate the growth of a variety of neoplasms, implying that both the pro-neoplastic and pro-inflammatory properties of Substance P may mutually-reinforce both pathways and yield a pathologically synergistic effect in both cases.

During acute and chronic inflammation, the pro-inflammatory effects of SP are upstream of cyclooxygenase-2 (COX-2) which is eventually activated by SP through the PLC/PLA_2 second-messenger pathways, yielding the pro-inflammatory products of arachidonic acid metabolism (prostaglandins). During recent years, the COX-2 selective inhibitors (most notably Vioxx), which have had such a marked ameliorative effect on chronic inflammation and pain in rheumatoid arthritis and related conditions, have also been shown to have significant deleterious cardiovascular effects and have been pulled

from the marketplace, creating a therapeutic drug vacuum for these conditions. Currently, the COX-2 selective inhibitor Celebrex remains on the market. However, this drug is still associated with adverse cardiovascular events. Interestingly, the most promising drug currently available for the treatment of chronic pain and inflammation (excluding the opiates from the discussion, as these drugs are strongly addicting and subject to the phenomenon of increasing tolerance as treatment time continues) is Enbrel (Etanercept), which is a soluble tumor-necrosis factor-α (TNF-α) receptor which sequesters this pro-inflammatory mediator in the bloodstream and extracellular space. Since the drug is protein-based, it is not orally-active and requires a maintenance regimen of injections for administration. Transcription, translation, and release of TNF-α are also at least partially under the control of the NK-1 receptor, so its levels may also be modulated by the inhibition of SP biosynthesis. Again, NK-1 activation is upstream of the events leading to the synthesis and release of TNF-α.

Certainly, then, reduction of peripheral levels of SP can be readily seen as a desirable target for pharmacological intervention for both chronic inflammation and cancer, via the inhibition/inactivation of the enzyme(s) responsible for its bioactivation. The thrust of the ensuing analysis hinges upon the development and evaluation of rationally-designed molecules which act as mechanism-based inactivators of PAM, the rate-limiting enzyme in the conversion of biologically-inactive SP-Gly to the pro-inflammatory/pro-neoplastic amidated SP. SP is known to affect (activate) nearly all of the cells of the innate immune system (leukocytes such as macrophages, neutrophils, eosinophils, as well as mast cells, dendritic cells, etc.) and exerts pro-inflammatory effects on cells of the acquired immune system as well (B- and T-lymphocytes) (O'Connor, 2004). Additionally, SP would be

expected to affect all neoplastic cells which express the NK-1 receptor, owing to its status as a mitogenic growth factor. Hence, owing to its stimulatory effects in both cases, reduction of SP levels via inhibition of PAM is certainly a very attractive target for pharmaceutical agents. Naturally, since PAM catalyzes the bioactivation of a wide variety of glycine-extended neuropeptides, inhibition of the rate-limiting monooxygenase leads necessarily to a depletion of all types of amidated neuropeptides. Therefore, it is also important that PAM inhibitors be targeted as specifically as possible to areas of chronic inflammation and neoplastic growth to reduce side-effects resulting from depletion of other biologically necessary neuropeptides required for homeostasis and general health of the organism. Moreover, it is of utmost importance that any PAM inhibitor not be able to penetrate the blood-brain barrier to any significant degree to avoid adverse neurological effects (treatment of brain tumors being one obvious exception). However, the work presented herein is interested primarily in evaluating these PAM inhibitors as anti-inflammatory and anti-cancer agents as proofs-of-concept, and further refinement to account for tissue-specific drug-targeting and prevention of CNS-associated side-effects is beyond the scope of this thesis.

Our second-generation mechanism-based PAM inactivator N-Ac-(L)-Phe-Acrylate (and its methyl ester prodrug) was evaluated as an anti-inflammatory agent in a variety of experiments including: acute inflammation initiated by carrageenan, chronic inflammation (adjuvant-induced polyarthritis), and mustard oil-induced neurogenic inflammation (MOINI). This compound was also evaluated for its inhibitory effects on purified COX-1 and COX-2 and for inhibition of these enzymes in human whole-blood assays. Experiments were also performed to evaluate this compound as an inhibitor of

soluble PLA_2 (V). Finally, the first-generation mechanism-based PAM inactivator 4-Phenyl-3-Butenoic Acid (PBA) (and its methyl ester prodrug) was evaluated for its ability to restore gap-junctional communication and a more normal phenotype to Ras-transformed (WB-Ras) epithelial cells. Its effects on the mitogen-activated protein kinase (MAP-K) pathway (involved in Ras activation) were also evaluated. In all cases involving animal experiments or cells, residual PAM activity levels were also tested in an attempt to correlate the anti-inflammatory or anti-neoplastic effects of these compounds to PAM inhibition. In all cases, the therapeutic effects of these inhibitors were indeed remarkable. In the following section, the effects of Substance P on the activities of cells of the innate and acquired immune system will be discussed in detail, as will the pathways involved in the pro-inflammatory and pro-neoplastic properties of SP, including the downstream effects of the activation of NF-κB and the Ras-pathway.

Substance P and Neurokinin Expression

Neurokinins are expressed from two separate genes, preprotachykinin-I (PPT-1) and preprotachykinin-2 (PPT-2). All *PPT-1* transcripts, of which there are four alternative splicing forms, encode for SP-Gly. Two of the transcripts also encode for Neurokinin A (NKA), Neuropeptide K, and Neuropeptide-γ, the latter two of which are extended forms of NKA. *PPT-II* does not code for SP. The bioactive, amidated form of SP has the following sequence: Arg-Pro-Lys-Pro-Gln-Gln-Phe-Phe-Gly-Leu-Met-NH_2. All tachykinins share a similar sequence at the C terminus: Phe-X-Gly-Leu-Met-NH_2, where X = Tyr, Phe, Val, or Ile, all aromatic or hydrophobic residues (Uddman, 1997). All, by

virtue of the requisite C-terminal amide for complete bioactivation, undergo catalysis by PAM and PGL from their respective glycine-extended precursors.

Each of the three major tachykinins, SP, NKA, and NKB, preferentially activate one of the three known neurokinin receptors. SP activates NK-1, NKA activates NK-2, and NKB activates NK-3 (Nakanishi, 1991). Although there is significant cross-reactivity between the various neurokinins and the three receptors at high concentrations of ligand, selectivity is marked at lower concentrations. The largely conserved carboxy-termini address the ligands to NK receptors in general, while the variable N-terminal regions dictate receptor subtype specificity. The NK-1 receptor has a 100-fold greater affinity for SP than for NKA, and 500-fold greater for SP than for NKB (Gerard, 1991). The NK-1 receptor is, as is typical for GPCRs, transcribed at low levels from what is characterized as "low-abundance" mRNA. The receptors are internalized after activation by SP, and are thus readily desensitized in the absence of any signals which increase either transcription of the receptor mRNA or translation of existing mRNA.

The human NK-1 receptor contains 407 amino acid residues and a molecular weight of 48,000 kDa (Hopkins, 1991). The SP binding site is located between the second and third transmembrane-spanning α-helices of the receptor, while the third intracellular loop appears to be responsible for interaction with the coupled G-protein. As with all GPCRs, agonist binding results in the exchange of bound (inactive) GDP for (active) GTP within the heterotrimeric G-protein, which precipitates the dissociation of the heterotrimeric complex into two subunits, G_{α} and $G_{\beta\gamma}$. The G_{α} subunit remains bound to GTP, but possesses an inherent GTPase activity which eventually hydrolyzes GTP back to GDP, allows the reassociation of the heterotrimeric complex, and inactivates the G-protein.

The activated G_{α} subunit may be one of several species, all of which serve to further activate different downstream pathways when dissociated from the $G_{\beta\gamma}$ subunit, but NK-1R activation results in the activation of the $G_{\alpha q/11}$, which goes on to activate membrane-bound Phopholipase C. This results, via hydrolysis of membrane phospholipids, in an increase in diacylglycerol (DAG) and inositol triphosophate (IP_3). These second messengers in turn mobilize intracellular calcium stores and activate Phospholipase A_2, which cleaves arachidonic acid from phospholipids, making them available as substrates for the COX enzymes (yielding the intermediate prostaglandin PGH_2) followed by catalysis of one of several prostaglandin synthase enzymes, yielding a variety of prostaglandins including PGE_2, $PGF_{2\alpha}$, PGI_2 (prostacyclin), and TXA_2 (thromboxane). Furthermore, Phospholipase C activity results in the activation of Protein Kinase C, which leads to further downstream effects.

The NK-1 receptor is rapidly desensitized via phosphorylation of a variety of Ser and Thr residues on the cytoplasmic tail, which encourage internalization (and deactivation) of the receptor. However, Phospholipase C remains active on a longer-term basis and exerts powerful cellular effects, even after the initial signal wave (SP) has abated. Therefore, in the absence of other destimulating factors, PKC and other downstream mediators will remain active even after SP-stimulation has terminated (Li, 1997).

Protein Kinase C and Downstream Cellular Signaling

Once Phospholipase C has been activated by the G_{α} subunit, the enzyme hydrolyzes phosphatidylinositol to inositol triphosphate (IP_3), which is released into the cytoplasm

and serves to liberate sequestered Ca^{+2} stores from intracellular reservoirs, and diacylglycerol (DAG), which remains associated with the plasma membrane. Calcium binds to soluble PKC, which allows it to associate with membrane-bound DAG and results in the fully active kinase.

PKC phosphorylates and actives Raf-1, a mitogen-activated protein kinase kinase kinase (MAP-KKK). MAP-KKK activates MEK (a MAP-kinase kinase), which in turn activates several Extracellular-Related Kinase-2 (ERK-2). ERK-2 is designated as a MAP-kinase, and leads to several important cellular processes, including the activation of various transcription factors, translation enhancers (e.g. MNK-1 and MNK-2 which increase the rate of translation of extant mRNAs), calcium-independent PLA_2, and other elements involved in cell survival and proliferation (such as p90RSK). An important transcription factor, Nuclear Factor κB (NF-κB), which promotes the transcription of a variety of cytokines and pro-inflammatory mediators, is thusly activated by SP binding to the NK-1 receptor. This will be discussed in further detail in the following sections.

In addition to the Raf-1-controlled pathway outlined above, another function of PKC is the activation of the Ras pathway. The *Ras* gene is a proto-oncogene, meaning that certain mutations result in a constituitively-activated p21 Ras proteins that, once activated, lacks the inherent GTPase activity necessary to deactivate itself, ultimately leading to a cascade of events that enhances cell survival and proliferation, and tends to oppose any pro-apoptotic signals which are concurrently trying to cause the transformed cell to undergo programmed cell death (Cesen-Cummings, 1998).

Indeed, the *Ras* genes are the most frequently mutated genes in solid tumors and blood cancers, and appear in *at least 30%* of all human cancers (Ahmadian, 2002; Hamad,

2002). p21 Ras proteins require farnesylation (by the enzyme farnesyltransferase) and association with the plasmalemma for full activity (Hancock, 1989). Permanent Ras activation results in potent downstream effects in the MAP-K pathway, also leading to upregulated transcription and translation of a variety of pro-growth genes and leading to the altered morphology typical of tumorigenic cells. When p21-Ras is thus activated, a further notable effect is the loss of gap junctions on the cell membrane which allow neighboring cells to directly communicate with each other (Ruch, 1993). As cells proliferate and begin to come into close contact with each other, various chemical signals may be passed between them via the gap-junctional pathway. Under normal circumstances, these chemical signals prevent further proliferation among adjacent cells. However, under the pathological conditions arising for constituitive Ras activation, less information is able to pass between cells via gap junctions and the requisite anti-proliferative signals are not "seen" as readily by these transformed cells. In a nascent solid tumor, adjacent cells continue to proliferate even as they are crowded in close contact with neighboring cells, and mitotic division continues unchecked, leading to continued tumor growth. Gap junctions are formed from connexin proteins, and the ability of these proteins to aggregate at the plasma membrane and form gap junctions is governed by the phosphorylation of connexin-43. Reduction in phosphorylation results in reduction of gap junction formation. (deFeijter, 1996), and Ras-activation appears to inhibit this phosphorylation. Previously, work performed on a variety of lung-tumor subtypes had shown that the proliferation of the tumorigenic cells was governed by autocrine growth loops controlled by gastrin-related peptide (GRP), which, like Substance P, requires C-terminal amidation by PAM/PGL for full biological activity

(Iwai, 1999). Indeed, since this GRP-mediated GPCR activation event is upstream of the Ras pathway, inhibition of amidation could possibly interrupt the autocrine growth loops which detrimentally govern (via Ras activation itself and therefore its downstream activation of ERK-2) the rampant growth of tumor cells. Hence, preventing the amidation of GRP (or SP, which controls many of the same pathways through the NK-1 receptor) may in fact block the activation of the transcriptional factors which influence the expression of pro-growth mediators, and upregulate gap-junctional communication. Both of these effects would be predicted to inhibit the growth and proliferation of tumor cells.

Nuclear Factor κB (NF-κB)

NF-κB is a transcription factor involved in the regulation of expression of a wide variety of pro-inflammatory mediators. Under normal physiological conditions, NF-κB is present in the cytoplasm of the cell in association with IκB. When these two molecules are thus associated, NF-κB is effectively sequestered and prevented from entering the nucleus to trigger the expression of the pro-inflammatory cascade. When extracellular stimuli result in the activation of the MAP-K/ERK-1 pathway, an enzyme known as IκK is phosphorylated and activated. The active form of IκK in turn phosphorylates IκB, which then dissociates from NF-κB, is ubiquinated and targeted for degradation by the proteasome. Once this occurs, NF-κB migrates to the nucleus where it promotes the expression of pro-inflammatory and pro-growth mediators (Maeda, 2008). The

expression of these mediators is therefore the ultimate downstream event associated with (among others) the activation of the NK-1 receptor.

NF-κB can also be activated by activation of several Toll-like receptors, including the lipopolysaccharide (LPS) receptor. LPS (or endotoxin) is a ubiquitous component of the cell-wall of Gram-negative bacteria, and thus bacterial infection is able, ultimately, to stimulate NF-κB activation and elicit an appropriate immunological response. However, in a variety of autoimmune pathologies associated with chronic inflammation, such as rheumatoid arthritis (RA), NF-κB is active in the absence of any bacteriological infection. Over recent years, a large body of literature has implicated elevated levels of SP in the pathology of RA, and since NF-κB can be activated as a downstream event of the occupation of the NK-1 receptor by SP, it is exceedingly likely that this amidated neuropeptide may be a major contributor to the continuation of the chronic inflammation which characterizes the disease (Marshall, 1990; Menkes, 1993).

Gene transcription and subsequent mRNA translation resulting from NF-κB translocation to the nucleus results in the formation of an abundance of pro-inflammatory chemokines, cytokines, enzymes, and adhesion molecules that serve to further amplify the inflammatory signal ultimately initiated by the binding of SP to the NK-1 receptor. First, the cytokine proteins of the acute phase response, including interleukin-1β (IL-1β), interleukin-6 (IL-6), and tumor necrosis factor-α (TNF-α) are produced and secreted. In a positive-feedback loop, IL-1β and TNF-α, upon secretion by an NF-κB-active cell, may act in an autocrine or paracrine manner by occupying cell-surface receptors which, when activated, serve *again* ultimately to stimulate NF-κB activation. When this occurs in the absence of viral or bacterial infection, it is easy to see how aberrant overexpression of SP

can result in unceasing activation and amplification of the expression of further pro-inflammatory mediators, leading ultimately to serious pathological conditions of chronic pain, inflammation, and the destruction of healthy tissue.

Further damaging effects occur with the expression and release of chemokines, molecules which serve as chemoattractants for a variety of cells of the innate (and adaptive) immune system. Most of these cells (macrophages, monocytes, granulocytes, dendritic cells, lymphocytes, etc.) also possess cell-surface receptors for the cytokines mentioned above, which are then also subject to NF-κB activation. Additionally, coexpressed with chemoattractants such as interleukin-8 (IL-8), RANTES (Regulated upon Activation, Normal T-Cell Expressed and Secreted, more commonly known now as CCL5), microphage inflammatory protein (MIP-1α), and monocyte chemotactic protein (MCP-1), are a variety of immune/inflammatory cell adhesion molecules which are expressed on the surface of vascular endothelial cells that serve to allow more efficient recruitment of immune cells. These include, but are not limited to, vascular cell-adhesion molecule (VCAM-1), intercellular-adhesion molecule (ICAM-1), and E-selectin. Coupled with the vasodilation induced by SP, which serves to slow blood flow in vessels near to the environment of the initial inflammatory stimulus, these adhesion molecules allow for even more efficient recruitment of immune cells from the circulation (Seidel, 2007).

Finally, but not least importantly, is the expression of a variety of inducible enzymes, such as Phospholipase A2 (which liberates arachidonic acid, the COX-1/COX-2 substrate), COX-2 itself, and inducible-nitric oxide synthase (iNOS). Nitric oxide causes further vasodilation, which indirectly enhances leukocyte recruitment, and when

subjected to the products of the respiratory burst (from NADPH oxidase in neutrophils and macrophages) such as superoxide, forms peroxynitrite and other reactive species which can cause further local cellular damage in an inflamed area already beset by a variety of other cytotoxic mediators. COX-2 catalyzes the formation of PGH_2 which, as mentioned previously, is the substrate for a variety of prostaglandin synthase enzymes which form the several prostaglandins, molecules which also exert potent pro-inflammatory effects. The cell surface receptors for the short-lived (autocrine or paracrine-acting) prostaglandins are also GPCRs. The COX isozymes themselves are integral membrane proteins of the endoplasmic reticulum and nuclear envelope. PGE_2 and PGI_2 (prostacyclin) potentiate the pain and edema-producing effects of bradykinin and histamine released from mast cells, cause further vasodilation (again facilitating leukocyte recruitment to the site of inflammation), and increase blood flow to the site of inflammation (bringing more leukocytes to the area). Furthermore, a variety of prostaglandins, via interaction with cell-surface GPCRs on immune cells, also serve to activate the Phospholipase C pathway, which ultimately leads to further NF-κB activation.

Overall, the pro-inflammatory positive-feedback cascade initiated by activation of the NK-1 receptor is nothing short of astounding. Inhibition of SP biosynthesis via inactivation of PAM (the rate-limiting step of peptide amidation) is therefore an extremely attractive target in the amelioration of the pathological conditions of a wide variety of chronic inflammatory conditions.

Effects of Substance P on Cells of the Immune System

The innate immune system is typically described as encompassing those populations of immune cells which are activated immediately upon insult to the organism, such as bacteriological invasion. Among this population of cells are monocytes, macrophages, neutrophils, basophils, eosinophils, neutrophils, fibroblasts, natural killer cells, and mast cells, to the exclusion of lymphocytes. Lymphocytes, on the other hand, are cells of the adaptive immune response, having generated immunity to specific pathogenic protein sequences or structures via interaction with antigen-presenting cells (APCs, e.g. macrophages and dendritic cells) and subsequent maturation and proliferation in the spleen or lymph-nodes. The semantic distinction notwithstanding, all cells of the innate immune system are recruited or stimulated to some extent by the mature T- and B-cells of the adaptive immune system, whether by direct cell-to-cell contact with T-cells, or via interaction and phagocytosis of pathogens coated with specific antibodies generated by B-cells (O'Connor, 2004).

As the innate immune system responds to physiological insult, the immediate tissues begin to swell and redden as blood flow is increased to the area and neighboring blood vessels become "leaky" and allow for the extravasation of cells and the accumulation of fluid into the extracellular space. Algesia is a secondary consequence of the infection or insult as nociceptive signals are transmitted along sensory neurons to the dorsal ganglia of the spinal cord. The eicosanoid prostaglandin products of the cyclooxygenase enzymes contribute to this response, but Substance P is thought to play the most major role. SP is released from vesicles of C-afferent sensory neurons in the area of insult, and

SP in transmitted in an anterograde (and retrograde) motion back and forth to the spinal ganglion (Bayliss, 1901). This SP cycle is characteristic of chronic pain. SP released from nerve terminals in inflamed areas contributes to the activation of the cells of the innate immune system in the area; inflammation generated through this pathway is known as neurogenic inflammation. Heat is a by-product of the vastly upregulated metabolic activity of immune cells in the area of inflammation. Proteins of the acute phase response produced by liver cells in response to pro-inflammatory mediators generated and secreted by immune cells lead to the induction of fever by the hypothalamus.

SP, via interaction with the NK-1R expressed by immune cells, not only enhances the immune response via direct effects on the production of pro-inflammatory cytokines and induction of the COX-2 isozyme, but also potentiates the effects of many other cytokines and chemokines. Generally, the role of SP is immunostimulatory but it has also been implicated in the resolution of inflammation as its mitogenic properties enhance the action of fibroblasts and other cell types which rebuild tissue damaged by injury or pathogenic invasion (Nilsson, 1985; Lotz, 1987; Ziche, 1990). The following is a brief recapitulation of the effects of SP on some of the major cell-types of the innate and adaptive immune system.

SP and Lymphocytes

SP is a powerful chemoattractant for lymphocytes, creating a chemical concentration gradient which increases the expression of various cell-to-cell adhesion molecules

(ICAM, ELAM, VCAM, etc.) in the area of inflammation or infection. As these molecules are upregulated (on the plasma membranes of the vascular endothelium and the immune cells themselves), lymphocytes are recruited and extravasated into the affected areas. SP is also a cofactor for the differentiation of B-lymphocytes and stimulates antibody secretion. Also upregulated is the secretion of interleukin-2 (IL-2) by T-lymphocytes, an autocrine/paracrine factor which enhances $CD4^+$ T-cell growth, enhances the natural killer activity of T-cells, and prolongs their life spans (Calvo, 1992). SP also stimulates the production and release of macrophage-inflammatory protein-1β (MIP-1β or CCL4) which not only attracts additional lymphocytes, but also activate granulocytes (neutrophils, eosinophils, etc.) and macrophages, upregulating their synthesis and secretion of the pro-inflammatory cytokines IL-1, IL-6, and TNF-α (Guo, 1992; Croitoru, 1990). This is one method by which SP affects the activities of the cells of the innate immune system via its interaction with cells of the adaptive immune system.

SP activates lymphocytes at concentrations as low as 0.1 nM, via interaction with the NK-1 receptor (Covas, 1994). While there is some evidence that lymphocytes themselves express and secrete SP, it would be more accurate to say that these cells express the *PPT-1* gene (which encodes SP). In other words, it is known that the mRNA for PPT-1 is expressed in lymphocytes. However, direct evidence of the production of SP has not been found. In order for SP itself to be produced by lymphocytes, these cells would also have to express PAM/PGL, which generates amidated, bioactive SP from SP-Gly (itself processed from the larger PPT-1 precursor). Immunological techniques have, to my knowledge, used only polyclonal anti-SP serum which would be cross-reactive with SP-Gly, and, to date, no PAM activity has been found in these cells.

SP and Macrophages/Monocytes

As for lymphocytes, SP is a potent chemoattractant for monocytes and macrophages (Schratzberger, 1997). It stimulates the production of IL-1, IL-6, and TNF-α, the three primary pro-inflammatory cytokines (Bill, 1979; Lotz, 1988). Interleukin-1 is classified as an endogenous pyrogen (fever-promoter), and promotes the recruitment of leukocytes and the expression of intercellular adhesion molecules. IL-1 also stimulates hematopoesis (myelocytes and erythrocytes) in response to infection. IL-6 acts as both a pro- and anti-inflammatory cytokine, and has many of the same pro-inflammatory effects as IL-1. TNF-α activates the apoptotic (programmed cell death) pathway, but also has many proliferative (pro-inflammatory) effects as well (activation of MAP-Kinase and NF-κB). These three cytokines are the major stimulators/markers of the acute phase response, which serves to stimulate the liver to increase the production of a variety of anti-microbial/pro-inflammatory proteins. These include C-reactive protein (an opsonin), whose plasma levels increase by nearly five orders of magnitude during the acute phase response, serum amyloid A (leukocyte recruitment, induction of matrix metalloproteinases (MMP)), the complement system (opsonin, components of "membrane attack complex" which lyse invading cells), ferritin (sequesters Fe^{+3} from pathogens), ceruloplasmin (oxidizes Fe^{+2} to facilitate sequestration by ferritin), and haptoglobin (binds hemoglobin, further iron sequestration. It is interesting that ceruloplasmin is one of the upregulated proteins of the acute phase response. Its normal function is as a copper-carrier protein in the bloodstream, and its activation during the

acute phase response for iron processing would seem to require that it dissociate from copper in areas of infection or inflammation. This could serve to increase local levels of copper ion, which is a requisite cofactor for PAM.

A more immediate effect of SP on macrophages/monocytes is the upregulation of phagocytic activity. Indeed, macrophages may be activated insofar as the production of cytokines, but do not reach their full phagocytic potential unless activated by SP (Bar-Shavit, 1980). SP also upregulates arachidonic acid metabolism by stimulating PLA_2 (via increase in free intracellular Ca^{+2} levels) activity and thus indirectly provides a greater substrate concentration for COX-2 catalysis, ultimately leading to the production of a wide variety of prostaglandins, leukotrienes, lipoxins, etc. In another instance of the involvement of SP in pro-inflammatory positive-feedback loops, SP also upregulates the expression of the NK-1 receptor in monocytes and macrophages, thereby serving to amplify its own signal. PPT-1 mRNA transcription is also upregulated. As mentioned above, this is suggestive of SP-Gly, rather than SP itself which may only be produced in the presence of PAM/PGL and the requisite cofactors. SP also upregulates the oxidative burst of macrophages/monocytes, the process whereby the enzyme NADPH oxidase reduces molecular oxygen to superoxide ion, the first in a chain reaction formation of reactive oxygen species (ROS) which include superoxide itself, peroxynitrite, hydroxyl radical, hydrogen peroxide, and a variety of halooxygen radicals such as hypochlorite (the anion of "bleach"). All are bactericidal, but also serve to damage "self" cells as well as invaders (Murris-Espin, 1995).

SP and Neutrophils

Neutrophils are the most common leukocyte present in the bloodstream, and the first line of defense against infection. These cells are a representative of the class of polymorphonuclear phagocytic cells (including eosinophils and basophils as well), also called granulocytes. These cells are also very proficient at the oxidative burst mechanism, and upon degranulation (release of granule contents) deliver further molecular species which are toxic to pathogens, including lysozyme, myeloperoxidase (generates hypochlorous acid), acid hydrolases (including phospholipase A_2), defensins (cationic, cysteine-rich proteins which form pores in bacterial cell walls), bactericidal permeability-increasing protein (BPI), elastase (degrades extracellular matrix), collagenase, and complement-activating factors (opsonins), among others (Haines, 1993; Serra, 1998). Neutrophils are short-lived, surviving an average or one or two days subsequent to recruitment (macrophages may live for months to years) and are the major component of pus formed at sites of infection.

As for lymphocytes/monocytes/macrophages, SP is chemotactic for neutrophils. In addition, SP induces the degranulation of neutrophils at sites of infection, leading to the release of a variety of products as described above. The respiratory burst, as for macrophages, is greatly enhanced upon SP stimulation. Through a process known as "neurogenic priming", SP potentiates the effects of a variety of other pro-inflammatory mediators on neutrophils (Perianin, 1989). As for other immune cells, SP stimulation results in the production and secretion of IL-1β and TNF-α.

SP and Other Cell Types

SP has profound effects on mast cells, which are related to the low-abundance basophils which circulate in the bloodstream. These cells are rich in granules containing histamine (associated largely with allergy/anaphylaxis) and heparin. Most notably, these cells are often in direct contact with sensory neurons, and can be drastically affected by the release of SP from these nerve terminals (Stead, 1987). Thus, mast cells are important contributors to neurogenic inflammation and have been shown to be important in a variety of autoimmune conditions such as rheumatoid arthritis, whereby they recruit other immune cells to the joints thus amplifying the inflammatory condition therein and resulting in further damaging effects to the local tissues. SP induces histamine and serotonin release by a receptor-independent mechanism (SP penetrates the cell membrane and interacts directly with the receptor-associated G-protein) (Shanahan, 1985). As for other cell types, SP activation results in an upregulation in the expression and secretion of TNF-α.

SP has similar effects on eosinophils as other cells of the innate immune system (stimulation of degranulation, respiratory burst, prostaglandin synthesis, etc.) but is tangential to our discussion owing to their role (mostly) as anti-helminth cells and cells which are involved in allergy/anaphylaxis. However, their activation may also lead to expression of pro-inflammatory mediators which affect other cells of the immune system or the acute phase response.

SP and Apoptosis

Apoptosis is a programmed cell death which arises in response to potentially deleterious changes to the cell itself (internal signals) or from interactions with various molecular signals from without. Although apoptosis can be triggered in response to a number of different conditions, perhaps the most notable function of programmed cell death is to prevent the proliferation and/or metastasis of transformed cells (i.e. cancer cells). The inability of cancer cells to respond appropriately to pro-apoptotic signals results, oftentimes, in runaway growth (failure to recognize the spatial limitations of its surroundings, mechanical displacement of healthy tissue by proliferating cancer cells) and *de facto* immortality.

Apoptosis is characterized by a variety of controlled cellular processes which allow for an orderly disposal of cellular contents and structural material. This controlled process differentiates apoptosis from a general, disorderly cellular necrosis which may result in a widespread dissemination of cellular contents and material into the surrounding extracellular space, often resulting in the release of a variety of potentially toxic mediators which may be deleterious to neighboring healthy tissue. Cells undergoing apoptosis are efficiently phagocytosed and disposed of by macrophages. When an apoptotic signal is recognized by a transformed, fatally-damaged, or virally-infected cell, a cascade of proteolytic activity governed by caspases (cysteine proteases) is initiated which leads to programmed cell death. Apoptosis requires a *functional* cell for culmination, and unlike generalized necrosis, requires the input of energy and hence

at least some minimal cellular metabolism able to regulate the required biochemical events.

Mitochondria are intimately involved in apoptotic events. Briefly, the equivalent of the membrane-attack complex (MAC) forms a pore in the mitochondrial membrane called the mitochondrial apoptosis-induced channel (also MAC). Formation of this channel is under the control of various proteins from the Bcl2 family, which contains members which both promote and prevent the initiation of apoptosis in the mitochondrion. The protein Bax (a component of the MAC channel) is a member of this family and its expression is under the regulatory control of the *p53* tumor suppression gene. Formation of the MAC allows for the leakage of cytochrome c (a member of the electron-transport chain) into the cytosol. Cytosolic cytochrome c leads to caspase activation and the initiation of apoptosis. The anti-apoptotic protein Bcl-2 prevents formation of the MAC and leakage of cytochrome c into the cytosol. Caspase-9 is activated by cytochrome c and serves to activate various effector caspases of the apoptotic pathway, ultimately resulting, among others, in the activation of poly-ADP ribose polymerase. This enzyme polymerizes nicotinamide adenosine diphosphate, effectively sequestering NADH from productive usage and restricting a wide variety of cellular processes.

Other notable pro-apoptotic pathways are the TNF-pathway and the *Fas* pathway, although TNF-α is able, as noted above, to initiate cell survival and pro-inflammatory pathways as well as sending pro-apoptotic signals. Incoming stimuli, from different receptors, may be both pro- and anti-apoptotic simultaneously. Indeed, it is unlikely that one cell will be exposed to *only* pro- or anti-apoptotic signals exclusively. The

preponderance of the signal, pro or anti, through expression and/or sequestration of the Bcl-2 members determines the ability of the MAC to form in mitochondria or other organelles, and the ultimate activation of the various pro-apoptotic effector caspases (CASP3, CASP6, CASP7).

As outlined above, SP is mitogenic and pro-inflammatory. In addition, SP has been shown to be directly anti-apoptotic in a variety of cell types, including macrophages, neutrophils, thymocytes, and small-cell lung carcinoma (deFea, 2000; Bockman, 2001). Treatment with NK-1R antagonists has been shown to increase levels of apoptosis in cultured small-cell carcinoma cells. Treatment of various cell types with glucocorticoids induces apoptosis, and coincubation with SP has been shown to limit glucocorticoid-induced apoptosis in these same cells. It must be noted that the anti-apoptotic effects of SP are tissue-specific, and SP has been shown to be actively pro-apoptotic in other cell types; hepatocytes undergo more efficient apoptosis when incubated with both TNF-α and SP, than when incubated with TNF-α alone. In other cases, SP has been shown to induce a caspase-independent non-apoptotic form of programmed cell death. In addition, the anti-apoptotic effects of SP may be dependent on the inflammatory microenvironment of a given tissue.

Thus, given the number of pathways under the control of the NK-1 receptor, stimulated by SP binding, we sought to investigate whether our novel PAM inhibitors, by prevented the amidation and bioactivation of SP, could act as anti-inflammatory and anti-cancer agents. First, that these drugs could display an anti-inflammatory effect against acute (carrageenan-induced edema) and chronic (adjuvant-induced polyarthritis) inflammation via, theoretically, preventing the induction and expression of pro-

inflammatory mediators under the control of the NK-1 receptor. Second, that these drugs could inhibit inducible COX-2 activity without directly inhibiting COX-2 itself, thereby displaying an effect upstream of PLA_2 and COX-2. Third, by investigating whether PAM activity was indeed present in Ras-transformed cells (WB-Ras), and whether our PAM inhibitors were selectively cytotoxic toward the transformed cell line (versus a normal cell line, WB-Neo) or were able to help return the transformed cells to a more normal phenotype. We also attempt to correlate the anti-inflammatory and anti-neoplastic effects of our PAM inhibitors with PAM activity in the serum and cell extracts, respectively.

Chapter 6: Materials and Methods

Animals

All animals in these experiments were male Sprague-Dawley rats purchased from Harlan Sprague Dawley, Inc. (Indianapolis, IN). All were allowed food and water *ad libitum* and allowed to acclimate for at least five days prior to experimentation at the Mercer University animal facility. The Mercer University Institutional Animal Care and Use Committee (Macon, GA) approved all animal experiments performed herein.

Reagents

4-phenyl-3-butenoic acid (PBA) and isothiocyanate were purchased from Aldrich Chemical Co. (Milwaukee, WI). N-acetyl-(L)-Phe-acrylic acid, methyl N-Acetyl-(L)-Phe-acrylate, methyl 4-phenyl-3-butenoic acid, and trinitrophenyl-(D)-Tyr-Val-Gly were all synthesized, and all reagents obtained for use in their syntheses procured, as described previously in Materials and Methods section 2.1. Indomethacin, EDTA, *Mycobacterium butyricum*, type IV lambda carrageenan, formamide, capsaicin, dithiothreitol, lipopolysaccharide (from *E. Coli* serotype 0111.B4), sodium citrate, sodium phosphate, and MES buffer (enzyme grade) were all obtained from Thermo Fisher Scientific (Pittsburgh, PA). Triton X-100 was purchased from Acros Organics (Pittsburgh, PA). COX colorimetric screening assays were purchased from Cayman Chemical (Ann Arbor,

MI). Prostaglandin E_2 ELISA kits were purchased from Oxford Biomedical (Oxford, MI). All other chemicals and reagents used in these experiments were analytical grade. WB-Ras and WB-Neo cells were kindly donated by Dr. James F. Trosko at Michigan State University (Lansing, MI). Alpha Modification of Eagle's Media was purchased from Mediatech (Herndon, VA). Fetal Bovine Serum (FBS), Neutral Red solution, and phenylmethylsulfonyl fluoride (PMSF) were obtained from Sigma Chemical Co. (St. Louis, MO).

Preparation and Administration of PBA and APAA-OMe

PBA was recrystallized prior to use by dissolution in boiling hexanes and overnight precipitation at -20° C. PBA was dissolved in phosphate-buffered saline (PBS) or water and the pH was adjusted to 7.4 with sodium hydroxide and hydrochloric acid. All PBA doses were administered by subcutaneous injection. Methyl-N-acetyl-(L)-Phe-acrylate was dissolved in 10/90 v/v DMSO/Ethanol.

Collection of Blood/Serum from Sprague-Dawley Rats

Blood was collected from rats at specified time points by clipping the tail of ether-anesthetized animals. The tails were electrocauterized post-collection. Briefly, 0.5 mL of blood was collected, allowed to clot at room temperature for 20 minutes, and centrifuged at 4° C for 5 minutes at 16,000 x g. The supernatant was collected and stored at -80º C until such time as it was thawed and assayed for PAM activity.

Analysis of Serum PAM Activity

PAM activity was determined using a previously-described method (Katopodis, 1991). Serum was allowed to thaw at room temperature, and 50 μL of serum was incubated in 200 μL of assay mixture containing saturating (greater than 50 μM) concentrations of TNP-YVG, 40 μM copper sulfate, 8 mM ascorbic acid, and 1 mg/mL catalase in 50 mM MES-Na buffer (pH 5.5). Samples were incubated for 45 minutes at 37º C in a water bath and the reaction was quenched via the addition of 25 μL 3M $HClO_4$. The assay mixture was then centrifuged at 4º C for 20 minutes at 16,000 x g. The supernatant was then assayed for product concentration (TNP-YV(OH)G and TNP-YV-NH_2) by RP-HPLC on an Alltech Allsphere C8 column connected to a Waters LC-Module 1 HPLC. 50 μL of sample were injected and monitored at 344 nm in a mobile phase of 44.0:55.9/0.1 acetonitrile/water/trifluoroacetic acid. Both hydroxy intermediate and amidated TNP-YVG products were quantified using HPLC standard curves. PAM activity is expressed in milliunits (mU) per mL, the amount of enzyme required to produce 1 nmol product per minute at saturating substrate concentrations.

Induction of Adjuvant Arthritis and Carrageenan Edema

Adjuvant arthritis was induced by a subplantar injection of Freund's Incomplete Adjuvant (1 mg/mL *M. butyricum* in mineral oil) into the right hindpaw. Control animals and the contralateral paw of animals receiving the adjuvant were injected with mineral oil

alone. Carrageenan edema was induced by the injection of 0.05 mL of carrageenan (20 mg/mL in PBS) into the subplantar region of the hindpaw. Control animals received injections of PBS only. Changes in paw volumes were measured plethysmographically by mercury displacement at various times post-induction of edema or arthritis.

WB-Ras and WB-Neo Cell Culture and PAM Activity

WB-Ras and WB-Neo rat liver epithelial cells derived from a WB-F344 cell line were subcloned from single cells to obtain WB-Neo_3 (WB-Neo) and WB-Ras_1 (WB-Ras) cell lines. All cells used for the following experiments were between passages 5-20. Cells were grown in Alpha Modification of Eagle's Media supplemented with 2 mM L-glutamine, 5% v/v fetal bovine serum (FBS), and 2% v/v G418 antibiotic solution (not used during experiments). Cells were grown to confluence, underwent trypsinization, and were plated at 5-10% confluence during each passage. Cells were incubated in an atmosphere of 5% CO_2 at 37º C.

To determine the effects of PBA and PBA-OMe on PAM activity in WB-Ras and WB-Neo cells, cells were grown to greater than 90% confluence in 15 mL Eagle's media including 150 µL of either vehicle or drug at the appropriate concentration. Each treatment group consisted of two 75 cm^2 T-flasks. After the appropriate incubation time, cells were washed 4 times with 0.9% w/v PBS, scraped from the flask using a rubber policeman, and collected. Cell suspensions were centrifuged for 20 minutes at 4,000 x g and the supernatant was discarded. The cell pellet was then resuspended in 500 µL of 50 mM MES-Na buffer (pH 6.6) and frozen (-80° C) and rethawed three times. Following

the last thaw, the suspension was again centrifuged as above and the supernatant was collected as the soluble protein/enzyme fraction. The pellet was then resuspended in MES buffer containing 1% v/v Triton X-100 detergent and allowed to sit for one hour. The suspension was then centrifuged again, as above, and the supernatant was collected as the membrane-associated protein/enzyme fraction. PAM activity (including both the hydroxyglycine intermediate and the fully amidated TNP-YVG) was measured as described above.

Statistical Analysis

All data are presented as the mean ± standard error of the mean (S.E.M.). Statistical significance was determined using the Student's *t* test when comparing means *between* two groups. One-way analysis of variance (ANOVA) was utilized to test for statistically-significant differences between repeated measures. Tukey's post-hoc test was then used to analyze statistical differences within groups. All measurements denoted with an asterisk as statistically significant have probability of $P < 0.05$ (95% confidence).

Chapter 7: Results

Previous work by this group in has established that PBA is a potent mechanism-based time-dependent inactivator of PAM *in vitro*. In addition, in later experiments in collaboration with Dr. Stanley Pollock at Mercer University, PBA was shown to have potent anti-inflammatory effects *in vivo* against carrageenan-induced edema, an acute inflammatory model (Ogonowski 1997). These anti-inflammatory effects correlated well with inactivation and reduction of rat serum PAM activity. Chronic inflammation, on the other hand, involves a variety of cells and mediators which do not participate on the short time-scale of acute inflammation, including, most notably, T- and B-lymphocytes. Therefore, the acute anti-inflammatory effects of a given compound do not necessarily translate into similar effects on a long-term basis. To that end, we investigated the potency of PBA (60 mg/kg/h) as an inhibitor of chronic inflammation, using the adjuvant-induced polyarthritis (AIP) model in Sprague-Dawley rats. AIP is characterized by three distinct phases. In the first phase (recognition phase), the injection of the adjuvant (subplantar injection of 0.1 mL of 1 mg/mL *M. butyricum* in mineral oil) in the hindpaw initiates an acute phase of inflammation which results in significant swelling of the injected paw, and lasts for approximately two days. Second, the proliferation phase (Days 2-10) is characterized by a plateau or modest reduction in the swelling of the injected paw. In the third phase (effector), specific T-cell-mediated inflammation results in a second period of increased swelling of the injected paw, with a concurrent inflammation of the contralateral hind paw and other systemic inflammatory effects. The inflammatory effects during the effector phase were monitored until Day 18. Indeed, the

PAM inactivator PBA was shown to diminish inflammation associated with AIP in each of the three phases of the progression of the disease, in both the injected and contralateral paws. This was a proof-of-concept which established that potent PAM inhibitors are potent anti-inflammatory compounds.

Therefore, since PBA (a commercially-available compound which resembles, structurally, the PAM substrate N-benzoylglycine) had been shown to have potent anti-inflammatory effects in both acute and chronic models of inflammation, we reasoned that our second-generation compound N-Ac-(L)-Phe-Acrylic Acid (and methyl ester prodrug), having shown greater *in vitro* potency as a mechanism-based PAM inactivator) should prove an even more potent anti-inflammatory drug. To that end, we evaluated the ability of the acrylate to inhibit serum PAM in comparison to PBA, its effectiveness against acute inflammation (carrageenan-induced edema model), and attempted to assay its ability to reduce the inflammation associated with AIP in Sprague-Dawley rats. Other experiments performed by our collaborators investigated the potency of this compound as inhibitors of purified ovine COX-1 and COX-2 and, in a human whole-blood assay, against the production of PGE_2 by lipopolysaccharide (LPS)-induced COX-2. Finally, we investigated, in collaboration with Dr. Diane Matesic (Mercer University), firstly, whether PAM activity was present in WB-Neo and WB-Ras-transformed epithelial cells, and secondly to what extent PBA could inhibit epithelial PAM and return the transformed cells to a more normal phenotype.

All animal experiments were performed at Mercer University, in collaboration with Professor Stanley Pollock. Work was performed with the involvement of one or more of the following: Dr. John Bauer, Dr. Jeffrey Sunman, or Mr. Jeremy Thompson, and I.

Interesting results from various experiments performed by one of the aforementioned researchers using chemicals synthesized by this researcher, but beyond which I was not directly involved will be presented in the Discussion section, in order to distinguish that work from such that I was involved with more directly and intimately, beyond synthesizing and providing the compound tested. This is especially the case for a variety of assays on SP immunoreactivity, phospholipase assays, COX-1 and COX-2 assays (whole-blood and kits), and other *in vivo* assays such as the mustard oil experiments.

Effect of PBA on Serum PAM Activity *in vivo*

PBA was administered to Sprague-Dawley rats either as a one-time dose of 500 mg/kg, or every three hours at doses of 500, 250, and 125 mg/kg. Blood samples were taken every three hours and the serum was assayed for PAM activity. The results of the study are shown in Figure 54. The one-time PBA dose resulted in a significant reduction (72%) of serum PAM activity after 3 hours, relative to time zero. This effect was fairly short-lived, and the serum PAM activity increased to 90% of control levels by 9 hours post-injection. By 24 hours, PAM activity was still at approximately 90% of controls. Dosing at 500 mg/kg every three hours, on the other hand, resulted in nearly 100% inhibition of PAM activity from six to twelve hours post-administration, after which the PAM activity began to rebound, even as maintenance doses of PBA continued to be administered. After 24 hours, serum PAM activity has increased to approximately

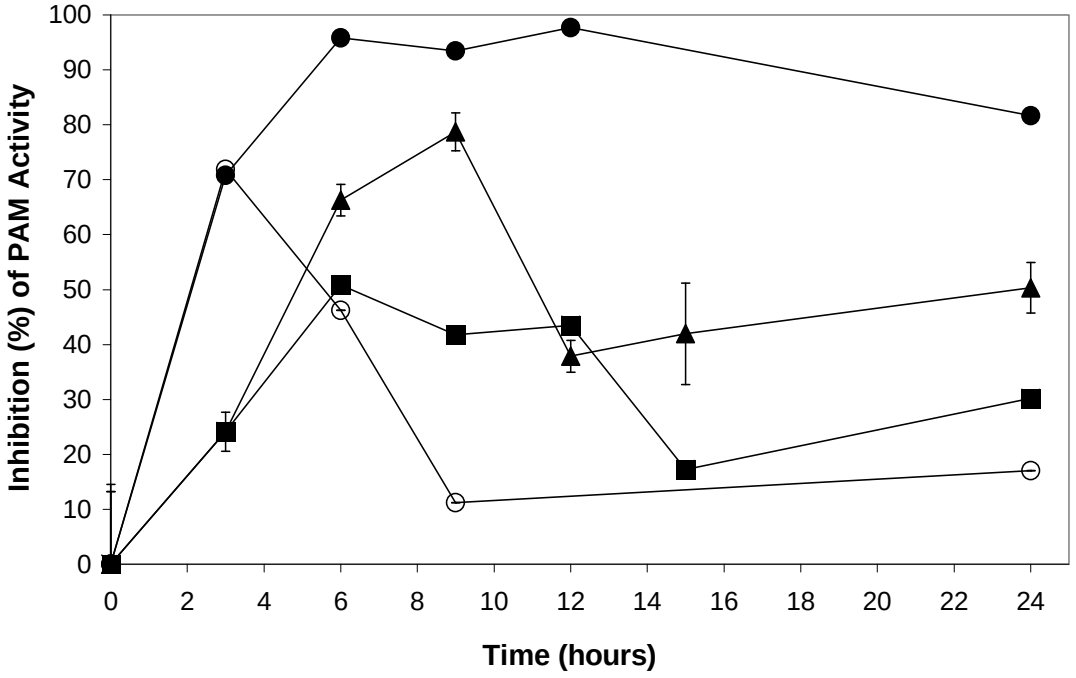

Figure 54. Inhibition of serum PAM by PBA *in vivo*. PBA was administered to Sprague-Dawley rats as a subcutaneous injection in aqueous PBS. Control animals received only vehicle injections. Blood was taken from the tail at various time points and the serum was analyzed for PAM activity as described in Experimental section. PBA 500 mg once (○); PBA 500 mg/kg every 3 hours (●); PBA 250 mg/kg every 3 hours (▲); PBA 125 mg/kg every 3 hours (■). Data are presented as the mean ± S.E.M. for each group (n=1-3).

15% of controls. At 125 mg/kg and 250 mg/kg, reduction in PAM activity was 45% and 65%, respectively, after three hours, and 30% and 45%, respectively, after 24 hours. All dosing was characterized by an initial and robust inactivation of serum PAM, which peaked after approximately 12 hours, and which could not be maintained beyond this time. This indicates that there is some mechanism by which PAM levels are able to rebound toward controls, even as the concentration of PBA is maintained (or even increased) in the bloodstream.

Continuous administration of PBA via osmotic pumps at 60 mg/kg/hr over the course of six days is shown in Figure 55. By 12-24 hours, PAM activity had been reduced by 65-70%. After two days, the inhibition was nearly 100%, and serum PAM levels remained virtually undetectable through Day 3. The final three days showed a slow decline in the inhibitory potential of the continuously administered PBA, and after 6 days, this compound was only able to maintain serum PAM activity at approximately 40% of controls (60% inhibition). This experiment shows the same rebound in PAM activity described with the higher doses (one-time 500 mg/kg and 125, 250, and 500 mg/kg every three hours)

Effect of N-Ac-(L)-Phe-Acrylate on Serum PAM Activity

One-time doses of N-Ac-(L)-Phe-Acrylate were administered to Sprague-Dawley rats at 10, 50, and 100 mg/kg to evaluate their effects on the inhibition of serum PAM activity, relative to control blood samples at t = 0 (Figure 56). After one hour, serum

PAM activity was reduced by 20, 28, and 38%, respectively. After one hour, the activity, as was the case for the PBA treated animals above, began slowly to return to baseline.

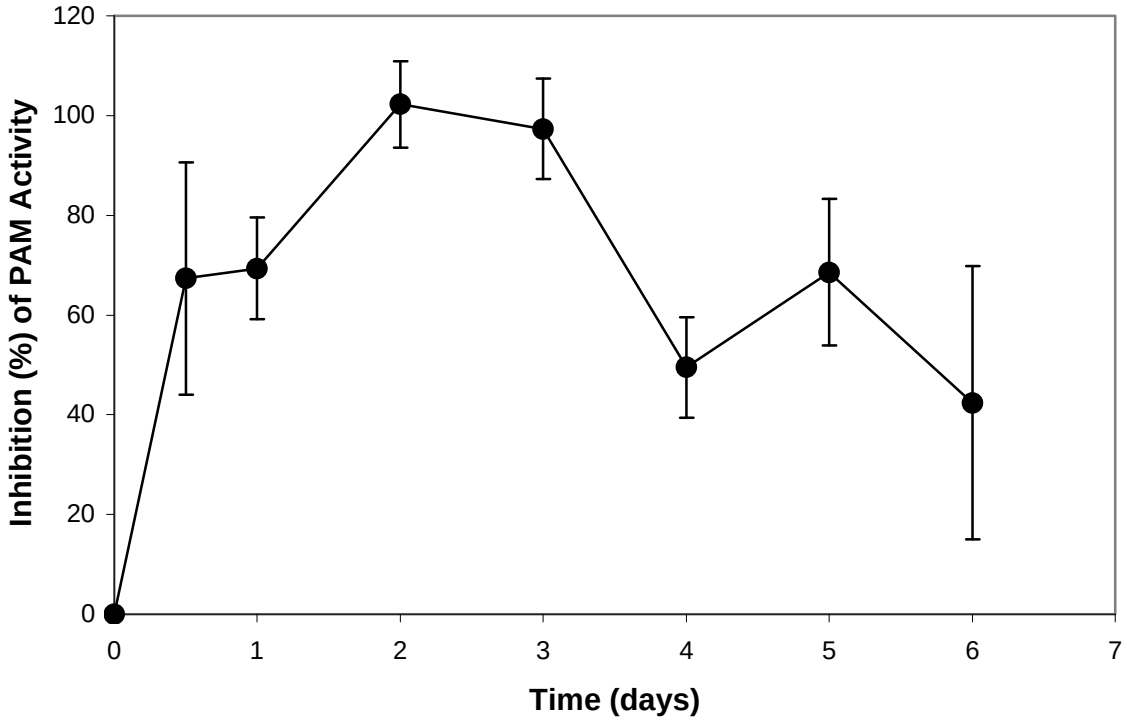

Figure 55. Effect on serum PAM activity in Sprague-Dawley rats dosed continuously with PBA for six days with an osmotic pump at 60 mg/kg/h. Control animals were sham treated. Serum samples were taken at time points between 0 and 6 days and assayed for PAM activity as described in "Methods". Data are presented as the mean ± S.E.M. for each group (n=3).
* Statistically significant ($P < .05$) compared to controls for that day (Student's *t* test).

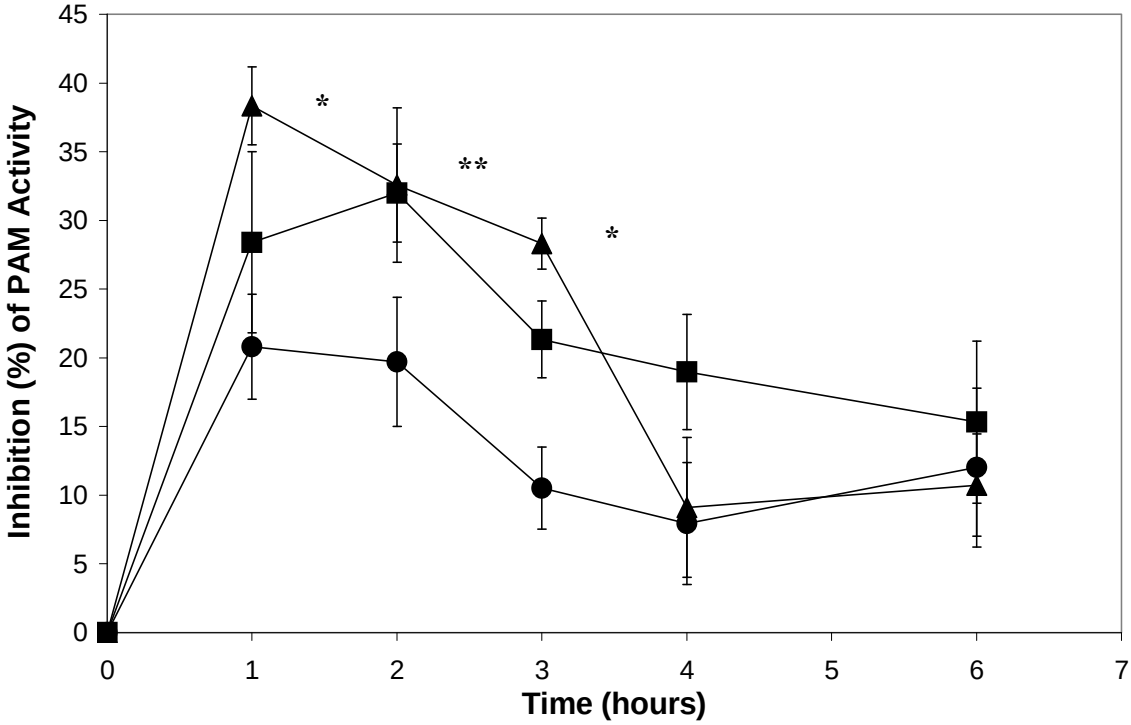

Figure 56. Effect of N-Ac-(L)-Phe-Acrylic Acid on serum PAM levels in Sprague-Dawley rats. N-Ac-(L)-Phe-Acrylate was administered subcutaneously at three different concentrations to Sprague-Dawley rats in order to determine the degree to which serum PAM is inhibited. Control animals received vehicle alone. Blood was collected and assayed for serum PAM activity over the course of six hours. APAA 10 mg/kg (●); APAA 50 mg/kg (■); APAA 100 mg/kg (▲). Data are presented as the mean ± S.E.M. for each group (n=6).
* Statistically significant ($P < .05$) compared to controls (Tukey's test).

After six hours, inhibition was 16, 14, and 12% for the 100, 10, and 50 mg/kg doses, respectively. Since these were one-time doses, it is not evident whether or not continued dosing would have allowed for a continued inhibition of serum PAM at peak levels.

Effect of N-Ac-(L)-Phe-Acrylate Methyl Ester on Serum PAM Activity

As with the free acid analog N-Ac-(L)-Phe-Acrylate, one-time doses were administered to Sprague-Dawley rats at concentrations of 10, 50, and 100 mg/kg and serum PAM activity was monitored for six hours post-administration (Figure 57). Only the free acid derivative is able to inactivate PAM *in vitro*, so presumably the ester analog requires *in vivo* hydrolysis prior to any PAM inactivation. Interestingly, although the inhibition of serum PAM was nearly identical for the methyl ester and the free acid at the higher doses (50 and 100 mg/kg), the lowest concentration did not significantly inhibit PAM until six hours post-administration. Also, the inhibition persisted for longer periods of time for the ester relative to the free acid. At 100 mg/kg, PAM activity was reduced by approximately 37% after one hour, and remained at this level until three hours post-administration, before declining to 25% of controls after six hours. The graph for the 50 mg/kg dose is nearly superimposable over that of the 100 mg/kg dose, although PAM activity levels were 5-7% greater in the former case. The 10 mg/kg dose actually reached peak levels of inhibition after six hours at 20%.

A direct graphical comparison of the effects on serum PAM levels of the free acid acrylate and the methyl ester prodrug (both at 100 mg/kg) are shown in Figure 58. Inhibition is nearly identical one hour post-injection (c. 35-40%), but the serum PAM

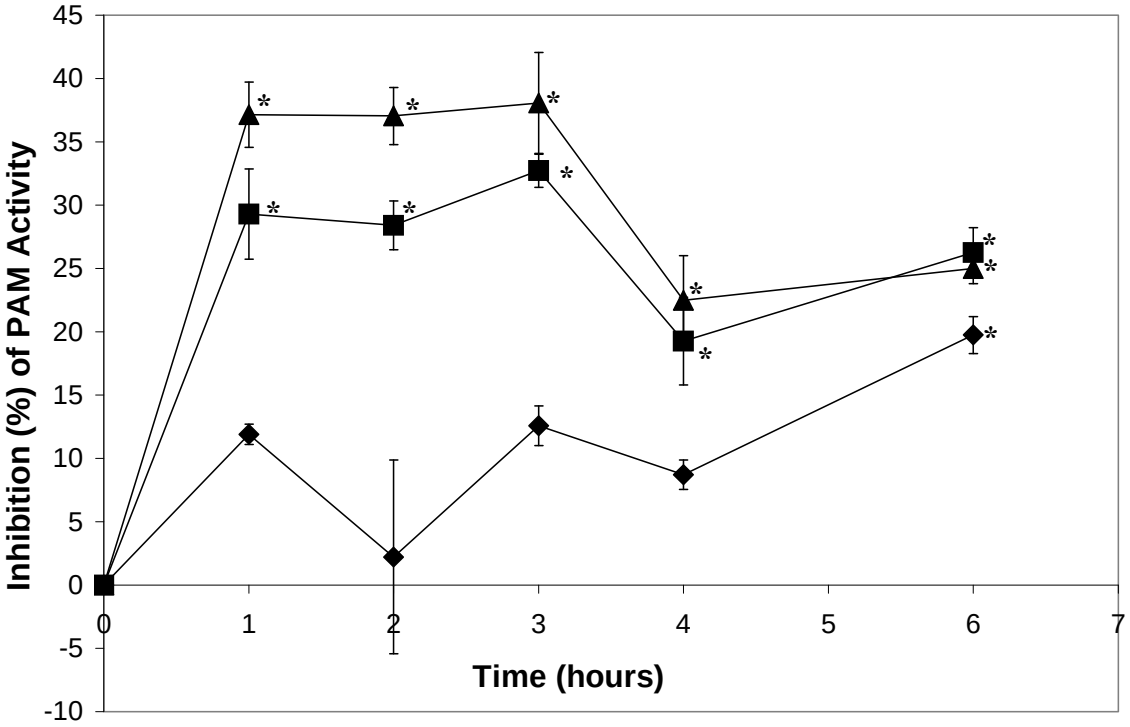

Figure 57. Effect of Methyl-N-Ac-(L)-Phe-Acrylate on serum PAM activity in Sprague-Dawley rats. Methyl-N-Ac-(L)-Phe-Acrylate was administered as a single subcutaneous dose at three concentrations to determine the effects on serum PAM activity *in vivo*. Control animals received injections of vehicle only. Time points were taken periodically over the course of six hours. APAA-Me 10 mg/kg (●); APAA-Me 50 mg/kg (■); APAA-Me 100 mg/kg (▲). Data are presented as the mean ± S.E.M. for each group (n=3).
* Statistically significant ($P < .05$) compared to controls (Tukey's test).

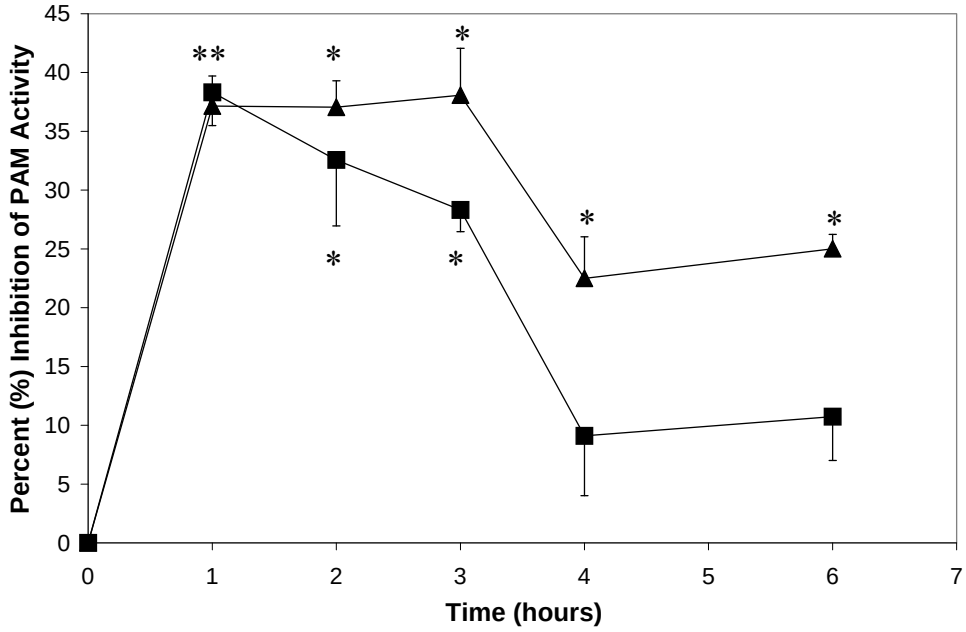

Figure 58. Effect of APAA and APAA-Me on serum PAM activity *in vivo*. Compounds were given as a single subcutaneous injection to determine their effect on serum PAM activity. Control animals received injections of vehicle. Serum was collected at time points between 0 and 6 hours. PAM activity was analyzed as described in "Methods". APAA 100 mg/kg (■); APAA-Me 100 mg/kg (▲). Data are presented as the mean ± SEM for each group (n=3). *Statistically significant ($P < 0.05$) compared to controls (Tukey's test).

activity rebounds more quickly toward basal levels in the case of the free acid. After three hours, PAM inhibition by the free acid has decreased to 28% of controls while the prodrug maintains its initial inhibition (38%). Between 3 and 4 hours post-injection, inhibition decreases sharply for both the free acid and the ester (by 20% and 15%, respectively). No further rebound in serum PAM activity is evident for either compound between four and six hours post-injection.

Anti-inflammatory Effect of APAA-OMe

As mentioned above, carrageenan-induced edema is an effective model of acute inflammation. Typically, the injected paw volume tends to increase dramatically by one hour and continues to increase until four or five hours post-administration, at which point the swelling begins to subside. Figure 59 shows the change in hindpaw volume after carrageenan administration in the presence and absence of N-Ac-(L)-Phe-Acrylate Methyl Ester at a dose of 150 mg/kg over six hours. Paw volume measurements were taken every hour for six hours. Remarkably, this compound completely abolished swelling and inflammation in the hindpaw throughout the entire time-frame of the experiment. The anti-inflammatory effect is most pronounced four hours post-administration, when untreated control paws had increased by 0.75 mL in volume while the prodrug-dosed group showed little to no increase in paw volume.

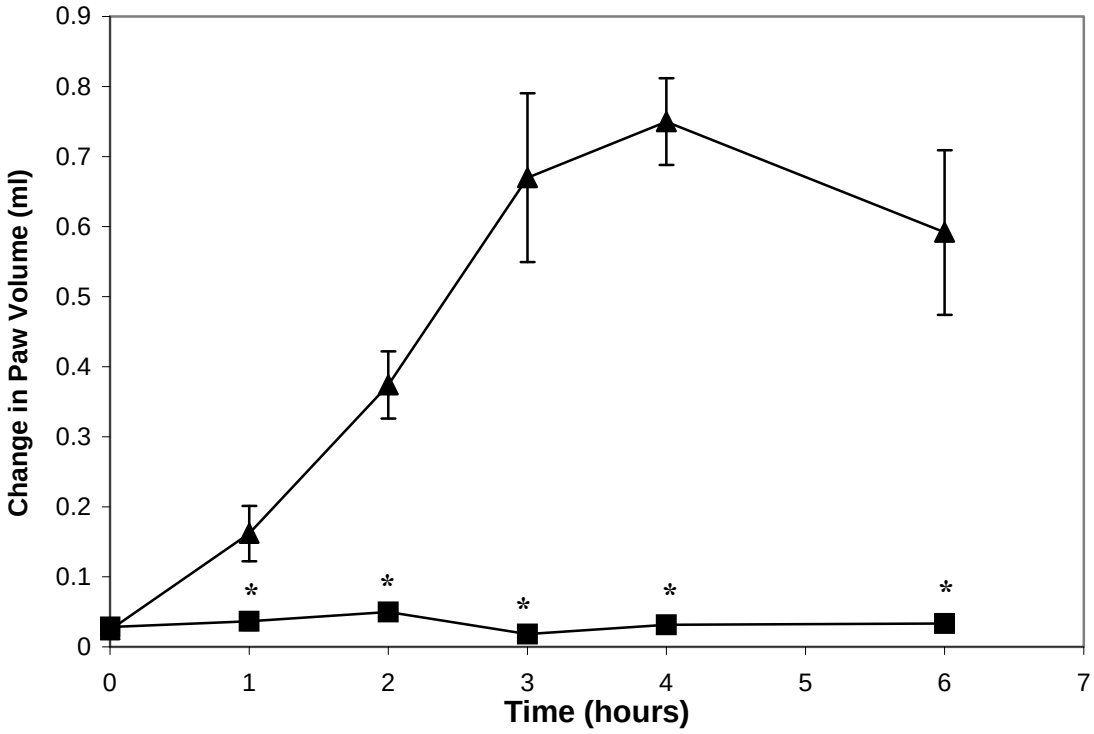

Figure 59. Effect of Methyl-N-Ac-(L)-Phe-Acrylate on acute inflammation of the hindpaw in carrageenan-induced edema. Methyl-N-Ac-(L)-Phe-Acrylate was administered subcutaneously at 150 mg/kg 30 minutes prior to the induction of carrageenan-induced edema. Control animals received vehicle only. Injected and contralateral paw volumes were analyzed plethysmographically by mercury displacement at 0, 1, 2, 3, 4, and 6 hours. Change in paw volume was calculated as the difference in injected and contralateral hindpaw volumes at each time point. Vehicle treated animals (▲); APAA-Me 150 mg/kg (■). Data are presented as the mean ± S.E.M. for each group (n=6).
* Statistically significant ($P < .05$) compared to controls for that time point (Student's *t* test)

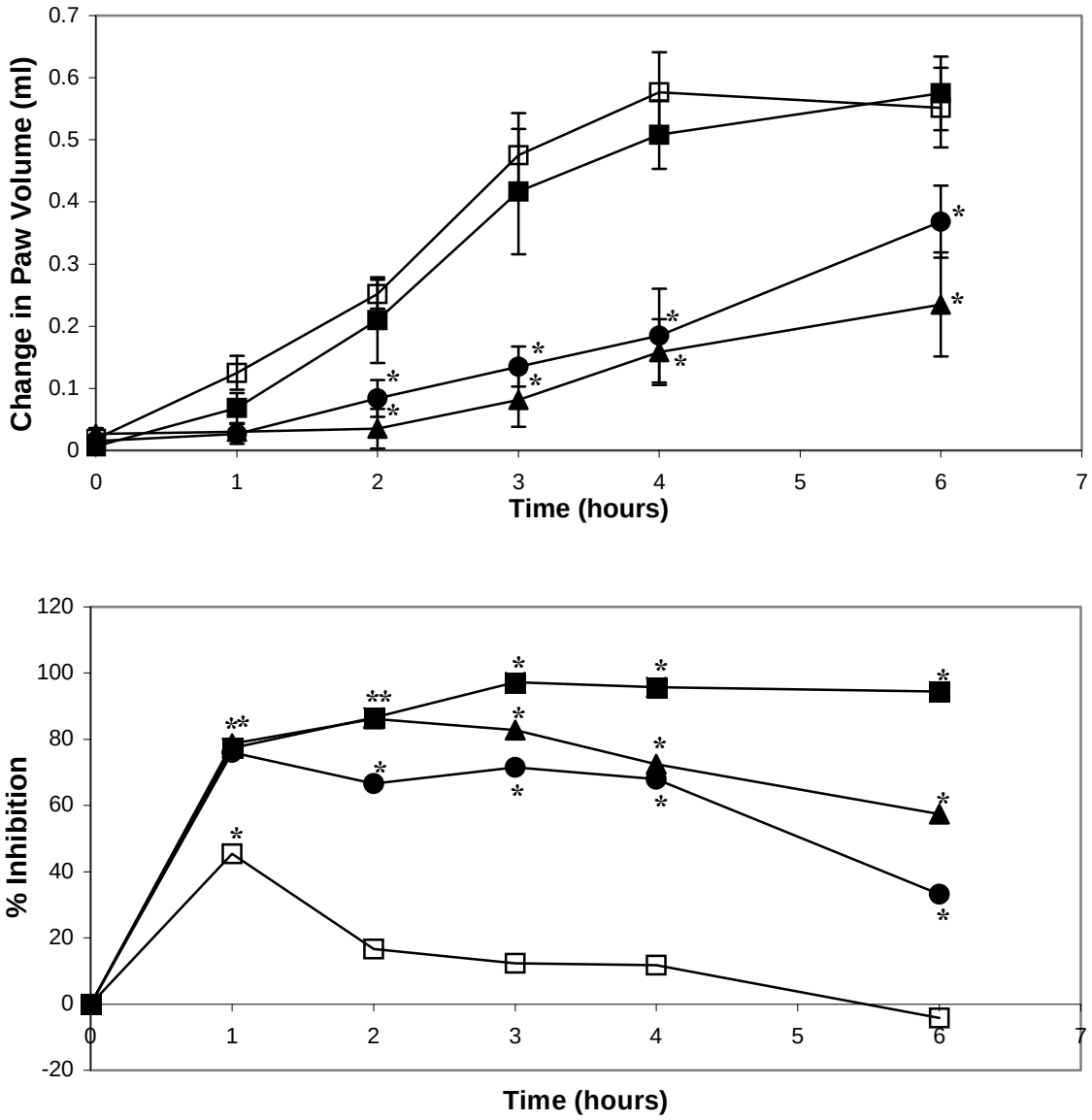

Figure 60. Effect of different doses of Methyl-N-Ac-(L)-Phe-Acrylate on acute inflammation in carrageenan-induced edema in Sprague-Dawley rats. Various concentrations of Methyl-N-Ac-(L)-Phe-Acrylate were delivered by subcutaneous injection into the hindpaw of rats 30 minutes prior to the induction of carrageenan-induced edema. Injected and contralateral hindpaw volumes were measured plethysmographically by mercury displacement at 0, 1, 2, 3, 4, and 6 hours. Change in paw volume was calculated as the difference in injected and contralateral hindpaw volumes at each time point. a) Vehicle treated animals (□); APAA-Me 10 mg/kg (■); APAA-Me 50 mg/kg (●); APAA-Me 100 mg/kg (▲). Data are presented as the mean ± S.E.M. for each group (n=6). b) APAA-Me 10 mg/kg (□); APAA-Me 50 mg/kg (●); APAA-Me 100 mg/kg (▲); APAA-Me 150 mg/kg (■).
* Statistically significant ($P < .05$) compared to control time point (Tukey's test).

Next, varying doses of N-Ac-(L)-Phe-Acrylate Methyl Ester (10, 50, 100 mg/kg) were administered to Sprague-Dawley rats injected with carrageenan. The results are shown in Figure 60. The top panel shows the change in paw volume with time. The 10 mg/kg dose was unable to reduce the inflammation and swelling associated with the carrageenan-induced edema in a statistically-significant manner. The 50, 100, and 150 mg/kg doses were all effective in preventing the inflammation of the paw induced by the carrageenan. The bottom panel shows the percent inhibition of swelling over a six hour time course. The three highest doses all inhibited the swelling to varying degrees. Again, the 150 mg/kg dose resulted in nearly 100% inhibition three hours after administration. After six hours, the 50, 100, and 150 mg/kg doses resulted in levels of inhibition of approximately 95%, 60%, and 40%, respectively. The low 10 mg/kg dose was indistinguishable from controls after six hours.

Figure 61 presents a dose-response curve of % inhibition vs. log [N-Ac-(L)-Phe-Acrylate Methyl Ester] (mg/kg). The curve is linear for the four points tested. A dose of 50 mg/kg results in 70% inhibition of inflammation, while the highest dose was able to completely abolish the carrageenan-induced inflammation by 3 hours post injection.

Effect of APAA-OMe on Adjuvant Induced Polyarthritis (AIP)

After our remarkable results with this compound in the amelioration of swelling associated with the acute inflammation induced by carrageenan injections, we attempted to assay the anti-inflammatory effects of this compound against the three stages of AIP

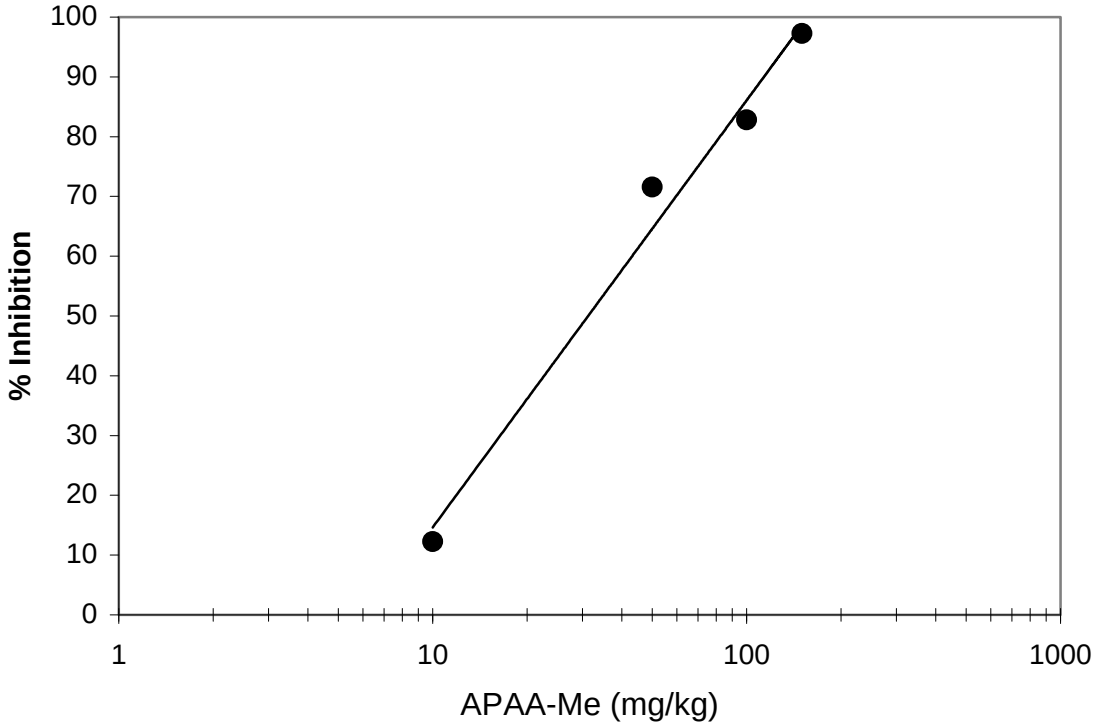

Figure 61. Anti-inflammatory effect of Methyl-N-Ac-(L)-Phe-Acrylate on carrageenan-induced edema three hours post-induction. The percent inhibition versus vehicle-treated animals was determined 3 hours post-induction of carrageenan edema for concentrations of APAA-Me ranging from 10 mg/kg to 150 mg/kg. Data are presented as the dose received versus the percent inhibition produced by each dose at 3 hours post-induction (n=6).

(recognition, proliferation, and effector), an animal model which more closely resembles the progression of rheumatoid arthritis in humans. Owing to the solubility problems and the difficulty of delivery of the extremely hydrophobic N-Ac-(L)-Phe-Acrylate Methyl Ester, we were forced to opt for a vehicle which contained 90:10 ethanol/DMSO. The subcutaneous injections of this compound in this particular vehicle resulted in local tissue necrosis and death in several of the animals over the course of the first 3 days of the experiment (Day 0, Day 1, and Day 2). Therefore, the drug injections were discontinued after Day 2. The results of the experiment are presented in Figure 62. At the end of the recognition phase (Day 2), the drug-treated animals did exhibit significantly smaller injected paw volumes relative to the positive controls (about 40%). The contralateral paw does not increase in volume during the recognition phase of adjuvant arthritis. By Day 4, the injected paw volumes were still less than those of the positive controls, but the results were not statistically significant. By Day 16 (the effector phase), both the injected and contralateral paws of the drug-treated animals were slightly higher in volume than the positive controls, although, again, this was not statistically significant. We were forced, then, to abandon further adjuvant experiments with this compound until a more reasonable vehicle was found which did not cause local necrosis and mortality.

PAM Activity in WB-Neo Cells and Inhibition by PBA

Intrinsic PAM activity in WB-Neo (rat liver epithelial) cells was calculated for both the membrane-bound and soluble fractions. Subsequently, the extracts were analyzed for PAM activity in the presence of 250 μM PBA, in order to determine whether PAM from

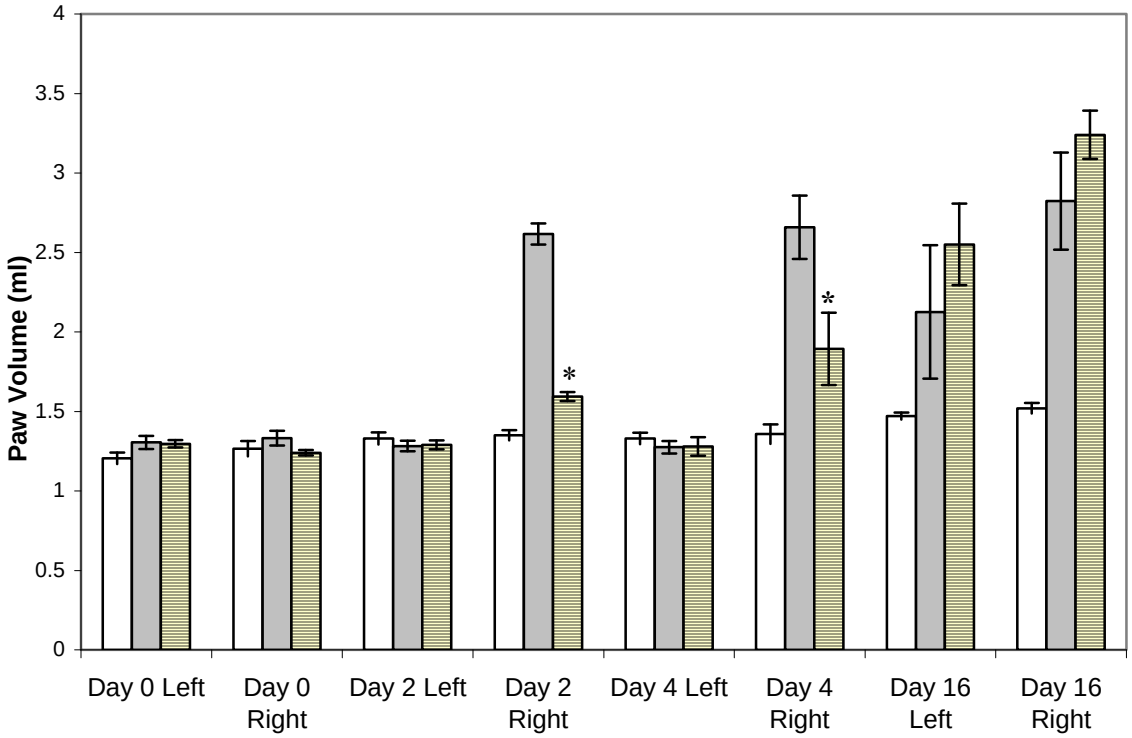

Figure 62. Effect of Methyl-N-Ac-(L)-Phe-Acrylate on Adjuvant-Induced Polyarthritis in Sprague-Dawley rats. Methyl-N-Ac-(L)-Phe-Acrylate was administered subcutaneously on Days 0-2 at 150 mg/kg to rats. Injections ceased after Day 2 owing to acute local and systemic toxicity. Injected (right) and uninjected (left) hindpaw volumes were measured plethysmographically by mercury displacement on day 0, 2, 4, and 16. Open bars – vehicle-treated controls (n=4); solid bars – vehicle-treated arthritic animals (n=4); dashed bars – APAA-Me-treated animals (n=3). Data are presented as the mean ± S.E.M. for each group.
* Statistically significant ($P < .05$) compared to arthritic controls (Student's *t* test).

this source was susceptible to PBA inhibition. The results are presented in Figure 63. Under normal culture conditions, in the absence of PBA, WB-Neo cells were shown to possess a significant amount of soluble and membrane-bound PAM activity. Soluble PAM was found to be present at 8 nmol product/mg protein/hour, while PAM activity from the membrane-bound extract was slightly more than twice as high as for soluble controls, at 18 nmol product/mg protein/hour. Incubation of the cell extracts with 250 μM PBA reduced PAM activity in the soluble and membrane-bound fractions by 75% and 85%, respectively, to 2 nmol product/mg protein/hour in both cases. Overall, for the WB-Neo cells, the ratio of membrane-bound/soluble PAM activity was found to be 2:1.

PAM Activity in WB-Ras Cells and Inhibition by PBA

WB-Ras (transformed rat liver epithelial) cells were evaluated for soluble and membrane-bound PAM activity, and this activity was again evaluated in the presence of PBA to determine its susceptibility to inhibition by this known *in vivo* mechanism-based PAM inactivator. Results are presented in Figure 63. Soluble PAM activity was found to be 0.6 nmol product/mg protein/hour. Coincubation of the soluble extract with 250 μM PBA in the PAM assay mix resulted in a 60% decrease in activity. The membrane-bound extract had activity of 3.5 nmol product/mg protein/hour, which in the presence of 250 μM PBA was reduced by 60% to 1.5 nmol product/mg protein/hr.

Cultured WB-Neo and WB-Ras Cells: Inhibition by PBA/PBA-OMe

WB-Neo and WB-Ras cells were cultured in the presence of either 0.1 mg/mL PBA or 0.01 mg/mL PBA-Methyl Ester. Cells were evaluated for residual PAM activity after one day and again after four days, and compared to untreated controls. Cells were harvested, counted, and the soluble and membrane-bound extracts were assayed for PAM activity as stated in the Experimental Section.

The results of the PBA-treated cells are presented in Figure 63. Soluble WB-Neo cells showed a progressive decrease in PAM specific activity over the course of the experiment. After 24 hours, the specific PAM activity in the PBA-treated cells had decreased by approximately 38%, and after 4 days incubation, had decreased by 43% relative to controls. The membrane-bound PAM activity in the WB-Neo cells evinced a 30% decrease relative to controls after the first day, with a sharp continued decline in activity after four days incubation (55%). It appears that the membrane-associated PAM activity was susceptible to inactivation by PBA for an extended period of time relative to the soluble PAM activity, and was inactivated to a greater degree over the time course of the experiment. In the WB-Neo controls, soluble PAM activity represented 58% of the total PAM activity, with 42% of the total activity found in the membrane-bound extract. After one day treatment with 0.1 mg/mL PBA, 56% of total PAM activity was found in the soluble extract, whereas 44% was present in the membrane-associated extract. After 4 days treatment, 63% of the activity was soluble and 37% membrane-associated.

The PBA-treated WB-Ras cells also showed a significant decrease in PAM activity after 24 hours treatment, similar to the WB-Neo cells, but after 4 days treatment, the

PAM activity had rebounded relative the activity after 24 hours, with membrane-associated PAM activity increasing to greater levels than were seen in the WB-Ras controls after 4 days treatment. After 24 hours, the soluble PAM activity in the WB-Ras cells decreased to 35% of controls. After 4 days, PAM activity was essentially the same as after 24 hours treatment (39% controls). Conversely, the membrane-associated PAM specific activity had decreased to 50% of controls after 24 hours, but after 4 days had rebounded to over 110% of control PAM levels. Overall, in the WB-Ras cells, 22% of the PAM activity in controls was found in the soluble extract, with 78% in the membrane-bound fraction. After 24 hours, only 17% of the total PAM activity was located in the soluble extract, with 83% membrane-associated. After 4 days, only 9% of the PAM activity was soluble, while 91% was membrane-bound. The most intriguing aspects of these results are twofold. First, that the PAM activity in the WB-Ras cells was able to return to control levels after 4 days treatment, whereas WB-Neo cells were not, implies that the WB-Ras cells are able to more efficiently upregulate PAM activity when incubated with an inactivating species than their WB-Neo counterparts. Secondly, and perhaps even more striking, is the change in distribution of PAM activity between soluble and membrane-bound forms of the enzyme between the two cell lines. In the WB-Ras cells, the membrane-associated PAM accounted for 78%, 83%, and 91% of the total PAM activity in the control, 24-hour PBA-treated, and 4-day PBA-treated cells, respectively. For the WB-Neo cells, the membrane-associated PAM activity accounted for only 42% (control), 44% (24 h), and 37% (4 days) of total activity.

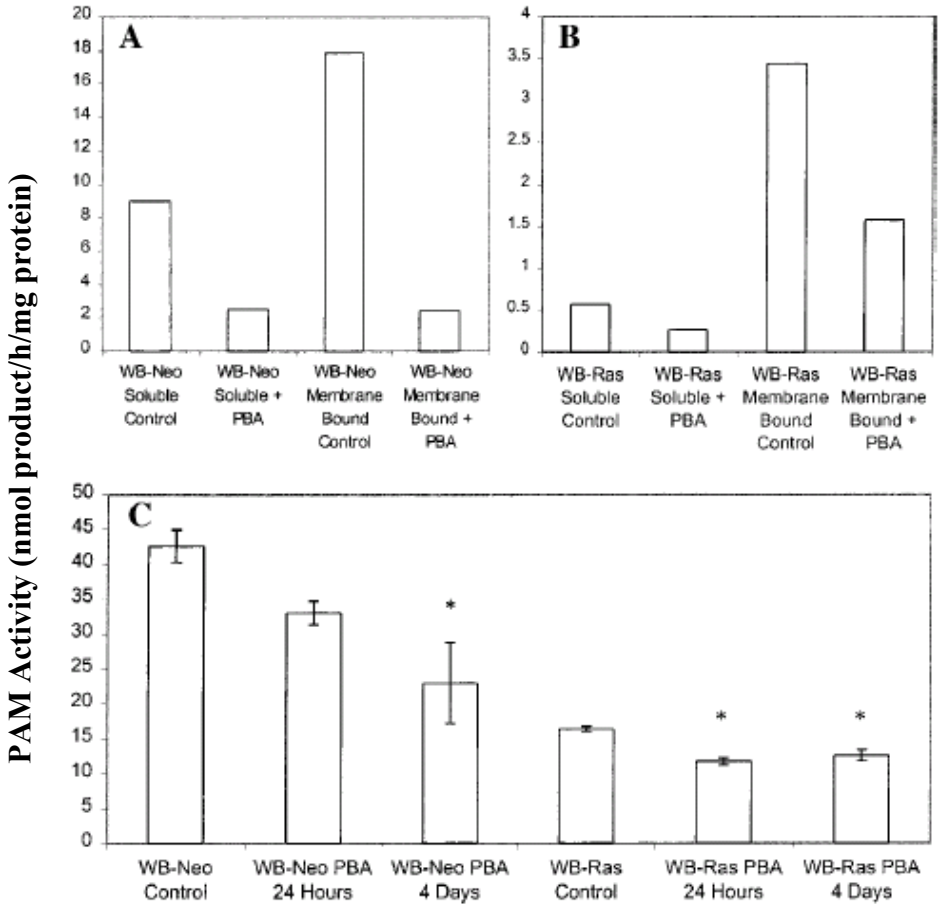

Figure 63. Effect of PBA on PAM activity in WB-Neo and WB-Ras cells. Each group consists of cells grown to 90-100% confluence from two 75 cm^2 flasks. Cell extracts and PAM assays were performed as described in "Methods". (A) Specific activity of PAM in soluble and membrane-associated extracts of WB-Neo Cells, with and without 250 μM PBA added to reaction mixture. (B) Specific Activity of PAM in soluble and membrane-associated extracts of WB-Ras cells, with and without 250 μM PBA added to reaction mixture. (C) Combined specific activity of PAM in WB-Neo and WB-Ras cells treated with 0.1 mg/mL PBA for 24 hours and 4 days. Data presented as mean PAM specific activity ± S.E.M. for each group (n=3). *, Statistically significant ($P<0.05$) compared to controls (Tukey's test).

Chapter 8: Discussion

As evident from the introductory remarks above, SP clearly plays a major role in the metabolic pathways which govern a wide variety of pro-inflammatory and pro-growth processes and functions. Bioactive SP-NH_2 is a product of the PAM reaction, the rate-limiting step of peptide amidation outlined in the first section. Therefore, interference with the enzyme responsible for the bioactivation of a species (SP) which lies near the upstream terminus of the activation of the PLC pathway, the COX-2 pathway, the MAP-Kinase pathway, and the Ras pathway would surely be expected to ameliorate many inflammatory and neoplastic pathologies. We have shown that our mechanism-based acrylate inhibitors are the most potent *in vitro* inactivators of PAM currently known, and the ability of these compounds to permanently inactivate PAM makes them especially desirable agents relative to simple competitive inhibitors. Naturally, permanent inactivation of *in vivo* PAM activity requires that new PAM be transcribed, translated, and post-translationally modified/processed in order to return enzyme concentrations (and its products) to pre-dosing levels.

Currently, a widespread therapeutic interest in blocking the effects of SP (or related pro-inflammatory neuropeptides such as calcitonin gene-related peptide) has become manifest, with the development of compounds which act as antagonists toward the NK-1 receptor (the receptor for SP), or compounds which deplete stores of SP from the vesicles of C-afferent nerve fibers (such as capsaicin). Both approaches have been shown to be effective in the amelioration of certain pathological conditions. However, the former approach (receptor antagonists) engenders only a competition between SP itself and the

therapeutic agent for the occupation of the NK-1 receptor. It does not serve to deplete or reduce actual physiological concentrations of SP. Indeed, SP has been shown to be able to initiate intracellular cascades via a receptor-independent mechanism in mast cells (cells which lie close to the C-afferent nerve terminals which contain stored SP), and thus these antagonists are of no account in preventing this type of activation. Indeed, the phenomenon of neurogenic inflammation involves both mast cells and the innervating afferent nerve terminals. SP released from the nerve terminals serves to activate a pro-inflammatory response in these mast cells, which are a major source of histamine, bradykinin, and serotonin, all factors which further contribute to the pathology of chronic inflammation. Capsaicin treatment, through interaction with a vanillin-like receptor, causes SP to be released from nerve terminals over a short time period, causing a sharp increase in the extracellular concentrations of SP. Although the nerve terminals are thusly depleted of SP, levels of which may not return to baseline for an extended period of time, the topical treatment is painful on the one hand, and the initial depletion of SP into the extracellular space can potentiate, on short time scales, any pro-inflammatory processes which have already begun in earnest.

Certainly, the most effective way to interfere with the pro-inflammatory (or pro-growth/neoplasticity) effects of SP is to prevent its formation in the first place. Inhibition/inactivation of PAM-catalyzed SP bioactivation obviates, in large measure, the needs for treatment with NK-1 receptor antagonists (which, as peptides, are not orally active and require hypodermic injection) or for the "scorched-earth" approach of capsaicin-induced SP depletion. On the basis of these considerations, we naturally wished to investigate the ability of our acrylate PAM inactivators to, firstly, inactivate

PAM *in vivo* and secondly, to see if this inactivation led to a blockade of the many downstream effectors of NK-1 receptor activation and indeed manifested as an anti-inflammatory agent. Our results clearly show that administration of PAM inhibitors (PBA, PBA methyl ester, N-Ac-(L)-Phe-Acrylate, and methyl N-Ac-(L)-Phe-Acrylate) is extremely effective in the amelioration of both acute inflammation (via the carrageenan-induced edema model) and chronic inflammation (via the adjuvant arthritis model) in Sprague-Dawley rates. Furthermore, the anti-inflammatory effects of these agents correlate strongly with a decrease in residual serum PAM levels post-treatment.

Finally, because SP is also a mitogenic growth factor, we reasoned that inactivation of PAM may also manifest an anti-neoplastic effect on transformed cells, possibly via the deactivation of the Ras pathway, an expected downstream effect of reducing physiological levels of SP. As outlined in the results above, treatment of Ras-transformed epithelial cells with the pro-drug of PBA, a first-generation, lipophilic mechanism-based PAM inactivator resulted in an increase in gap-junctional communication (i.e. cell-to-cell communication) via an increase in the phosphorylation levels of the gap-junction component protein connexin-43. In this case, as in that of the anti-inflammatory studies mentioned, it must be stressed that inactivation of PAM by these compounds does not exclusively prevent the bioactivation of SP, but also that of any peptide which requires amidation for full biological activity. Nevertheless, these results show that PAM inhibition/inactivation is a valid target for both anti-inflammatory and anti-cancer agents, and certainly warrants continued study and refinement, as the proof of concept is clearly evident.

Previous work by our laboratories has demonstrated that continuously-administered PBA (via osmotic pump) is able to significantly inhibit serum PAM activity in Sprague-Dawley rats (Ogonowski, 1997). These studies also showed that PBA was able to inhibit the swelling typical of carrageenan-induced edema in rats, in conjunction with a decrease in SP immunoreactivity in injected rat hindpaw tissue. Taken together, these studies indicated that PBA was a bioactive PAM inhibitor, that serum PAM levels decreased commensurate with PBA dosing, and that the PAM product SP is also found to be decreased in the hindpaw tissues of rats that had been injected with carrageenan and dosed with PBA. These three pieces of information (anti-inflammatory effect based on reduced paw volume of PBA-treated animals, correlation of the inhibition of serum PAM activity with the anti-inflammatory effect, and the correlation of reduced SP levels with reduced PAM activity in dosed animals) certainly provide remarkable evidence that PAM inhibition *in vivo* leads to the downstream effects which had been postulated.

While the carrageenan studies were certainly encouraging, these experiments are models of acute, rather than chronic, inflammation. Certain diseases, most notably rheumatoid arthritis (RA), are characterized by a chronic type of inflammation that involves a specific cellular immune response which causes the long-term activation of pro-inflammatory pathways, and which is characterized by a failure to resolve the inflammation caused by the initial insult. Indeed, RA can be characterized as an autoimmune disease, where unresolved inflammation in a given area has led to a cross-reactivity with "self" cells of the joints and cartilage. As T-cells become involved in the process, a positive-feedback loop is engaged whereby the T-cells may be releasing pro-inflammatory mediators (which in turn stimulate the effector cells of the innate immune

system as described above) in response to the recognition of self antigen in a process which simply cannot be resolved by current conventional treatments. The processes which occur in acute inflammation are a major subset of the processes which occur in ongoing chronic inflammation, and many of these effector cells are influenced to continue the release of pro-inflammatory mediators by Substance P. Indeed, research has shown that SP is directly involved in the pathogenesis of adjuvant-induced polyarthritis (AIP) in rats, which is seen as one of the best animal models of (human) RA itself (Donaldson, 1995; Walker, 2003). Therefore, we reasoned the acute anti-inflammatory effect of PBA could translate into an amelioration of the chronic inflammation characteristic of AIP. AIP is initiated by the administration of heat-denatured *Mycobacterium butyricum* in mineral oil, which causes an initial, acute phase of inflammation (Phase 1) in the injected paw which peaks after approximately two days, and is mediated by the cells of the innate immune system (macrophages, neutrophils, etc.). The inflammation of the hindpaw plateaus at this point, and generally remains unchanged until nine or ten days post-adjuvant administration (Phase 2). During this time, it is believed that a T-cell proliferation process occurs, where T-cells exposed to the antigen, and likely cross-reactive with the injected tissue, mature in the lymphatic system. As these cells are selected for and proliferate, they migrate to the area of insult and, via the co-stimulation of the effector cells of the innate immune system, potentiate the inflammation which has already occurred therein. From Day 9 to Day 16 (Phase 3), the injected hindpaw swelling worsens, and in addition, the contralateral (non-injected) hindpaw begins progressively to inflame as well. The inflammation of the contralateral hindpaw is indicative of a systemic immune reaction, whereby the self-reactivity of the

T-cells engendered by the initial bacterial insult has allowed for the activation of pro-inflammatory pathways at sites far removed from the site of injection. The reported involvement of SP in the progression of this disease led us to believe that PBA would also be effective in the amelioration of this chronic inflammation. Moreover, by choosing PBA-dosing regimens which administered drug to animals in Phase 1 (starting 5 days prior to the adjuvant injection, through Day 2 post-injection), Phase 2 (from Day 2-9), and Phase 3 (Days 10-16), we were able to investigate whether our PAM inactivators were effective in the different stages of the disease progression. Also, by monitoring the volume (swelling or lack thereof) of both the injected and contralateral hindpaws, we were able to determine whether PBA dosing could affect the later-developing inflammation at sites far-removed from the initial site of injection.

Our results clearly indicate the phenomenal efficacy of PBA as an anti-inflammatory agent in all phases of AIP, and at both the injected and contralateral hindpaw at a dosing regimen of 60 mg/kg/hour. Certainly, it was not surprising that the Phase 1 dosing would evince a profound anti-inflammatory effect, as this stage of the disease would be expected to be very similar to the acute inflammation caused by carrageenan injections. Also, the reduction in paw volume in the experimental animals was maintained throughout the proliferation phase of AIP (Phase 2) relative to untreated arthritic animals and continued into Phase 3 (the effector phase). This shows that interfering with peptide amidation, very early in the experiment, results in a continued suppression of inflammation, even two weeks after PBA-dosing is terminated. This was true for both the injected and contralateral paws throughout the time-frame of the experiment.

Dosing during Phase 2 (the proliferation phase) significantly decreased the swelling in PBA dosed animals by Day 9 by more than 50%. This is an interesting result because it indicates that although the level of inflammation indeed plateaus during this period, it can still be positively affected by PAM inactivators. Furthermore, it indicates an active process of inflammation in the injected paw during this phase, even though the injected paws of vehicle-treated arthritic animals do not undergo further increases in volume over this seven day period. Based largely on the reduction in swelling effected by Phase 2 dosing, the effects of PBA remain pronounced through Phase 3, although the slopes of the lines representing paw volume with time are very similar for the injected paws of both PBA-treated and vehicle-treated arthritic animals. This Phase 3 effect is identical to that seen in animals dosed on Day -5 through Day 2 in the first set of animals outlined above. The interpretation of these results is that PBA dosing in Phase 1 and Phase 2 do not significantly affect the progression of inflammation and paw swelling in Phase 3, but that the overall swelling is reduced exclusively during Phase 1 and Phase 2, and that during Phase 3, the observed anti-inflammatory effect is a result of the initial decrease in swelling during the earlier two phases. Phase 2 dosing also significantly reduces the swelling in the contralateral paw during Phase 3. It is unknown whether this is the result of local PBA effects at the site of the joints (which persist into Phase 3 after dosing has been terminated), or whether PBA is able to interfere (through an SP-mediated mechanism) with the proliferation or maturation of the T-cells which are involved in the effector phase (Phase 3).

Finally, Phase 3 dosing (Days 10-16) also demonstrated the anti-inflammatory effects of PBA during the effector phase. The injected paws of PBA-treated animals underwent

no further swelling concurrent with dosing, and this effect seemed to be more pronounced that the anti-inflammatory effects when PBA was administered during Phase 1. The anti-inflammatory effect was also statistically significant in the contralateral paws of animals dosed during Phase 3, although some swelling was evident relative to the injected hindpaws during this time-frame. As mentioned above, when serum PAM activity was monitored over the course of seven days at 50 mg/kg/hour PBA, residual enzyme activity was maintained at 30% or less of controls throughout the course of the experiment. Although we did not directly evaluate serum PAM activity during the course of our AIP experiment (to prevent further insult to the animal), the above indicates a strong likelihood that the anti-inflammatory effects of PBA are correlated in some manner to this decrease in activity. In any event, this is the first evidence that a PAM inhibitor is effective in treating the chronic inflammation characteristic of AIP.

Owing to the success of the treatment of AIP by PBA, we next attempted to run another adjuvant experiment with our second-generation pro-drug ester, methyl-N-Ac-(L)-Phe-acrylate. However, we encountered solubility problems with this compound. Various cyclodextrins were employed to improve aqueous solubility but were unsuccessful. Attempts to formulate a drug solution in corn oil or mineral oil were also unsuccessful. Ultimately, we settled on a vehicle of 90:10 EtOH/DMSO. It must be noted that to create the PBA drug formulation, the free acid of PBA was simply titrated into phosphate-buffered saline with sodium hydroxide. This was not a problem with the achiral PBA, but because our acrylates are enantiomerically pure we were loath to employ this method for fear that base-catalyzed racemization might occur at the phenylalanine stereocenter. In addition, the results of our carrageenan-induced edema

studies with this acrylate and its pro-drug methyl ester had indicated that the pro-drug produced more impressive *in vivo* results. These concerns led to the rather undesirable vehicle formulation described above. Unfortunately, the pro-drug/vehicle combination was found to be toxic, both locally (causing tissue necrosis at the injection site) and systemically, and resulted in a high mortality rate among the animals involved in the AIP study, and the study was therefore discontinued two days into Phase 1 of the experiment. Nevertheless, some anti-inflammatory effect was evident in the injected paws of drug-treated animals after two days and after four days post-arthritis induction. Unlike the PBA AIP experiment outlined above, this effect did not persist into Phase 3, and the injected and contralateral hindpaws of drug-treated animals were statistically unchanged relative to controls.

A recent experiment (data not included in this thesis) with a microparticle formulation of Methyl-N-Ac-(L)-Phe-Acrylate encapsulated with poly(cyclohexane-1,4-diyl acetone dimethylene ketal) (PCADK) clearly showed that this compound was effective, as was PBA, in treating inflammation associated with all three phases of AIP, as per the dosing regimen outlined above. The particles were injected intra-peritoneally (IP), and it must be noted that the control animals were given ethanol vehicle, which caused early mortality. Therefore, the control animals were adversely affected by this ethanol vehicle (IP) as were the animals in the original AIP experiment where Methyl-N-Ac-(L)-Phe-Acrylate in 10:90 DMSO/ethanol was delivered subcutaneously. However, there appeared to be no toxicity or necrosis associated with the particle formulation (delivered as a suspension in phosphate-buffered saline). This indicates that the vehicle, and not the drug, was the cause of the mortality in the first AIP experiment. Experiments are

ongoing to maximize drug loading in the microparticles, in the anticipation of another AIP experiment with proper controls.

Since the PBA experiments on acute (carrageenan-induced edema) inflammation seemed to correlate the anti-inflammatory effects of the compound to the reduction in paw swelling, we reinvestigated the effects of different doses of PBA on serum PAM activity, and investigated the effects of N-Ac-(L)-Phe-Acrylate and its prodrug methyl ester as well. Whether or not the drop in serum PAM activity is actually causative of the anti-inflammatory effect is beyond the scope of this thesis. Nevertheless, an anti-inflammatory effect of a PAM inhibitor has never been seen in the absence of this concomitant drop in serum PAM activity.

Both PBA and N-Ac-(L)-Phe-Acrylate are completely ionized at physiological pH (7.4). It is, therefore, unlikely that either molecule is able to diffuse through the plasma membrane into cells and cause an anti-inflammatory effect via inactivation of intracellular PAM, which, to make matters more difficult for these anion species, is sequestered in secretory vesicles with the cell. However, the methyl ester prodrug would likely be able to diffuse into cells by virtue of its neutral character and general lipophilicity. Conversely, only the free acid is able to inhibit and inactivate PAM *in vitro*, so the effective concentration of the free acid in the bloodstream, when delivered as the methyl ester prodrug, is not readily known in the absence of further experimental data. Therefore, comparing the ability of each of the three compounds (PBA, N-Ac-(L)-Phe-Acrylate, and Methyl-N-Ac-(L)-Phe-Acrylate) to reduce serum PAM activity, and the time-course of that reduction in activity, relative to the anti-inflammatory effects of these compounds is very important.

We have seen that repeated dosing with PBA at 500 mg/kg (every three hours) results in a 70% reduction in serum PAM activity after two hours, a 95% reduction after six hours which is maintained until 12 hours after the initial PBA injection, and then a slight decrease to 80% inhibition after 24 hours. On the other hand, the one-time dose of 500 mg/kg, naturally, shows the same 70% inhibition after two hours, but the effect rapidly dissipates, with 45% inhibition after six hours and only 10% inhibition after nine hours. The increase in PAM activity after the one-time dose between two and nine hours post-injection indicates that the enzyme is being replenished by some physiological source, owing to the fact that the inactivated enzyme cannot "reactivate" itself. Additionally, since additional PBA (multiple dosing) maintains the decrease in serum PAM activity (which is not maintained by the one-time dose) it is evident that PBA is cleared rapidly from the bloodstream (or chemically altered to a form which does not inhibit/inactivate PAM). Certainly, it is well-known that ionic species are more readily excreted by the kidneys than neutral species, which often require one or more passes through the liver before they can be efficiently excreted in the urine.

N-Ac-(L)-Phe-Acrylate, like PBA, is an anionic species at physiological pH. Although this compound was only administered as a one-time dose (subcutaneously) at 10, 50, and 100 mg/kg, we can see from the resulting inhibition of serum PAM activity that the profile is much the same as was the case for the one-time PBA dose. It must be mentioned that although doses for these studies are calculated as "mg/kg", this is not the best metric for the actual concentration of the drug in the bloodstream (presuming, of course, that all of the administered drug enters the bloodstream). Here, the molecular weights of PBA, N-Ac-(L)-Phe-Acrylate, and Methyl-N-Ac-(L)-Phe-Acrylate are 162,

261, and 273 g/mol, respectively. Therefore, equal doses of PBA and the free acid acrylate (in mg/kg), for instance, would provide for a greater concentration in the animal of PBA than the acrylate (about 1.6-fold greater). Additionally, the highest dose of the acrylate was only 100 mg/kg (vs. 500 mg/kg for PBA), so the effective concentration of the highest acrylate dose would be, all else being equal, only about 1/8 that of the highest PBA dose. Keeping that in mind, the 100 mg/kg dose of the acrylate evinced serum PAM inhibition of about 40% after one hour, which decreased to 10% inhibition after six hours. As was the case for anionic PBA, it is evident that anionic N-Ac-(L)-Phe-Acrylate is cleared from the bloodstream fairly rapidly, and likely this contributes to the decrease in inhibition with time, along with PAM being replenished in the bloodstream at the basal rate, or at an upregulated rate as the homeostatic concentration of serum PAM is decreased below a certain level. Further experiments are needed at higher concentrations of the free acid acrylate in order to determine whether this compound is able to inactivate serum PAM at the 95% levels seen with PBA at 500 mg/kg. That being said, after three hours serum PAM was inhibited by approximately 30% in the case of N-Ac-(L)-Phe-Acrylate, and similarly by about 25% in the case of 125 mg/kg PBA.

Finally, the methyl ester prodrug Methyl-N-Ac-(L)-Phe-Acrylate is uncharged at physiological pH and the ester must be cleaved (either enzymatically by an esterase or spontaneously at the alkaline pH of bloodstream) prior to inactivating/inhibiting serum PAM. By virtue of its charge-neutrality, it would be expected *a priori* to persist longer in the bloodstream than the free acid analog, and, if this were the case, would be expected to maintain serum PAM inactivation for a longer time period. Of course, contrary to the beneficial effect of persisting for a greater length of time in the bloodstream, the effective

concentrations of the actual free acid drug (compared to the inactivity of the methyl ester prodrug as a PAM inhibitor) would, at the same initial dosage, be lower at any given time than when the free acid is delivered subcutaneously. Which of these two contrary factors comes into play can be revealed by the serum PAM activity profile of the prodrug vs. that of the free acid. First, the prodrug, injected at the same level (mg/kg; because the molecular weights of these compounds differ only by 12 Daltons out of 261 g/mol and 273 g/mol the concentration differences are not as stark as between either one as compared to PBA) as the free acid yielded the approximately the same results as regards inhibition of serum PAM activity. The 10, 50, and 100 mg/kg prodrug doses caused serum PAM activity to drop to 10%, 30%, and 35% of controls three hours post-dosing, respectively. Compare this to drops in activity of 10%, 20%, and 30% for the free acid at the same three doses. This would seem to indicate that, by three hours after dosing, the effective concentration of the free acid are the same, whether the free acid is delivered directly to the animal, or whether the prodrug is administered. Conversely, after six hours, serum PAM levels in animals given the prodrug at 10, 50, and 100 mg/kg are 15%, 25%, and 25%, respectively, compared to 10%, 10%, and 15% for the free acid at these same dosing regimens. This indicates a paradoxical situation: on the one hand, the inhibitory effect of the prodrug persists for a much longer period, at a much higher level of efficacy than the free acid; on the other hand, the prodrug reduces serum PAM activity just as quickly (at the first measured time point) as the free acid. The former indicates that the ester persists for a longer period in the bloodstream than the free acid. The latter indicates that the effective concentration of free acid is the same as that of the prodrug after one hour. This is certainly an interesting situation which bears further investigation.

It is possible, as an example, that the prodrug is able to penetrate certain cells which secrete PAM into the bloodstream (possibly atrial myocytes) and inactivate newly synthesized PAM prior to its release (yielding the persistent inhibitory effects) while concurrently enough is hydrolyzed to the free acid in the circulation to inactivate PAM which is already circulating in the bloodstream (yielding the initial, rapid inactivation and decrease in serum PAM activity).

Since the prodrug was more effective in reducing serum PAM activity, and for a longer time, than the free acid (also, the methyl ester is a synthetic precursor of the free acid and therefore requires less work to obtain) we decided to evaluate the prodrug as an anti-inflammatory agent against carrageenan-induced edema. Remarkably, at a dose of 150 mg/kg, the methyl ester prodrug was able to reduce inflammation, relative to untreated controls, by nearly 100% over the six hour course of the experiment. Lower doses of 50 and 100 mg/kg also exhibited a potent anti-inflammatory effect. After one hour, paw volumes were 80% of untreated positive controls for animals dosed at 50, 100, or 150 mg/kg. The 150 mg/kg dose increased to near 100% inhibition of inflammation by three hours post-dosing, and this effect persisted throughout the time frame of the experiment (6 hours). After six hours, the 50 and 100 mg/kg doses yielded paws which were approximately 30% and 60%, respectively, less inflamed than the untreated controls. The 10 mg/kg dose was 40% inhibitory after one hour, and after six hours there was no difference in paw volumes between treated and untreated animals.

It is certainly interesting that the anti-inflammatory effect of the prodrug is so much more pronounced than its ability to inhibit serum PAM. Although we have no data for serum PAM inhibition at 150 mg/kg prodrug, where inflammation was almost entirely

abolished, the 100 mg/kg dose was at least 80% anti-inflammatory for four hours in the carrageenan edema experiment, while only inhibiting serum PAM by 25% after four hours, and reaching a maximum of 35% inhibition of serum PAM after three hours. Earlier experiments by this laboratory (Ogonowski, 1997) using 500 mg/kg of PBA exhibited a 67% inhibition of carrageenan-related paw swelling relative to untreated controls, where they saw, with this same dose of PBA, nearly 100% abolition of serum PAM activity. Recall that, for Methyl-N-Ac-(L)-Phe-Acrylate, the opposite was true; inflammation was nearly completely abolished but inhibition of serum PAM never exceeded 40%. Therefore, although inhibition of serum PAM appears to be a marker for anti-inflammatory properties, there is apparently not a direct correlation between the two events. Again, the methyl ester prodrug is lipophilic and uncharged and may be able to diffuse into macrophages or neutrophils (or mast cells) and inactivate PAM therein, whereas PBA or the free acid acrylate are not.

Finally, our collaborators at Mercer (Bauer, 2007) performed some further experiments with out acrylate inhibitors to investigate whether they could inhibit purified COX-1 and COX-2, or COX-2 stimulated by LPS in whole blood assays. As discussed above, inhibiting peptide amidation and preventing the biosynthesis of SP prevents NK-1 receptor activation. SP occupation of the NK-1 receptor would be expected to induce COX-2 activity via downstream events (NF-κB and others) while at the same time stimulating PLA_2 which serves to liberate the COX-2 substrate arachidonic acid from membrane phospholipids. Therefore, we expected that the acrylates would NOT inhibit purified COX-2, but would inhibit the formation of the COX-2 product PGE_2 in the whole blood assay by preventing PLA_2 activation and COX-2 induction. Indeed, this was

the case as the acrylates were unable to inhibit purified COX-2, even at concentrations as high as 1 mM, while1 mM PBA and 0.5 mM Methyl-N-Ac-(L)-Phe-Acrylate were able to significantly inhibit COX-2 in the whole blood assay (82% and 63%, respectively). To lend further credence to the above, COX-1 (which is constituitively expressed and not subject to induction by LPS) was not inhibited by either PBA or the prodrug acrylate at these concentrations.

As mentioned above, PAM had been shown to be active in small-cell lung carcinoma and is involved in a variety of autocrine growth loops which allow transformed cells to remain in an abnormally active and proliferative state. In addition, Ras-transformed cells have been shown to have decreased expression of various connexin proteins which serve to form gap-junctions, areas of cell-to-cell contact whereby neighboring cells may pass "information" to each other, especially with the idea of limiting the proliferation of healthy cells which are directly in contact with each other. By evaluating the levels of PAM in the normal (WB-Neo) and transformed (WB-Ras) cell lines, in the presence and absence of PBA, we attempted to correlate inhibition of PAM activity with the ability of the transformed cells to form gap-junctions and return to a more normal phenotype. The ability of the cells to form gap junctions is thought to be governed by connexin-43 phosphorylation (de Feijter, 1996), where lack of phosphorylation translates into a lessened ability to form these junctions. This phosphorylation is thought to be governed downstream of the MAP-Kinase pathway, with constituitively-active MAP-Kinase resulting in a decrease in connexin phosphorylation. As discussed above, MAP-Kinase activity, through PLC and PKC activation, is stimulated by occupation of the NK-1 receptor (or perhaps other serpentine receptors with amidated peptide agonists).

Therefore, we believed that inhibition of peptide amidation could conceivably lead to a decrease in MAP-Kinase activity, even though Ras itself is slightly upstream of MAP-K.

Indeed, treatment with PBA resulted in a decrease in PAM activity in both WB-Neo and WB-Ras cells. Concurrently, immunostaining for connexin showed an increase in immunoreactivity at the membrane of Ras-transformed cells, indicating that gap junctions were forming in greater abundance in the PBA-treated cells. Furthermore, a dye-transfer assay indicated that the permeability of transformed cells, through newly-formed gap junctions, presumably, increased upon PBA treatment. Also, our collaborators (Dr. Diane Matesic, et al., Mercer University) noted that the PBA-treated WB-Ras cells returned to a more normal (resembling WB-Neo) morphology and phenotype. Finally, the phosphorylation of connexin-43 was increased in the PBA-treated WB-Ras cells, which was expected to (and did) result in increased gap-junctional communication between the Ras-transformed cells (Sunman, 2004).

We have shown that our acrylate inhibitors are remarkable anti-inflammatory agents in both adjuvant-induced arthritis and carrageenan-induced edema, and that this effect is at least partially correlated to decreases in serum PAM activity. We also predicted, on the basis of the second-messenger pathways stimulated by SP occupation of the NK-1 receptor that these compounds should inhibit the induction of COX-2, and that indeed proved to be the case. In addition, our studies on WB-Ras and WB-Neo cells indicated that inhibition of peptide amidation is able, through restoration of gap-junctional communication, to return Ras-transformed cells to a more normal phenotype while concurrently showing that these cells contained active PAM which could be inhibited by PBA and PBA-OMe. All of these results indicate that inhibition of PAM activity *in vivo*

is able to ameliorate chronic and acute inflammation and to have positive effects on transformed cells. These compounds and their descendants are certainly worthy of further study and refinement as anti-inflammatory and anti-neoplastic agents.

References

Abou-Mohamed GA, Huang JZ, Oldham CD, Taylor TA, Jin LM, Caldwell RB, May SW, Caldwell RW. Vascular and endothelial actions of inhibitors of substance P amidation. J Card Pharm 2000;35:871-80.

Ahmadian MR. Prospects for anti-Ras drugs. Br J Haematol 2002;116:511-18.

Barratt BJ, Easton CJ, Henry DJ, Li IHW, Radom L, Simpson JS. Inhibition of Peptidylglycine -Amidating Monooxygenase by Exploitation of Factors Affecting the Stability and Ease of Formation of Glycyl Radicals. J Am Chem Soc 2004;126:13306-11.

Bar-Shavit Z, Goldman R, Stabinsky Y, Gottlieb P, Fridkin M, Teichberg VI, Blumberg S. Enhancement of phagocytosis – a newly found activity of substance P residing in its N-terminal tetrapeptide sequence. Biochem Biophys Res Comm 1980;94:1445-51.

Bastiaensen E, DePotter W. A peptidyl alpha-amidation activity in chromaffin granules of bovine adrenal medulla. FEBS Letters 1989;244:477-80.

Bauer JD, Sunman JA, Foster MS, Thompson JR, Ogonowski AA, Cutler SJ, May SW, Pollock SH. Anti-inflammatory effects of 4-phenyl-3-butenoic acid and 5-(acetylamino)-4-oxo-6-phenyl-2-hexenoic acid methyl ester, potential inhibitors of neuropeptide bioactivation. J Pharm Exp Ther 2007;320:1171-77.

Bauman AT, Yukl ET, Alkevich K, McCormack AL, Blackburn NJ. The hydrogen peroxide reactivity of peptidylglycine monooxygenase supports a Cu(II)-superoxo intermediate. J Biol Chem 2006;281:4190-98.

Bayliss WM. On the origin of the spinal cord of the vasodilator fibres of the hind-limb and the nature of these fibres. J Phys (London) 1901;26:173-209.

Bell J, El Meskini R, D'Amato D, Mains RE, Eipper BA. Mechanistic investigation of peptidylglycine alpha-hydroxylating monooxygenase via intrinsic tryptophan fluorescence and mutagenesis. Biochemistry 2003;42:7133-42.

Bill A, Stjernschantz J, Mandahl A, Brodin E, Nilsson G. Substance P: Release on trigeminal nerve stimulation, effects in the eye. Acta Physiol Scand 1979;106:371-73.

Bockmann S, Seep J, Jonas L. Delay of neutrophil apoptosis by the neuropeptide substance P. Involvement of the caspase cascade. Peptides 2001;22:661-70.

Boswell JS, Reedy BJ, Kulathila R, Merkler D, Blackburn NJ. Structural investigations on the coordination environment of the active-site coppers of recombinant bifunctional peptidylglycine alpha-amidating enzyme. Biochemistry 1996;35:12241-50.

Braas KM, Stoffers DA, Eipper BA, May V. Tissue specific expression of rat peptidylglycine alpha-amidating monooxygenase activity and messenger-RNA. Mol Endocrinology 1989;3:1387-98.

Braas KM, Harakall SA, Ouafik L, Eipper BA, May V. Expression of peptidylglycine alpha-amidating monooxygenase – an in situ hybridization and immunocytochemical study. Endcrinology 1992;130:2778-88.

Bradbury AF, Finnie MDA, Smthy DG. Mechanism of C-terminal amide formation in peptide hormones. Nature 1982;298:686-8.

Bradbury AF, Smyth DG. Substrate-specificity of an amidating enzyme in porcine pituitary. Biochem Biophys Res Comm 1983;112:372-77.

Bradbury AF, Smyth DG. Biosynthesis of the C-terminal amide in peptide hormones. Bioscience Reports 1987;7:907-16.

Bradbury AF, Smyth DG. Amidation: Isolation of a stable intermediate formed from an imino acid. Eur J Biochem 1987;169:579-84.

Bradbury AF, Mistry J, Roos BA, Smyth DG. 4-Phenyl-3-butenoic acid, an in vivo inhibitor of peptidylglycine hydroxylase (peptide amidating enzyme). Eur J Biochem 1990;189:363-68.

Bradbury AF, Smyth DG. Peptide Amidation. Trends Biol Sci 1991;16:112-15.

Bresnihan B. Pathogenesis of joint damage in rheumatoid arthritis. J Rheumatol 1999;26:717-9.

Calvo CF, Chavanel G, Senik A. Substance P enhances IL-2 expression in activated human T-cells. J Immunol 1992;148:3498-504.

Cesen-Cummings K, Warner KA, Ruch RJ. Role of protein kinase C in the deficient gap-junctional intercellular communication of K-ras-transformed murine lung epithelial cells. Anticancer Res 1998;18:4343-46.

Chen P, Bell J, Eipper BA, Solomon EI. Oxygen activation by the noncoupled binuclear copper site in peptidylglycine alpha-hydroxylating monooxygenase. Reaction mechanism and role of the noncoupled nature of the active site. JACS 2003;126:4991-5000.

Chew GH, Galloway LC, McIntyre NR, Schroder LA, Richards KM, Miller SA, Wright DW, Merkler DJ. Ubiquitin and ubiquitin-derived peptides as substrates for peptidylglycine alpha-amidating monooxygenase. FEBS Letters 2005;579:4678-84.

Covas MJ, Pinto LA, Victorino RM. Disturbed immunoregulatory properties of the neuropeptide substance P on lymphocyte proliferation in HIV infection. Clin Exp Immunol 1994;96:384-88.

Crespo A, Marti MA, Roitberg AE, Amzel LM, Estrin DA. The catalytic mechanism of peptidylglycine alpha-hydroxylating monooxygenase investigated by computer simulation. J Am Chem Soc 2006;128:12817-28.

Croitoru K, Ernst PB, Bienenstock J, Padol I, Stanisz AM. Selective modulation of the natural killer activity of murine intestinal intraepithelial leucocytes by the neuropeptide substance P. Immunology 1990;71:196-201.

DeBlassio JL, deLong MA, Glufke U, Kulathila R, Merkler KA, Vederas JC, Merkler DJ. Amidation of salicyluric acid and gentisuric acid: A possible role for peptidylglycine alpha-amidating monooxygenase in the metabolism of aspirin. Arch Biochem Biophys 2000;383:46-55.

DeBold AJ. Atrial natriuretic factor - a hormone produced by the heart. Science 1985;230:767-70

DeFea KA, Vaughn ZD, O'Bryan EM, Nishijima D, Dery O, Bunnett NW. The proliferative and anti-apoptotic effects of substance P are facilitated by formation of a beta-arrestin-dependent scaffolding complex. PNAS 2000;97:11086-91.

de Feijter AW, Matesic, DF, Ruch RJ, Guan X, Chang CC, Trosko JE. Localization and function of the connexin-43 gap-junction protein in normal and various oncogene-expressing rat liver epithelial cells. Mol Carcin 1996;16:203-12.

Dickinson CJ, Yamada T. Gastrin-amidating enzyme in the porcine pituitary and antrum – characterization of molecular forms and substrate specificity. J Biol Chem 1991;266:334-38.

Dickinson CJ, Daugherty D, Guo YJ, Stadler B, Finniss S, Yamada T. Substrate specificity of the gastrin amidating enzyme. J Biol Chem 1993;268:15929-34.

Driscoll WJ, Konig S, Fales HM, Pannell LK, Eipper BA, Mueller GP. Peptidylglycine-alpha-hydroxylating monooxygenase generates two hydroxylated products from its mechanism-based suicide substrate, 4-phenyl-3-butenoic acid. Biochemistry 2000;39:8007-16.

Eipper BA, Mains RE, Glembotski CC. Identification in pituitary tissue of a peptide alpha-amidation activity that acts on glycine-extended peptides and requires molecular oxygen, copper, and ascorbic acid. PNAS 1983;80:5144-48.

Eipper BA, Glembotski CC, Mains RE. Selective loss of alpha-melanotropin-amidating activity in primary cultures of rat intermediate pituitary-cells. J Biol Chem 1983;258:7292-98.

Eipper BA, Myers AC, Mains RE. Peptidyl-glycine alpha-amidation activity in tissues and serum of the adult-rat. Endocrinology 1985;116:2497-504.

Eipper BA, May V, Braas KM. Membrane-associated peptidylglycine alpha-amidating monooxygenase in the heart. J Biol Chem 1988;263:8371-79.

Eipper BA, Green CBR, Campbell TA, Stoffers DA, Keutmann HT, Mains RE, Ouafik L. Alternative splicing and endoproteolytic processing generate tissue-specific forms of pituitary peptidylglycine alpha-amidating monooxygenase (PAM). J Biol Chem 1992;267:4008-15.

Erion MD, Tan J, Wong M, Jeng AY. Inhibition of peptidylglycine alpha-amidating :monooxygenase by N-substituted homocysteine analogs. J Med Chem 1994;37:4430-37.

Evans JP, Blackburn NJ, Klinman JP. The catalytic role of the copper ligand H172 of peptidylglycine alpha-hydroxylating monooxygenase: A kinetic study of the H172A mutant. Biochemistry 2006;45:15419-29.

Feng J, Shi J, Sirimanne SR, Mounier-Lee CE, May SW. Kinetic and stereochemical studies on novel inactivators of C-terminal amidation. Biochem J 2000;350:521-30.

Feng J, May SW. High-performance liquid chromatographic enantiomeric separation of an enzyme inhibitor which possesses both a chiral center and tautomeric moieties. J Chrom A 2001;905:103-09.

Fenger M, Hilsted L. Influence of ascorbic acid on in vivo amidation of alpha-melanocyte stimulating hormone in guinea-pig pituitary. Acta Endocrinology 1988;118:119-24.

Firestein GS. Invasive fibroblast-like synoviocytes in rhematoid arthritis. Passive responders or transformed aggressors? Arthritis Rheum 1996;39:1781-90.

Francisco WA, Merkler DJ, Blackburn NJ, Klinman JP. Kinetic mechanism and intrinsic isotope effects for the peptidylglycine alpha-amidating enzyme reaction. Biochemistry 1998;37:824452.

Francisco WA, Knapp MJ, Blackburn NJ, Klinman JP. Hydrogen tunneling in peptidylglycine alpha-hydroxylating monooxygenase. J Am Chem Soc 2002;124:8194-5.

Francisco WA, Blackburn NJ, Klinman JP. Oxygen and hydrogen isotope effects in an active site tyrosine to phenylalanine mutant of peptidylglycine alpha-hydroxylating monooxygenase: Mechanistic implications. Biochemistry 2003;42:1813-19.

Frimer AA, Rosenthal L. Superoxide radical anion – oxidative cleavage of chalcones. Tetrahedron Lett 1976:2805-08.

Frimer AA, Rosenthal L. Chemical reactions of superoxide ions in aprotic solvents. Photochem Photobiol 1978;28:711-19.

Gale JS, McIntosh JEA, McIntosh RP. Peptidyl-glycine alpha-amidating mono-oxygenase activity towards a gonadotropin-releasing-hormone C-terminal peptide substrate, in subcellular-fractions of sheep brain and pituitary. Biochem J 1988;251:251-59.

Gerard NP, Eddy RL, Shows TB, Gerard C. The human neurokinin-A (Substance-K) receptor - molecular-cloning of the gene, chromosome localization, and isolation of cDNA from tracheal and gastric tissues. J Biol Chem 1990;265:20455-62.

Gerard NP, Garraway LA, Eddy RL, Shows TB, Iijima H, Paquet JL, Gerard C. Human Substance-P receptor (NK-1) - organization of the gene, chromosome localization, and functional expression of cDNA clones. Biochemistry 1991;30:10640-46.

Gibian, MJ, Russo S. Electron transfer between superoxide ion and an α,β-unsaturated ketone. J Org Chem 1984;49:4304-06.

Gilligan JP, Lovato SJ, Mehta NM, Bertelsen AH, Jeng AY, Tamburini PP. Multiple forms of peptidyl alpha-amidating enzyme - purification from rat medullary-thyroid carcinoma CA-77 cell-conditioned medium. Endocrinology 1989;124:2729-36.

Glembotski CC, Eipper BA, Mains RE. Characterization of a peptide alpha-amidation activity from rat anterior-pituitary. J Biol Chem 1984;259:6385-92.

Glembotski CC. The characterization of the ascorbic acid-mediated alpha-amidation of alpha-melanotropin in cultured intermediate pituitary lobe cells. Endocrinology 1986;118:1461-68.

Gomez S, DiBello C, Hung LT, Genet R, Morgat JL, Fromageot P, Cohen P. C-terminal amidation of neuropeptides - Gly-Lys-Arg extension an efficient precursor of C-terminal amide. FEBS Lett 1984;167:160-64.

Guembe L, Villaro AC, Treston AM. Immunocytochemical mapping of the amidating enzyme PAM in the developing and adult mouse lung. J Hist Cytochem 1999;47:623-36.

Guo CJ, Lai JP, Luo HM, Douglas Sd, Ho WZ. Substance P upregulates macrophage inflammatory protein-1beta expression in human T-lymphocytes. J Neuroimmunol 2002:131:160-67.

Haines KA, Kolasinski SL, Cronstein BN, Reibma J, Gold LI, Weissmann G. Chemoattraction of neutrophils by substance P and transforming growth factor-beta1 is inadequately explained by current models of lipid remodeling. J Immunol 1993;151:1491-99.

Hamad NM, Elconin JH, Karnoub AE, Bai WL, Rich JN, Abraham RT, Der CJ, Counter CM. Distinct requirements for Ras oncogenesis in human versus mouse cells. Genes Development;16:2045-57.

Hancock JF, Magee AI, Childs JE, Marshall CJ. All ras proteins are polyisoprenylated but only some are palmitoylated. Cell 1989;57:1167-77.

Hershey AD, Krause JE. Molecular characterization of a functional cDNA encoding the rat Substance P receptor. Science 1990;247:958-62.

Hopkins B, Powell SJ, Danks P, Briggs I, Graham A. Isolation and characterization of the human lung NK-1 receptor cDNA. Biochem Biophys Res Comm 1991;180:1110-14.

Iwai N, Martinez A, Miller MJ, Vos M, Mulshine JL, Treston AM. Autocrine growth loops dependent on peptidyl alpha-amidating enzyme as targets for novel tumor cell growth inhibitors. Lung Cancer 1999;23:209-22.

Jaron S, Blackburn NJ. Characterization of a half-apo derivative of peptidylglycine monooxygenase. Insight into the reactivity of each active-site copper. Biochemistry 2001;40:6867-75.

Jaron S, Mains RE, Eipper BA, Blackburn NJ. The catalytic role of the copper ligand H172 of peptidylglycine alpha-hydroxylating monooxygenase (PHM): A spectroscopic study of the H172A mutant. Biochemistry 2002;41:13274-82.

Jeng AY, Fujimoto RA, Chou M, Tan J, Erion MD. Suppression of substance P biosynthesis in sensory neurons of dorsal root ganglion by prodrug esters of potent peptidylglycine alpha-amidating monooxygenase inhibitors. J Biol Chem 1997;272:14666-71.

Katopodis AG, May SW. A new facile trinitrophenylated substrate for peptide alpha-amidation and its use to characterize PAM activity in chromaffin granules. Biochem Biophys Res Comm 1988;151:499-505.

Katopodis AG, May SW. Novel substrates and inhibitors of peptidylglycine alpha-amidating monooxygenase. Biochemistry 1990;29:4541-48.

Katopodis AG, Ping DS, May SW. A novel enzyme from bovine neurointermediate pituitary catalyzes dealkylation of alpha-hydroxyglycine derivatives, thereby functioning sequentially with peptidylglycine alpha-amidating monooxygenase in peptide amidation. Biochemistry 1990;29:6115-20.

Katopodis AG, Ping DS, Smith CE, May SW. Functional and structural characterization of peptidylamidoglycolate lyase, the enzyme catalyzing the second step in peptide amidation. Biochemistry 1991;30:6189-94.

Klinge M, Cheng HM, Zabriskie TM, Vederas JC. Irreversible inhibition of mammalian and insect peptidylglycine alpha-hydroxylating monooxygenases (PHMs), peptide amidating enzymes, by N-formyl amides. J Chem Soc Comm 1994;11:1379-80.

Klinman JP. The copper-enzyme family of dopamine beta-monooxygenase and peptidylglycine alpha-hydroxylating monooxygenase: Resolving the chemical pathway for substrate hydroxylation. J Biol Chem 2006;281:3013-16.

Kolhekar AS, Keutmann HT, Mains RE, Quon ASW, Eipper BA. Peptidylglycine alpha-hydroxylating monooxygenase: Active site residues, disulfide linkages, and a two-domain model of the catalytic core. Biochemistry 1997;36:10901-09.

Leeman S. Substance P and neurotensin: Discovery, isolation, chemical characterization, and physiological studies. J Exp Biol 1980;89:193-200.

Li H, Leeman SE, Slack BE, Hauser G, Saltsman WS, Krause JE, Blusztajn JK, Boyd ND. A Substance P (neurokinin-1) mutant carboxy-terminally truncated to resemble a naturally-occurring receptor isoform displays enhanced responsiveness and resistance to desensitization. PNAS 1997;94:9475-80.

Lotz M, Carson DA, Vaughan JH. Substance P activation of rheumatoid synoviocytes: Neural pathway in the pathogenesis of arthritis. Science 1987;235:893-95.

Lotz M, Vaughan JH, Carson DA. Effect of neuropeptides on production of inflammatory cytokines from human monocytes. Science 1988;241:893-95.

Maeda S, Omata M. Inflammation and cancer: Role of nuclear factor-kappaB activation. Cancer Sci 2008;99:836-42.

Mains RE, Myers AC, Eipper BA. Hormonal, drug, and dietary factors affecting peptidyl glycine alpha-amidating monooxygenase activity in various tissues of the adult male-rat. Endocrinology 1985;116:2505-15.

Mains RE, Park LP, Eipper BA. Inhibition of peptide amidation by disulfiram and diethyldithiocarbamate. J Biol Chem 1988;261:11938-41.

Marshall KW, Chiu B, Inman RD. Substance P and arthritis: Analysis of plasma and synovial fluid levels. Arthritis Rheum 1990;33:87-90.

Masu Y, Nakayama K, Tamaki H, Harada Y, Kuno M, Nakanishi S. cDNA cloning of bovine Substance-K receptor through oocyte expression system. Nature 1987;329:836-38.

May V, Eipper BA. Regulation of peptide amidation in cultured pituitary-cells. J Biol Chem 1985;260:6224-31.

May V, Cullen EI, Braas KM, Eipper BA. Membrane-associated forms of peptidylglycine alpha-amidating monooxygenase activity in rat pituitary - tissue-specificity. J Biol Chem 1988;263:7550-54.

May V, Ouafik L, Eipper BA, Braas KM. Immunocytochemical and in situ hybridization studies of peptidylglycine-alpha-amidating monooxygenase in pituitary gland. Endocrinology 1990;127:358-64.

McIninch JK, Geiser F, Prickett KB, May SW. Determination of the absolute configuration of alpha-hydroxyglycine derivatives by enzymatic conversion and chiral high-performance liquid chromatography. J Chrom A 1998;828:191-98.

McIntyre NR, Lowe EW, Chew GH, Owen TC, Merkler DJ. Thiorphan, tiopronin, and related analogs as substrates and inhibitors of peptidylglycine alpha-amidating monooxygenase (PAM). FEBS Lett 2006;580:521-32.

Mehta NM, Gilligan JP, Jones BN, Bertelsen AH, Roos BA, Birnbaum RS. Purification of a peptidylglycine alpha-amidating enzyme from transplantable rat medullary-thyroid carcinomas. Arch Biochem Biophys 1988;261:44-54.

Menkes CJ, Renoux M, Laoussadi S, Mauborgne A, Bruxelle J, Cesselin F. Substance P levels in the synovium and synovial fluid from patients with rheumatoid arthritis and osteoarthritis. J Rheum 1993;20:714-17.

Merkler DJ, Kulathila R, Consalvo AP, Young SD, Ash DE. O-18 isotopic C-13 NMR shift as proof that bifunctional peptidylglycine alpha-amidating enzyme is a monooxygenase. Biochemistry 1992;31:7282-88.

Merkler DJ, Kulathila R, Francisco WA, Ash DE, Bell J. The irreversible inactivation of 2 copper-dependent monooxygenases by sulfite - peptidylglycine alpha-amidating enzyme and dopamine beta-monooxygenase. FEBS Lett 1995;366:165-69.

Merkler DJ, Merkler KA, Stern W, Fleming FF. Fatty acid amide biosynthesis: A possible new role for peptidylglycine alpha-amidating enzyme and acyl-coenzyme A:glycine N-acyltransferase. Arch Biochem Biophys 1996;330:430-34.

Merkler DJ, Glufke U, Ritenour-Rodgers KJ, Baumgart LE, DeBlassio JL, Merkler KA, Vederas JC. Formation of nicotinamide from nicotinuric acid by peptidylglycine alpha-amidating monooxygenase (PAM): A possible alternative route from nicotinic acid (niacin) to NADP in mammals. J Am Chem Soc 1999;121:4904-05.

Milgram SL, Johnson RC, Mains RE. Expression of individual forms of peptidylglycine alpha-amidating monooxygenase in ATt-20 cells - endoproteolytic processing and routing to secretory granules. J Cell Biol 1992;117:717-28.

Milgram SL, Mains RE, Eipper BA. COOH-terminal signals mediate the trafficking of a peptide processing enzyme in endocrine-cells. J Cell Biol 1993;121:23-36.

Milgram SL, Mains RE, Eipper BA. Differential trafficking of soluble and integral membrane secretory granule-associated proteins. J Cell Biol 1994;124:33-41.

Milgram SL, Mains RE, Eipper BA. Identification of routing determinants in the cytosolic domain of a secretory granule-associated integral membrane protein. J Biol Chem 1996;271:17526-35.

Mizuno K, Sakata J, Kojima M, Kangawa K, Matsuo H. Peptide C-terminal alpha-amidating enzyme purified to homogeneity from xenopus-laevis skin. Biochem Biophys Res Comm 1986;137:984-91.

Moore AB, May SW. Kinetic and inhibition studies on substrate channelling in the bifunctional enzyme catalysing C-terminal amidation. Biochem J 1999;341:33-40.

Mounier CE, Shi J, Sirimanne SR, Chen BH, Moore AB, GillWoznichak MM, Ping DS, May SW. Pyruvate-extended amino acid derivatives as highly potent inhibitors of carboxyl-terminal peptide amidation. J Biol Chem 1997;272:5016-23.

Mueller GP, Husten EJ, Mains RE, Eipper BA. Peptide alpha-amidation and peptidylglycine alpha-hydroxylating monooxygenase - control by disulfiram. Mol Pharmacol 1993;44:972-80.

Mueller GP, Altarac M. Peptide alpha-amidation - differential regulation by disulfiram and its metabolite, diethyldithiocarbamate. Neuropeptides 1995;28:333-40.

Mueller GP, Driscoll WJ, Eipper BA. In vivo inhibition of peptidylglycine-alpha-hydroxylating monooxygenase by 4-phenyl-3-butenoic acid. J Pharm Exp Ther 1999;290:1331-36.

Murris-Espin M, Pinelli E, Pipy B, Leophonte P, Didier A. Substance P and alveolar macrophages: Effects on oxidative metabolism and eicosanoid production. Allergy 1995;50:334-39.

Murthy ASN, Mains RE, Eipper BA. Purification and characterization of peptidylglycine alpha-amidating monooxygenase from bovine neurointermediate pituitary. J Biol Chem 1986;261:1815-22.

Murthy ASN, Keutmann HT, Eipper BA. Further characterization of peptidylglycine alpha-amidating monooxygenase from bovine neurointermediate pituitary. Mol Endocrinology 1987;1:290-99.

Nakanishi S. Mammalian tachykinin receptors. Ann Rev Neurosci 1991;14:123-36.

Nilsson J, von Euler AM, Dalsgaard CJ. Stimulation of connective tissue cell growth by substance P and substance K. Nature 1985;315:61-63.

Noe BD, Katopodis AG, May SW. Kinetic analyses of peptidylglycine alpha-amidating monooxygenase from pancreatic-islets. Gen Comp Endocrinology 1991;83:183-92.

O'Connor TM, O'Connell JO, O'Brien DI, Goode T, Bredin CP, Shanahan F. The role of substance P in inflammatory disease. J Cell Phys 2004;201:167-80.

Oldham CD, Li CZ, Girard PR, Nerem RM, May SW. Peptide amidating enzymes are present in cultured endothelial cells. Biochem Biophys Res Comm 1992;184:323-29.

Ormo M, Regnstrom K, Wang ZG, Que L, Sahlin M, Sjoberg BM. Residues important for radical stability in ribonucleotide reductase from E. Coli. J Biol Chem 1995;270:6570-76.

Ouafik L, May V, Keutmann HT, Eipper BA. Developmental regulation of peptidylglycine alpha-amidating monooxygenase (PAM) in rat-heart atrium and ventricle - tissue-specific changes in distribution of PAM activity, messenger-RNA levels, and protein forms. J Biol Chem 1989;264:5839-45.

Ouafik L, Stoffers DA, Campbell TA, Johnson RC, Bloomquist BT, Mains RE, Eipper BA. The multifunctional peptidylglycine alpha-amidating monooxygenase gene - exon intron organization of catalytic, processing, and routing domains. Mol Endocrinology 1992;6:1571-84.

Oyarce AM, Eipper BA. Neurosecretory vesicles contain soluble and membrane-associated monofunctional and bifunctional peptidylglycine alpha-amidating monooxygenase proteins. J Neurochemistry 1993;60:1105-14.

Oyarce AM, Eipper BA. Identification of subcellular compartments containing peptidylglycine alpha-amidating monooxygenase in rat anterior-pituitary. J Cell Sci 1995;108:287-97.

Perianin A, Snyderman R, Malfroy B. Substance P primes human neutrophil activation: A mechanism for neurological regulation of inflammation. Biochem Biophys Res Comm 1989;161:520-24.

Ping DS, Katopodis AG, May SW. Tandem stereochemistry of peptidylglycine alpha-monooxygenase and peptidylamidoglycolate lyase, the two enzymes involved in peptide amidation. J Am Chem Soc 1992;114:3998-4000.

Ping DS, Mounier CE, May SW. Reaction versus subsite stereospecificity of peptidylglycine alpha-monooxygenase and peptidylamidoglycolate lyase, the two enzymes involved in peptide amidation. J Biol Chem 1995;270:29250-55.

Prigge ST, Kolhekar AS, Eipper BA, Mains RE, Amzel LM. Amidation of bioactive peptides: The structure of peptidylglycine alpha-hydroxylating monooxygenase. Science 1997;278:1300-05.

Prigge ST, Eipper BA, Mains RE, Amzel LM. Dioxygen binds end-on to mononuclear copper in a precatalytic enzyme complex. Science 2004;304:864-67.

Rhodes CH, Xu RY, Angeletti RH. Peptidylglycine alpha-amidating monooxygenase (PAM) in Schwann-cells and glia as well as neurons. J Histochem Cytochem 1990;38:1301-11.

Ruch RJ, Sigler K. Growth inhibition of rat liver epithelial tumor cells by monoterpenes does not involve ras plasma membrane association. Carcinogenesis 1994;15:787-89.

Sakata J, Mizuno K, Matsuo H. Tissue distribution and characterization of peptide C-terminal alpha-amidating activity in rat. Biochem Biophys Res Comm 1986;140:230-36.

Saldise L, Martinez A, Montuenga LM, Treston A, Springall DR, Polak JM, Vazquez JJ. Distribution of peptidyl-glycine alpha-amidating mono-oxygenase (PAM) enzymes in normal human lung and in lung epithelial tumors. J Histochem Cytochem 1996;44:3-12.

Sawyer DT, Gibian MJ. The chemistry of superoxide ion. Tetrahedron 1979;351:1471-81.

Schafer MKH, Stoffers DA, Eipper BA, Watson SJ. Expression of peptidylglycine alpha-amidating monooxygenase (E.C.1.14.17.3) in the rat central-nervous-system. J Neurosci 1992;12:222-34.

Schratzberger P, Reinisch N, Prodinger WM, Kahler CM, Sitte BA, Bellmann R, Fischer-Colbrie R, Winkler H, Wiedermann CJ. Differential chemotactic activities of sensory neuropeptides for human peripheral blood mononuclear cells. J Immunol 1997;158:3895-901.

Scopsi L, Lee R, Gullo M, Collini P, Husten EJ, Eipper BA. Peptidylglycine alpha-amidating monooxygenase in neuroendocrine tumors - Its identification, characterization, quantification, and relation to the grade of morphologic differentiation, amidated peptide content, and granin immunocytochemistry. App Immunohistochem 1998;6:120-32.

Seidel MF, Tsalik J, Vetter H, Muller W. Substance P in rheumatic diseases. Curr Rheum Rev 2007;3:17-30.

Serra MC, Bazzoni F, Della Bianca V, Greskowiak M, Rossi F. Activation of human neutrophils by substance P. Effect on oxidative metabolism, exocytosis, cytosolic Ca^{+2} concentration, and inositol phosphate formation. J Immunol 1988;141:2118-24.

Siebert X, Eipper BA, Mains RE, Prigge ST, Blackburn NJ, Amzel LM. The catalytic copper of peptidylglycine alpha-hydroxylating monooxygenase also plays a critical structural role. Biophys J 2005;89:3312-19.

Stead RH, Tomioka M, Quinonez G, Simon GT, Felten SY, Bienenstock J. Intestinal mucosal mast cells in normal and nematode-infected rat intestines are in intimate contact with peptidergic nerves. PNAS 1987;84:2975-79.

Suchanek G, Kreil G. Translation of melittin messenger-RNA *in vitro* yields a product terminating with glutaminylglycine rather than with glutaminamide. PNAS 1977;74:975-78.

Sunman JA, Foster MS, Folse SL, May SW, Matesic DF. Reversal of the transformed phenotype and inhibition of peptidylglycine alpha-monooxygenase in Ras-transformed cells by 4-phenyl-3-butenoic acid. Mol Carcinogen 2004;41:231-46.

Suzuki K, Ohta M, Okatmoto M, Nishikawa Y. Functional expression and characterization of a Xenopus laevis peptidylglycine alpha-amidating monooxygenase, AE-II, in insect-cell culture. Eur J Biochem 1993;213:93-98.

Takahashi K, Okamoto H, Seino H, Noguchi M. Peptidylglycine alpha-amidating reaction - evidence for a 2-step mechanism involving a stable intermediate at neutral pH. Biochem Biophys Res Comm 1990;169:524-530.

Tamburini PP, Jones BN, Consalvo AP, Young SD, Lovato SJ, Gilligan JP, Wennogle LP, Erion M, Jeng AY. Structure-activity relationships for glycine-extended peptides and the alpha-amidating enzyme derived from medullary-thyroid CA-77 cells. Arch Biochem Biophys 1998;267:623-31.

Tamburini PP, Young SD, Jones BN, Palmesino RA, Consalvo AP. Peptide substrate-specificity of the alpha-amidating enzyme isolated from rat medullary-thyroid CA-77 cells. Int J Pep Prot Res 1990;35:153-56.

Tateishi K, Arakawa F, Misumi Y, Treston AM, Vos M, Matsuoka Y. Isolation and functional expression of human pancreatic peptidylglycine alpha-amidating monooxygenase. Biochem Biophys Res Comm 1994;205:282-90.

Thiele EA, Marek KL, Eipper BA. Tissue-specific regulation of peptidyl-glycine alpha-amidating monooxygenase expression. Endocrinology 1989;125:2279-88.

Tuppy H. The amino acid sequence in oxytocin. Biochim Biophys Acta 1953;11:449-50.

Uddman R, Hakanson R, Luts A, Sundler F. Autonomic control of the respiratory system. In: Barnes PJ, editor. Distribution of neuropeptides in airways. London: Harvard Academic 1997.

Vollhardt KPC, Schore NE. Organic Chemistry Second Edition 1994. W.H. Freeman and Company.

Von Euler US, Gaddum JH. An unidentified depressor substance in certain tissue extracts. J Physiology 1931;72:74-87.

Von Zastrow M, Tritton TR, Castle JD. Exocrine Secretion Granules Contain Peptide Amidation Activity. PNAS 1986;83:3297-301.

Wilcox BJ, Ritenour-Rodgers KJ, Asser AS, Baumgart LE, Baumgart MA, Boger DL, DeBlassio JL, deLong MA, Glufke U, Henz ME, King L, Merkler KA, Patterson JE, Robleski JJ, Vederas JC, Merkler DJ. N-acylglycine amidation: Implications for the biosynthesis of fatty acid primary amides. Biochemistry 1999;38:3235-45.

Young SD, Tamburini PP. Enzymatic peptidyl alpha-amidation proceeds through formation of an alpha-hydroxyglycine intermediate. J Am Chem Soc 1989;111:1933-34.

Zabriskie TM, Cheng HM, Vederas JC. Incorporation of aerobic oxygen into the hydroxyglycyl intermediate during formation of C-terminal peptide amides by peptidylglycine alpha-amidating monooxygenase (PAM). J Chem Soc Comm 1991;8:571-2.

Zabriskie TM, Cheng HM, Vederas JC. Mechanism-based inactivation of peptidylglycine alpha-hydroxylating monooxygenase (PHM) by a substrate-analog, D-phenylalanyl-L-phenylalanyl-D-vinylglycine - inhibition of formation of peptide C-terminal amides. J Am Chem Soc 1992;114:2270-72.

Ziche M, Morbidelli L, Pacini M, Geppetti P, Alessandri G, Maggi CA. Substance P stimulates neovascularization in vivo and proliferation of cultured endothelial cells. Microvasc Res 1990;40:264-78.